INSTITUT D'OPTIQUE GRADUATE SCHOOL

ÉCOLE DOCTORALE ONDES ET MATIERE

DISCIPLINE : PHYSIQUE

THÈSE
pour l'obtention du grade de Docteur en science de l'Institut d'Optique Graduate School
préparée au Laboratoire Charles Fabry

soutenue le 12/12/2014

par

Samuel LELLOUCH

COLLECTIVE LOCALIZATION TRANSITIONS IN INTERACTING DISORDERED AND QUASIPERIODIC BOSE SUPERFLUIDS

Composition du jury

Directeur de thèse :	Laurent SANCHEZ-PALENCIA	–	Institut d'Optique, Palaiseau
Président du jury :	Pascal SIMON	–	Université Paris Sud, Orsay
Rapporteurs :	Jean-Claude GARREAU	–	Université de Lille 1
	Tommaso ROSCILDE	–	ENS Lyon
Examinateurs :	Anna MINGUZZI	–	LPMMC, Grenoble
	Giovanni MODUGNO	–	LENS, Florence

Ibergekumene tsores iz gut tsu dertseylin.
(C'est un plaisir de raconter les ennuis passés.)

Proverbe yiddish
voir Primo Levi, Le système périodique

Remerciements

J'ai effectué mon travail de thèse au laboratoire Charles Fabry (LCF) de l'Institut d'Optique (Palaiseau), unité mixte de recherche du CNRS et de l'Université Paris-Sud, et au sein de l'École doctorale Ondes et Matière (EDOM) de l'Université Paris-Sud. Ces travaux ont été financés par une allocation AMX de l'École Polytechnique et un monitorat de l'Université Paris-Sud. Mes premiers remerciements vont donc naturellement à l'ensemble des services de ces différentes institutions, qui ont permis que ma thèse se déroule dans les meilleures conditions. Je suis tout particulièrement reconnaissant à Christian Chardonnet et Pierre Chavel, directeurs successifs du LCF, de m'avoir accueilli dans ce laboratoire agréable et dynamique, et de l'attention qu'ils ont toujours manifestée vis-à-vis des nombreux doctorants.

La logique voudrait que je poursuive du plus général au plus particulier, mais je dois tellement à Laurent Sanchez-Palencia qu'il m'est impossible de ne pas commencer par là. Avoir un directeur de thèse comme Laurent est une chance inouïe. Sa disponibilité permanente, son souci -au-delà de l'encadrement scientifique de mon travail- de me procurer un environnement idéal et une formation complète, ainsi que le subtil dosage dont il a toujours fait preuve entre un suivi attentif de mes travaux et l'autonomie qu'il me laissait pour les mener, représentent pour tout étudiant en thèse un bénéfice inestimable. Dans de telles conditions, j'ai eu ce luxe d'avoir pu sereinement goûter aux multiples ennuis que la physique se plaît à distiller. Il ne serait pas exagéré non plus de dire que Laurent m'a appris à faire de la physique. Son habileté à extraire d'un problème les grandeurs pertinentes, son sens du détail poussé à l'extrême, m'ont montré combien il peut être profitable de reprendre de fond en comble un problème a priori compris pour en dégager une image plus simple et plus limpide. La liste de ses enseignements serait bien trop longue pour figurer ici -j'avais pensé un temps y consacrer une annexe...-, je me contenterai simplement d'un immense merci, en espérant ne pas avoir trop abusé de ces conditions de luxe.

J'ai eu également la chance de travailler au sein de la jeune équipe de Théorie de la Matière Quantique qui, passée de quatre à huit membres entre septembre 2011 et septembre 2014, s'apparente de plus en plus à un authentique système à N corps. Les interactions multiples au sein du groupe ont toujours été aussi enrichissantes que sympathiques, et j'en remercie donc tous les membres, Tung-Lam Dao, Luca Pezzè, Marie Piraud, Giuseppe Carleo, Guilhem Boéris (avec l'accent sur le "e" je vous prie), Lih-King Lim, Lorenzo Cevolani, Cécile Crosnier, et Christian Trefzger.

Plus largement, c'est à l'ensemble du groupe d'Optique atomique que je souhaite exprimer ma profonde gratitude. Un grand merci à son directeur Alain Aspect, qui m'a si chaleureusement accueilli dans ce haut lieu de la matière ultrafroide. La passion d'Alain est à n'en pas douter contagieuse, l'étendue de ses connaissances impressionnante, et sa curiosité autant que

son exigence sont pour l'ensemble de son groupe de véritables stimulateurs (quantiques). Par ailleurs, la proximité avec les équipes expérimentales, matérialisée par les réunions de groupe communes, représente un plus indéniable que j'ai eu un réel plaisir à apprécier - abstraction faite, bien sûr, des problèmes de voltage, qui font disjoncter plus d'un théoricien en réunion de groupe.

Je suis reconnaissant à Jean-Claude Garreau et Tommaso Roscilde qui ont gentiment accepté d'être mes rapporteurs et ont pris le temps de lire ce manuscrit avec attention. Je remercie également tous les membres de mon jury, Anna Minguzzi, Giovanni Modugno et Pascal Simon, pour les discussions constructives que nous avons eues et pour leurs efforts à aménager leurs emplois du temps bien remplis, qui ont permis de dégager ce créneau commun de 3h53 (allers-retours vers Massy TGV compris !) le jour de ma soutenance.

Je ne saurai oublier toutes les personnes avec qui j'ai eu le plaisir d'enseigner durant mes trois années de monitorat. Un grand merci à Gaétan Messin (mécanique quantique), Sylvie Lebrun (informatique) et François Goudail (analyse de Fourier et traitement du signal) pour la confiance qu'ils m'ont accordée, en me confiant notamment, alors que je n'en avais jamais suivi le moindre cours, les TDs de traitement du signal -signal que j'espère en l'occurrence ne pas avoir trop maltraité. Une pensée également pour tous les élèves de l'Institut d'Optique, qui ont été un public indulgent -et que j'espère également ne pas avoir trop maltraités.

Je remercie enfin tous les services techniques de l'Institut d'Optique qui, bien que je les aie nettement moins sollicités qu'un expérimentateur, ont toujours répondu rapidement et efficacement à mes requêtes. Une attention particulière au service de reprographie et à Graça Martins qui a assuré le tirage et la reliure de ce manuscrit.

Je souhaiterais pour terminer réserver mes derniers remerciements à toutes les personnes que j'ai eu le plaisir de côtoyer pendant ces années. A tous les membres de ma famille, qui ont participé de façon -plus ou moins- décisive à la relecture de mon manuscrit et qui, dans une sorte d'excitation collective, se sont déplacés en masse le jour ma soutenance; leur contribution non moins décisive au pot de thèse a été unanimement appréciée. A tous mes amis d'orchestre et de musique de chambre, professeurs de musique à Paris et à Bruxelles, ainsi qu'à Niccolò, Jean-Sébastien, Johannes, Piotr Illytch, Eugène et tous les autres, qui m'ont apporté bien plus que la néanmoins indispensable antidote à l'overdose de physique quantique. A tous mes coéquipiers de la glorieuse équipe de foot du laboratoire, à qui j'adresse mes sincères excuses pour tous les buts encaissés et mes profondes condoléances, à tous mes amis, à tous ceux qui ont insisté pour figurer dans ces pages comme à ceux que j'aurais involontairement oubliés, au lecteur téméraire enfin, à qui je souhaite une bonne lecture et qui, probablement, se demande encore ce qui diable a pu le pousser à aller jusqu'au bout de cet interminable -et quelque peu désordonné (évidemment !)- paragraphe.

Brussel Zuid, le 18/12/2014

Contents

Introduction

L'ordre est le plaisir de la raison,
mais le désordre est le délice de l'imagination.
Platon

Physics have always liked simple systems, and managed to explain the world in terms of basic laws and equations. As pointed out by Goldenfeld and Kadanov [1],

"One of the most striking aspects of physics is the simplicity of its laws. [...] The world is lawful, and [...] everything is simple, neat, and expressible in terms of everyday mathematics [...]. Everything is simple and neat -except, of course, the world."

Indeed, complex systems are in fact everywhere. When trying to find out the properties and the states of matter, be it in solid-state, nuclear, or liquid physics, one faces incredibly complex structures, which can no longer be understood from simple equations. Such complexity arises from two reasons.

A first one is that when looking at them at the microscopic scale, all macroscopic systems are made of many elementary components, which unavoidably interact with each other. Electrons and atoms in solids, nucleons in nuclei, molecules in liquids, do not behave independently of each other, but interact via forces of all kinds. Therefore, the behaviour of the whole system is intrinsically a many-body one, which generally cannot be described as the sum of all one-body behaviours. As summarized by Anderson, *"More is different"*, and new approaches are needed. Although statistical physics provides the tools to deal with such systems, finding a simple and intuitive description of the physics at stake remains in most cases extremely difficult.

The second reason is that real-life systems are never perfect, in the sense that they always display uncontrolled imperfections at the microscopic scale. For instance in solid-state physics, crystals are modelled by periodic arrangements of atoms, but in practice, such structures always exhibit unavoidable defects, whose nature or positions are not necessarily known. All those unknown degrees of freedom, which are traditionally referred to as *disorder*, make the system impossible to exactly describe microscopically, and one has to develop other approaches to still make reliable -and useful- predictions.

Somehow fascinatingly, both interactions and disorder turn out to play a prominent role when entering the quantum world.

Interactions in quantum mechanics can have several origins, e.g. conservative external forces, spin-spin or spin-orbit couplings, matter-light interactions... Additionally, one puzzling feature

of quantum mechanics is the existence of several quantum statistics. Due to their indistinguishability, identical particles in quantum mechanics obey a specific statistics, which depends on their nature (bosonic or fermionic). As a result, they do not behave independently but display, even in the absence of interactions, a many-body behaviour, as illustrated by the Pauli exclusion principle for fermions and Bose-Einstein condensation for bosons. More generally, interactions and quantum statistics are responsible for collective behaviours, and underlie original phenomena and fascinating quantum phases, such as superconductivity and superfluidity.

As regards disorder, it has been known since Anderson that in phase coherent systems, disorder can dramatically alter the physics, not only quantitatively, but also qualitatively. The most celebrated example in undoubtedly Anderson localization [2], an interference effect where a small amount of disorder can lead to a total suppression of transport in disordered samples.

Furthermore, disorder and interactions interplay in a very complex way [3]. While disorder is now recognized to possibly destroy superfluidity [4,5] or superconductivity [6,7], it has been shown that disorder and interactions can compete or cooperate depending on situations, yielding non-trivial localization effects. A theory of localization with interactions, a long-standing quest that Anderson himself has dreamt of in the early days after his seminal discovery [8], is far from being achieved. While new concepts have emerged, such as many-body localization [9,10], new questions have arised and many aspects of the field remain still unexplored. This is for instance the case of the disorder-induced superfluid to insulator transition [11, 12] and of the localization properties of collective excitations [13, 14].

Somehow unexpectedly, a renewed interest in the field has emerged from the development of quantum gases. Such systems, which offer unprecedented control over their parameters, including disorder and interactions, have stimulated both experimental and theoretical research in the field and produced landmark results. Moreover, they have proved to feature their own original effects, which are worth studying in their own right.

From a theoretical point of view, addressing the question of disorder in interacting systems represents a considerable challenge, firstly because the many-body problem is an extraordinary difficult one. Describing the intricate motions of all individual particles is impossible and pointless, and new approaches are required. Among the concepts that have emerged, a central one is the concept of quasiparticle. Instead of considering individual particles, the idea is to think in terms of elementary fictitious bodies. For instance, as the motion of one particle affects all the neighboring ones, this amounts altogether to a global motion of a cloud of particles. This fictitious body, which has its own physical properties (mass, lifetime...), is called a *quasi-particle*, and corresponds to an elementary *collective excitation* of the system. Remarkably in many cases, all motions within a complex interacting system can be described in terms of the *independent* motions of elementary excitations. Therefore, a central question in the field of disordered interacting quantum systems is to understand how disorder affects those collective excitations.

In this thesis, we theoretically investigate the collective localization properties of disordered Bose systems, focusing on the localization properties of their collective excitations. Since the latter govern most elementary processes in interacting systems, understanding how they behave in the presence of disorder is of prime importance to penetrate both dynamical (energy transfer, thermalization properties...) and static (phase transitions) properties of disordered many-body systems. We will focus on the case of a Bose gas in the weakly-interacting regime, for which the Bogoliubov theory has proved an efficient tool, and address the question of col-

lective localization transitions in several contexts : the disordered Bose gas, the quasiperiodic Bose gas, and the two-component Bose gas. This manuscript is organized as follows.

In chapter 1, we introduce the basic concepts and the general framework of our study. We review the main notions about disordered systems, among which Anderson localization, before addressing in details the question of disorder in interacting quantum systems. We show that those topics, which originally emerged in condensed matter, have known a renewed interest sparked by the development of ultracold gases. A brief state of the art concludes this chapter.

Chapter 2 is devoted to an introductory presentation of the Bose gas in the weakly-interacting regime, and provides the technical tools to be used in this thesis. Much attention is devoted to the Bogoliubov theory, which successfully describes the gas in terms of elementary quasiparticles. The theory is presented in details in the most general inhomogeneous situation. General features of Bose gases, such as condensation, quasi-condensation, and superfluidity, are also discussed.

Then, chapters 3 to 5, which constitute the heart of this manuscript, study the influence of disorder on collective excitations in three different cases.

Chapter 3 considers the case of a weakly-interacting Bose gas in the continuous space and in arbitrary dimension, in the presence of a truly disordered potential. While the 1D case was already studied by weak-disorder approaches, revealing that collective excitations are also subjected to Anderson localization, no study has so far been performed in the strong-disorder case, which is however needed to address the problem in higher dimensions. This is done in this chapter, which provides us with a generic and rather complete description of the localization behaviour of collective excitations in arbitrary dimension. We discuss universal and non-universal features of their propagation and present a microscopic interpretation of the observed behaviours. Implications on ultracold-atom experiments are discussed.

Chapter 4 is devoted to the case of a weakly-interacting Bose gas in the presence of a one-dimensional quasiperiodic potential. Quasiperiodic potentials are known to display an intermediate behaviour between truly disordered and periodic ones. However, the influence of such potentials on the collective excitations of the gas has been little studied so far. We perform here a numerical and analytical treatment of this problem. We quantitatively characterize the localization transition of the excitations and provide an interpretation of our results in terms of localization in an effective multiharmonic model.

Finally, chapter 5 is devoted to the case of a two-component Bose gas. Although such systems are expected to display their own original effects when subjected to disorder, a unified formalism to address those questions in the most general inhomogeneous situation is missing. We develop such a formalism here, and apply it to the homogeneous case to enlighten the basic -but already rich and non-trivial- physics at stake.

A conclusion summarizes the obtained results and discusses both theoretical and experimental perspectives of this work.

Version française

La physique a toujours aimé les systèmes simples, et cherché à expliquer le monde à l'aide de lois et d'équations élémentaires. Comme le soulignaient Goldenfeld et Kadanov [1], *"l'un des aspects les plus fascinants de la physique est la simplicité de ses lois [...] Le monde est régi par des lois [...] tout est simple, net, et peut s'exprimer à l'aide des mathématiques de tous les jours [...] Tout est simple et net - excepté bien sûr le monde".*

En effet, les systèmes complexes sont en réalité partout. Dès que l'on cherche à comprendre les propriétés et les états de la matière, que ce soit en physique des solides, en physique nucléaire ou en physique des liquides, l'on est immédiatement confronté à des structures prodigieusement complexes, qui ne peuvent plus être décrites par des équations simples. Les raisons d'une telle complexité sont multiples.

La première d'entre elles est que dès qu'on les regarde à l'échelle microscopique, tous les systèmes macroscopiques sont constitués d'une multitude de constituants élémentaires qui, inévitablement, interagissent les uns avec les autres. Les électrons et les atomes dans les solides, les nucléons dans les noyaux atomiques, ou encore les molécules dans les liquides, ne se comportent pas indépendamment les uns des autres mais interagissent via des forces de toutes sortes. De ce fait, le système tout entier possède un comportement intrinsèquement collectif, qui ne peut généralement pas se réduire à une somme de comportements individuels. *"More is different"*, résumait Anderson, soulignant la nécessité de recourir à des approches radicalement nouvelles. Si celles-ci ont en partie été fournies par le développement de la physique statistique, trouver une image simple et intuitive de la physique à l'oeuvre dans ces systèmes demeure, dans la plupart des cas, extrêmement difficile.

La seconde raison est que les systèmes réels ne sont jamais parfaits, mais présentent toujours, à l'échelle microscopique, des imperfections impossibles à prendre en compte de façon exacte. En physique des solides par exemple, les structures cristallines, bien que modélisées par un arrangement périodique d'atomes, contiennent en pratique toujours d'inévitables défauts, dont la nature et la position sont rarement connues. Ces degrés de liberté non contrôlés, que l'on rassemble traditionnellement sous l'appellation de *désordre*, rendent le systèmes impossible à décrire exactement au niveau microscopique, et d'autres approches sont nécessaires pour obtenir malgré tout des prédictions fiables et utiles.

D'une façon tout à fait remarquable, les interactions comme le désordre ont une influence accrue dès que l'on entre dans l'univers quantique.

Les interactions en mécanique quantique peuvent avoir des origines diverses, qu'il s'agisse de forces extérieures conservatives, de couplages spin-spin ou spin-orbite, d'interactions lumière-matière... A cela s'ajoute l'existence des statistiques quantiques -une spécificité de la physique quantique. Les particules identiques étant indiscernables en mécanique quantique, elles obéissent à une statistique différente des particules classiques, qui dépend qui plus est de leur nature (bosonique ou fermionique). De ce fait, les particules identiques ne se comportent pas indépendamment mais ont, même en l'absence d'interactions, un comportement intrinsèquement collectif, illustré par exemple par le principe d'exclusion de Pauli pour les fermions et la condensation de Bose-Einstein pour les bosons. Plus généralement, interactions et statistiques quantiques sont à l'origine de comportements collectifs qui sous-tendent l'existence de phases et d'états de la matière originaux et fascinants, tels la supraconductivité et la superfluidité.

En ce qui concerne le désordre, il est désormais bien connu, depuis les travaux

d'Anderson [2], que dans les systèmes cohérents, celui-ci peut profondément altérer la physique à l'oeuvre, non seulement quantitativement mais aussi qualitativement. L'exemple le plus emblématique est sans conteste la localisation d'Anderson, un effet d'interférence multiple où une quantité même infime de désordre peut conduire à une suppression totale du transport à travers l'échantillon.

De plus, les effets du désordre et des interactions se combinent d'une façon extrêmement complexe. S'il est communément admis que le désordre peut détruire la superfluidité [4, 5] et la supraconductivité [6, 7], on sait également que désordre et interactions peuvent s'opposer ou coopérer selon les situations, conduisant à des effets de localisation non triviaux. Plus d'un demi-siècle après la découverte d'Anderson, une théorie unifiée de la localisation en présence d'interactions, théorie dont Anderson lui-même a longtemps rêvé [8], n'est encore qu'une lointaine utopie. Si de nouveaux concepts ont émergé, comme celui de localisation d'Anderson à N corps [9, 10], de nouvelles questions ont surgi et bien des aspects du domaine demeurent inexplorés. C'est par exemple le cas des transitions de phase induites par le désordre [11, 12], et des propriétés de localisation des excitations collectives [13, 14].

D'une façon quelque peu inattendue, c'est le développement récent des gaz quantiques ultrafroids qui a ravivé l'intérêt pour ces questions-là. Ces systèmes, qui permettent un contrôle sans précédent de tous leurs paramètres, y compris désordre et interactions, ont stimulé des recherches aussi bien expérimentales que théoriques et permis des avancées majeures. Ils présentent de surcroît de nombreux effets originaux qui leur sont propres, et sont donc intéressants à étudier en tant que tels.

D'un point de vue théorique, comprendre le rôle du désordre dans les systèmes quantiques en interaction représente un défi considérable, avant tout parce qu'il s'agit d'un problème à N corps. De fait, chercher à décrire les mouvements individuels, enchevêtrés à l'extrême, de toutes les particules qui constituent le système est impossible et inutile, et il faut adopter un nouveau point de vue. Parmi les approches qui se sont développées, un concept fondamental est celui de quasi-particule : au lieu de considérer les particules individuelles, l'idée est de raisonner en termes d'objets fictifs élémentaires. Pour s'en faire une idée, on peut se représenter le mouvement d'une particule qui, affectant toutes ses voisines, va résulter en un mouvement global de tout un nuage de particules. Cet objet fictif, qui possède ses caractéristiques propres (masse, durée de vie...) est appelé *quasi-particule*, et correspond de fait à une *excitation collective* élémentaire du système. De façon tout à fait remarquable, dans bien des cas, tous les mouvements se produisant au sein d'un système en interaction peuvent se décomposer en mouvements indépendants de ses excitations élémentaires. Ainsi, une question centrale dans le domaine des systèmes désordonnés est de comprendre comment le désordre affecte ces excitations collectives.

Ce manuscrit présente une étude théorique des propriétés de localisation collective dans les systèmes bosoniques désordonnés en interaction, en se focalisant sur la question de la localisation de leurs excitations collectives. Dans la mesure où ces dernières gouvernent la plupart des processus élémentaires à l'oeuvre dans les systèmes en interaction, appréhender leur comportement en présence de désordre revêt une importance particulière, en vue de comprendre les propriétés dynamiques (transfert d'énergie, thermalisation...) et statiques (diagramme de phase) de ces systèmes désordonnés. En nous focalisant sur le cas d'un gaz de Bose dans le régime de faibles interactions, très bien décrit par la théorie de Bogoliubov, nous étudions cette question dans différents contextes : le gaz de Bose désordonné en dimension arbitraire, le gaz de Bose quasi-périodique unidimensionnel , et le gaz de Bose à deux

composants. Le manuscrit est organisé comme suit.

Le chapitre 1 introduit les notions de base et le contexte général dans lequel s'inscrit notre étude. Nous passons en revue les concepts utiles à la description des systèmes désordonnés, au premier chef desquels la localisation d'Anderson, avant de discuter en détail de la question des systèmes en interaction. Nous montrons que ces sujets, bien qu'originellement introduits dans le contexte de la matière condensée, ont connu un renouveau récent stimulé par le développement des gaz quantiques ultrafroids. Un bref état de l'art conclut ce chapitre.

Le chapitre 2 s'ouvre avec une présentation introductive du gaz de Bose dans le régime de faibles interactions, puis fournit la plupart des outils techniques qui seront utilisés par la suite. Nous consacrons une large part à la théorie de Bogoliubov, qui décrit avec succès les excitations élémentaires du gaz de Bose. Cette théorie est présentée en détail, dans sa formulation la plus générale. Les principales propriétés physiques du gaz de Bose, telles que condensation, quasi-condensation et superfluidité sont également discutées.

Les chapitres 3 à 5, qui constituent le coeur du travail présenté ici, étudient ensuite l'influence du désordre sur les excitations collectives dans différentes situations.

Le chapitre 3 considère le cas d'un gaz de Bose en dimension arbitraire dans l'espace continu, en présence d'un vrai potentiel désordonné. Une telle situation avait déjà été étudiée en 1D à faible désordre, au moyen d'approches perturbatives, révélant en particulier que les excitations élémentaires étaient sujettes à la localisation d'Anderson. Toutefois, pour traiter le cas des dimensions supérieures, où la localisation survient à plus fort désordre, de nouvelles méthodes doivent être adoptées afin de pouvoir décrire un régime de fort désordre. Dans ce chapitre, nous développons une telle approche, aboutissant à une description générique et complète du comportement de localisation des excitations en dimension arbitraire. Nous discutons en particulier leurs propriétés universelles et non universelles de transport, et présentons une interprétation microscopique des comportements observés. Les implications expérimentales des ces résultats sont également discutées.

Le chapitre 4 est consacré au cas d'un gaz de Bose soumis à un potentiel quasi-périodique unidimensionnel. Si les potentiels quasi-périodiques sont connus pour posséder des propriétés intermédiaires entre les potentiels périodiques et désordonnés, la question des propriétés de localisation collective dans ces systèmes a jusqu'alors été très peu étudiée. Nous effectuons ici un traitement analytique et numérique du problème. Nous caractérisons quantitativement la transition de localisation observée, et l'interprétons en termes de localisation dans un modèle effectif multiharmonique.

Enfin, le chapitre 5 traite du gaz de Bose à deux composants. Bien que ces systèmes soient connus pour présenter des effets originaux en présence de désordre, l'absence d'un formalisme unifié dans le régime inhomogène le plus général manque cruellement à ce jour. Nous développons ici un tel formalisme, avant de l'appliquer au cas homogène qui renferme une physique riche et déjà non triviale.

Une conclusion récapitule les résultats obtenus et discute d'un certain nombre de perspectives à ce travail, aussi bien théoriques qu'expérimentales.

Chapter 1

Disorder and interactions : from condensed matter to ultracold gases

On se fait une idée précise de l'ordre, mais non pas du désordre.
Jacques-Henri Bernardin de Saint-Pierre

Solid-state systems, which are made of the spatial arrangement of atoms sharing their valency electrons, are tremendously complex structures. They result from elaborate *interactions* processes between their numerous elementary components, and unavoidably feature structural imperfections, which are generically referred to as *disorder*. Fascinatingly, both interactions and disorder turn out to have a crucial impact on their physical properties.

On the one hand, interactions are intrinsically present in all solids. As charged particles, electrons necessarily interact with each other and with the crystalline structure via the Coulomb force, the coupling with the material phonons, or via spin and magnetic exchanges. Although conduction properties of solids can be obtained at the simplest level from a description in terms of free electrons propagating in a frozen cristalline structure, interactions are crucial to account for some of the most fascinating phenomena in condensed matter, such as superconductivity [15] or superfluidity [16]. Whatever their origin, interactions and quantum statistics underlie a specific *many-body* physics.

On the other hand, disorder, which refers to all uncontrolled imperfections of the system, is necessarily present in all real-life systems. As a non-desirable ingredient, it is often neglected when interested in a macroscopic behaviour, mostly resulting in uncertainties on the predicted results or on the experimental measurements. However, it is well-established today that even at the macroscopic scale, disorder can have dramatic effects, as illustrated by the emblematic phenomenon of Anderson localization [2], in which weak disorder can turn a metallic sample into an insulator. In condensed-matter systems, disorder is recognized today to underlie numerous properties of solids, such as the physics of spin glasses, disorder-induced phase transitions, quantum Hall effect, quantum chaos and -presumably- high-Tc-superconductivity.

From a fundamental point of view, disorder and interactions are very difficult to study. A first reason is that both are immuable in solid samples, and mostly unknown at the microscopic level, being in the best case taken into account via idealized models. A second and more conceptual reason is that either interacting or disordered systems are *complex systems*, in the sense that they cannot be understood from the properties of their elementary components. As regards interactions, they turn the problem into a many-body one, coupling $\sim 10^{23}$ particles,

and approximations are indispensible, although very difficult to control. As regards disorder, complexity means that in the presence of disorder, novel behaviours arise at the macroscopic scale, that cannot be extrapolated from the microscopic properties of the sample.

Moreover, the interplay between disorder and interactions in quantum systems is today among the most challenging questions in the field. While it is of crucial importance to describe condensed-matter systems, it raises fundamental questions which are still the subject of vivid debates. This topic has attracted a renewed interest over the past decades thanks to the developement of ultracold gases. As remarkably well-controlled systems, they can promisingly be used for a systematic study of such questions.

This introductive chapter is devoted to a basic review of the previous concepts and provides a background overview for the remainder of this manuscript. In Sec. 1.1, we introduce disorder and review the basics of transport in disordered media, among which Anderson localization. In Sec. 1.2, we discuss the interplay between disorder and interactions, first in general terms, before enlightening the questions of disordered bosons, many-body localization, and disordered many-body dynamics, which are directly relevant for this work. Finally, Sec.1.3 provides an introduction to ultracold gases, focusing on their contribution to the field of disordered interacting quantum systems.

1.1 Matter waves in disorder : from diffusion to Anderson localization

1.1.1 Disorder in solids

Disorder is ubiquitous in all solid-state systems. Traditionally, the understanding of electronic transport in solids relies on Bloch's theory, which requires a perfect underlying cristalline structure. In this case, the periodicity of the cristalline potential felt by the conduction electrons results in the existence of extended Bloch waves, whose occupancy accounts for the insulator or conducting behaviour of the system. In practice however, the cristalline structure is never perfect, and always contains defects, which break the translational invariance. This lack of regularity, which is referred to as *disorder*, can take the form of local impurities (an atom which is replaced by another), excess atoms or atomic vacancies, as well as dislocations of the cristalline structure. Furthermore, disorder can also be structural in glasses and amorphous materials, where the atoms are irregularly arranged in space.

Dealing with disorder proves to be difficult and the latter is often neglected in first approximations. However, it is now recognized after Anderson [2] that even a small amount of disorder can qualitatively -and dramatically- alter the physics. It should be realized that dealing with disorder requires a conceptual change of viewpoint. In a disordered sample, the exact microscopic structure is not known, neither experimentally accessible. Furthermore, all samples are different since they correspond to different configurations of defects. Therefore, a useful theory should not deal with one single specific sample -which would be pointless-, but rather describe a whole class of systems which share global common properties. This can be achieved by the introduction of *randomness* to inlude all degrees of freedom that we cannot or do not want to control (e.g. the exact position of defects will be replaced by a random potential). Disordered systems of a same class will be characterized by common statistical properties -although each sample is unique since it corresponds to a specific *realization* of disorder-, and their universal features will be obtained by statistical averaging. Theoretical approaches therefore provide

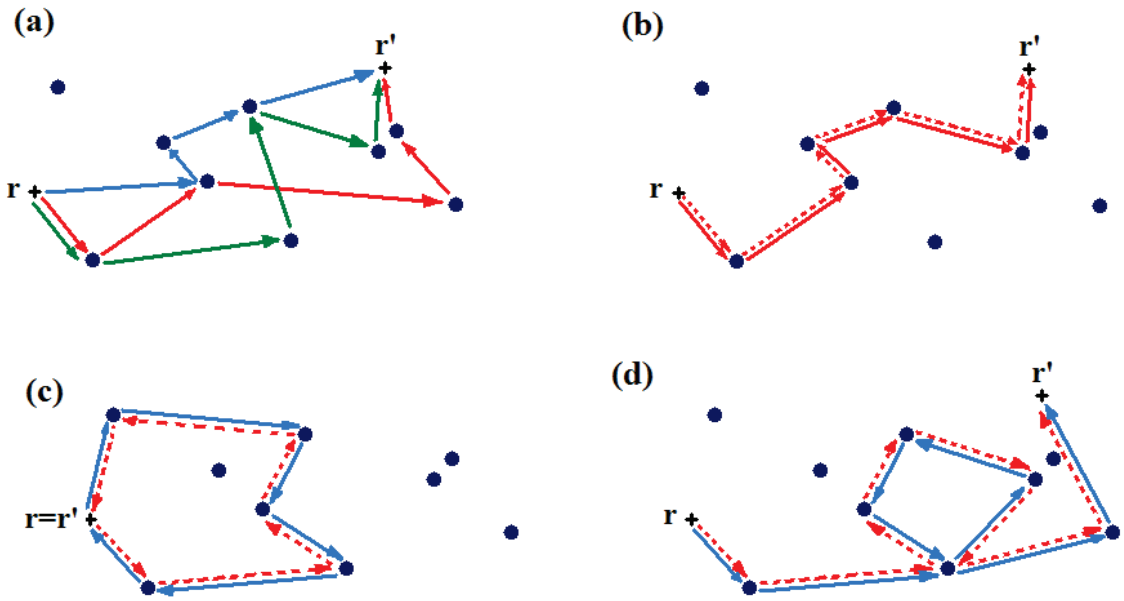

Figure 1.1: Interference contributions of several multiple-scattering trajectories in the disorder medium. (a) Three typical paths from $\mathbf{r}$ to $\mathbf{r}'$; each path is a random walk in the impurity landscape, and is represented by a specific color. (b-d) Three contributions which survive disorder averaging. Solid lines represent the field amplitude, and dashed lines represent its conjugate. (b) Classical contribution leading to diffusion (first term of Eq. (1.1). (c) Loop trajectories in the case $\mathbf{r} = \mathbf{r}'$, where a path i (blue) interferes with a different conjugate path j (red), leading to an enhancement of the return probability to the origin. (d) Loop trajectories in the case $\mathbf{r} \neq \mathbf{r}'$, which dominate the weak localization corrections and lead to reduced diffusion.

access to average quantities (or possibly their fluctuations), and a key question is then to relate them to the results of a given experiment, which generally concerns one single realization. In many cases, large disordered systems are *self-averaging*, and observables take their average values, but it may not be the case, and one has to think at which level the averaging is performed.

1.1.2 Wave transport in disordered media

To understand the key role of disorder, let us start with a simplified description of solids which neglects both interactions and quantum statistics, and consider the elementary problem of the propagation of a single wave (or quantum particle, as an electron in a solid) in a disordered medium.

This problem can be formalized in the framework of an elaborate quantum transport theory [17, 18] [see appendix B]. However, its main qualitative features, among which weak and strong localization, can be captured by a multiple-scattering picture, which proves an intuitive tool to appreciate the effect of disorder. Let us describe a given realization of the disordered medium by a static random arrangement of point-like impurities. The incoming wave is assumed to propagate freely in space and to undergo elastic scattering from each impurity. All multiply-scattered wavelets can then interfere, and the wave density (or energy) is the result of this complex interference process. The problem of the propagation of a quantum particle turns out to be exactly equivalent. Indeed, in Feynman's approach of quantum mechanics, the

propagation of a quantum particle from a point $\mathbf{r}$ to $\mathbf{r}'$ is described by a complex amplitude $G(\mathbf{r},\mathbf{r}')$, known as well as the *Green function*. The latest is the sum of all contributions associated to coherent multiple-scattering paths from $\mathbf{r}$ to $\mathbf{r}'$ [see Fig. 1.1(a)], each contribution i being described by a complex amplitude $A_i(\mathbf{r},\mathbf{r}')$, whose phase is notably proportional to the full path length and to all individual dephasings induced at each scattering event. The probability to go from $\mathbf{r}$ to $\mathbf{r}'$, which is the square modulus of the Green function, thus reads

$$P(\mathbf{r},\mathbf{r}') = |G(\mathbf{r},\mathbf{r}')|^2 = \sum_{paths\ j} |A_j(\mathbf{r},\mathbf{r}')|^2 + \sum_{paths\ i\neq j} A_i(\mathbf{r},\mathbf{r}')A_j^*(\mathbf{r},\mathbf{r}') \tag{1.1}$$

and depends, via the second term, on interferences between all possible paths from $\mathbf{r}$ to $\mathbf{r}'$.

In practice, dephasing or inelastic processes (phonons, photon absorption,...) may destroy the coherence of the paths, for instance by regularly randomizing the phase of the amplitudes, leading to decoherence and suppression of interference effects. The coherence length L_ϕ, which is the typical length before the particle undergoes such a dephasing event, determines the maximal length of the paths for being added coherently. We will neglect such effects and consider only the coherent regime where $L_\phi \gg l_S$, with l_S the scattering mean-free path, i.e. the average length travelled by the particle before it undergoes one scattering event.

The structure of Eq. (1.1) is exactly similar to the Young experiments. The first term, where all phases have disappeared, is purely classical : the probability to travel from $\mathbf{r}$ to $\mathbf{r}'$ is the sum of all probabilities of individual paths, and leads to diffusive transport, recovering Drude-Boltzman theory [see Fig. 1.1(b)]. The second term represents quantum interferences between *different* paths. Since each path represents a random walk in the landscape of the impurity configuration, two different paths *a priori* accumulate two different phases which depend on the precise disorder realization, and their interferences can therefore be expected to vanish after disorder averaging. However, there exist contributions which survive disorder averaging. This is the case when a path A_i and a conjugate path A_j^* visit both the same scatterers. For instance, if $\mathbf{r} = \mathbf{r}'$, this happens when paths i and j correspond to reversed trajectories [see Fig. 1.1(c)], and quantum interferences increase in that case the probability to come back to the origin. If $\mathbf{r} \neq \mathbf{r}'$, the same argument applies to any trajectory containing a loop [see Fig. 1.1(d)], since it can interfere with a trajectory where the loop is travelled backwards; in that case, quantum interferences reduce transport from $\mathbf{r}$ to $\mathbf{r}'$, and although the motion remains diffusive, the diffusive constant and the conductivity are reduced.

This effect, which is referred to as *weak localization*, has been intensely studied experimentally [7, 19, 20]. Reduction of the conductivity has been studied as a function of disorder (e.g. impurity concentration), dimensionality, and temperature (which activates decoherence processes). The effect of a magnetic field, which breaks the time-reversal invariance and dephases reversed trajectories, alters weak localization and especially results in negative magnetoresistance. Among the other numerous signatures of weak localization, let us mention coherent backscattering (enhancement in the backwards direction of the intensity of a wave reflected by a disordered medium), which has been observed in various systems (colloids [21–23], light diffusing on cold atoms [24], BEC in speckle potential [25, 26]), as well as universal conductance fluctuations.

So far, we have considered only trajectories containing a single loop, but many other contributions (multiple-loop trajectories,...and more generally all pairs of paths visiting the same

scatterers) yield non-vanishing interference effects. The latter may lead not only to reduction of conductivity, but to complete suppression of transport, an effect called *strong localization* or *Anderson localization.*

1.1.3 Anderson localization

Anderson localization was first predicted [2] within the framework of the so-called Anderson model. The latter is a tight-binding Hamiltonian

$$\hat{H} = -\sum_{\langle i,j \rangle} t(\hat{c}_i^\dagger \hat{c}_j + h.c.) + \sum_i \epsilon_i \hat{c}_i^\dagger \hat{c}_i \tag{1.2}$$

describing free particles on a lattice (here, $\hat{c}_i$ and $\hat{c}_i^\dagger$ are the annihilation and creation operators on site i), with a uniform hopping parameter t between nearest-neighbor sites $\langle i,j \rangle$, and in the presence of random on-site energies ϵ_i, independently and uniformly distributed in $[-W/2; W/2]$. By analysing the time evolution of the probability amplitude of a particle at a given energy E, Anderson found that in three dimensions, and for a sufficiently strong disorder (measured by the width W), the particle remains exponentially localized around its original position, yielding a total suppression of transport. Conversely, at fixed disorder strength, the energy spectrum displays a mobility edge separating localized low-energy states from extended high-energy ones. When increasing the disorder strength, more and more states turn localized. Since transport properties are determined by the states located at the Fermi level, the system undergoes, at the point where the mobility edge crosses the Fermi level, a phase transition from a metallic to an insulator phase, named the *Anderson transition.* For strong enough disorder, the whole spectrum is localized (the energy spectrum on a lattice is indeed upper-bounded), yielding an insulator whatever the position of the Fermi level.

Although originally predicted in the specific case of the above model, Anderson localization was realized later to be very general in nature, and to arise from destructive interference between all coherent paths associated to multiple scattering within the disordered medium. This ubiquitous phenomenon possesses many universal features :

- First, it is a single-particle effect, where interactions between waves/particles and quantum statistics have been discarded. The effect of interactions and quantum statistics on Anderson localization [see Sec. 1.2] is one of the most challenging questions in the field of disordered systems.

- Anderson localization strongly differs from classical trapping and can notably occur even if the particle energy lies far above the potential maxima. It is characterized by an exponential localization of the wavefunctions and the absence of diffusion.

- Anderson localization applies to all kinds of waves (among which quantum particles) and all type of disorder. Although introduced in the framework of electronic transport and quantum particles, it has so far been widely studied outside its original context, and reported in numerous experimental systems [27]. In particular, experiments with classical waves, such as light, offer the advantage of circumventing the problem of interactions, which are difficult to control in electronic systems. By studying the transmission through a disordered sample of variable length, one can discriminate between an exponential

decay characteristic of Anderson localization and a linear one typical of Ohm's law [1]. Observation of Anderson localization was reported for microwaves [28, 29] and visible light [30, 31], and more recently in disordered photonic crystals [32, 33], as well as for ultrasound [34–36] and seismic waves [37]. Observation of Anderson localization with matter waves in various situations [38–42] is discussed in more details in Sec. 1.3.3.

- Similarly to weak localization, Anderson localization crucially depends on dimensionality, since the existence of loop paths is governed by the probability for a random walk to come back to its origin in a finite time or not. In 1D and 2D where every random walk has a loop (asymptotically in 2D), all states are localized in infinite systems (2D being thus the marginal dimension), whatever their energy or the disorder strength. Conversely in 3D, a phase transition in energy [2] called the Anderson transition shows up at the so-called *mobility edge* energy E_c. The latter can be approximately captured by the Ioffe-Regel criterion [43], which states that localization requires that the phase accumulated between two successive scattering events be less than 2π, yielding $kl_S \lesssim 1$ (with l_S the scattering mean-free path).

So far, there exists no exact theory of Anderson localization near the critical point, especially as regards the exact location of the mobility edge and the values of the critical exponents s and ν, which characterize the behaviour of both the conductance σ (on the conducting side) and the localization length $L_{\rm loc}$ (on the insulating side) at the transition

$$L_{\rm loc} \propto (E_c - E)^{-\nu} \quad , \quad \sigma \propto (E - E_c)^s. \tag{1.3}$$

The scaling theory of localization, introduced in the late 1970s by Abrahams, Anderson, Licciardello and Ramakrishnan [44], and which we will review in a general form in Sec. 3.1.2, remarkably captures the dependence on dimensionality. Although being qualitative, it provides a correct scaling of the localization length as a function of the microscopic parameter l_S, in 1D ($L_{\rm loc} \propto l_S$) and 2D ($\log(L_{\rm loc}/l_S) \propto kl_S$), and recovers the Ioffe-Regel criterion in 3D. It predicts as well the relation $s = (d-2)\nu$ (which yields $s = \nu$ in 3D), but cannot give the values of the critical exponents.

Quantitative approaches based on perturbative quantum transport theory [17, 18] [see appendix B] can successfully describe classical diffusive transport, as well as weak localization corrections, which can be obtained from the lowest-order terms of the perturbative series. Such theories however break down in the strong localization regime, which would require to take into account all diagrams an resum them all. The self-consistent theory [45, 46] circumvents this problem by taking the weak-localization correction expressed as a function of a self-consistently renormalized diffusion constant. Although not being justified a priori, such a procedure amounts to sum up a whole class of diagrams of all orders, although not all. It reproduces the qualitative features of the Anderson transition, provides a good estimation of the mobility edge for weak disorder [47, 48], and predicts the values of $s = \nu = 1$ for critical exponents. The latter were evaluated numerically as $s = \nu = 1.58$ in simulations of the Anderson model [49].

[1] Absorption effects, which also induce an exponential decay, can be excluded by studying the transmission fluctuations, unambiguously identifying Anderson localization.

[2] or equivalently in disorder, if the energy is fixed.

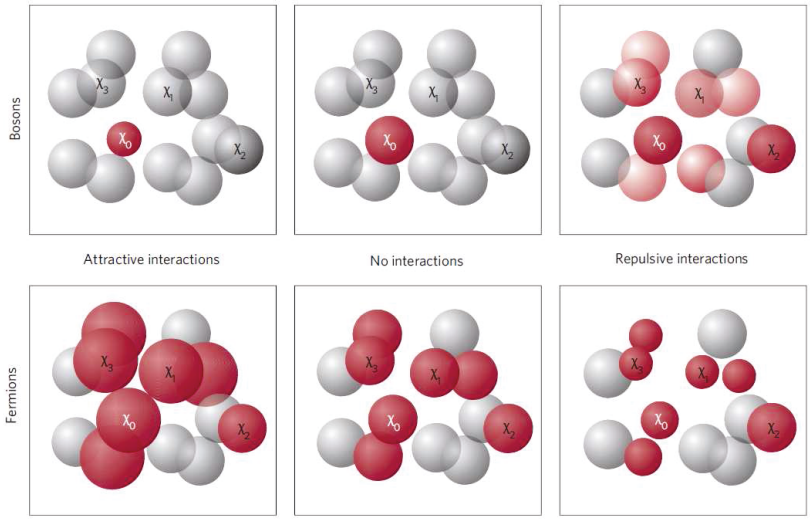

Figure 1.2: Qualitative effect of weak interactions on the localization properties of Bose and Fermi gases. For bosons, attractive interactions enhance localization while repulsive interactions compete with it. It is the opposite for fermions.

1.2 Disorder and interactions

So far, we have considered only non-interacting particles evolving in purely disordered potentials. Although conceptually well understood, such a description is however oversimplistic, since a complete theory of disordered solids should take into account the Coulomb interaction, the underlying cristalline structure, the fermionic statistics of electrons, as well as interactions with phonons and possible magnetic effects. Incorporating all those ingredients is a priori essential to capture most phenomena reported in condensed-matter systems. Indeed, interactions of all kinds and quantum statistics underlie a rich and specific *many-body* physics, which is not only quantitatively different, but also qualitatively : they can induce collective behaviours, phase transitions (e.g. the Mott transition on a lattice, a metal-insulator transition driven by interactions) [50, 51], and lie at the heart of the most spectacular phenomena in condensed matter, such as superfluidity [52] and superconductivity [15].

Unfortunately, dealing with disorder in many-body systems represents a formidable challenge, since even the simplest models including all minimal ingredients are hardly solvable, and often lead to unsolved questions and controversial answers. The most challenging one is the interplay of disorder with interparticle interactions and quantum statistics.

1.2.1 General issues

To address this question, one can consider two different angles, which are nevertheless interrelated. On the one hand, one can wonder how interactions affect Anderson localization, or more generally, all disorder-induced single-particle effects. On the other hand, one can study what happens to the many-body states and phase transitions in the presence of disorder.

How interactions challenge Anderson localization ?

Strictly speaking, Anderson localization is a single-particle effect, but the question of interactions, which could presumably destroy localization, was raised immediately after it was

introduced. Anderson himself, in his Nobel lecture [8], presented it as the major challenge for the next generations :

"A reason why I felt discouraged in the early days was that I couldn't fathom how to reinsert interactions, and was afraid they, too, would delocalize. The realization that, of course, the Mott insulator localizes without randomness, because of interactions, was my liberation on this [...] The present excitement of the field for me is that I feel a theory of localization with interactions is beginning to appear..."

Although such a theory is still missing, it seems today well established that interactions can compete or cooperate with localization, depending on their sign and on quantum statistics. In particular, the effect of weak interactions on localization can be efficiently captured by a useful picture [3] that we briefly review [see Fig. 1.2].

Let us start with bosons. In the absence of interactions, all bosons condense in the same single-particle state, which is localized in the disorder. Then, weak attractive interactions are expected to further contract the gas, enhancing localization. Conversely, for weak repulsive interactions, bosons will populate an increasing number of single-particle states, thus competing with localization. In this case, if interactions are weak, the overlap between all populated single-particle states, which are only a few and exponentially localized in space, is small and the whole system remains localized; then, when increasing interactions, the overlap increases and the gas can eventually form a connected cloud, being globally delocalized. This competition between disorder and repulsive interactions in Bose systems can in particular underlie a metal-insulator transition, as reviewed below (Sec. 1.2.2).

For fermions, the situation is very different. In the absence of interactions, free fermions form a Fermi sea and populate all lowest-energy states, which are localized in the disorder. Then, for attractive interactions, a given state will tend to expand, so as to maximize its overlap with the others, thus competing with localization. Conversely, for repulsive interactions, a given state will tend to contract, enhancing localization. In the latter case, localization thus remains the rule, which should be of no surprise since repulsive interactions in Fermi systems are known to lead only to a renormalization of the single-particle physics (the Fermi liquid theory). Remarkably, the conclusion seems inverted for bosons and for fermions.

Notice that the previous conclusions can be challenged in strongly-correlated regimes. For instance with bosons, strong attractive interactions can lead to delocalizing instabilities, while strong repulsive interactions can lead to a localized Mott insulator phase in the presence of a lattice.

How disorder alters many-body phases ?

The second question that has been puzzling for decades concerns the effect of disorder on many-body phases, in particular superfluidity and superconductivity. The latter are generically believed to be possibly destroyed by disorder, in agreement with the previous conclusions that disorder competes with repulsive interactions (which support superfluidity) in Bose systems and with attractive interactions (which support superconductivity) in Fermi systems. Many questions are nevertheless open : are such states completely destroyed in the presence of disorder ? Are the associated phase transitions suppressed, or only quantitatively, or qualitatively, modified ? What are the mechanisms for such a destruction ?

As regards superfluidity, much attention has been devoted to understanding the influence of disorder on the BKT transition (finite-temperature superfluid transition in 2D), and to the

phase diagram of disordered bosons (see Sec. 1.2.2).

As for superconductivity, it seems today established that weak disorder only shifts the normal to superconductor transition temperature [53], while strong disorder can totally suppress the existence of the superconducting state [54]. However, understanding the mechanisms of such a destruction, as well as the microscopic nature of the strongly-disordered superconducting and insulating phases, on both sides of the transition, remains an open challenge. Several scenarii have been proposed (a bosonic scenario of localization of preformed Cooper pairs and a fermionic one of destruction of pairs), and the possibility to have a two-step transition, with two criticalities, is not excluded.

In the following, we will specifically enlighten three current topics which are directly relevant for our work : disordered bosons (Sec. 1.2.2), many-body localization (Sec. 1.2.3) and disordered many-body dynamics (Sec. 1.2.4).

1.2.2 Disordered bosons

Although condensed matter mainly deals with electrons in solids, which are fermions, much attention has been devoted, somehow paradoxically, to disordered bosons. The latter have been investigated first in the context of the superfluidity of ^{4}He in porous media [4], and in the field of disordered superconductors, where charge carriers are bosonic Cooper pairs. They can furthermore prove useful to understand fermions in 1D, where the paradigm of the Luttinger liquid allows for an explicit mapping between the two. More recently, the development of ultracold gases, which can simulate bosonic Hamiltonians, has renewed the interest for disordered bosons, all the more that bosons are more easily coolable than fermions.

From a fundamental point of view, repulsively interacting disordered bosons represent a great theoretical challenge. Their intrinsically collective behaviour and the competition between repulsive interactions and disorder in Bose systems suggest rich and non trivial localization effects. This strikingly contrasts with fermions, where repulsive interactions only quantitatively renormalize the free-particle case (see sec. 1.2.1). In particular, while for fermions, the non-interacting case is a good starting point around which interactions can be tackled perturbatively [7, 55], such an approach is impossible with bosons [3], where the non-interacting disordered case is pathological [57]. Indeed, such a state has all particles in the lowest eigenstate of the single-particle Hamiltonian (which is localized), and is therefore unstable to the introduction of even the weakest interaction.

The *dirty boson problem* is traditionally defined as understanding the nature of the phases, and the transitions between them, in a system of interacting bosons in a random potential at zero temperature. It was originally studied in 1D by bosonization and renormalization group (RG) techniques, treating disorder as a perturbation [11, 58]. Relying on those results, much attention was devoted to understanding the physics of the disordered Bose-Hubbard model

$$\hat{H} = -\sum_{\langle i,j \rangle} J(\hat{a}_i^\dagger \hat{a}_j + h.c.) + \sum_i V_i \hat{a}_i^\dagger \hat{a}_i + \sum_i \frac{U}{2} \hat{a}_i^\dagger \hat{a}_i^\dagger \hat{a}_i \hat{a}_i \tag{1.4}$$

This model, which describes lattice bosons ($\hat{a}_i$ and $\hat{a}_i^\dagger$ being the annihilation and creation

[3] For weak interactions, generalizations of this approach nevertheless exist, by considering for instance not only the single-particle ground-state, but a whole set of low-energy states [10, 56].

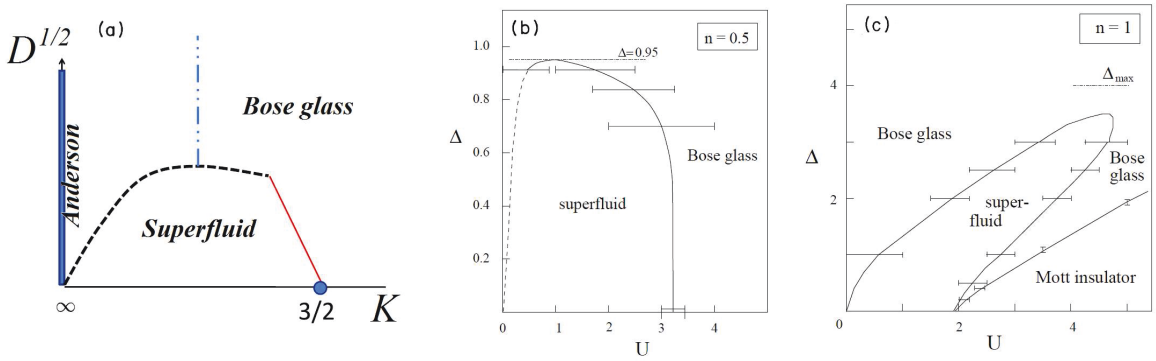

Figure 1.3: Phase diagrams of 1D disordered bosons at zero temperature as a function of interaction (x-axis) and disorder (y-axis) strengths. (a) Original phase diagram obtained from renormalization group (RG), for bosons in the continuum (or equivalently on a lattice at incommensurate filling); K is the Luttinger parameter ($K = \infty$ for free bosons and decreases for increasing repulsion) and D is the strength of the disorder. The red solid line is the SF-BG transition computed from RG, and has to bend down (dashed line) at weak interactions to be compatible with the non-interacting limit (Anderson phase, in blue). The possible existence of two distinct localized phases (suggested by the dash-dotted line) is still an open question. Figure based on Ref. [57]. (b)-(c) Phase diagrams for the 1D Bose-Hubbard model with onsite energy V_i randomly distributed in $[-\Delta; -\Delta]$, as obtained from density-matrix renormalization group (DMRG), at half (b) and integer (c) filling. Figures extracted from [59].

operators on site i) with tunelling rate J, random on-site energies V_i, and interaction energy U when placed in the same site, contains all minimal ingredients of the dirty boson problem. In particular, it features two fundamental metal-insulator transitions, the Anderson transition (for $U = 0$) and the Mott transition (for $V_i = 0$). Its study permitted to predict most qualitative features of the phase diagram of disordered bosons in arbitrary dimensions [12], which were then completed by many numerical studies (density-matrix renormalization group, quantum Monte-Carlo) [59], and investigation of other models (e.g. Josephson model and strongly-disordered RG [60]).

We review here the obtained phase diagrams at zero temperature, which to some extent constitute a background for this work.

Bosons on the continuum or on a lattice at incommensurate filling

The case of bosons on the continuum and bosons on a lattice at incommensurate filling are very similar [4]. The 1D phase diagram as originally obtained by perturbative RG [11] is presented on Fig. 1.3(a). Two phases were predicted : a superfluid phase (SF), obtained in the RG approach when the disorder becomes irrelevant on large scales, and a localized phase, when the disorder becomes increasingly relevant. The later was named *Bose glass* (BG) and shown to be insulating, gapless and compressible.

For vanishing interactions, all bosons are Anderson localized in a single state and the system is insulating. For finite interactions, several states are populated, but the system remains insulating while their overlap remains small (see Sec. 1.2.1). When increasing the interactions, this overlap eventually connects the whole system and the gas enters the superfluid regime [56, 60]. Superfluidity is then destroyed again for stronger interactions, where the 1D Bose gas enters the Tonks-Girardeau regime.

[4] Subtle differences between the two situations may exist, as explained in [61].

In the strongly-interacting regime, the transition (red line) was precisely characterized [11]. It was shown to be of BKT type, with a Luttinger parameter of $K = 3/2$ jumping discontinuously at the transition. Critical exponents were as well predicted. The SF-BG transition was interpreted as a localization-delocalization phase transition, driven by the enhanced role of the phase slips (long-range phase fluctuations) which reduce the coherence over large distances.

Conversely, because of strong spatial modulations of the density, the perturbative RG fails describing the weakly-interacting transition, which mostly remains uncharacterized. The qualitative reentrant shape on Fig 1.3(a), originally argued as an extrapolation to connect to the free bosons case, was confirmed by numerical studies [10, 56, 62, 63]. However, the mechanism at stake seems to be rather different, and to involve the fragmentation of the density.

Investigation of the Bose-Hubbard model at incommensurate filling by density-matrix renormalization group (DMRG) [59] confirmed the 1D phase diagram [see Fig. 1.3(b)], as well as the evidence for a localized bosonic phase and a superfluid-insulating transition [11]. The latter was then shown to exist in higher dimensions as well, where the qualitative physics of the Bose-Hubbard model and the critical properties of the transition were elucidated by general scaling arguments [12]. So far, numerical simulations are however needed for quantitative results.

Many questions still remain open. The very different mechanisms and universal properties for the weakly- and strongly- interacting transitions could indicate the existence of two different localized phases (as suggested by the dash-dotted line on Fig. 1.3(a)), with a possible phase transition between the two. If it were the case, this would raise the question of an order parameter to distinguish the two. On that point, numerical studies have so far provided conflicting answers [61, 64].

Bosons on a lattice at commensurate filling

Let us turn to the case of bosons on a lattice at commensurate filling. In this case, it should be reminded first that a phase transition towards a Mott insulator (MI), driven by strong repulsive interactions, occurs in the absence of disorder [see Fig. 1.4(a)]. This phase, where each single site is occupied by a fixed number of particles, is insulating, incompressible and gapped (at variance with the Bose glass).

The 1D phase diagram of the disordered Bose-Hubbard model at commensurate filling was elucidated first by Fisher [12], and more recently by numerical studies [59]. As shown on Fig. 1.3(c), it is very similar to that of the incommensurate case, except that a Mott insulator appears for strong interactions. Remarkably here, strong interactions cooperate with disorder while weak interactions compete with disorder. The MI-BG phase transition was found to be of Griffiths type [65].

One puzzling question is whether the Bose glass phase totally surrounds the Mott lobes of the phase diagram as in Fig. 1.4(b), or whether a direct MI-SF transition is possible as in Fig. 1.4(c). In 1D, the first analysis based on RG [12], confirmed later by further arguments [66, 67], proved that a Bose glass phase always shows up between the MI and the SF phases. After controversial theories, it was finally shown to be the case in higher dimensions as well [68, 69], proving that in the presence of disorder, a direct transition MI-SF is not possible.

Today, one major challenge concerns the possible extension of such phase diagrams to finite temperature regimes. Such an issue, which requires to take into account two-body processes and collective excitations of the gas, is in fact intimately related to the question of the conductivity of the Bose glass phase and the concept of many-body localization, that we review now.

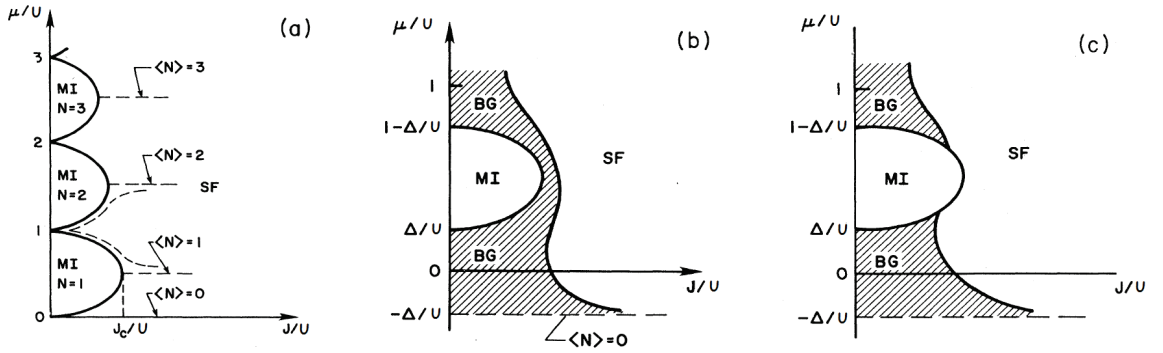

Figure 1.4: (a) Zero-temperature phase diagram for the Bose-Hubbard model in the absence of disorder. For a commensurate filling, a transition to a Mott insulating (MI) phase occurs at strong interaction strength (small J/U). (b)-(c) Two possible scenarii when adding weak bounded disorder $V_i \in [-\Delta; -\Delta]$ with $\Delta < U/2$. Figure (b), where the SF-MI transition occurs only through the Bose glass phase (BG), has been proved to be the correct scenario. Figures extracted from Ref. [12].

1.2.3 Many-body localization

Many-body localization, which was originally introduced for fermions, concerns the possible extension to the interacting case of a metal-insulator transition similar to the Anderson transition.

For free electrons, we recall that the Anderson model (see Sec. 1.1.3) predicts that for sufficiently strong disorder, the zero-temperature conductivity should identically vanish since all states are localized [5]. When introducing weak repulsive interactions, it was found [9] that all states should remain localized, and that the conductivity should be exactly zero below a certain temperature, and finite above, signaling a finite-temperature metal-insulator transition. This so-called many-body localized phase was claimed to occur because the interaction term only couples a finite number of energy levels, which all correspond to localized excitations.

The *many-body localization* transition was then studied using renormalization procedures [70] or exact diagonalization [71], which helped characterize its critical properties and the two phases. In particular, it was shown that the existence of a localized phase at finite temperature for weak interactions necessarily implies its persistence for strong interactions and high temperature [72]. A similar finite-temperature many-body localization transition was then predicted and investigated for interacting bosons in 1D [10].

More generally, many-body localization refers to the existence of a finite-temperature phase with vanishing transport coefficients. Such a transition generically arises because of the competition between a local coupling and the random levels discreteness. Indeed, while the Anderson transition can be viewed as the result of a competition between the possible hybridization of two quantum states located on different lattice sites and their random energy difference, the many-body localization-delocalization transition can be qualitatively understood by extending this physical picture to states with more than one particle. Therefore, it is intimately linked with the 'localization' properties of the many-body eigenstates of the system in the Fock space. In the conducting phase, the latter are thermal and ergodic in the Fock space. In the insulating phase, many-body excitations are localized in the Fock space; due to the resulting *lack of ergodicity*, the localized phase is characterized by an absence of relaxation and a breakdown of thermalization. Refs. [73, 74] discuss the connections between localization in Fock space,

[5] For weak disorder, only part of the spectrum is localized and it therefore depends on the position of the Fermi level respectively to the mobility edge.

thermalization processes and dynamical properties, which we review now.

1.2.4 Disordered many-body dynamics

Many-body dynamics is generically defined as the study of the dynamical properties and of the conditions for thermalization in isolated many-body systems.

In classical physics, the requirements for thermalization are well understood, and intimately linked with the concept of ergodicity, which establishes a connection between long-time averages of observables and statistical ensemble averages. As established by Boltzman, a condition for ergodicity is that the motion of the individual particles be fully chaotic. In classical physics then, violation of ergodicity may occur only for integrable (or close to being integrable) systems. Integrability indeed implies the existence of constants of motion, which restricts the ergodic exploration of the microcanonical energy shell. Conversely, disorder in classical physics is expected to break integrability, hence favoring ergodicity and thermalization of any observable [6]

The situation in quantum mechanics is less clear, and first pioneering works date back to Von Neumann [75, 76]. At variance with the classical case, ergodicity in quantum systems can be broken by integrability, interactions [77, 78], and more importantly by disorder, via one-body [2] or many-body [9, 10, 13, 70–72, 79–81] Anderson localization. For instance, it was shown [82] that many-body localization effects can invalidate the expectation that classical chaos leads to thermalization of the quantum counterpart. More precisely, absence of thermalization and persistence of local fluctuations have been reported in one-dimensional spin [73, 74] and Fermi [77, 82, 83] systems. Therefore, understanding the effect of disorder in many-body quantum dynamics has become an increasingly attractive issue [77, 82, 83]. A renewed interest has in particular been sparked by the new experimental possibilities offered by ultracold atomic gases. In such systems, out-of-equilibrium dynamics can indeed be induced by a very simple setting, which is that of a *quantum quench*, i.e. an abrupt change of some Hamiltonian parameter. The system abruptly gets out of equilibrium, and thermalization to a new equilibrium state can be monitored.

More generally, studying the interplay between disorder and interactions has long remained difficult to address experimentally, since disorder and interactions in condensed-matter samples are frozen, and mostly unknown. New approaches to these issues have emerged from atomic physics, where ultracold gases have proved to be versatile and flexible simulators.

1.3 Ultracold atoms

Over the second half of the 20^{th} century, advances in the understanding of matter-light interaction gradually allowed for considerable progress in cooling and trapping atoms. The regime of quantum degeneracy finally became accessible, as illustrated by the pioneering experimental realizations of a Bose-Einstein condensate (BEC) [84–86] and first interference experiments on BECs [87]. Although more challenging, the obtention of quantum degenerate Fermi gases soon followed [88,89], while observation and manipulation techniques improved rapidly. Today, *ultracold gases* are dilute atomic (or molecular) systems cooled down to very low temperatures (a few nKs), and confined in immaterial traps thanks to appropriate combinations of optical beams. Such systems offer unpreceedented control and versatility, and have proved very promising tools to investigate the field of disordered systems [3].

[6] except the energy, which is the only conserved quantity.

1.3.1 Versatile and controlled simulators

Compared to condensed-matter systems, ultracold gases offer numerous advantages in terms of control and versatility.

Firstly, one can choose to work with bosons, fermions, or even mixtures, and can precisely control the number of atoms and the temperature.

Secondly, electromagnetic fields can be used to design at will optical potentials for the atoms, which can then be controlled and varied by continuously tuning experimental parameters, such as light intensities or frequencies. Harmonic traps of adjustable anisotropy may be obtained from magnetic fields or laser light; a tight anisotropic confinement can reduce the effective dimensionality, realizing low-dimensional systems. Waveguides can as well be realized using a strongly focused laser beam. More importantly, the dipolar force induced by laser light proves a powerful tool to design external potentials. Lattice potentials mimicking condensed-matter systems can be produced from the interference pattern of several laser beams; for instance, using pairs of counterpropagating laser beams creates a periodic potential, simulating the Hubbard model. The dipolar force may also be used to design disordered optical potential, as reviewed in the next section 1.3.2.

Thirdly, interactions between atoms can be controlled using Feshbach resonances, making it possible to go from non-interacting to strongly-correlated regimes by simply tuning the magnetic field. Manipulating the internal states of atoms offers as well the possibility to simulate spin systems or new types of interactions in spinor and dipolar gases. Artificial gauge fields can be realized, simulating magnetism for neutral atoms.

Finally, ultracold gases are relatively robust to decoherence processes, which are intrinsically present (e.g. via phonons) in condensed-matter systems.

Furthermore, ultracold gases have come with new experimental techniques, measurement tools and can advantageously be probed over relatively long times (up to a few seconds). Imaging techniques (by fluorescence or absorption) give access to density profiles in situ, while momentum distributions can be inferred from time-of-flight techniques. Light-shift tomography may be used to precisely determine the energy or positions of atoms, and correlation functions of the gas can be obtained from interference experiments, and Raman or Bragg spectroscopy.

For all those reasons, ultracold gases are often referred to as *quantum simulators*, in the sense that they realize model Hamiltonians, whose parameters can be experimentally controlled and continuously varied, as well as calculated *ab initio* from the experimental parameters. Their original approaches prove complementary to theoretical and numerical tools. Most importantly, they permit to explore new regimes that are hardly accessible in condensed matter, leading to unexpected findings and raising new challenges for theory. Their successes no longer have to be demonstrated, since they have led for instance to the observation of the Mott transition [90–92], and Tonks-Girardeau [93, 94] and Berezinskii-Kosterlitz-Thouless [95] physics. They have as well provided a decisive contribution to the field of disordered systems, as we review below.

1.3.2 Disordered optical potentials

Disorder may be introduced in ultracold systems in several ways. From a theoretical point of view, disorder can be modelled by any random parameter in the Hamiltonian (e.g. a random on-site energy, a random tunneling rate...). In this work, we will focus only on time-independent

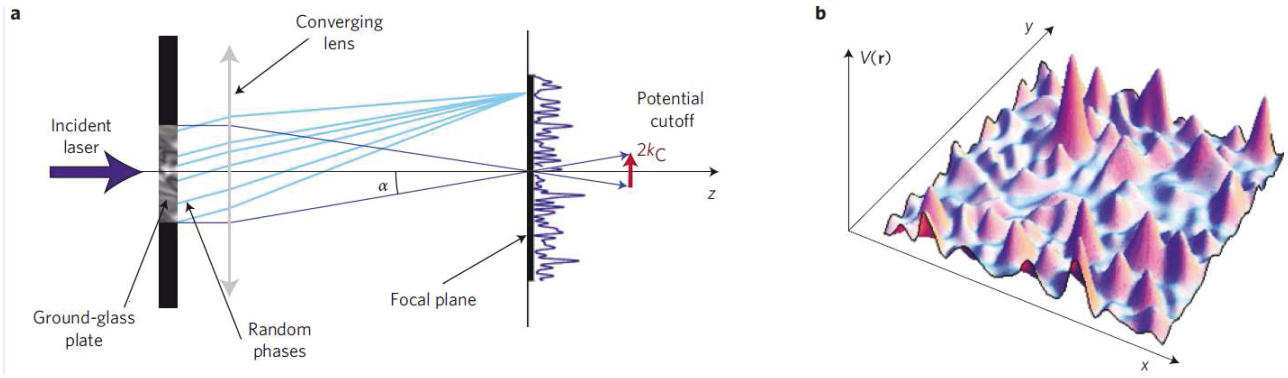

Figure 1.5: Optical apparatus to create a speckle potential (see description in the text), and typical realization of a 2D speckle field. Figure extracted from Ref. [3].

(*quenched*) disorder, which takes the form of a static external random potential $V(\mathbf{r})$. A random potential is generically characterized by its statistical properties, which depend on the precise way it is experimentally generated. In Appendix A, we review the basic concepts of disorder statistics, and set the conventions used in this thesis.

A fruitful way to generate a random potential relies on the *dipolar force* induced by an electromagnetic field on an atom. Indeed, when submitted to an electromagnetic field $\mathcal{E}(\mathbf{r})$ such as that of a laser, an atom experiences a conservative dipolar force which results from the coupling between the electric field and the induced atomic electric dipole [7], and which derives from the so-called dipolar potential [18]

$$V(\mathbf{r}) = \frac{3\pi c^2 \Gamma I(\mathbf{r})}{2\omega_0^3 \delta}, \tag{1.5}$$

where $I(\mathbf{r}) = |\mathcal{E}(\mathbf{r})|^2$ is the intensity of the field, Γ is the decay rate of the excited state, and $\delta = \omega_L - \omega_0$ is the detuning between the laser frequency ω_L and the atomic transition frequency ω_0 : if $\delta < 0$ (*red-detuned* laser), the potential is attractive, whereas it is repulsive for $\delta > 0$ (*blue-detuned* laser). Therefore, designing any suitable intensity pattern $I(\mathbf{r})$ permits to tailor an optical potential for the atoms, and possibly a disordered one.

Speckle potentials and quasiperiodic lattices, which rely on this technique, but also impurity disorder, which proceeds rather differently, are among the most commonly implemented models of disorder. Since they will be considered later in this manuscript, we review below their main features in some details.

Speckle potentials

A speckle field [96,97] results from the reflection or transmission of a coherent beam through a rough diffusive plate, which is then focused by a convergent lens, as illustrated on Fig. 1.5. The rough plate imprints a random phase to each partial wave emitted from each of its points. The complex electric field $\mathcal{E}(\mathbf{r})$ in the observation focal plane at point $\mathbf{r} = (x, y)$ results from the coherent superposition of those elementary contributions. In the paraxial approximation, it

[7] There is as well a dissipative part, the radiation pressure, but since the two scale differently with the laser parameters, both can be idenpendently controlled; in particular, the radiation pressure can be made negligible at high detuning.

can be expressed as a function of the electric field $\mathcal{E}_D(\rho)$ at a point $\rho = (\rho_x, \rho_y)$ of the diffusive plate,

$$\mathcal{E}(\mathbf{r}) = \frac{e^{2\pi i f/\lambda}}{if\lambda} e^{\pi i f(x^2+y^2)/\lambda} \int e^{\pi i(\rho_x^2+\rho_y^2)/f\lambda} e^{-2\pi i(x\rho_x+y\rho_y)/f\lambda} \mathcal{E}_D(\rho) d^d\rho. \tag{1.6}$$

with f the focal distance and λ the laser wavelength. Since the phases of all $\mathcal{E}_D(\rho)$ at all points ρ of the diffusor are identically and independently distributed random variables, the electric field $\mathcal{E}(\mathbf{r})$ in the observation plane is a complex Gaussian random variable, by virtue of the central limit theorem. The statistical properties of the intensity $I(\mathbf{r}) = |\mathcal{E}(\mathbf{r})|^2$ -and of the speckle field deriving from Eq. (1.5)- can then be inferred from the Gaussian statistics of the electric field.

- The *one-point intensity*, $I(\mathbf{r})$, is the sum of two squared Gaussian random variables (namely the real and imaginary parts of the electric field). It therefore follows an exponential probability distribution [97]

$$P(I) = \frac{1}{\overline{I}} e^{-I/\overline{I}} \tag{1.7}$$

  and so does the speckle potential, up to a shift which ensures that it is of zero average. Since such distribution is highly asymmetric and unbounded, the speckle field $V(\mathbf{r})$ will be as well asymmetrically distributed, as exemplified on Fig. 1.5. From Eqs. (1.5) and (1.7), it appears that it has no upper (resp. lower) bound for a blue (resp. red)-detuned speckle. Furthermore, such a distribution yields the standard deviation

$$V_{\mathrm{R}} = \frac{3\pi c^2 \Gamma \overline{I}}{2\omega_0^3 \delta} \tag{1.8}$$

  for the speckle potential. Notice that all those single-point properties require only the central limit theorem to be valid, and therefore apply to any speckle pattern, independently of the dimensions or transmission properties of the diffusive plate.

- The *two-point correlation function* or autocorrelation function, $C(\mathbf{r}, \mathbf{r}') = \overline{V(\mathbf{r})V(\mathbf{r}')}$, can be expressed as a function of the electric field four-point correlation function, which can be computed using Wick's theorem. This yields

$$C(\mathbf{r} - \mathbf{r}') = V_{\mathrm{R}}^2 \left| \frac{\int e^{-2\pi i(\mathbf{r}-\mathbf{r}').\rho/f\lambda} I_D(\rho) d^d\rho}{\int I_D(\rho) d^d\rho} \right|^2 \tag{1.9}$$

  where $I_D(\rho) = |\mathcal{E}_D(\rho)|^2$, which is the intensity distribution in the diffusive plate, is referred to as the *pupil function*. The two-point correlation function is therefore the squared modulus of the Fourier transform of the pupil function. It can be entirely controlled experimentally by designing the pupil shape and transmission factor. The translation of Eq. (1.9) to Fourier space expresses that the power spectrum of the speckle potential (i.e. the Fourier transform of its autocorrelation function) is the autoconvolution of the pupil function.

- Higher-order correlation functions can in the same manner be computed from the underlying Gaussian structure of the electric field. Importantly, for a speckle potential, they *do not* vanish, at variance with the case of a Gaussian disorder [see appendix A].

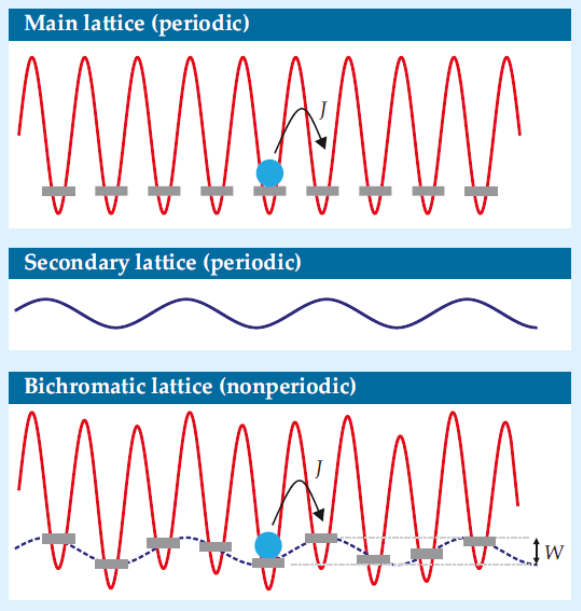

Figure 1.6: Realization of a one-dimensional quasi-periodic potential by superimposing two periodic lattices of incommensurate frequencies. Figure extracted from Ref. [111].

Speckle potentials offer numerous advantages. They are easily (and widely) implemented in cold atom experiments [25, 38, 41, 42, 96, 98–107]. As seen above, their statistical properties are well-known and can be designed by tailoring the optical apparatus. Speckle potentials offer an example of *correlated* potentials, allowing for the investigation of disorder correlations. They are also an example of non-Gaussian potentials, suitable though for analytical calculations thanks to the underlying Gaussian structure of the electric field.

Impurity disorder

Speckle potentials are however not the only way of generating disordered potentials. An alternative proposal, which does not involve the dipolar force, consists in creating an *impurity disorder* for one atomic species [108, 109] by using a secondary atomic species trapped on random sites of an optical lattice. If the main species is insensitive to the lattice, it experiences only the impurity potential created by the second species,

$$V(\mathbf{r}) = \sum_i U(\mathbf{r} - \mathbf{r}_i), \tag{1.10}$$

with U the potential created by a single atom of the second species, and $\mathbf{r}_i$ its random position. This proposal realizes the so-called Edwards model and has been implemented in cold atom experiments [110]. It notably proves useful to investigate disorder correlations, since the latter are determined by the shape of $U(\mathbf{r})$. For instance, for delta-correlated impurities (i.e. $U(\mathbf{r}) = \delta(\mathbf{r})$), it realizes a *white-noise disorder* (see appendix A). The latter is widely used in the literature since it allows for analytical calculations while containing in most cases the relevant physics [8]. A *Gaussian disorder* (see appendix A) can also be obtained within this framework in the limit of infinite impurity density of vansihingly small amplitudes.

[8] Many continuous potentials reduce as well to a white-noise potential in the low-energy limit.

Quasiperiodic potentials

When considering a lattice configuration, such as in the Hubbard model, several ways exist to experimentally add a disorder. One can of course superimpose to the main optical lattice a speckle potential, resulting in random on-site energies whose statistics are determined by those of the speckle potential. However, an alternative and fruitful approach consists in designing a so-called *quasiperiodic potential*, which strictly speaking is not a purely disordered one but has very similar properties. To do so [39, 100, 112–114], the idea is to superimpose a shallow *periodic* lattice, whose frequency is incommensurate with that of the main lattice (see Fig.1.6). In such a bichromatic lattice, the on-site energy is then pseudo-periodic, $\epsilon_i = \Delta\cos(2\pi\beta i + \phi)$, with Δ and ϕ being determined by the depth and the phase of the secondary lattice, and $\beta = k_2/k_1$ being given by the (incommensurate) ratio between the two lattice wavelengths. Although deterministic, such a configuration mimics a disordered potential for finite size-systems [9]. Localization properties of quasiperiodic potentials however differ from those of a *true* disorder, as will be widely discussed in chapter 4.

1.3.3 State of the art

Let us conclude this section by a brief state of the art of the main achievements and challenges in the field of disordered cold atoms.

Anderson localization of non-interacting matter waves was experimentally observed for the first time in 2008 in one dimension, simultaneously for cold atoms in a speckle potential [38], and in a quasiperiodic lattice [39]. In 2012, three-dimensional Anderson localization was reported as well in ultracold atomic systems, for BEC in a speckle potential [42], and in fermionic gases [41]. The quest for Anderson localization in 2D is more challenging : since it is the marginal dimension, localization lengths can be exponentially large, and the window between a detectable localized state and a classically trapped one is very narrow. Let us mention as well the realization of quantum versions of kicked-rotor models [40], which can be mapped onto the Anderson Hamiltonian [115]. In such systems, *dynamical localization* [116, 117] (localization in momentum space) has been observed, allowing for an experimental determination of the critical exponents of the Anderson transition [118].

Those pioneering works have opened numerous perspectives, paving the way to the investigation of many other challenges [3], among which the most exciting one is undoubtedly the interplay between disorder and interactions.

As regards the problem of disordered bosons, most efforts have been devoted to experimentally study the superfluid to Bose glass transition. The latter was in particular observed in 1D in the weakly-interacting regime, in LENS with a quasiperiodic lattice [112–114], in Stony Brook with an impurity disorder on a lattice [110], and in Houston in the presence of a speckle potential [105]. In such experiments, evidence of a Bose glass phase has been reported, and the transition was characterized using both dynamical (damping of a BEC in the disorder, subdiffusive transport) and static (BEC fragmentation) criteria. Since experiments are carried out at (small but) finite temperature, some observations could be linked to the questions of many-body localization and localization of excitations, which are attracting an increasing attention. In 2D, where the clean system displays a finite-temperature superfluid transition

[9] The system size should indeed not be too large, to avoid periodic replicas of the potential.

(the BKT transition), most experiments have focused on studying the influence of the disorder on the BKT transition [106, 107]. Experiments exist as well in strongly-correlated regimes, for instance at Urbana Champaign where disorder-induced condensate depletion has been studied for 3D strongly-correlated lattice bosons, in the presence of a superimposed speckle potential [99].

The field of disordered many-body dynamics is more recent. As briefly mentionned previously, out-of-equilibrium dynamics can be induced in ultracold gases by a *quantum quench*, i.e. an abrupt change of some Hamiltonian parameter (e.g. a lattice depth, a trapping frequency...). Propagation of correlations in the system and relaxation to a new equilibrium state can then be monitored. So far, first studies have been performed in clean systems [119–124], focusing on light-cone propagation of correlations and Lieb-Robinson theorem. Quantum quenches in the presence of disorder have not been realized yet, but theoretical studies have started [77, 82, 83]. This field can be expected to become very active in a close future, since it is related to the questions of localization of collective excitations and many-body localization, which remain far from being understood.

Let us mention as well several studies with disorder in multi-component ultracold gases. The latter can be used to mimic spin systems and simulate spin glasses [125], whose phase diagrams remain an outstanding challenge in condensed matter. Moreover, multi-component disordered ultracold gases are known to exhibit their own specific features, such as disorder-induced order [126–129].

Outlook

While disorder and interactions lie at the heart of the most complex phenomena in solid-state physics, understanding their interplay represents a formidable challenge. Among the most puzzling issues, the question of collective localization transitions is particularly intriguing. It is expected to underlie some celebrated disorder-induced phase transitions, such as the superfluid-to-insulator and superconducting-to-insulator ones, as well as many-body localization effects, and dynamical properties of disordered many-body systems. While theoretical questions remain far from being fully explored, recent experiments carried out with ultracold atoms are now in a position to address those long-standing issues.

The theoretical study of collective localization transitions is the main topic of this thesis. More precisely, we will focus in this manuscript on the localization transitions of collective excitations in the case of Bose superfluids. We will successively address this question in different contexts, which are all realized by current ultracold-atom experiments (disordered, quasiperiodic, and multi-component Bose gases).

Chapter 2

Ultracold Bose gases - Bogoliubov theory

1.	d2-d4	Cg8-f6
2.	c2-c4	e7-e6
3.	Cg1-f3	Ff8-b4+

Défense Bogoliubov

This chapter is devoted to an introductory presentation of the quantum degenerate Bose gas, in particular in the weakly-interacting regime. It constitutes a preliminary step before addressing the question of disorder, whose interplay with interactions in weakly-interacting Bose systems is the main topic of this manuscript. Therefore, the objectives of this chapter are twofold. On the one hand, it reviews the main features and physical properties of Bose gases *without* disorder, among which Bose-Einstein condensation, quasicondensation, superfluidity, and coherence properties. On the other hand, it provides the theoretical tools to be used when dealing with weakly-interacting Bose gases. Much attention will be devoted to the Bogoliubov method, which will be widely used in this work, and which is therefore presented here in its most general inhomogeneous formulation.

In Sec. 2.1, after a brief history, we discuss the basics of Bose-Einstein condensation. We first introduce it in the case of an ideal Bose gas (Sec. 2.1.2), before generalizing the concept to the most general inhomogeneous situation, where we establish the link between condensation and long-range order (Sec. 2.1.3). We then move to the case of the weakly-interacting Bose gas in Sec. 2.2. After introducing the principle of meanfield approaches (Sec. 2.2.1), we present in details the Bogoliubov theory (Sec. 2.2.2), and apply it to a homogeneous gas to enlighten its main physical properties (Sec. 2.2.3). The case of low dimensions is addressed in Sec. 2.2.4, where we discuss the phenomenon of quasicondensation and possible extensions of the Bogoliubov theory.

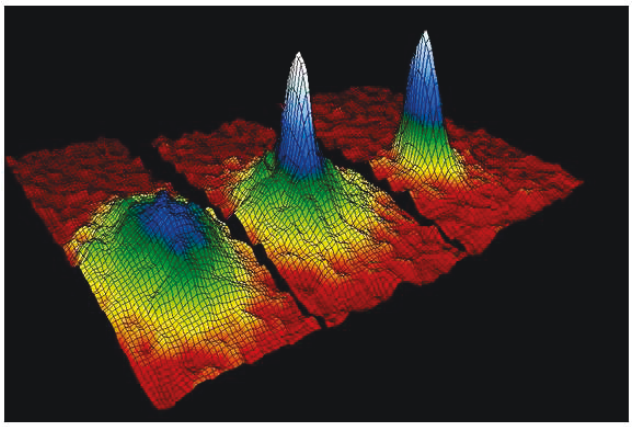

Figure 2.1: Three successive steps in the obtention of a BEC (from left to right, $T \sim 400nK$, $T \sim 200nK$, $T \sim 50nK$), obtained by imaging the velocity distribution of the gas after time-of-flight expansion of the cloud (the trap is suddenly released so that the atoms expand freely according to their initial velocity). At very low temperature, the central peak reveals a high number of atoms with the same velocity (the signature of BEC), surrounded by a cloud of thermal atoms with random velocities. Image provided by JILA, University of Colorado, Boulder.

2.1 Bose-Einstein condensation

2.1.1 History

Bose-Einstein condensation is undoubtedly one of the most spectacular manifestations of quantum statistics, which sees bosons acquire a collective behaviour, even in the absence of interactions. Pioneering works date back to Bose, who studied the quantum statistics of photons, and proposed a different statistics from the classical Boltzman one, assuming that photons are indistinguishable and can occupy the same quantum state. This idea was then generalized by Einstein to all bosonic particles, defining the so-called *Bose-Einstein statistics*. Applying this concept to an ideal (i.e. non-interacting) gas of bosons [130], Einstein found that, as a direct consequence of this statistics, a phase transition was predicted to happen at finite temperature, between a classical gas and a state where bosons accumulate in the same single-particle quantum state. This new state of matter was nicknamed Bose-Einstein condensate (BEC), but Einstein himself doubted about its reality :

"It is a nice theory, but does it contain any truth ?"

It took until 1937, and the discovery of superfluidity in liquid helium ^{4}He [16], before Einstein's prediction was considered with a renewed interest. Superfluidity is a macrsocopic hydrodynamic property of some fluids which, below a critical temperature, flow with zero viscosity. Noticing that the superfluid critical temperature of ^{4}He ($2.2K$), was remarkably close to the condensation temperature of an ideal Bose gas with the density of helium ($3.2K$), London suggested that superfluidity might be a manifestation of BEC [1]. At the same time, studies on superconductivity, where charge carriers were identified as bosonic Cooper pairs, reinforced the idea that it could as well be a consequence of BEC. Simultaneously, theoretical

[1]It is today known that the link between BEC and superfluidity is more subtle, since superfluidity requires in particular interactions between particles.

works [131] developed rapidly, revealing that Bose-Einstein condensation was not specific to the non-interacting gas, but expected to be a rather generic feature in Bose systems.

The experimental observation of Bose-Einstein condensates was finally made possible by the development of ultracold gases over the last decades of the 20^{th} century. On the one hand, significant advances in atom trapping and cooling enabled to reach the quantum degeneracy regime (low temperature/high density) where BEC arises. On the other hand, the development of new diagnostic apparatuses, among which time-of-flight measurements, provided the decisive tools to unambiguously identify a BEC. In 1995, in Boulder, Cornell and Wieman managed to observe a BEC of rubidium atoms at $\sim 100nK$ for a few seconds, soon followed by other observations [84–86] (see Fig. 2.1). Such efforts have been honoured by the Nobel prize in 2001 to Cornell, Wieman and Ketterle, "for the achievement of Bose-Einstein condensation in dilute gases [...] and for early fundamental studies of the properties of condensates". Since then, BECs have been realized for many atomic species [132–135], in the presence of dipolar interactions [136], for molecules of fermionic atoms [137–139], as well as for magnons [140,141], exciton polaritons [142,143] and photons [144]. Direct observation of condensation and measurements of BEC coherence properties have today reached an impressive degree of precision.

2.1.2 The ideal Bose gas

The ideal (i.e. non-interacting) Bose gas case is treated in most statistical physics textbooks, and we refer to them for an exhaustive presentation, especially as regards all thermodynamical properties of condensates. In this section, we mostly recall the general picture, and provide an intuitive criterion for condensation to occur.

In an ideal gas, the N-body Hamiltonian is the sum of identical independent single-particle Hamiltonians, whose eigenstates and eigenenergies are respectively denoted $|\lambda\rangle$ and ε_λ. A many-body state is then entirely characterized by the number of particles populating each single-particle eignestate $|\lambda\rangle$. At $T = 0$, all particles occupy the single-particle ground state (labelled by $\lambda = 0$ for simplicity) and the ideal Bose gas is always perfectly condensed. At finite temperature T, the number of atoms N_λ in a given state $|\lambda\rangle$ obeys the Bose-Einstein distribution

$$N_\lambda = \frac{1}{e^{\beta(\varepsilon_\lambda - \mu)} - 1} \tag{2.1}$$

where $\beta = 1/k_B T$ and the chemical potential μ is adjusted to fulfill the condition of fixed number of particles $N = \sum_\lambda N_\lambda$ (necessarily, $\mu < \varepsilon_0$ to ensure stability of the gas). In finite-size systems, the single-particle spectrum ε_λ is discrete and will be labelled for simplicity by $\lambda \in \mathbb{N}$. In this case, the number of particles in the excited states (i.e. $\lambda \neq 0$) is upper-bounded by

$$N_e^{max} = \sum_{\lambda>0} \frac{1}{e^{\beta(\varepsilon_\lambda - \varepsilon_0)} - 1}. \tag{2.2}$$

Because of this *saturation of excited states*, if the gas contains $N > N_e^{max}$ particles, at least $N - N_e^{max}$ will populate the ground state, which will be macroscopically occupied. Therefore, a BEC always arises at finite temperature in finite-size systems. However, a true phase transition can only exist in the thermodynamic limit, and the key question is whether this saturation of excited states survives in this limit, i.e. when the spectrum becomes continuous, $\varepsilon_1 \to \varepsilon_0$. Replacing the discrete sum in Eq. (2.2) by an integral, it is immediate to see that N_e^{max}

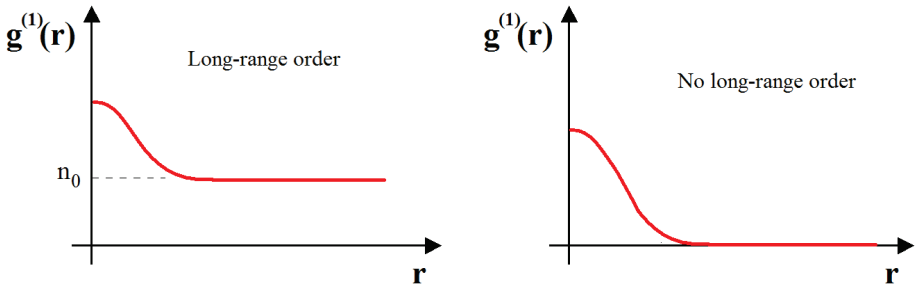

Figure 2.2: When a true condensate is present, the $g^{(1)}$ function exhibits long-range order, in the sense that it decreases to a finite value at large separations. In a homogeneous system, the latter is given by the condensate density. When $g^{(1)}$ goes to zero at infinity, no BEC occurs; it is for instance the case in low dimensional Bose gases.

remains finite provided

$$\int_0^\infty \frac{\rho(\varepsilon)}{e^{\beta\varepsilon}-1} d\varepsilon < \infty, \tag{2.3}$$

with $\rho(\varepsilon)$ the single-particle density of states. A simple criterion to have a BEC at finite temperature in the thermodynamic limit is therefore that $\int \frac{\rho(\varepsilon)}{\varepsilon} d\varepsilon$ converge for $\varepsilon \to 0$. It strongly depends on dimensionality and on the single-particle density of states. For instance, while BEC occurs in free space in 3D, and in harmonics traps in 2D and 3D, it cannot occur in free space in 1D and 2D, as well as in 1D harmonics traps [2]. The difficulty to condense in low dimensions is a general feature which will be discussed later in this chapter.

2.1.3 Long-range order

It has however taken a long time before a univeral definition of BEC was admitted, encapsulating both ideal or interacting, as well as uniform or inhomogeneous, systems. It is now recognized that one of the key concepts is the first-order correlation function, or one-body density matrix (OBDM), defined by

$$g^{(1)}(\mathbf{r},\mathbf{r}') = \langle \hat{\psi}^\dagger(\mathbf{r})\hat{\psi}(\mathbf{r}')\rangle \tag{2.4}$$

where $\hat{\psi}(\mathbf{r})$ (resp. $\hat{\psi}^\dagger(\mathbf{r})$) is the bosonic annihilation (resp. creation) operator of a particle at position $\mathbf{r}$, which satisfies the bosonic commutation rule $[\hat{\psi}(\mathbf{r}), \hat{\psi}^\dagger(\mathbf{r}')] = \delta(\mathbf{r}-\mathbf{r}')$. The OBDM contains information about the spatial density of the gas, its momentum distribution, and correlations of the field. It was first proposed by Yang [145] to define a BEC by the existence of *off-diagonal long range order* (ODLRO), namely the fact that $g^{(1)}(\mathbf{r},\mathbf{r}')$ does not vanish at large distance, $|\mathbf{r}-\mathbf{r}'| \to \infty$, but goes to a finite value (see Fig. 2.2),

$$\lim_{|\mathbf{r}-\mathbf{r}'|\to\infty} g^{(1)}(\mathbf{r},\mathbf{r}') \equiv \psi_0^*(\mathbf{r})\psi_0(\mathbf{r}') \neq 0. \tag{2.5}$$

For a homogeneous gas, the translation of this property to Fourier space [3] indeed expresses that the momentum distribution is not regular, $n(k) = n_0\delta(k) + \tilde{n}(k)$ with $\tilde{n}(k)$ a regular function,

[2] We recall that the single-particle density of states scales as $\rho(\varepsilon) \propto \varepsilon^{d/2-1}$ in free space, and $\rho(\varepsilon) \propto \varepsilon^{d-1}$ in harmonic traps.

[3] We recall that for a homogeneous gas, the momentum distribution $n(k)$ is the Fourier transform of the function $g^{(1)}(s)$, which depends only on the separation $s = \mathbf{r}-\mathbf{r}'$.

the $k = 0$ single-state thus being macroscopically occupied. The Yang definition also applies to inhomogeneous systems, ψ_0 defining the *condensate wavefunction*. However, it cannot hold for finite-size systems where $g^{(1)}(\mathbf{r}, \mathbf{r}')$ always vanishes at large distances. Threfore, a more general definition was proposed by Penrose and Onsager [146], which is based on the eigenvalues of the OBDM. Let us denote by N_i the eigenvalues and $\phi_i(\mathbf{r})$ the eigenvectors of $g^{(1)}(\mathbf{r}, \mathbf{r}')$, which are solutions of

$$\begin{aligned} \int g^{(1)}(\mathbf{r}, \mathbf{r}')\phi_i(\mathbf{r}')d\mathbf{r}' &= N_i\phi_i(\mathbf{r}) \\ \int |\phi_i|^2 &= 1. \end{aligned} \tag{2.6}$$

In this diagonal basis, the OBDM rewrites

$$g^{(1)}(\mathbf{r}, \mathbf{r}') = \sum_i N_i\phi_i^*(\mathbf{r})\phi_i(\mathbf{r}'). \tag{2.7}$$

A BEC is then defined by the existence of one macroscopic (extensive) eigenvalue, N_0, which is of the order of the total number of particles N. In the thermodynamic limit, this definition coincides with Yang's criterion of ODLRO, since

$$g^{(1)}(\mathbf{r}, \mathbf{r}') = N_0\phi_0^*(\mathbf{r})\phi_0(\mathbf{r}') + \sum_i N_i\phi_i^*(\mathbf{r})\phi_i(\mathbf{r}') \underset{|\mathbf{r}-\mathbf{r}'|\to\infty}{\longrightarrow} N_0\phi_0^*(\mathbf{r})\phi_0(\mathbf{r}') \tag{2.8}$$

as the discrete sum can be replaced by an integral which vanishes in the thermodynamic limit. The BEC wavefunction therefore expresses $\psi_0(\mathbf{r}) = \sqrt{N_0}\phi_0(\mathbf{r})$, where N_0 is the number of atoms populating the macroscopically occupied single-particle state ϕ_0. It is the order parameter of the BEC phase transition, and BEC is thus related to the symmetry breaking of the gauge invariance [147]. The Penrose-Onsager defintion is very general, and applies for both inhomogeneous and finite-size systems. From this defintion, BEC is thus related to first-order, or phase, coherence.

Diagonalizing the OBDM enables to clearly identify the single-particle wavefunctions, ϕ_i, usually referred to as *natural orbitals*[4]. Interestingly, a BEC can only arise in one of those states [5]. Let us further denote by $\hat{a}_i$ the annihilation operator in state ϕ_i. The field operator may be written :

$$\hat{\psi}(\mathbf{r}) = \phi_0(\mathbf{r})\hat{a}_0 + \sum_{i\neq 0} \phi_i(\mathbf{r})\hat{a}_i. \tag{2.9}$$

If $N_0 \approx N$, one may treat the macrocopic component as a classical field, by replacing $\hat{a}_0, \hat{a}_0^\dagger$ by $\sqrt{N_0}$. The field operator then rewrites

$$\hat{\psi}(\mathbf{r}) = \psi_0(\mathbf{r}) + \delta\hat{\psi}(\mathbf{r}) \tag{2.10}$$

where $\psi_0(\mathbf{r})$ is the BEC wavefunction and the *depletion operator* $\delta\hat{\psi}(\mathbf{r}) = \sum_i \phi_i(\mathbf{r})\hat{a}_i$ includes quantum and thermal fluctuations. This is the starting point of mean-field theories for the condensed phase, such as the Bogoliubov theory for the weakly-interacting Bose gas (see Sec. 2.2).

[4] For a homogeneous systems, the natural orbitals are the plane waves of well defined momentum, and Eq. (2.9) is nothing but the Fourier transform for the field operator, $\hat{\psi}(\mathbf{r}) = \frac{1}{\sqrt{\mathcal{V}}}\sum_{\mathbf{k}} \hat{a}_{\mathbf{k}}e^{i\mathbf{k}.\mathbf{r}} = \frac{\hat{a}_0}{\sqrt{\mathcal{V}}} + \sum_{\mathbf{k}\neq 0} \hat{a}_{\mathbf{k}}e^{i\mathbf{k}.\mathbf{r}}$.

[5] When several eigenvalues N_i of the OBDM are of the order of N, one speaks of a *fragmented BEC*.

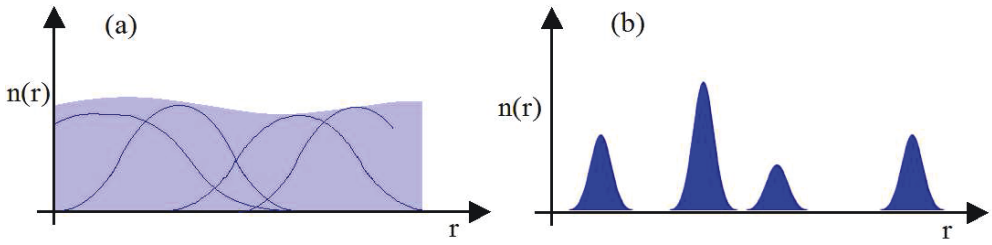

Figure 2.3: (a) Weakly-interacting configuration where the wavefunctions of individual particles (blue lines) overlap, yielding a roughly homogeneous mean-field density profile (shaded area). In this case, there is no kinetic energy and the interaction energy is $E_I = gn$. (b) Strongly-correlated configuration where the wavefunctions of different particles (shaded areas) exclude each other. In this case, there is no interaction energy and the typical kinetic energy is $E_K = \hbar^2 n^{d/2}/2m$. Comparing their energies, one can find which of those two configurations is the more favourable, yielding a criterion for the weakly-interacring regime.

2.2 The weakly-interacting Bose gas

2.2.1 Weak interactions and mean-field theories

In dilute Bose gases, interactions mainly reduce to two-body collisions. At low temperatures, the latter are dominated for bosons by s-wave scattering, and interactions can be accurately modelled by a contact pseudopotential $V(\mathbf{r}) = g\delta(\mathbf{r})$, where the coupling constant g can be expressed as a function of the scattering length a_S. The latter encodes the interaction strength and is an intrinsic property of the considered atomic species. For instance in 3D, $g = 4\pi\hbar^2 a_S/m$, while in lower dimensions, the expression can depend on the transverse confinement, which determines whether collisions still take place in 3D or not.

A general criterion for the weakly-interacting regime can be found by requiring that the typical interaction energy $E_I = gn$, in a weakly-interacting meanfield configuration where the wavefunctions of all particles completely overlap, be much smaller than the typical kinetic energy $E_K = \hbar^2 n^{d/2}/2m$, in a strongly-interacting configuration where the wavefunctions of different particles exclude each other (see Fig. 2.3). In 3D, this criterion yields the condition $na_S^3 \ll 1$, stating that the weakly-interacting regime is reached at low density. In 2D, the criterion is found to weakly depend on the density, while in 1D, weak interactions occur at high density !

In the weakly-interacting regime, one can rely on mean-field theory. The starting point of meanfield theories for the condensed phase is to assume the existence of a condensate (an assumption which is checked a posteriori in the theory), and to develop the field operator around the condensate wavefunction [see Eq. (2.10)], assuming a small depletion of the condensate, $|\delta\hat{\psi}(\mathbf{r})| \ll \psi_0(\mathbf{r})$. Such an assumption requires weak quantum and thermal fluctuations, which in 3D is achieved in the weakly-interacting regime ($na_S^3 \ll 1$) at low-temperatures ($T \ll T_c$). Conversely, it breaks down in *strongly-correlated* regimes where *many-body* physics dominates. Such regimes are hardly accessible in 3D experiments, except in the presence of a lattice, where the strong confinement at each lattice site causes strong correlations between particles. More importantly, the assumption of an existing condensate can also break down in low dimensions, where large phase fluctuations can possibly prevent condensation. Extensions of meanfield theories, with reduced hypotheses, nevertheless exist (see Sec. 2.2.4).

In the following, we will present in details the mean-field theory for the weakly-interacting Bose gas (the so-called Bogoliubov theory), focusing first on the simple (3D) case where a true condensate exists, as originally introduced by Bogoliubov [131]. Possible extensions of the theory to lower dimensions, where no true condensate wavefunction can be identified due to large phase fluctuations, will be discussed in Sec. 2.2.4.

2.2.2 Bogoliubov theory

The Hamiltonian of the weakly-interacting Bose gas writes

$$\hat{\mathcal{H}} = \int \left\{ \hat{\psi}^\dagger \left[\frac{-\hbar^2 \nabla^2}{2m} + V(\mathbf{r}) \right] \hat{\psi} + \frac{g}{2} \hat{\psi}^\dagger \hat{\psi}^\dagger \hat{\psi} \hat{\psi} \right\} \mathrm{d}^d\mathbf{r}, \tag{2.11}$$

where $\hat{\psi}(\mathbf{r})$ is the field operator of a particle at position $\mathbf{r}$, g is the interaction coupling constant, and $V(\mathbf{r})$ is a static external potential. The general idea of the Bogoliubov theory consists in a perturbative expansion of $\hat{\mathcal{H}}$ in the fluctuation part $\delta\hat{\psi}$ of the field operator. As discussed above, it is expected to be valid for dilute ($n a_S^3 \ll 1$) gases at low-temperatures ($T \ll T_c$). Although originally formulated in momentum space for homogeneous systems, we will present here the real-space formulation of the theory, which can advantageously apply to the most general inhomogeneous situation we will consider later in this manuscript.

Ground-state and Gross-Pitaevskii equation

To lowest order, fluctuations are neglected and the field operator $\hat{\psi}^\dagger(\mathbf{r})$ is replaced by the condensate wavefunction $\psi_0(\mathbf{r})$. Furthermore, at this order, $N_0 = N$, so that $\psi_0(\mathbf{r}) = \sqrt{N}\phi_0(\mathbf{r})$. The N-body wavefunction then describes all particles in the same single-particle state, $\phi_0(\mathbf{r})$, $\psi(\mathbf{r}_1, \mathbf{r}_2, ...\mathbf{r}_n) = \prod_{i=1}^N \phi_0(\mathbf{r}_i)$.

There are several ways to derive the equation governing the condensate wavefunction $\psi_0(\mathbf{r})$. A first one is to minimize the classical energy functional,

$$E[\psi_0] = \int \Big[\frac{\hbar^2}{2m} |\nabla\psi_0(\mathbf{r})|^2 + V(\mathbf{r})|\psi_0(\mathbf{r})|^2 + \frac{1}{2} g |\psi_0(\mathbf{r})|^4 \Big] \mathrm{d}^d\mathbf{r}, \tag{2.12}$$

which is obtained by replacing $\hat{\psi}^\dagger(\mathbf{r})$ by $\psi_0(\mathbf{r})$ in Hamiltonian (2.11), under the constraint of fixed average number of particles. This yields the stationary Gross-Pitaevskii equation (GPE) [148–150]

$$\Big[-\frac{\hbar^2\nabla^2}{2m} + V(\mathbf{r}) - \mu + g|\psi_0(\mathbf{r})|^2 \Big] \psi_0(\mathbf{r}) = 0, \tag{2.13}$$

where the chemical potential μ is the Lagrange multiplier associated to the constraint of fixed average number of particles, which reads

$$\mu = \frac{1}{N} \int \Big[\frac{\hbar^2}{2m} |\nabla\psi_0(\mathbf{r})|^2 + V(\mathbf{r})|\psi_0(\mathbf{r})|^2 + g|\psi_0(\mathbf{r})|^4 \Big] \mathrm{d}^d\mathbf{r}. \tag{2.14}$$

The GPE (2.13) governs static properties of the condensate, and determines for instance the density profile $|\psi_0(\mathbf{r})|^2$ of the condensate.

An alternative way to derive the GPE consists in replacing $\hat{\psi}^\dagger(\mathbf{r}, t)$ by $\psi_0(\mathbf{r}, t)$ in the Heisenberg equation of motion, which yields the dynamical GPE

$$i\hbar\partial_t\psi_0(\mathbf{r}, t) = \Big[-\frac{\hbar^2\nabla^2}{2m} + V(\mathbf{r}) + g|\psi_0(\mathbf{r}, t)|^2 \Big] \psi_0(\mathbf{r}, t). \tag{2.15}$$

Apart from recovering the static GPE by writing $\psi_0(\mathbf{r},t) = \psi_0(\mathbf{r})e^{-i\mu t/\hbar}$, this equation governs all dynamical properties of the condensate [6]. More importantly, the linearization of the dynamical GPE around the stationary solution $\psi_0(\mathbf{r})$ enables to compute the eigenmodes of the condensate or determine its response to a perturbation.

Elementary excitations and Bogoliubov equations

The next order in the Bogoliubov expansion corresponds to a quadratization of Hamiltonian (2.11) in fluctuation terms. Indeed, the linear terms are found to vanish, using the fact that ψ_0 solves the GPE. Keeping terms up to second order in Hamiltonian (2.11) yields the so-called Bogoliubov Hamiltonian

$$\hat{\mathcal{H}}^{(2)} = \frac{1}{2}\int \left(\delta\hat{\psi}^\dagger, -\delta\hat{\psi}\right) \mathcal{L}_{GP}(\mathbf{r}) \begin{pmatrix} \delta\hat{\psi} \\ \delta\hat{\psi}^\dagger \end{pmatrix} \mathrm{d}^d\mathbf{r} \; + cst. \tag{2.16}$$

where

$$\mathcal{L}_{GP} = \begin{pmatrix} -\dfrac{\hbar^2\nabla^2}{2m} + V(\mathbf{r}) - \mu + 2g|\psi_0(\mathbf{r})|^2 & g\psi_0(\mathbf{r})^2 \\ -g\psi_0^*(\mathbf{r})^2 & -\left[-\dfrac{\hbar^2\nabla^2}{2m} + V(\mathbf{r}) - \mu + 2g|\psi_0(\mathbf{r})|^2\right]^* \end{pmatrix}. \tag{2.17}$$

As a quadratic form in $\delta\hat{\psi}$ and $\delta\hat{\psi}^\dagger$, the Bogoliubov Hamiltonian can *a priori* be diagonalized, i.e. put into the canonic form

$$\hat{\mathcal{H}}^{(2)} = \sum_\nu \varepsilon_\nu \hat{b}_\nu^\dagger \hat{b}_\nu + cst. \tag{2.18}$$

thanks to a suitable linear transformation

$$\begin{aligned} \hat{b}_\nu &= \int \mathrm{d}\mathbf{r} \left[u_\nu^*(\mathbf{r})\delta\hat{\psi}(\mathbf{r}) - v_\nu^*(\mathbf{r})\delta\hat{\psi}^\dagger(\mathbf{r})\right] \\ \hat{b}_\nu^\dagger &= \int \mathrm{d}\mathbf{r} \left[u_\nu(\mathbf{r})\delta\hat{\psi}^\dagger(\mathbf{r}) - v_\nu(\mathbf{r})\delta\hat{\psi}(\mathbf{r})\right] \end{aligned} \tag{2.19}$$

Such a form [Eq. (2.18)] describes non-interacting *quasi-particles* of energy ε_ν, which are created (resp. annihilated) by the Bogoliubov operator $\hat{b}_\nu^\dagger$ (resp. $\hat{b}_\nu$). In practice, to obtain such a canonic form, one can show that the suitable u_ν and v_ν wavefunctions in the linear transformation Eq. (2.19) should be the solutions of *positive* energy $\varepsilon_\nu > 0$ of the so-called *Bogoliubov De-Gennes equations* (BdGEs)

$$\mathcal{L}_{GP}\begin{pmatrix} u_\nu \\ v_\nu \end{pmatrix} = \varepsilon_\nu \begin{pmatrix} u_\nu \\ v_\nu \end{pmatrix}, \tag{2.20}$$

together with the bi-orthogonality conditions

$$\begin{aligned} \sum_\sigma \int \mathrm{d}\mathbf{r} \left[u_\nu(\mathbf{r})u_{\nu'}^*(\mathbf{r}) - v_\nu(\mathbf{r})v_{\nu'}^*(\mathbf{r})\right] &= \delta_{\nu\nu'} \\ \sum_\sigma \int \mathrm{d}\mathbf{r} \left[u_\nu(\mathbf{r})v_{\nu'}(\mathbf{r}) - v_\nu(\mathbf{r})u_{\nu'}(\mathbf{r})\right] &= 0\,. \end{aligned} \tag{2.21}$$

[6] Hydrodynamic equations can for instance be inferred from Eq. (2.15) [147].

The latter ensure that the operators $\hat{b}^\dagger$ and $\hat{b}$ satisfy the bosonic commutation relations. It is important to note that only positive energies $\varepsilon_\nu > 0$ enter Eq. (2.18), which means that populating quasiparticle modes necessarily increases the total energy, as required by stability conditions.

Therefore, the Bogoliubov theory amounts to describe a complex N-body gas of *interacting particles* as a gas of *non-interacting quasi-particles* [7]. The latter can thus be treated as an ideal Bose gas, the populations of the quasiparticle modes obeying the Bose-Einstein statistics. To obtain all the thermodynamics of the gas, it is therefore crucial to determine the quasi-particle energy spectrum and wavefunctions. This is achieved by solving the BdGEs, Eq. (2.20), which take the form of an eigenproblem.

The solution to this eigenproblem is commonly treated in literature [151, 152]. All eigenmodes

$$\begin{pmatrix} u_\nu \\ v_\nu \end{pmatrix}$$

of the operator $\mathcal{L}_{GP}$ of energy $\varepsilon_\nu > 0$ come along with an eigenmode

$$\begin{pmatrix} v_\nu^* \\ u_\nu^* \end{pmatrix}$$

of energy $-\varepsilon_\nu$, which however does not enter into the sum in Eq. (2.18). Besides this, $\mathcal{L}_{GP}$ has a mode of zero energy

$$\begin{pmatrix} \psi_0(\mathbf{r}) \\ -\psi_0^*(\mathbf{r}) \end{pmatrix}.$$

However, since the operator $\mathcal{L}_{GP}$ is *not* Hermitian, it is in general not diagonalizable and one cannot in principle reduce the Bogoliubov Hamiltonian to the canonic form Eq. (2.18). In this case however, the symmetries of $\mathcal{L}_{GP}$ and the assumption that $\psi_0(\mathbf{r})$ is a local minimum of the GPE are sufficient to make $\mathcal{L}_{GP}$ *almost diagonalizable*, in the sense that only one eigenvector is missing to span the whole space. As we shall see, this is sufficient to put the Bogoliubov Hamiltonian in a form which is very close to Eq. (2.18). More precisely, an additional vector

$$\begin{pmatrix} \partial\psi_0(\mathbf{r}) \\ \partial\psi_0^*(\mathbf{r}) \end{pmatrix}$$

is introduced to obtain a complete basis. In this basis, the field operator expands as

$$\begin{pmatrix} \delta\hat{\psi} \\ \delta\hat{\psi}^\dagger \end{pmatrix} = \sum_\nu \begin{pmatrix} u_\nu(\mathbf{r}) \\ v_\nu(\mathbf{r}) \end{pmatrix} \hat{b}_\nu + \begin{pmatrix} v_\nu^*(\mathbf{r}) \\ u_\nu^*(\mathbf{r}) \end{pmatrix} \hat{b}_\nu^\dagger + \frac{1}{i\hbar}\hat{Q} \begin{pmatrix} \psi_0(\mathbf{r}) \\ -\psi_0^*(\mathbf{r}) \end{pmatrix} + \hat{P} \begin{pmatrix} \partial\psi_0(\mathbf{r}) \\ \partial\psi_0^*(\mathbf{r}) \end{pmatrix}, \quad (2.22)$$

where $\hat{b}_\nu^\dagger$ and $\hat{b}_\nu$ are still given by Eqs. (2.19), and

$$\begin{aligned} \hat{P} &= \int \mathrm{d}\mathbf{r} \left[\psi_0^*(\mathbf{r})\delta\hat{\psi}(\mathbf{r}) + \psi_0(\mathbf{r})\delta\hat{\psi}^\dagger(\mathbf{r})\right] \\ \hat{Q} &= i\hbar \int \mathrm{d}\mathbf{r} \left[\partial\psi_0(\mathbf{r})\delta\hat{\psi}^\dagger(\mathbf{r}) - \partial\psi_0^*(\mathbf{r})\delta\hat{\psi}(\mathbf{r})\right], \end{aligned} \quad (2.23)$$

[7] Interactions between quasi-particles arise when considering higher orders (i.e. cubic and quartic) in Bogoliubov expansion, and confer to them a finite lifetime, which is purely neglected at this level.

represent additional conjugate operators. With this expansion, the Bogoliubov Hamiltonian is finally *almost*-diagonalized under the form

$$\hat{\mathcal{H}}^{(2)} = \sum_\nu \varepsilon_\nu \hat{b}_\nu^\dagger \hat{b}_\nu + \frac{\hat{P}^2}{2m_{\text{eff}}} + cst. \tag{2.24}$$

It is made of a canonic part similar to Eq. (2.18) describing quasi-particle excitations. Additionnally, the spurious modes and the corresponding conjugate operators $\hat{Q}$ and $\hat{P}$ play no role on the dynamics, but should be interpreted as a collective phase coordinate and its conjugate momentum. They induce quantum phase diffusion and fluctuations of the number of particles [153, 154]. Their presence can indeed be traced to the fact that the Bogoliubov Hamiltonian (2.16) does not conserve the total number of particles which, from a mathematical point of view, is intimately related to the fact that the operator $\mathcal{L}_{GP}$, as discussed above, is not diagonalizable (its eigenvectors do not span the whole space).

A solution to this problem can be achieved by making $\mathcal{L}_{GP}$ diagonalizable by extracting only the "relevant" part of $\delta\hat{\psi}$, i.e. restricted to an appropriate subspace [151]. This idea is formalized by the so-called "number-conserving" approach, which consists in expanding Hamiltonian (2.11) up to second order in the operator

$$\hat{\Lambda}(\mathbf{r}) = \frac{\hat{a}_{\psi_0}^\dagger \delta\hat{\psi}(\mathbf{r})}{\hat{N}^{1/2}},$$

which, at variance with $\delta\hat{\psi}(\mathbf{r})$, *does conserve* the number of particles. The resulting Bogoliubov Hamiltonian writes

$$\hat{\mathcal{H}}^{(2)} = \frac{1}{2}\int \left(\hat{\Lambda}^\dagger - \hat{\Lambda}\right) \mathcal{L}(\mathbf{r}) \begin{pmatrix} \hat{\Lambda} \\ \hat{\Lambda}^\dagger \end{pmatrix} \mathrm{d}^d\mathbf{r} \; + cst. \tag{2.25}$$

where

$$\mathcal{L} = \begin{pmatrix} -\dfrac{\hbar^2\nabla^2}{2m} + V(\mathbf{r}) - \mu + 2gQ_{\psi_0}|\psi_0(\mathbf{r})|^2 Q_{\psi_0} & gQ_{\psi_0}\psi_0(\mathbf{r})^2 Q_{\psi_0}^* \\ -gQ_{\psi_0}^*\psi_0^*(\mathbf{r})^2 Q_{\psi_0} & -\left[-\dfrac{\hbar^2\nabla^2}{2m} + V(\mathbf{r}) - \mu + 2gQ_{\psi_0}|\psi_0(\mathbf{r})|^2 Q_{\psi_0}\right]^* \end{pmatrix},$$

with Q_{ψ_0} (resp. $Q_{\psi_0}^*$) denoting the projection operator orthogonally to ψ_0 (resp. ψ_0^*). Contrary to $\mathcal{L}_{GP}$, $\mathcal{L}$ is diagonalizable. Most importantly, one has the remarkable result that if (u_ν, v_ν) is an eigenvector of $\mathcal{L}_{GP}$ of eigenvalue $\varepsilon_\nu > 0$, then $(Q_{\psi_0}u_\nu, Q_{\psi_0}^* v_\nu)$ is an eigenvector of $\mathcal{L}$ of same eigenvalue ε_ν. Therefore, the Bogoliubov transformation

$$\begin{pmatrix} \hat{\Lambda} \\ \hat{\Lambda}^\dagger \end{pmatrix} = \sum_\nu \begin{pmatrix} u_\nu^\perp(\mathbf{r}) \\ v_\nu^\perp(\mathbf{r}) \end{pmatrix} \hat{b}_\nu + \begin{pmatrix} v_\nu^{*\perp}(\mathbf{r}) \\ u_\nu^{*\perp}(\mathbf{r}) \end{pmatrix} \hat{b}_\nu^\dagger, \, , \tag{2.26}$$

where $u_\nu^\perp$ (resp. $v_\nu^\perp$) stands for $Q_{\psi_0}u_\nu$ (resp. $Q_{\psi_0}^* v_\nu$), exactly diagonalizes the Bogoliubov Hamiltonian (2.25) into $\sum_\nu \varepsilon_\nu \hat{b}_\nu^\dagger \hat{b}_\nu + cst$, where no spurious mode appears any longer. In particular, the particle-number conserving and non-conserving approaches yield the same excitation spectrum, while the excitation wavefunctions in the two approaches are related by a simple projection operation. This justifies the common use of the non-conserving approach, simply omitting the spurious modes is the modal expansion, provided that the eigenvectors are then correctly orthogonalized with respect to the condensate wavefunction.

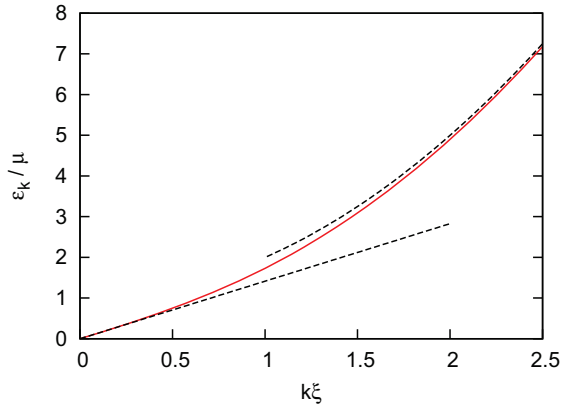

Figure 2.4: Bogoliubov excitation spectrum of the weakly-interacting Bose gas, in units of the homogeneous chemical potential $\mu = gn$, and as a function of $k\xi$, with $\xi = \frac{\hbar}{\sqrt{2m\mu}}$ the healing length of the condensate. The spectrum is phononic at low-energy and particle-like at high-energy, as indicated by the dashed lines.

2.2.3 Results for the homogeneous weakly-interacting Bose gas

Although approximate, the Bogoliubov theory remarkably reproduces the main features of dilute weakly-interacting Bose gases at low temperature, as observed experimentally. In this section, we focus on the homogeneous case, and review the main predictions of the theory. We recall that in this case, the condensate wavefunction is homogeneous, $n_0(\mathbf{r}) = n = \mu/g$, as straightforwardly obtained from Gross-Pitaevskii equation. Equivalently, condensation occurs in the state of zero momentum $k = 0$.

Excitation spectrum and wavefunctions

The *excitation spectrum* can be obtained from the Bogoliubov equations (2.20). In the homogeneous case, the latter rewrite

$$\begin{pmatrix} -\frac{\hbar^2\nabla^2}{2m} + gn & gn \\ -gn & \frac{\hbar^2\nabla^2}{2m} - gn \end{pmatrix} \begin{pmatrix} u_\nu \\ v_\nu \end{pmatrix} = \varepsilon_\nu \begin{pmatrix} u_\nu \\ v_\nu \end{pmatrix}. \tag{2.27}$$

Translation invariance ensures that the excitation wavefunctions u_ν (resp. v_ν) are plane waves labelled by a well-defined momentum $\mathbf{k}$ (instead of ν), $u_\mathbf{k} e^{i\mathbf{k}.\mathbf{r}}/\mathcal{V}$, with $\mathcal{V}$ the volume of the system. The eigenproblem (2.27) then reduces to diagonalizing a 2×2 matrix

$$\begin{pmatrix} \frac{\hbar^2 k^2}{2m} + gn & gn \\ -gn & -\frac{\hbar^2 k^2}{2m} - gn \end{pmatrix} \begin{pmatrix} u_\mathbf{k} \\ v_\mathbf{k} \end{pmatrix} = \varepsilon_k \begin{pmatrix} u_\mathbf{k} \\ v_\mathbf{k} \end{pmatrix}, \tag{2.28}$$

yielding the Bogoliubov spectrum

$$\varepsilon_\mathbf{k} = \sqrt{\frac{\hbar^2\mathbf{k}^2}{2m}\left(\frac{\hbar^2\mathbf{k}^2}{2m} + 2gn\right)}. \tag{2.29}$$

The latter is plotted on Fig. 2.4, and is found to be gapless. At high energy, it is particle-like, $\varepsilon_\mathbf{k} = \hbar^2k^2/2m + gn$. At low energy, it is phononic, $\varepsilon_\mathbf{k} = \hbar ck = cp$, and the velocity $c = \sqrt{gn/m}$

coincides with the macroscopic sound velocity as measured in experiments. Moreover, this linear low-energy dispersion accounts for the superfluidity of the weakly-interacting Bose gas as expressed by the Landau criterion [8].

As regards *excitation wavefunctions*, they are plane waves of well-defined momentum, whose amplitudes are found to be

$$u_{\mathbf{k}}^2 = \frac{1}{2}\left(\frac{\frac{\hbar^2\mathbf{k}^2}{2m}+gn}{\varepsilon_{\mathbf{k}}}+1\right), \qquad v_{\mathbf{k}}^2 = \frac{1}{2}\left(\frac{\frac{\hbar^2\mathbf{k}^2}{2m}+gn}{\varepsilon_{\mathbf{k}}}-1\right) \tag{2.30}$$

Moreover, the Bogoliubov transform Eq. (2.19) can be explicitely rewritten as a function of the creation/annihilation operators of k-states [9]

$$\begin{aligned} \hat{b}_{\mathbf{k}} &= u_{\mathbf{k}}^*\hat{a}_{\mathbf{k}} - v_{\mathbf{k}}^*\hat{a}_{-\mathbf{k}}^\dagger & \hat{a}_{\mathbf{k}} &= u_{\mathbf{k}}\hat{b}_{\mathbf{k}} + v_{-\mathbf{k}}^*\hat{b}_{-\mathbf{k}}^\dagger \\ \hat{b}_{\mathbf{k}}^\dagger &= u_{\mathbf{k}}\hat{a}_{\mathbf{k}}^\dagger - v_{\mathbf{k}}\hat{a}_{-\mathbf{k}} & \hat{a}_{\mathbf{k}}^\dagger &= u_{\mathbf{k}}^*\hat{b}_{\mathbf{k}}^\dagger + v_{-\mathbf{k}}\hat{b}_{-\mathbf{k}} \end{aligned} \tag{2.31}$$

This in particular enlightens the nature of a Bogoliubov quasiparticle, which can be viewed as a pair excitation made of a particle of momentum $\mathbf{k}$ and a hole of momentum $-\mathbf{k}$. At high energy, $u_{\mathbf{k}} \approx 1$ and $v_{\mathbf{k}} \approx 0$, so that Bogoliubov quasiparticles are simlar to free bosons, while at low energy, $u_{\mathbf{k}} \approx v_{\mathbf{k}}$, so that they are particle-hole excitations.

Condensate depletion, ground-state energy and chemical potential

In the Bogoliubov description, quasiparticles are non-interacting, and can therefore be treated as an ideal Bose gas. In particular, their thermal occupancy at finite temperature T is given by the Bose-Einstein distribution, $N_{\mathbf{k}} \equiv \langle \hat{b}_{\mathbf{k}}^\dagger \hat{b}_{\mathbf{k}} \rangle = 1/(e^{\beta\varepsilon_{\mathbf{k}}}-1)$, and all the thermodynamics can then be computed.

For instance, the *condensate depletion*, i.e. the number of non-condensed particles, defined by $N' = \langle \sum_{\mathbf{k}\neq 0} \hat{a}_{\mathbf{k}}^\dagger \hat{a}_{\mathbf{k}} \rangle$ ($\langle ... \rangle$ denoting thermal average), is straightforwardly obtained by reinserting Eqs. (2.31) for $\hat{a}_{\mathbf{k}}$ in its definition, yielding

$$N' = \frac{\mathcal{V}}{2\pi}\int \left[v_{\mathbf{k}}^2 + (u_{\mathbf{k}}^2 + v_{\mathbf{k}}^2) N_{\mathbf{k}} \right] d^d\mathbf{k}. \tag{2.32}$$

In 3D at $T = 0$, this yields the celebrated result $N'(T=0) = 8/3\sqrt{\pi}(na_S^3)^{1/2}N$ [151], which scales as the small parameter of the weakly-interacting Bose gas, $(na_S^3)^{1/2}$. This quantity is referred to as the *quantum depletion* of the condensate. At finite temperature, there is an additional *thermal depletion* which is given by $N'(T) = N'(T=0)[1 + (\pi k_{\mathrm{B}}T/2gn)^2 + ...]$ for low temperatures.

In lower dimensions, infrared divergences may appear in Eq. (2.32), suggesting the absence of condensation, as discussed in the next section.

[8] We recall that the Landau criterion discriminates between a superfluid and a viscous fluid by examining the possibility for a dissipative process to take place within the fluid, via the creation of an excitation. According to this criterion, a fluid is superfluid at velocity v if $v < v_c \equiv \min_p \frac{\varepsilon_p}{p}$. Here, the critical velocity v_c is finite and equal to the sound velocity c, so that the fluid is superfluid at zero velocity. This is in striking contrast with the ideal Bose gas, for which $\varepsilon_p = p^2/2m$ yields $v_c = 0$.

[9] We recall that the depletion operator $\delta\hat{\psi}(\mathbf{r})$ indeed develops in the basis of k-states as $\delta\hat{\psi}(\mathbf{r}) = \sum_{\mathbf{k}\neq 0} \hat{a}_{\mathbf{k}} e^{i\mathbf{k}.\mathbf{r}}$ (see footnote 3, page 39).

Corrections to the mean-field *ground state energy* and *chemical potential* can as well be computed, yielding in 3D the well-known Lee-Huang-Yang corrections

$$E^0 = \frac{gN^2}{2\mathcal{V}}\Big[1 + \frac{128}{15\sqrt{\pi}}(na_S^3)^{1/2}\Big] \tag{2.33}$$

and

$$\mu = \frac{gN}{\mathcal{V}}\Big[1 + \frac{32}{3\sqrt{\pi}}(na_S^3)^{1/2}\Big] \tag{2.34}$$

Notice that here as well, corrections scales as $(na_S^3)^{1/2}$.

Fluctuations and correlations

Density and phase *correlations and fluctuations* can finally be inferred from the computation of the coherence functions $g^{(1)}(\mathbf{r},\mathbf{r}') = \langle\hat\psi^\dagger(\mathbf{r})\hat\psi(\mathbf{r}')\rangle$ and $g^{(2)}(\mathbf{r},\mathbf{r}') = \langle\hat\psi^\dagger(\mathbf{r})\hat\psi^\dagger(\mathbf{r}')\hat\psi(\mathbf{r}')\hat\psi(\mathbf{r})\rangle$, which express, in the Bogoliubov approach,

$$g^{(1)}(\mathbf{r}-\mathbf{r}') = n_0 + \frac{1}{N}\sum_{\mathbf{k}\neq 0} e^{-i\mathbf{k}(\mathbf{r}-\mathbf{r}')}[v_\mathbf{k}^2 + (u_\mathbf{k}^2 + v_\mathbf{k}^2)N_\mathbf{k}] \tag{2.35}$$

and

$$g^{(2)}(\mathbf{r}-\mathbf{r}') = n^2 + \frac{2n}{\mathcal{V}}\sum_{\mathbf{k}\neq 0}[(u_\mathbf{k}+v_\mathbf{k})^2 N_\mathbf{k} + (u_\mathbf{k}+v_\mathbf{k})v_\mathbf{k}]\cos[\mathbf{k}(\mathbf{r}-\mathbf{r}')]. \tag{2.36}$$

The $g^{(2)}$ function provides access to density correlations $\langle\hat n(\mathbf{r})\hat n(\mathbf{r}')\rangle = g^{(2)}(\mathbf{r}-\mathbf{r}')$ [10]; in particular, one finds here that $g^{(2)}(\mathbf{r}-\mathbf{r}') \neq n^2 = n(\mathbf{r})n(\mathbf{r}')$, the Bogoliubov theory successfully accounting for density correlations in the gas. Density fluctuations $\langle\delta\hat n(\mathbf{r})\delta\hat n(\mathbf{r}')\rangle = g^{(2)}(\mathbf{r}-\mathbf{r}') - n^2$ can as well be inferred from the $g^{(2)}$ function.

Conversely, the $g^{(1)}$ function provides information about phase coherence. For instance in 3D, Eq. (2.35) yields $g^{(1)}(s) \simeq_{s\to\infty} n_0$, recovering the existence of a long-range order given by the condensate density. The case of lower dimensions, where long-range order may not exist, is discussed in the next section. As already mentioned, the Bogoliubov theory is *a priori* not valid in this case and a proper treatement of the $g^{(1)}$ function should be performed.

Let us finally give a more precise link between the behaviour of $g^{(1)}$ at large separations and phase fluctuations, which will be useful to understand why phase fluctuations can prevent condensation and long-range order. At large separations, density fluctuations may be neglected, and one may rewrite

$$\begin{aligned} g^{(1)}(\mathbf{r}) &= \langle\hat\psi^\dagger(\mathbf{r})\hat\psi(0)\rangle \\ &\simeq \sqrt{n_0(\mathbf{r})n_0(0)}\langle \mathrm{e}^{-i\hat\theta(\mathbf{r})}\mathrm{e}^{i\hat\theta(0)}\rangle \\ &\simeq \sqrt{n_0(\mathbf{r})n_0(0)}e^{\langle(\Delta\theta(\mathbf{r}))^2\rangle} \qquad \text{(assuming Gaussian fluctuations)} \\ &\simeq \sqrt{n_0(\mathbf{r})n_0(0)}e^{-(\chi(\mathbf{r})-\chi(0))} \end{aligned} \tag{2.37}$$

where $\Delta\theta(\mathbf{r}) = \hat\theta(\mathbf{r}) - \hat\theta(0)$ and $\chi(\mathbf{r}) = \langle\hat\theta(\mathbf{r})\hat\theta(0)\rangle$. Therefore, long-range order arises when the phase fluctuations $\chi(\mathbf{r}) = \langle\hat\theta(\mathbf{r})\hat\theta(0)\rangle$ remain finite at large separations. On the contrary, phase fluctuations diverging when the separation increases prevent the establishment of long-range order.

[10] There is in principle an additional singular term $n\delta(\mathbf{r}-\mathbf{r}')$, but the latter can be left aside provided correlations are computed taking the normal order.

2.2.4 Low dimensions : extensions of Bogoliubov theory and quasicondensation

So far, we have focused on the 3D case, which is well described by mean-field theories. In low dimensions however (i.e. when the confinement is so strong that the motion along the tight direction(s) is frozen), the physics can be significantly different. Due to the confinement, interactions are generally stronger and strongly-correlated regimes are easier to access, while meanfield theories become questionnable. Most importantly, one generically expects as well larger fluctuations, which can possibly prevent condensation.

Condensation and quasi-condensation

The absence of condensation/long-range order in low dimensions can be viewed as a consequence of the *Hohenberg-Mermin-Wagner theorem*. The latter applies to any system (classical or quantum) in the presence of short-range interactions, and states that in low dimensions, fluctuations are too strong to allow for the spontaneous breaking of a continuous symmetry (in particular the $U(1)$ symmetry, thus prohibiting the establishment of long-range order and the formation of a BEC). At $T = 0$, this arises from quantum fluctuations and applies only to 1D systems, while at $T > 0$, it comes from thermal fluctuations and concerns both 1D and 2D systems.

This general statement is remarkably corroborated by the previous results of the Bogoliubov theory.

As regards the condensate depletion (2.32), a divergence is found in 2D at $T > 0$ and 1D at $T = 0$ (which are logarithmic with $\mathcal{V}$), as well as in 1D at $T > 0$ (which is linear with $\mathcal{V}$), suggesting that no condensate can exist.

The same conclusions arise from an analysis of phase fluctuations and first-order coherence, which are related by Eq. (2.37). Phase fluctuations can for instance be estimated within a hydrodynamic approach [147], yielding

$$\chi(\mathbf{s}) = \frac{mc^2}{n} \int (n_{\mathbf{k}} + 1/2) \frac{e^{i\mathbf{k}.\mathbf{s}}}{\hbar k} \frac{d^d\mathbf{k}}{(2\pi)^2}. \tag{2.38}$$

This gives the following results :

- in 3D at any T, or in 2D at $T = 0$, the integral in Eq. (2.38) always converges and phase fluctuations remain finite, guaranteeing the existence of true long-range order;

- in 2D at $T > 0$ and 1D at $T = 0$, the integral in Eq. (2.38) diverges logarithmically, yielding an algebraic decay of $g^{(1)}(\mathbf{r})$ by virtue of Eq. (2.37), $g^{(1)}(\mathbf{r}) \propto r^{-\nu}$, referred to as *quasi-long range order*.

- in 1D at $T > 0$, the integral in Eq. (2.38) diverges linearly, yielding an exponential decay of $g^{(1)}(\mathbf{r})$, $g^{(1)}(\mathbf{r}) \propto e^{-r/r_0}$.

Therefore, in the last two cases, which correspond to low dimensions, large phase fluctuations prevent the establishment of long-range order.

However, although large *phase* fluctuations forbid condensation, a kind of "coherent" state can be identified at sufficiently low temperatures. Indeed, the computation of *density* fluctuations, either from Bogoliubov theory (2.36) or from hydrodynamic approaches [155], reveals that *in the presence of interactions*, density fluctuations are suppressed below a critical tem-

perature [11]. Such a state, characterized by weak density fluctuations, has been referred to since Popov [156] as a *quasi-condensate* (QBEC), and is defined by the condition $\langle \delta^2 n \rangle \ll n^2$. Equivalently, this implies that the second-order correlation function $g^{(2)}$ satisfies $g^{(2)}(0) = 1$ [12]. In other words, a QBEC does not have first-order (phase) coherence as a BEC, but exhibits second-order (density) coherence. An alternative definition of a QBEC indeed requires that the phase coherence length be much larger than the density coherence length [157–159]. In a quasicondensate, the density is close to its average value and thermodynamic properties are locally similar to those of a BEC.

Bogoliubov theory in the density-phase representation

As we have discussed above, the hypothesis on which relied the Bogoliubov theory (i.e. the existence of a condensate wavefunction) is invalidated in low-dimensions where large phase fluctuations prevent condensation in a state of well defined phase. An alternative and more general formulation of the theory, which does not require the existence of a condensate, was introduced by Popov [156], and proves particularly relevant in low dimensions. The latter relies on the density-phase representation of the field operator,

$$\hat{\psi}(\mathbf{r}) = \mathrm{e}^{i\hat{\theta}(\mathbf{r})}\sqrt{\hat{n}(\mathbf{r})}, \tag{2.39}$$

where the density ($\hat{n}$) and phase ($\hat{\theta}$) operators satisfy the bosonic commutation rule $[\hat{n}(\mathbf{r}), \hat{\theta}(\mathbf{r}')] = i\delta(\mathbf{r} - \mathbf{r}')$. In this representation, the general Hamiltonian of the weakly-interacting Bose gas (2.11) rewrites

$$\hat{H} = \int \sqrt{\hat{n}}\Big[\frac{-\hbar^2}{2m}\left(\nabla^2 - |\nabla\hat{\theta}|^2\right) + V(\mathbf{r}) + \frac{g}{2}\hat{n}\Big]\sqrt{\hat{n}}\,\mathrm{d}\mathbf{r}. \tag{2.40}$$

Similarly to the standard Bogoliubov approach, Popov's idea consists in developing density and phase operators around classical fields,

$$\hat{n}(\mathbf{r}) = n_0(\mathbf{r}) + \delta\hat{n}(\mathbf{r}), \qquad \hat{\theta}(\mathbf{r}) = \theta_0(\mathbf{r}) + \delta\hat{\theta}(\mathbf{r}), \tag{2.41}$$

assuming small density and small gradient of phase fluctuations [13]. Importantly, this hypothesis of slowly variating phase fluctuations does not require phase fluctuations to be weak. For instance, Popov's theory can be used in situations where no condensate exists due to large phase fluctuations (e.g. varying from 0 to 2π over the whole system size), provided the phase fluctuations locally vary sufficiently slowly. It is therefore particularly well-suited to describe quasicondensates.

Hamiltonian (2.40) is then perturbatively expanded in fluctuation terms.

To zeroth order, it yields the two-coupled equations for the classical fields $n_0(\mathbf{r})$ and $\theta_0(\mathbf{r})$,

$$-\frac{\hbar^2}{2m}\left(\frac{\nabla^2\sqrt{n_0}}{\sqrt{n_0}} - |\nabla\theta_0|^2\right) + V - \mu + gn_0 = 0 \tag{2.42}$$

$$\nabla(n_0\nabla\theta_0) = 0. \tag{2.43}$$

Remarkably, Eqs. (2.42) and (2.43) exactly coincide with the GPE (2.13) for the field $\psi_0(\mathbf{r}) = \mathrm{e}^{i\theta_0(\mathbf{r})}\sqrt{n_0(\mathbf{r})}$. In many cases, when no constraint is imposed on the phase, one

[11] The critical temperature goes to zero when the interactions vanish.

[12] Notice that interactions are indeed crucial to have a quasicondensate since $g^{(2)}(0) = 2$ for an ideal gas.

[13] It can in fact be shown that weak density fluctuations also imply weak fluctuations of the phase gradient [160].

immediately gets $\theta_0(\mathbf{r}) = 0$, while $\sqrt{n_0(\mathbf{r})}$ obeys then the usual Gross-Pitaevskii equation. Exceptions to this situation can be encountered when considering phase-twisted boundary conditions, as commonly done when studying the superfluidity [14], or when studying the relative phase between coupled BECs, as done in chapter 5 . Therefore, we will consider here the most general situation.

At second order in the fluctuation terms, Hamiltonian (2.40) reads

$$\hat{\mathcal{H}}^{(2)} = \frac{1}{2}\int \left(\hat{B}^\dagger - \hat{B}\right) \mathcal{L}_{GP}(\mathbf{r}) \begin{pmatrix} \hat{B} \\ \hat{B}^\dagger \end{pmatrix} \mathrm{d}^d\mathbf{r} \; + cst. \tag{2.44}$$

where

$$\hat{B} \equiv \frac{\delta\hat{n}(\mathbf{r})}{2\sqrt{n_0(\mathbf{r})}} + i\sqrt{n_0(\mathbf{r})}\delta\hat{\theta}(\mathbf{r}) \tag{2.45}$$

and

$$\mathcal{L}_{GP} = \begin{pmatrix} \left[-\frac{\hbar^2}{2m}\left(\nabla^2 + 2i\nabla\theta_0\cdot\nabla - |\nabla\theta_0|^2\right) + V - \mu + 2gn_0 \right] & gn_0 \\ -gn_0 & -\left[-\frac{\hbar^2}{2m}\left(\nabla^2 + 2i\nabla\theta_0\cdot\nabla - |\nabla\theta_0|^2\right) + V - \mu + 2gn_0 \right]^* \end{pmatrix}. \tag{2.46}$$

Remarkably, Hamiltonian $\hat{\mathcal{H}}^{(2)}$ is diagonalized in the same canonic form as in the usual Bogoliubov approach [Eq. (2.24)], using the same Bogoliubov transform [Eq. (2.22)] (with $\hat{B}$ replacing $\delta\hat{\psi}$), provided the Bogoliubov wavefunctions u_ν and v_ν are solutions of the Bogoliubov equations

$$\mathcal{L}_{GP}\begin{pmatrix} u_\nu \\ v_\nu \end{pmatrix} = \varepsilon_\nu \begin{pmatrix} u_\nu \\ v_\nu \end{pmatrix}. \tag{2.47}$$

Note that here again, the zero-modes $\hat{P}$ and $\hat{Q}$ can be left aside provided the Bogoliubov wavefunctions are properly orthogonalized with respect to the ground state. In the density-phase picture, the Bogoliubov transformation (2.22) is more likely rewritten explicitely in terms of phase and density fluctuations,

$$\delta\hat{n}(\mathbf{r}) = \sqrt{n_0(\mathbf{r})}\sum_\nu \left(f_\nu^{-\perp}\hat{b}_\nu + f_\nu^{-\perp *}\hat{b}_\nu^\dagger\right) \tag{2.48}$$

$$\delta\hat{\theta}(\mathbf{r}) = \frac{1}{2i\sqrt{n_0(\mathbf{r})}}\sum_\nu \left(f_\nu^{+\perp}\hat{b}_\nu - f_\nu^{+\perp *}\hat{b}_\nu^\dagger\right) \tag{2.49}$$

with $f_\nu^{\pm\perp} = u_\nu^\perp \mp v_\nu^\perp$, the superscript $\perp$ indicating orthogonalization with respect to the ground-state.

The density-phase representation yields the same excitation spectrum and wavefunctions, as well as ground-state energy and second-order correlation function $g^{(2)}$, Eq. (2.36). It is thus remarkable that the previous results also apply in low dimensions, although no true condensate

[14] The superfluidity is indeed obtained from the answer of the fluid to an imposed velocity flow, which amounts to impose a gradient in the phase of the condensate wavefunction.

exists. As regards the first-order correlation function $g^{(1)}$, the situation is less simple. The density-phase representation yields

$$g^{(1)}(\mathbf{r}-\mathbf{r}') = \frac{1}{N}\sum_{\mathbf{k}\neq 0} e^{-i\mathbf{k}(\mathbf{r}-\mathbf{r}')}[v_{\mathbf{k}}^2 + (u_{\mathbf{k}}^2 + v_{\mathbf{k}}^2)N_{\mathbf{k}}] \tag{2.50}$$

which is the same expression as Eq. (2.35), but without the first term n_0. Although this result captures the absence of long-range order in low dimensions, it is inconsistent with the usual Bogoliubov theory in 3D, which is well-described by Eq. (2.35). Moreover, a more careful inspection of Eq. (2.50) reveals the presence of divergences in low dimensions. Those inconsistencies can in fact be traced to the fact that the density-phase picture does not rely on a precise definition of the phase operator, and needs to be regularized.

Regularizations of Bogoliubov theory

Several attempts have been made to overcome this long-standing issue. Popov first developed a functional integral approach [156], but the latest requires the introduction of an arbitrary cutoff, so that there is no full equivalence in 3D with the Bogoliubov theory. A successful method to treat this problem was provided by Mora and Castin [154], who improved the density-phase formulation by introducing a grid discretisation to properly define the phase and density operators, and built a unified theory where all divergences have been solved. The latter in particular recovers all the results of the usual Bogoliubov theory, for instance as regards density fluctuations and second-order correlation function $g^{(2)}$. Most interestingly, their proper treatment enabled them to exactly compute phase fluctuations and the first-order correlation function (and not only their asymptotic behaviour) in all dimensions. In the case where a true condensate is present, their formula for $g^{(1)}$ coincides with the usual Bogoliubov theory, Eq. (2.35). More importantly, in low dimensions, they find the remarkable formula

$$g^{(1)}(\mathbf{r}) = \sqrt{n(\mathbf{r})n(0)}\exp\left[\frac{g^{(1),Bogo}(\mathbf{r})}{\sqrt{n(\mathbf{r})n(0)}} - 1\right], \tag{2.51}$$

where $g^{(1),Bogo}(\mathbf{r})$ is given by Eq. (2.50).

Conclusion

The Bogoliubov theory successfully describes the Bose gas in the weakly-interacting regime. Although originally introduced in the 3D case where a true condensates exists, it can also apply to quasicondensates, and is therefore very general. Moreover, it can advantageously be used in inhomogeneous systems, proving thus a powerful tool when addressing the question of disorder. Since it precisely describes the collective elementary excitations of the system, it is particularly well-suited for an investigation of the collective localization transitions, which is the main topic of this manuscript. Therefore, it is to some extent one of the cornerstones of this manuscript, and will be widely used in the next chapters in various situations.

Chapter 3

Propagation of collective pair excitations in disordered many-body Bose superfluids

Plus il y a de gruyère, plus il y a de trous,
et malheureusement, plus il y a de trous,
eh bien moins il y a de gruyère.
Coluche

Collective excitations govern most *dynamical* properties of many-body quantum systems. In many-body dynamics, propagation of correlations, relaxation of integrable systems, and thermalization processes, are for instance determined by the transport properties of collective excitations [161]. Those issues have known a renewed interest sparked by the recent development of quantum devices with long coherence times and dynamically controlable parameters, such as ultracold atomic gases and superconducting circuits [162]. In those systems, out-of-equilibrium dynamics can for instance be induced by a *quantum quench*, i.e. an abrupt change of some Hamiltonian parameter [119, 121–124]. A quantum quench generates collective excitations, which can then propagate and mediate long-range energy transfer throughout the system.

As discussed in Sec. 1.2.4, understanding how disorder alters this dynamics remains a challenging issue, especially in quantum systems where one-body [2] or many-body [9, 10, 13, 70–72, 79–81] Anderson localization is expected to possibly break ergodicity. So far, absence of thermalization and persistence of local fluctuations were only reported for systems where localization is the rule, e.g. one-dimensional spin [73, 74] and Fermi [77, 82, 83] systems. The case of Bose systems in higher dimensions, on which we will focus in this chapter, is much less advanced, although one can anticipate a richer behavior. On the one hand, disorder in dimension higher than one sparks a variety of transport regimes, including incoherent diffusion, weak localization, and strong localization [163]. On the other hand, repulsive interactions in Bose systems can compete or cooperate with disorder, inducing nontrivial localization effects [11, 12, 164, 165], which are still debated.

Furthermore, it should be pointed out that collective excitations govern also some *static* properties of interacting quantum systems. They generically determine the finite-temperature

behaviour of most observables, as well as quantum fluctuations around the ground state at zero temperature. In particular, in the case of a Bose gas we will consider in this chapter, collective excitations are directly linked with coherence properties and macroscopic quantities, such as superfluidity. Understanding the effect of disorder on collective excitations can thus help understand how disorder destroys those quantities and characterize the superfluid to Bose glass phase transition at finite temperature (see Sec.1.2.2), which remains an open question.

Therefore, understanding the localization properties of collective excitations in Bose gases is not only directly relevant to describe many-body dynamical properties, but can as well pave the way towards the investigation of the disordered bosons phase diagram at finite temperature.

A generic and important starting point in the understanding of localization in correlated quantum systems relies on a classification according to the symmetries of their excitations [166]. For Fermi systems, it is mostly based on the three classes of random matrices [167] as well as chiral or particle-hole symmetries [168]. For Bose systems, a strong distinction arises between Goldstone and non-Golstone modes [14,169]. In particular, localization is generically suppressed for low-energy Goldstone modes.

In the precise case of a repulsively interacting Bose superfluid, it has been shown that although weak interactions destroy single-particle localization (the system being an extended superfluid), localization can survive at the level of collective excitations, which are in this case Bogoliubov quasiparticles [13, 79]. Localization properties of collective excitations have then been investigated, and several studies have agreed that localization should generically be suppressed for phonon excitations [13, 79, 170], in agreement with the anticipated behaviour for Goldstone modes. However, such conclusions were based on a weak disorder analysis, which holds only in dimension $d \leq 2$ where localization occurs for arbitrary weak disorder. They are challenged in higher dimension, where the onset of the Anderson transition requires sufficiently strong disorder. Strong disorder may then affect the very nature of the excitations, and deeply alter this localization picture.

In this chapter, we develop a formalism allowing us to treat both the weak and strong disorder case, which will permit to study localization in 3D as well, and provide an intuitive description of the nature of the excitations and the physics at stake. The chapter is organized as follows. In Sec. 3.1, we use the Bogoliubov theory to set up a scattering problem describing the transport of the excitations. This problem is then reformulated in terms of an effective screened scattering problem. The latter is solved in Sec. 3.2, first for a generic impurity model, before extending the results to others models of disorder. In particular, we find that the competition of disorder, screening, and density depletion yields a strongly non-monotonic and non-universal energy dependence of the disorder parameter, which controls the localization properties. In three dimensions, the resulting localization diagram exhibits several classes of mobility spectra, characterized by either no or several mobility edges. Section 3.3 is devoted to a more detailed analysis of the effect on disorder correlations, which may be used to obtain richer and tailored localization diagrams. Finally, we quantify the validity conditions of our approach in Sec. 3.4, before discussing observability and experimental implications of our predictions.

3.1 Devising a scattering problem for the excitations

We consider a disordered Bose fluid in arbitrary dimension d, in the presence of weak repulsive interactions. Its dynamics can be captured by the many-body grand-canonical Hamiltonian

$$\hat{\mathcal{H}} = \int \left\{ \hat{\Psi}^\dagger \left[\frac{-\hbar^2 \nabla^2}{2m} + V(\mathbf{r}) - \mu \right] \hat{\Psi} + \frac{g}{2} \hat{\Psi}^\dagger \hat{\Psi}^\dagger \hat{\Psi} \hat{\Psi} \right\} \mathrm{d}^d\mathbf{r} \tag{3.1}$$

where m is the particle mass, μ denotes the chemical potential, and the repulsive interactions are modeled by a contact potential of coupling constant $g > 0$. The field operator is conveniently written $\hat{\Psi} = \mathrm{e}^{i\hat{\theta}}\sqrt{\hat{n}}$, where the phase ($\hat{\theta}$) and density ($\hat{n}$) operators obey the commutation rule $[\hat{n}(\mathbf{r}), \hat{\theta}(\mathbf{r}')] = i\delta(\mathbf{r} - \mathbf{r}')$.

The disordered potential, V, is chosen to be a random field with spatially homogeneous statistical properties. We assume without loss of generality that it is of vanishing average $\langle V \rangle = 0$ (which amounts to choose the zero of energies adequately). We denote by $V_\mathrm{R} = \sqrt{\langle V^2 \rangle}$ its root-mean-square amplitude and

$$C(\mathbf{r}) = \langle V(\mathbf{r}')V(\mathbf{r}+\mathbf{r}') \rangle \equiv V_\mathrm{R}^2 c_2(\mathbf{r}/\sigma_\mathrm{R}) \tag{3.2}$$

its two-point correlation function, where σ_R is the correlation length and c_2 is the dimensionless correlation function (see appendix A). We will also assume the disorder to be isotropic, which means that $C(\mathbf{r})$ is a radial function, $C(\mathbf{r}) = C(r)$. In Fourier space, isotropy ensures that the power spectrum of the disorder $\tilde{C}(\mathbf{q}) = \int C(\mathbf{r}) e^{-i\mathbf{q}.\mathbf{r}} d^d\mathbf{r}$ is as well a radial function.

Furthermore, the translation of Eq. (3.2) to Fourier space reads

$$\tilde{C}(\mathbf{q}) = V_\mathrm{R}^2 \sigma_\mathrm{R}^d \tilde{c_2}(\mathbf{q}\sigma_\mathrm{R}) \tag{3.3}$$

and

$$\langle \tilde{V}(\mathbf{q}) \tilde{V}^*(\mathbf{q}') \rangle = (2\pi)^d \delta(\mathbf{q} - \mathbf{q}').\tilde{C}(\mathbf{q}) \tag{3.4}$$

The dimensionless power spectrum $\tilde{c_2}$ is therefore a radial [$\tilde{c_2}(\mathbf{q}) = \tilde{c_2}(q)$)], positive [$\tilde{c_2}(\mathbf{q}) \geq 0$] and normalized [$\int \tilde{c_2}(\mathbf{q}) d^d\mathbf{q} = (2\pi)^d$] function.

In the weakly-interacting regime we are interested in ($n \gg mg/\hbar^2$), meanfield theory provides a good description of the Bose gas, as detailed in chapter 2. Therefore, to devise a scattering problem for the excitations, we will follow the Bogoliubov-Popov approach [156]. As already explained, such an approach mostly consists in a perturbative expansion of Hamiltonian (3.1) in weak fluctuation terms, around the inhomogeneous classical fields ($\nabla\theta_\mathrm{c}, n_\mathrm{c}$) which minimize the classical energy functional associated to Hamiltonian (3.1).

Therefore, we will proceed in three successive steps. Firstly, we will determine the inhomogeneous classical fields ($\nabla\theta_\mathrm{c}, n_\mathrm{c}$), which will in particular provide us with a precise description of the disordered density profile of the condensate. This will be the object of Sec. 3.1.1. Then, in Sec. 3.1.2, expanding Hamiltonian (3.1) in the weak fluctuation terms $\nabla\hat{\theta}(\mathbf{r})$ and $\hat{\delta n}(\mathbf{r}) = \hat{n}(\mathbf{r}) - n_\mathrm{c}(\mathbf{r})$ will allow us to write the Bogoliubov equations which govern the behaviour of collective excitations. As we shall see, this will define a scattering problem for the excitations, whose universal transport properties can be straightforwardly inferred from one-parameter scaling theory. However, to obtain non-universal transport properties, which are necessary to completely characterize the localization behaviour of collective excitations, we will have to resort to a microscopic approach, which will be the object of Sec. 3.1.3. This will set up an explicit scattering problem, which we will be in a position to solve for any model of disorder in the next sections.

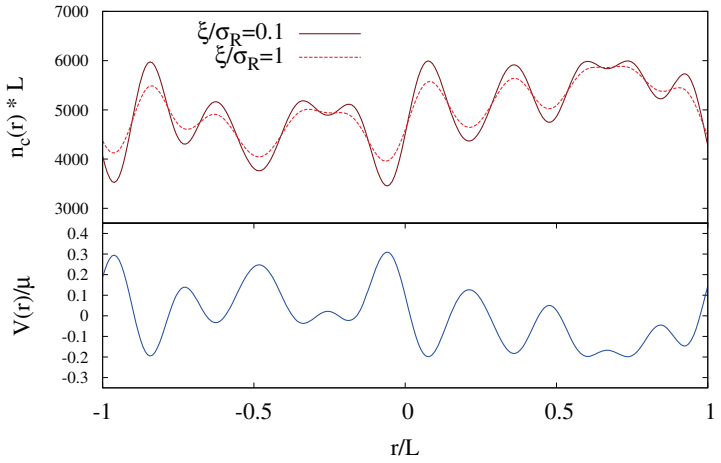

Figure 3.1: Density background in the weak disorder case, as numerically obtained by solving the GPE (3.5) using imaginary time propagation. The system has a size $2L$ and contains $N = 10^4$ atoms. Due to the disorder, the density is modulated around its average value $Ln_c = 5000$. If the limit $\xi \ll \sigma_R$ (solid red line), the density profile follows the spatial modulations of the bare disorder. For $\xi \gtrsim \sigma_R$ (dashed red line), it follows the modulations of a smoothed potential $\tilde{V}$ where short-wavelength variations of the bare potenital have been smoothed out.

3.1.1 The inhomogeneous density background

The fields $\nabla\theta_c$ and n_c are the solutions of the Gross-Pitaevskii equation, Eqs. (2.42) and (2.43). Since no constraint is imposed on the phase of the condensate, one immediately sees that the latter is uniform, $\nabla\theta_c = 0$, and that n_c is the solution of the Gross-Pitaevskii equation (GPE) for the density

$$\Big[-\frac{\hbar^2\nabla^2}{2m} + V(\mathbf{r}) - \mu + g n_c(\mathbf{r}) \Big] \sqrt{n_c(\mathbf{r})} = 0, \tag{3.5}$$

In the following, we determine and describe the disordered density background n_c, which is given by the solution of Eq. (3.5).

Let us first recall that contrary to the disordered Schrödinger equation, which can yield exponentially localized wavefunctions, the non linear term of the GPE always makes the ground state delocalized, in the sense that no localization of the density profile can occur on asymptotically large scales. Indeed, two distant finite subsystems with typically similar variations of $V(\mathbf{r})$ and similar kinetic energy cannot have significantly different average densities, since the GPE would then yield different chemical potentials for the two subsystems, violating equilibrium. In other words, contrary to the single-particle Schrödinger equation, which does not involve directly the absolute amplitude of the wavefunction, the iteracting term here does so; it balances the external potential, the kinetic energy and the chemical potential, and therefore cannot drop on lagre scales if the potential has homogeneous properties.

Therefore, the disordered density profile is traditionally determined as a perturbation of the homogeneous density profile $n_c = \mu/g$. More precisely, for weak disorder, Eq. (3.5) can be solved using straightforward perturbation theory [171, 172]. It is now well-known that at first

order, the density profile follows the modulations of a so-called *smoothed* disorder,

$$n_{\rm c}(\mathbf{r}) = \frac{\mu - \tilde{V}(\mathbf{r})}{g}, \tag{3.6}$$

where, in Fourier space,

$$\tilde{V}(\mathbf{q}) = \frac{V(\mathbf{q})}{1 + \xi^2 |\mathbf{q}|^2}, \tag{3.7}$$

with $\xi = \hbar/\sqrt{4m\mu}$ denoting the *healing length* of the condensate. The latter is traditionally interpreted as the typical length over which the condensate density can accomodate to spatial variations of an external potential. If $\xi \ll \sigma_{\rm R}$ (*Thomas-Fermi regime*), the potential V varies on a length scale much larger than ξ, so that the density profile can follow its spatial modulations, $\tilde{V} = V$. If $\xi \gg \sigma_{\rm R}$, the potential V varies on a length scale shorter than ξ. In this case, a density profile following the modulations of the bare potential is thus no longer energetically favorable since it generates too much kinetic energy. The density then follows the modulations of a smoothed potential $\tilde{V}$, where short-wavelength variations of the bare potenital have been smoothed out (see Fig. 3.1).

However, the previous approach is not valid for strong disorder, mainly because it does not take into account the possible depletion of the density around the local maxima of the disordered potential. To incorporate this effect, which will play a crucial role in the following, we extend the perturbative approach by writing the density field in the generic form

$$n_{\rm c}(\mathbf{r}) = \frac{\mu + \Delta - \eta(\mathbf{r})}{g}, \tag{3.8}$$

where the field $\eta(\mathbf{r})$ describes the modulations of the density due to the disorder, and the quantity Δ is a shift in the chemical potential which allows us to impose the conventional condition that $\eta(\mathbf{r})$ is of zero statistical average. Since the density is positive everywhere, $n_{\rm c}(\mathbf{r}) \geq 0$, the field $\eta(\mathbf{r})$ is bounded above, $\eta(\mathbf{r}) \leq \mu + \Delta$. Notice that necessarily, $\mu + \Delta \geq 0$ since $\eta(\mathbf{r})$ cannot be negative everywhere.

Then, the general idea of the approach consists in inserting the generic expression Eq. (3.8) into the Gross-Pitaevskii equation (3.5), and solving it self-consistently for $\eta(\mathbf{r})$ and Δ. We detail below the resolution before analysing the physics of the solution.

Self-consistent resolution

To solve self-consistently the GPE for $\eta(\mathbf{r})$ and Δ, we first rewrite Eq. (3.8) in the form $\sqrt{n_{\rm c}} = \sqrt{\dfrac{\mu + \Delta}{g}}(1 + \psi_1)$, and insert it in the GPE, lifting temporarily the constraint $\psi_1 \geq -1$. We then linearize it at first order in ψ_1 and V. This yields

$$\psi_1(\mathbf{r}) = -\frac{\Delta + \tilde{V}(\mathbf{r})}{2\mu + 3\Delta} \tag{3.9}$$

where, in Fourier space,

$$\tilde{V}(\mathbf{q}) = \frac{V(\mathbf{q})}{1 + \xi_\Delta^2 |\mathbf{q}|^2}. \tag{3.10}$$

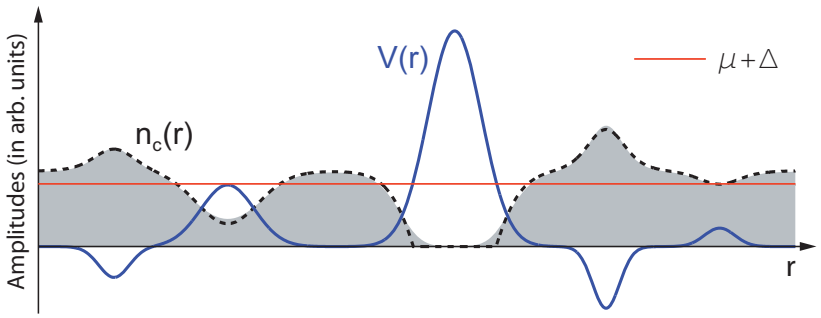

Figure 3.2: One-dimensional cut of the density profile of a Bose superfluid in a disordered potential [full line, $V(\mathbf{r})$]: exact numerical solution of the GPE (3.5) [shaded area, $n_c(\mathbf{r})$] vs. self-consistent solution using Eq (3.8) [dashed line], for a disorder of amplitude $V_R/\mu = 0.87$ and correlation length $\sigma_R = \xi$. The density profile may be locally depleted around disorder maxima.

The quantity $\tilde{V}(\mathbf{r})$ is a generalized smoothed potential [171], where the healing length is renormalized by the shift Δ to the value $\xi_\Delta = \hbar/\sqrt{4m(\mu + 3\Delta/2)}$. From ψ_1, we immediately infer n_c and η, which yields, putting back the constraint that it is bounded above,

$$\eta(\mathbf{r}) = (\mu + \Delta) \ \min\left\{\frac{\Delta + \tilde{V}(\mathbf{r})}{\mu + 3\Delta/2}, 1\right\}. \tag{3.11}$$

The quantity Δ is then determined using the condition $\langle\eta(\mathbf{r})\rangle = 0$, which yields

$$0 = \Delta + \langle\min\{\tilde{V}(\mathbf{r}), \mu + \Delta/2\}\rangle, \tag{3.12}$$

where $\langle\ldots\rangle$ denotes statistical averaging. Note that Eq. (3.12) ensures that $\mu + 3\Delta/2 \geq 0$, so that the above quantity ξ_Δ is well defined.

Therefore, the density field $n_c(\mathbf{r})$ (3.8) is finally found by solving self-consistently Eqs. (3.10) and (3.12) for Δ and $\tilde{V}(\mathbf{r})$, and using Eq. (3.11) to deduce $\eta(\mathbf{r})$.

Discussion

The previous solution, Eq. (3.11), shows that the density modulations $\eta(\mathbf{r})$ follow those of a disordered field $\tilde{V}(\mathbf{r})$, which is smoother than the bare disorder due to a finite healing length. However, due to the presence of the *min* function, the field $\eta(\mathbf{r})$ locally saturates to the constant value $\mu + \Delta$ at positions where $\tilde{V}(\mathbf{r})$ typically exceeds the chemical potential μ (more precisely, where $\tilde{V}(\mathbf{r}) \geq \mu + \Delta/2$). In those regions, which will be referred to as *depleted regions*, we thus have $n_c(\mathbf{r}) \approx 0$ (see Fig. 3.2).

In order to interpret the shift Δ, we may rewrite Eq. (3.12) in the form

$$\begin{aligned}
\Delta &= -\langle\min\{\tilde{V}, \mu + \Delta/2\}\rangle \\
&= -\int d\tilde{V}\, P(\tilde{V})\, \min\{\tilde{V}, \mu + \Delta/2\} \\
&= -\int_{\text{depl.}} d\tilde{V}\, P(\tilde{V})(\mu + \Delta/2) - \int_{\text{non depl.}} d\tilde{V}\, P(\tilde{V})\tilde{V} \\
&= \int_{\text{depl.}} d\tilde{V}\, P(\tilde{V})\, [\tilde{V} - (\mu + \Delta/2)],
\end{aligned} \tag{3.13}$$

where $P(\tilde{V})$ is the probability distribution of the smoothed potential, "depl." (resp. "non depl.") denotes the depleted (resp. non depleted) regions, and where we have used the fact that $\tilde{V}$ is of zero statistical average.

From Eq. (3.13), it appears that the quantity Δ represents the weight of the part of the smoothed potential that is truncated in the depleted regions, as illustrated below :

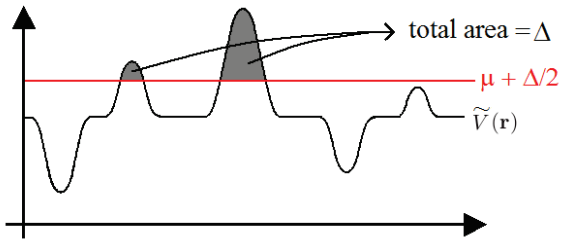

In particular, in the case of weak disorder for which $\tilde{V}(\mathbf{r})$ never exceeds μ, we get $\Delta = 0$, so that we recover from Eqs. (3.10) and (3.12) the solution given by usual perturbation theory, Eq. (3.6) [171, 172]. For stronger disorder, Δ is finite and depleted regions appear at positions where $\tilde{V}(\mathbf{r}) \geq \mu + \Delta/2$. Moreover, both the amplitude of the density modulations and the healing length are then renormalized by the shift Δ. Therefore, the self-consistent solution Eq. (3.11) accounts for the local depletion of the density field around the disorder maxima, an effect that will crucially affect the propagation of collective excitations.

The above self-consistent procedure can be numerically implemented in a very simple way. Starting from $\Delta = 0$, we iterate the following two-step process until convergence :

(i) Use Eq. (3.10) to compute $\tilde{V}$ from Δ and the bare disorder;

(ii) Use Eq. (3.12) to compute a new value of Δ (Δ^{new}) from $\tilde{V}$ and the current value of Δ (Δ^{old}), by $\Delta^{new} = -\langle \min\{\tilde{V}(\mathbf{r}), \mu + \Delta^{old}/2\}\rangle$.

Once Δ and $\tilde{V}(\mathbf{r})$ have been determined, $\eta(\mathbf{r})$ is straightforwardly inferred from Eq. (3.11), and so is $n_c(\mathbf{r})$ from Eq. (3.8). Note that in the numerical calculation, the statistical average is simply replaced by the spatial average of the considered realzation, which allows to determine the density profile for one single disorder realization. Figure 3.2 shows that this procedure is in very good agreement with the exact density profile, which is numerically obtained by imaginary time propagation.

3.1.2 Transport equation for the excitations - Universal properties

Bogoliubov equations : a two-wave scattering problem

Knowing the density field $n_c(\mathbf{r})$, we now turn to the collective excitations. In the density-phase picture [see chapter (2)], Hamiltonian (3.1) is developed up to second order in the Bogoliubov operator

$$\hat{B}(\mathbf{r}) \equiv \frac{\delta\hat{n}(\mathbf{r})}{2\sqrt{n_c(\mathbf{r})}} + i\sqrt{n_c(\mathbf{r})}\hat{\theta}(\mathbf{r}) \tag{3.14}$$

where $\hat{\theta}$ and $\delta\hat{n}$ denote phase and density fluctuations. The resulting quadratic Hamiltonian is then diagonalized by expanding the Bogoliubov operator into the excitation basis,

$$\hat{B}(\mathbf{r}) = \sum_{\varepsilon}\{u_\varepsilon(\mathbf{r})\hat{b}_\varepsilon + v^*_\varepsilon(\mathbf{r})\hat{b}^\dagger_\varepsilon\}, \tag{3.15}$$

where $\hat{b}_\varepsilon$ is the annihilation operator of a Bogoliubov quasiparticle of energy ε. The excitation fields $u_\varepsilon(\mathbf{r})$ and $v_\varepsilon(\mathbf{r})$ are then determined by the Bogoliubov-de-Gennes equations (2.47). The latter involve the density field n_c, and rewrite, after replacing it by its expression (3.8),

$$\mathcal{L}_0 \begin{pmatrix} u_\varepsilon \\ v_\varepsilon \end{pmatrix} + \mathcal{U}(\mathbf{r}) \begin{pmatrix} u_\varepsilon \\ v_\varepsilon \end{pmatrix} = \varepsilon \begin{pmatrix} u_\varepsilon \\ v_\varepsilon \end{pmatrix}, \tag{3.16}$$

where we have on purpose separated the two contributions

$$\mathcal{L}_0 = \begin{pmatrix} -\dfrac{\hbar^2\nabla^2}{2m} + \mu + 2\Delta & +\mu + \Delta \\ -\mu - \Delta & +\dfrac{\hbar^2\nabla^2}{2m} - \mu - 2\Delta \end{pmatrix}$$

and

$$\mathcal{U}(\mathbf{r}) = \begin{pmatrix} +V(\mathbf{r}) - 2\eta(\mathbf{r}) & -\eta(\mathbf{r}) \\ +\eta(\mathbf{r}) & -V(\mathbf{r}) + 2\eta(\mathbf{r}) \end{pmatrix}.$$

In this form, Eq. (3.16) devises a well-defined two-wave scattering problem. The dynamics of a given excitation at energy ε is governed by the homogeneous propagator $\mathcal{L}_0$ and scattering from a disordered medium defined by $\mathcal{U}(\mathbf{r})$. The latter combines the two random fields $V(\mathbf{r})$ and $\eta(\mathbf{r})$, which are strongly correlated according to Eqs. (3.10) and (3.11).

Universal transport properties

Universal transport properties can be obtained using the one-parameter scaling (OPS) theory [44], which proved successful for analyzing linear [166,173,174] as well as nonlinear [175] disordered systems. As we shall see, it is easily extended to the case of excitations.

The general idea of a scaling theory is that the relevant macroscopic properties of a system can be inferred by analysing how those properties evolve when increasing the system size. The scaling theory of localization is traditionnaly formulated in terms of a dimensionless conductance, which is supposed to be the only scaling variable of the system. The latter is identified to the so-called *Thouless number* [176], which is the ratio of the energy-scale associated to diffusion across a finite sample of size L,

$$\delta\varepsilon = \hbar D_\mathrm{B}/L^2$$

(with $D_\mathrm{B} = w l_\mathrm{B}/d$ the classical diffusion constant, $w = \hbar^{-1}|\partial\varepsilon/\partial\mathbf{k}|$ the excitation velocity, and l_B the Boltzmann transport mean-free path), to the energy-level spacing,

$$\Delta\varepsilon = 1/N(\varepsilon)L^d$$

(with $N(\varepsilon)$ the density of states per unit volume). In the diffusive regime, if k_ε is the momentum associated to energy ε, then $N(\varepsilon) \propto k_\varepsilon^{d-1}/|\partial\varepsilon/\partial\mathbf{k}| = k_\varepsilon^{d-1}/\hbar w$, so that

$$G(L) \propto (k_\varepsilon l_\mathrm{B})(k_\varepsilon L)^{d-2}.$$

In the localized regime, the conductance is exponentially small,

$$G(L) \sim \exp(-L/L_\mathrm{loc})$$

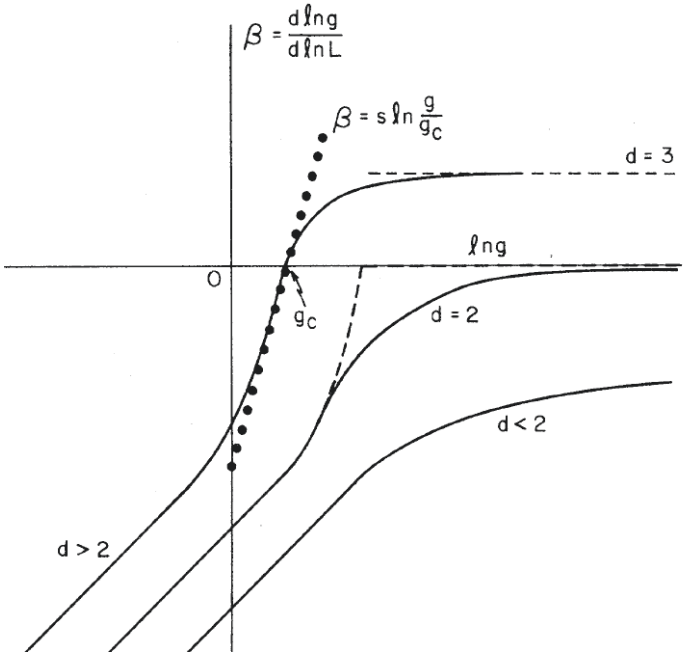

Figure 3.3: RG flow $\beta(L)$ of the one-parameter scaling theory of localization in dimensions 1, 2 and 3. In 3D, the crossing with the horizontal axis indicates the transition point between the diffusive and the localized regimes. Figure from the original paper [44].

with $L_{\rm loc}$ the localization length.

The idea is then to develop a renormalization-group (RG) analysis of this size-dependent conductance. The evolution of the conductance under a change in the system size is determined by the RG flow $\beta \equiv d\log G/d\log L$. It can be shown that it is a regular, monotonic function of G only [44]. The latter is plotted on Fig. 3.3. In the diffusive regime (large G, right part of the figure), $\beta \equiv d\log G/d\log L \sim d-2$. In the localized regime (small G, left part of the figure), $\beta \sim \log G$. The OPS then predicts the following well-known behavior. For $d \leq 2$, $\beta(G)$ is strictly negative and $G(L)$ always flows down to the localized regime when increasing the system size. In such case, all states are localized, and the localization length $L_{\rm loc}$ is found to scale linearly with $l_{\rm B}$ in 1D, $L_{\rm loc} \propto l_{\rm B}$, and exponentially in 2D, $\log(L_{\rm loc}/l_{\rm B}) \propto k_\varepsilon l_{\rm B}$. Conversely, for $d > 2$, $\beta(G)$ has both negative (for small G) and positive (for large G) values and crosses zero at $G_{\rm c} \sim 1$. This point is an unstable RG fixed point, known as the mobility edge, which separates a diffusive regime from a localized regime. Therefore, a localization transition occurs for $k_\varepsilon l_{\rm B} \simeq 1$.

At this stage, there is virtually no difference between single-particle and many-body localization universal scaling laws, for they are independent of the dispersion relation. In particular, all excitations are localized in 1D and 2D, while a localization transition shows up in 3D. Nevertheless the localization behaviour crucially depends on the *inverse disorder parameter* (IDP) $k_\varepsilon l_{\rm B}$, which determines the onset of 3D Anderson localization for $k_\varepsilon l_{\rm B} \lesssim 1$. For single particles in continuous space, $k_\varepsilon l_{\rm B}$ usually increases monotonously with energy, giving rise to a single mobility edge [1]. What happens for pair excitations in the interacting Bose fluid ?

[1] Exceptions exist for some disorder correlations (see for instance Refs [47,177–179]), a case that we disregard here.

3.1.3 Microscopic approach

To completely solve the scattering problem (3.16), one therefore has to estimate the disorder parameter $k_\varepsilon l_\mathrm{B}$, which requires to resort to a microscopic approach. A fruitful, although approximate, approach is to use diagrammatic perturbation theory and retain the leading-order disorder terms [17]. For single particles, it is now a well-established method, whose basics are reviewed in appendix B. This in paricular permits to characterize field and intensity transport, and compute, among others, the Boltzmann transport mean-free path l_B. For pair excitations, it is a much more complicated problem, since the scattering problem (3.16) involves twice as many waves as for single-particles. So far, this two-wave problem has been solved at the level of field transport, i.e. for single-scattering only [172]. As regards intensity transport, from which is traditionally computed the transport mean-free path, it is much more involved, since it a priori involves all possible diagrams coupling the two Bogoliubov waves and their conjugates.

A solution to this problem can be achieved by finding an appropriate linear combination of the two Bogoliubov modes which will dominate the diagrammatic expansion. In other words, this will enable us to reduce the two-wave scattering problem (3.16) to an effective single-wave problem, which can then be solved by applying the standard diagrammatic perturbation theory procedure.

Decoupling into an effective single-wave problem

To do so, we generalize the approach of Ref. [79] to the strong disorder case where $\Delta \neq 0$. We first rewritte Eq. (3.16) in the form

$$\frac{\hbar^2}{2m}\nabla^2 \begin{pmatrix} u_\varepsilon \\ v_\varepsilon \end{pmatrix} = \begin{pmatrix} -\varepsilon+\mu+2\Delta & \mu+\Delta \\ \mu+\Delta & \varepsilon+\mu+2\Delta \end{pmatrix} \begin{pmatrix} u_\varepsilon \\ v_\varepsilon \end{pmatrix} + \begin{pmatrix} V(\mathbf{r})-2\eta(\mathbf{r}) & -\eta(\mathbf{r}) \\ -\eta(\mathbf{r}) & V(\mathbf{r})-2\eta(\mathbf{r}) \end{pmatrix} \begin{pmatrix} u_\varepsilon \\ v_\varepsilon \end{pmatrix}. \tag{3.17}$$

A suitable basis to perform a diagrammatic expansion in leading disorder terms is found by applying the linear transform $(u_\varepsilon, v_\varepsilon) \to (g_\varepsilon^+, g_\varepsilon^-)$ that diagonalises the homogeneous term in Eq. (3.17), i.e. the matrix $M \equiv \begin{pmatrix} -\varepsilon+\mu+2\Delta & \mu+\Delta \\ \mu+\Delta & \varepsilon+\mu+2\Delta \end{pmatrix}$. It yields

$$\begin{pmatrix} g_\varepsilon^+ \\ g_\varepsilon^- \end{pmatrix} = \begin{pmatrix} \hbar^2\gamma_\varepsilon^2/2m-\Delta+\varepsilon & -\hbar^2\gamma_\varepsilon^2/2m+\Delta+\varepsilon \\ \hbar^2 k_\varepsilon^2/2m+\Delta-\varepsilon & -\hbar^2 k_\varepsilon^2/2m-\Delta-\varepsilon \end{pmatrix} \begin{pmatrix} u_\varepsilon \\ v_\varepsilon \end{pmatrix}, \tag{3.18}$$

where $-\hbar^2 k_\varepsilon^2/2m \equiv -\sqrt{\varepsilon^2+(\mu+\Delta)^2}+(\mu+2\Delta)$ and $\hbar^2\gamma_\varepsilon^2/2m \equiv \sqrt{\varepsilon^2+(\mu+\Delta)^2}+(\mu+2\Delta)$ are the eigenvalues of the homogeneous matrix M.

Without any approximation at this stage, the BdGEs in the $(g_\varepsilon^+, g_\varepsilon^-)$ basis then read

$$\frac{\hbar^2 k_\varepsilon^2}{2m} g_\varepsilon^+(\mathbf{r}) = -\frac{\hbar^2}{2m}\nabla^2 g_\varepsilon^+(\mathbf{r}) + \Big[V(\mathbf{r}) - f_-(\epsilon)\eta(\mathbf{r})\Big] g_\varepsilon^+(\mathbf{r}) + \Phi_+(\epsilon)\eta(\mathbf{r}) g_\varepsilon^-(\mathbf{r}) \tag{3.19}$$

$$-\frac{\hbar^2 \gamma_\varepsilon^2}{2m} g_\varepsilon^-(\mathbf{r}) = -\frac{\hbar^2}{2m}\nabla^2 g_\varepsilon^-(\mathbf{r}) + \Big[V(\mathbf{r}) - f_+(\epsilon)\eta(\mathbf{r})\Big] g_\varepsilon^-(\mathbf{r}) + \Phi_-(\epsilon)\eta(\mathbf{r}) g_\varepsilon^+(\mathbf{r}), \tag{3.20}$$

with $f_\pm(\epsilon) = \frac{2\sqrt{\varepsilon^2+(\mu+\Delta)^2}\pm(\mu+\Delta)}{\sqrt{\varepsilon^2+(\mu+\Delta)^2}}$ and $\Phi_\pm(\epsilon) = \frac{\sqrt{\varepsilon^2+(\mu+\Delta)^2}\pm(\mu+\Delta)}{\sqrt{\varepsilon^2+(\mu+\Delta)^2}}$.

In the absence of disorder, Eqs. (3.19) and (3.20) are now decoupled and are straightforward to solve. The g_ε^+ modes are plane waves of momentum k_ε, while the g_ε^- are evanescent waves of penetration length γ_ε^{-1}. The latter vanish identically if the system is infinite or has periodic boundary conditions [2].

In the presence of disorder, we can therefore make the assumption that $|g_\varepsilon^-| \ll |g_\varepsilon^+|$ by at least one order in $V_{\rm R}/\mu$ and Δ/μ. Keeping only the leading-order terms in disorder in Eq. (3.20), one can neglect the second term of the r.h.s. Equation (3.20) is then straightforwardly solved by

$$g_\varepsilon^- \simeq -\frac{2m}{\hbar^2\beta_\varepsilon^2}\Phi_-(\varepsilon)\int d\mathbf{r}'\; G_{1/\gamma_\varepsilon}(\mathbf{r}-\mathbf{r}')\eta(\mathbf{r}')g_\varepsilon^+(\mathbf{r}') \tag{3.21}$$

where G_{1/γ_ε} is the Green function associated to the differential operator $-\nabla^2/\gamma_\varepsilon^2+1$. In Fourier space,

$$G_{1/\gamma_\varepsilon}(\mathbf{q}) = \frac{(2\pi)^{-d/2}}{1+q^2/\gamma_\varepsilon^2}.$$

In real space, it is a positive function of integral 1 decaying on a length scale $1/\gamma_\varepsilon$. Then, since $\dfrac{2m}{\hbar^2\gamma_\varepsilon^2} < \mu$ and $|\Phi_-(\varepsilon)| < 1$ for all energy ε, we have

$$|g_\varepsilon^-| \lesssim \int G_{1/\gamma_\varepsilon}(\mathbf{r}-\mathbf{r}')|\eta(\mathbf{r}')||g_\varepsilon^+(\mathbf{r}')|d\mathbf{r}'/\mu \lesssim V_{\rm R}/\mu|g_\varepsilon^+|,$$

which is consistent with our initial assumption $|g_\varepsilon^-| \ll |g_\varepsilon^+|$. Therefore, the last term of Eq. (3.19) can be neglected, yielding a closed equation for g_ε^+ :

$$\frac{\hbar^2 k_\varepsilon^2}{2m}g_\varepsilon^+(\mathbf{r}) = -\frac{\hbar^2}{2m}\nabla^2 g_\varepsilon^+(\mathbf{r}) + \mathcal{V}_\varepsilon(\mathbf{r})g_\varepsilon^+(\mathbf{r}) \tag{3.22}$$

with

$$\mathcal{V}_\varepsilon(\mathbf{r}) = V(\mathbf{r}) - f(\varepsilon)\eta(\mathbf{r}) \tag{3.23}$$

where for simplicity, we now denote by $f(\epsilon)$ the quantity $f_-(\epsilon) = \frac{2\sqrt{\varepsilon^2+(\mu+\Delta)^2}-(\mu+\Delta)}{\sqrt{\varepsilon^2+(\mu+\Delta)^2}}$.

Equation (3.22) contains the leading disorder terms and features an effective single-wave scattering problem. Transport properties are entirely determined by the wave g_ε^+. The g_ε^- wave is enslaved on g_ε^+, as expressed by Eq. (3.21), and only renormalizes the disorder seen by g_ε^+. The quantity $\mathcal{V}_\varepsilon(\mathbf{r})$ indeed defines a so-called *screened potential*, in the sense that it can be viewed as the screening of the bare potential $V(\mathbf{r})$ by the density background encoded in $\eta(\mathbf{r})$. It notably depends on the energy ε of the Bogoliubov excitation. Note as well that since $\langle\eta(\mathbf{r})\rangle = 0$ by construction, the screened potential is of zero statistical average.

Disorder parameter of excitations

The effective single-wave scattering problem (3.22) can now be solved by standard quantum transport theory [17]. Details of this procedure are provided in appendix B. In brief,

[2] This is rigorously true only for excitations of energy $\varepsilon > \sqrt{2\Delta(\mu+3\Delta/2)}$ -otherwise both modes are evanescent-. However, it is indeed the case of almost all excitations, except for a very narrow energy range at the bottom of the spectrum. Therefore, in the following, we will always assume that it is the case for the considered excitations.

localization properties are determined by a two-step process [45, 46].

Firstly, the transport mean-free path is calculated in the Boltzmann approximation where interference between multiple-scattering paths are neglected. Within the *on-shell* approximation, which amounts to assimilate the spectral function to the disorder-free one, diagrammatic theory (see appendix B) yields, in $d > 1$:

$$\frac{1}{k_\varepsilon l_{\rm B}(\varepsilon)} \simeq \frac{2\pi m^2}{\hbar^4 k_\varepsilon^{4-d}} \int \frac{d\Omega_d}{(2\pi)^d} (1-\cos\theta) \mathcal{C}_\varepsilon[2k_\varepsilon \sin(\theta/2)], \tag{3.24}$$

where $\mathcal{C}_\varepsilon$ is the power spectrum of the screened potential and $d\Omega_d$ the infinitesimal solid angle in d dimensions. Notice that Eq. (3.24) is valid only for models of disorder with isotropic correlation functions [18], as considered here [3]. The 1D case is particular, as the angular integral reduces to the two angles $\theta = 0$ and $\theta = \pi$. Moreover, since the contribution of $\theta = 0$ vanishes due to the anisotropy factor $(1 - \cos\theta)$, the IDP in that case is entirely determined by the backscattering process $\theta = \pi$, which yields the formula

$$\frac{1}{k_\varepsilon l_{\rm B}(\varepsilon)} \simeq \frac{2\pi m^2}{\hbar^4 k_\varepsilon^{4-d}} \mathcal{C}_\varepsilon[2k_\varepsilon], \tag{3.25}$$

This expression in 1D can be derived in a more rigorous way [13] by considering the Lyapunov exponent which, according to the scaling theory, scales as $\Gamma = 1/L_{loc} \propto 1/l_{\rm B}$. Therefore, our approach captures as well the 1D case provided Eq. (3.25) is used instead of Eq. (3.24).

Secondly, localization is found using either the one-parameter scaling theory [44], as discussed in the previous Sec. 3.1.2, or the self-consistent approach [45, 46]. The self-consistent theory incorporates interference corrections on the top of diffusive dynamics, which yields a self-consistent equation for the diffusive constant or the localization length. Both approaches give in 3D the approximate localization threshold $k_\varepsilon l_{\rm B} \sim 1$, and the respective scalings $L_{\rm loc} \propto l_{\rm B}$ and $\log(L_{\rm loc}/l_{\rm B}) \propto k_\varepsilon l_{\rm B}$ in 1D and 2D, which we will use in the following.

The calculation of the IDP $k_\varepsilon l_{\rm B}$ from Eq. (3.24) requires to know the power spectrum of the screened potential. Since the latter depends on the density background $\eta(\mathbf{r})$, which includes both density modulations and depletion induced by the disorder [see Eq. (3.11)], it is in general non universal, in the sense that it depends on the precise model of the disorder. For any given model of disorder, one can in principle numercially solve the density background, Eq. (3.11), compute the screened potential, Eq. (3.23), and deduce the IDP from Eq. (3.24).

3.2 Localization of excitations for an impurity model

For the sake of concreteness, and to facilitate the discussion, we will in this section focus on a precise impurity model. The reasons of such a choice are twofold. The first one is pedagocical, since an impurity model more easily allows for a physical interpretation, as positive and negative peaks are clearly identified. The second one is technical : one shall indeed see that in the limit of dilute impurities, the power spectrum of the screened potential can be expressed as a sum over impurities of decoupled individual terms. This dispenses us to generate a full disorder realization, which can be computationnally demanding in 3D, but allows us to solve instead the meanfield background and the screened potential at the level of each single impurity.

[3] For extension to anisotropic correlation functions, see Refs. [47, 180].

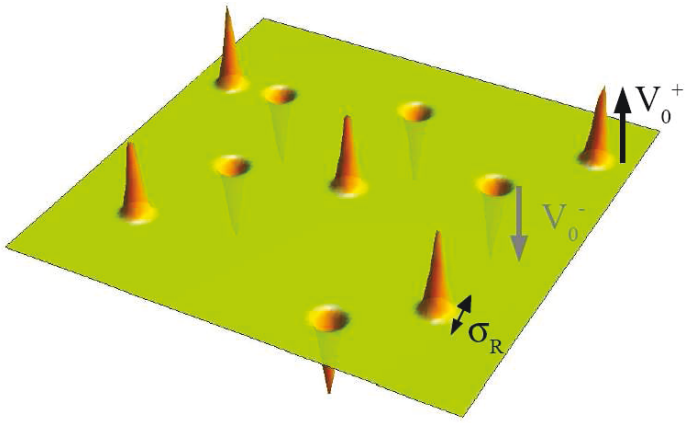

Figure 3.4: Schematic view of the impurity model (3.26).

3.2.1 The imbalanced impurity model

The model

The generic impurity model we will consider (see Fig .3.4) is described by the potential

$$V(\mathbf{r}) = \sum_j V_j^0 h(\mathbf{r} - \mathbf{r}_j) - \overline{V}. \tag{3.26}$$

It is made of identical Gaussian-shaped impurities of width $\sigma_{\rm R}$, $h(\mathbf{r}) = \exp(-\mathbf{r}^2/2\sigma_{\rm R}^2)$, which are independently and randomly distributed in space, with a uniform probability distribution. Their amplitudes V_j^0 are independent random variables which can only take two values $+V_0^+ > 0$ or $-V_0^- < 0$, with equal probability. The impurity density is denoted ρ. The constant term $\overline{V} \equiv \rho(\sqrt{2\pi}\sigma_{\rm R})^d(V_0^+ - V_0^-)/2$ ensures that the potential $V(\mathbf{r})$ is of vanishing statistical average.

Let us emphasize a few properties of this model of disorder. Such a potential is by construction stationnary and of zero statistical average. Its correlation function reads, in the thermodynamic limit where both the volume and the number N of impurities go to infinity at fixed impurity density ρ :

$$C(\mathbf{r}) = \langle V(0)V(\mathbf{r})\rangle = \rho(\sqrt{\pi}\sigma_{\rm R})^d e^{-r^2/4\sigma_{\rm R}^2}[(V_0^+)^2 + (V_0^-)^2]/2. \tag{3.27}$$

Therefore, the standard deviation of this potential reads $V_{\rm R}^2 = \rho(\sqrt{\pi}\sigma_{\rm R})^d[(V_0^+)^2 + (V_0^-)^2]/2$. Moreover, since $\tilde{C}(0)$ is finite, such a potential has a white-noise limit (see appendix A), in the sense that its low-energy properties can be obtained by replacing it by a delta-correlated potential, $C(\mathbf{r}) = D\delta(\mathbf{r})$ with $D = \tilde{c}_2(0)V_{\rm R}^2\sigma_{\rm R}^d = 2^d\pi^{d/2}V_{\rm R}^2\sigma_{\rm R}^d$.

The dilute limit

We will further assume that the impurities are dilute, namely $\rho\sigma_{\rm R}^d \ll 1$. In this limit, we show below that the impurities decouple, in the sense that the power spectrum of the screened disorder expresses as a sum over each single impurity.

To show this, we recall that the screened potential can be expressed [see Eqs. (3.23) and (3.11)] by

$$\mathcal{V}_\varepsilon(\mathbf{r}) = V(\mathbf{r}) - f(\varepsilon)\frac{\mu+\Delta}{\mu+3\Delta/2}\left[\min\left(\mu+\Delta/2,\tilde{V}(\mathbf{r})\right)+\Delta\right] \tag{3.28}$$

The quantity $\min[\mu+\Delta/2,\tilde{V}(\mathbf{r})]$ can then be calculated in the limit of dilute impurities,

$$\begin{aligned}\min\left(\mu+\Delta/2,\tilde{V}(\mathbf{r})\right) &= \min\left(\mu+\Delta/2,\sum_j V_j^0\tilde{h}(\mathbf{r}-\mathbf{r}_j)-\overline{V}\right)\\ &= \min\left(\mu+\Delta/2+\overline{V},\sum_j V_j^0\tilde{h}(\mathbf{r}-\mathbf{r}_j)\right)-\overline{V}\\ &\simeq \sum_j\left[\min\left(\mu+\Delta/2+\overline{V},V_j^0\tilde{h}(\mathbf{r}-\mathbf{r}_j)\right),\right]-\overline{V}\end{aligned}$$

where we have used the fact that in the dilute limit, distinct impurities do not overlap. Note that adding and substracting $\overline{V}$ as done above is essential since the second argument of the *min* function has to be zero far from the impurities for the decoupling to work. Therefore,

$$\begin{aligned}\mathcal{V}_\varepsilon(\mathbf{r}) &= \sum_j V_j^0 h(\mathbf{r}-\mathbf{r}_j)-\overline{V}\\ &\quad -f(\varepsilon)\frac{\mu+\Delta}{\mu+3\Delta/2}\sum_j\min\left(\mu+\Delta/2+\overline{V},V_j^0\tilde{h}(\mathbf{r}-\mathbf{r}_j)\right)+f(\varepsilon)\frac{\mu+\Delta}{\mu+3\Delta/2}(\overline{V}-\Delta)\end{aligned} \tag{3.29}$$

Since the screened potential is of zero statistical average, its correlation function reads $\mathcal{C}_\varepsilon(\mathbf{r}) = \langle\mathcal{V}_\varepsilon(0)\mathcal{V}_\varepsilon(\mathbf{r})\rangle$, which yields:

$$\begin{aligned}\mathcal{C}_\varepsilon(\mathbf{r}) &= \left\langle\sum_{i,j}V_i^0V_j^0h(0-\mathbf{r}_i)h(\mathbf{r}-\mathbf{r}_j)\right\rangle\\ &\quad -2f(\varepsilon)\frac{\mu+\Delta}{\mu+3\Delta/2}\left\langle\sum_{i,j}V_i^0h(0-\mathbf{r}_i)\min\left(\mu+\Delta/2+\overline{V},V_j^0\tilde{h}(\mathbf{r}-\mathbf{r}_j)\right)\right\rangle\\ &\quad +f(\varepsilon)^2\left(\frac{\mu+\Delta}{\mu+3\Delta/2}\right)^2\left\langle\sum_{i,j}\min\left(\mu+\Delta/2+\overline{V},V_i^0\tilde{h}(0-\mathbf{r}_i)\right)\min\left(\mu+\Delta/2+\overline{V},V_j^0\tilde{h}(\mathbf{r}-\mathbf{r}_j)\right)\right\rangle\end{aligned} \tag{3.30}$$

up to constant terms which will have no impact on the IDP [see Eq. (3.24)]. To simplify this expression, we then use the fact that the statistical average is an average over all the random parameters of the disorder model (positions $\mathbf{r}_j$ and amplitudes V_j^0),

$$\langle\ldots\rangle = \prod_j\int\ldots P(V_j^0)dV_j^0\frac{d^d\mathbf{r}_j}{\mathcal{V}},$$

where $\mathcal{V}$ denotes the volume of the system, and the probability density for the impurity amplitudes $P(V)$ is simply for our model $P(V) = (\delta(V-V_0^+)+\delta(V+V_0^-))/2$. This yields the final

expression

$$\begin{aligned}
\mathcal{C}_\varepsilon(\mathbf{r}) &= \frac{\rho}{2}(V_0^+)^2\int h(\mathbf{r}')h(\mathbf{r}+\mathbf{r}')d\mathbf{r}' \qquad (3.31)\\
&-2f(\varepsilon)\frac{\mu+\Delta}{\mu+3\Delta/2}\frac{\rho}{2}\int V_0^+ h(\mathbf{r}')\min\left(\mu+\Delta/2+\overline{V},V_0^+\tilde{h}(\mathbf{r}+\mathbf{r}')\right)d\mathbf{r}'\\
&+\frac{\rho}{2}f(\varepsilon)^2\left(\frac{\mu+\Delta}{\mu+3\Delta/2}\right)^2\int \min\left(\mu+\Delta/2+\overline{V},V_0^+\tilde{h}(\mathbf{r}')\right)\min\left(\mu+\Delta/2+\overline{V},V_0^+\tilde{h}(\mathbf{r}+\mathbf{r}')\right)d\mathbf{r}'\\
&+\frac{\rho}{2}(V_0^-)^2\int h(\mathbf{r}')h(\mathbf{r}+\mathbf{r}')d\mathbf{r}'\\
&-2f(\varepsilon)\frac{\mu+\Delta}{\mu+3\Delta/2}\frac{\rho}{2}\int (-V_0^-)h(\mathbf{r}')\min\left(\mu+\Delta/2+\overline{V},-V_0^-\tilde{h}(\mathbf{r}+\mathbf{r}')\right)d\mathbf{r}'\\
&+\frac{\rho}{2}f(\varepsilon)^2\left(\frac{\mu+\Delta}{\mu+3\Delta/2}\right)^2\int \min\left(\mu+\Delta/2+\overline{V},-V_0^-\tilde{h}(\mathbf{r}')\right)\min\left(\mu+\Delta/2+\overline{V},-V_0^-\tilde{h}(\mathbf{r}+\mathbf{r}')\right)d\mathbf{r}'.
\end{aligned}$$

One now sees the advantage of considering the dilute limit. Since impurities are decoupled in this expression, one does not have necessarily to generate a full impurity disorder, but can directly use Eq. (3.31). In other words, to infer the correlation function of the *full* screened potential, the only quantities to know are the smoothed function of a *single* impurity $\tilde{h}$ and Δ. A priori, those are determined by applying the self-consistent procedure detailed in Sec. 3.1.1 to the *full* disordered potential, which amounts to iterate Eqs. (3.10) and (3.12). However, here again, this latter equation can be rewritten in the dilute limit

$$\begin{aligned}
\Delta = -\langle\min\{\tilde{V}(\mathbf{r}),\mu+\Delta/2\}\rangle &= -\frac{\rho}{2}\int \min\left(\mu+\Delta/2+\overline{V},V_0^+\tilde{h}(\mathbf{r})\right)d^d\mathbf{r} \qquad (3.32)\\
&-\frac{\rho}{2}\int \min\left(\mu+\Delta/2+\overline{V},-V_0^-\tilde{h}(\mathbf{r})\right)d^d\mathbf{r}+\overline{V}
\end{aligned}$$

using the same trick as above to decouple the impurities. This permits to calculate $\tilde{h}$ and Δ without necessarily having to generate the full disordered potential, but by simply iterating Eqs. (3.10) and (3.32).

3.2.2 The disorder parameter of excitations

Using the above procedure, we can now compute from Eq. (3.24) the IDP of the excitations for our impurity model. Figure 3.5 shows the energy dependence of the IDP for the 3D impurity model, in the balanced impurity case ($V_0^+ = V_0^- \equiv V_0$) for three different impurity amplitudes V_0. Depending on the disorder strength, it can exhibit three generic behaviors, that will be analysed in the following :

- case (A) (weak disorder) : non monotonic curve diverging at low and high energy, with one local minimum in-between;

- case (B) (intermediate disorder) : non monotonic curve going to zero at low energy and diverging at high energy, with one local maximum and one local minimum in-between;

- case (C) (strong disorder) : monotonic increasing curve going to zero at low energy and diverging at high energy.

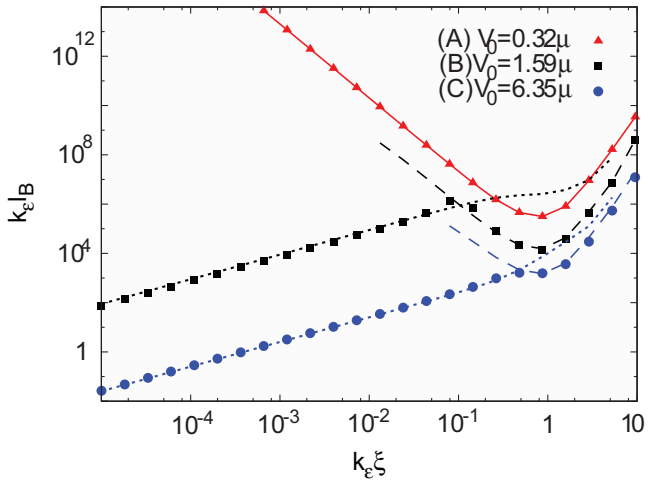

Figure 3.5: Inverse disorder parameter (IDP) versus pair-excitation momentum for the 3D balanced impurity model, with $\sigma_{\rm R} = \xi$, $\rho\sigma_{\rm R}^3 = 2\times10^{-4}$, and for various values of the disorder amplitude $V_0 \equiv V_0^+ = V_0^-$. Shown are the results of Eq. (3.24), with the full screened power spectrum $\mathcal{C}_\varepsilon(\mathbf{q})$ (dots) or with Eq. (3.33) (solid line), as well as the contributions of the bulk (dashed lines) and depleted (dotted lines) regions.

Qualitatively similar curves are found for lower dimensions and for imbalanced impurity cases ($V_0^+ \neq V_0^-$). In all cases, they are of type A, B, or C. The exact positions of the local maximum and minimum then depend on the parameters of the disorder potential. The variety of behaviours for the IDP curves strongly differs from the free-particle case, where the IDP increases monotonously with energy. As we shall see below, it is the result of a non universal interplay between disorder, sceening, and density depletion.

Weak disorder : screening at low-energy

For weak disorder (case A in Fig 3.5), the nonmonotonic energy dependence of the IDP can qualitatively be understood as follows. At high energy, the excitations are insensitive to the density background and behave as free particles in the bare disordered potential. Conversely, at low energy, the excitations are strongly affected by the density background, which screens the disorder and suppresses scattering, enhancing transport.

More precisely, this holds provided the chemical potential exceeds the maximum of the smoothed potential (i.e. for $V_0^+\tilde{h}(0) - \overline{V} < \mu$) so that the density background has no depleted region. In this case, one has $\Delta = 0$ and $\eta(\mathbf{r}) = \tilde{V}(\mathbf{r})$, so that $\mathcal{V}_\varepsilon(\mathbf{r}) = V(\mathbf{r}) - f(\varepsilon)\tilde{V}(\mathbf{r})$. The power spectrum of the screened potential, $\mathcal{C}_\varepsilon(\mathbf{q})$, can then be computed explicitly as a function of that of the bare disorder, $C(\mathbf{q})$, and of the excitation energy, ε. It yields

$$\mathcal{C}_\varepsilon(\mathbf{q}) = \left(1 - \frac{1+4k_\varepsilon^2\xi^2}{1+2k_\varepsilon^2\xi^2}\frac{1}{1+\mathbf{q}^2\xi^2}\right)^2 C(\mathbf{q}). \tag{3.33}$$

From Eqs. (3.24) and (3.25), the IDP is then given by

$$\frac{1}{k_\varepsilon l_{\rm B}(\varepsilon)} \simeq \frac{2\pi m^2}{\hbar^4 k_\varepsilon^{4-d}} \int \frac{d\Omega_d}{(2\pi)^d}(1-\cos\theta)S^2(k_\varepsilon\xi,\cos\theta)C[2k_\varepsilon\sin(\theta/2)] \tag{3.34}$$

in $d > 1$, and

$$\frac{1}{k_\varepsilon l_{\rm B}(\varepsilon)} \simeq \frac{2\pi m^2}{\hbar^4 k_\varepsilon^{4-d}} S^2(k_\varepsilon\xi,\cos\pi)C[2k_\varepsilon] \tag{3.35}$$

in 1D, where

$$S(k_\varepsilon\xi,\cos\theta)=\left(1-\frac{1+4k_\varepsilon^2\xi^2}{1+2k_\varepsilon^2\xi^2}\frac{1}{1+4k_\varepsilon^2\xi^2\sin^2\theta/2}\right)=\frac{2k_\varepsilon^2\xi^2}{1+2k_\varepsilon^2\xi^2}\frac{2k_\varepsilon^2\xi^2(1-\cos\theta)-\cos\theta}{2k_\varepsilon^2\xi^2(1-\cos\theta)+1}. \tag{3.36}$$

Remarkably, the IDP is determined only by the power spectrum of the bare disorder. The so-called *screening function*, S, which is the only difference compared to the free-particle case in Eqs. (3.34) and (3.35), is completely universal. It contains all the influence of interactions, which renormalize the disorder seen by an excitation. At low-energy ($k_\varepsilon\xi\ll 1$), $S^2(k_\varepsilon\xi,\cos\theta)\sim 4(k_\varepsilon\xi)^4\cos^2(\theta)$ vanishes, the bare disorder being efficiently screened by the density background. At high-energy ($k_\varepsilon\xi\gg 1$), $S^2(k_\varepsilon\xi,\cos\theta)\sim 1$ for almost all θ : the screening is irrelevant and one recovers the free-particle physics.

The same function has also been identified in single-scattering processes [172], and in previous studies in the 1D case [13, 79]. However, in $d>1$, Eq. (3.34) shows that the transport length of an excitation results from the contribution of the full on-shell integral. In particular, it is not simply proportional to the free-particule one as it is in the 1D case [13, 79] [see Eq. (3.35)].

Equation (3.34) yields the solid line in Fig. 3.5, which reproduces very well the data in the full energy range for case A.

The behavior of the IDP can now be found by inspection of Eqs. (3.34) and (3.35), which are entirely analytical. A fully detailed discussion of this behaviour is provided in the supplement at the end of this chapter, Sec. 3.6. In brief, we find the following results.

The IDP is directly proportional to the disorder strength $V_{\rm R}^2$, which trivially acts as an *overall magnitude*. Increasing the disorder strength amounts to shift down the IDP curves as those of Fig. 3.5.

For $k_\varepsilon\gg\xi^{-1},\sigma_{\rm R}^{-1}$, the screening function is irrelevant in Eq. (3.34). We then recover the free-particle behavior [18, 47, 180]. In $d>1$, this yields [4]

$$k_\varepsilon l_{\rm B}\sim\frac{\mu^2}{V_{\rm R}^2}\frac{\sigma_{\rm R}}{\xi}(k_\varepsilon\xi)^5. \tag{3.37}$$

Conversely, for $k_\varepsilon\ll\xi^{-1},\sigma_{\rm R}^{-1}$, the screening strongly enhances $k_\varepsilon l_{\rm B}$ compared to the free-particle case and we find, in any dimension

$$k_\varepsilon l_{\rm B}\sim\frac{\mu^2}{V_{\rm R}^2}\Big(\frac{\xi}{\sigma_{\rm R}}\Big)^d(k_\varepsilon\xi)^{-d}. \tag{3.38}$$

Both low-energy and high-energy scalings reproduce the behavior of case A. In-betwwen, the local minimum of the IDP is generically located at

$$k_\varepsilon^{\rm min}\sim\min(1/\xi,1/\sigma_{\rm R}), \tag{3.39}$$

as derived in the supplement at the end of this chapter, Sec. 3.6.

The divergence of the IDP observed at low energy has already been reported in the 1D case, where previous studies [13, 79] have in particular concluded to protected transport

[4] The 1D case is particular, and the scaling can depend on the precise form of the correlation function of the bare disorder, as discussed in the supplement at the end of this chapter, Sec. 3.6.

for low-energy excitations [170]. Most importantly, it is as well in agreement with the universal behavior expected for bosonic Goldstone modes [14, 169]. In a study based on general symmetries properties of the excitations, Gurarie and Chalker indeed found that the localization length for Goldstone modes necessarily diverges at low energy, according to the scalings $L_{\rm loc} \propto \omega^{-2}$ in 1D and $L_{\rm loc} \propto exp^{(\omega_0/\omega)^2}$ in 2D. Those scalings coincide with our low energy expression (3.38), since $\omega \propto k_\varepsilon$ at low energy, and recalling that $L_{\rm loc} \propto l_{\rm B}$ in 1D while $\log(L_{\rm loc}/l_{\rm B}) \propto k_\varepsilon l_{\rm B}$ in 2D.

Let us emphasize that all the previous conclusions rely on a weak disorder assumption, be it the absence of density depletion or the assumption of having Goldstone modes. They accurately describe localization properties in 1D and 2D, where localization occurs for arbitrary weak disorder, but predict the absence of localization at low enegry in 3D. We shall however see below that this picture no longer holds when considering stronger disorder.

Strong disorder : the impact of density depletion

For intermediate to strong disorder (cases B and C in Fig. 3.5), the energy dependence of the IDP strongly differs from the weak disorder case at low energy, where $k_\varepsilon l_{\rm B}$ now increases with the energy. To understand this, it should be noticed that in this case, $V_0^+ \tilde{h}(0) - \overline{V} > \mu$, so that the background density is now locally depleted around the positive impurities. Hence, during its propagation, an excitation goes through two types of regions, namely the *density depleted* region, and the rest, which constitutes the *density bulk* (see Fig. 3.6). Therefore, it will prove convenient to split the screened potential into two contributions

$$\mathcal{V}_\varepsilon(\mathbf{r}) = \mathcal{V}_\varepsilon^{Bulk}(\mathbf{r}) + \mathcal{V}_\varepsilon^{Depl}(\mathbf{r}) \tag{3.40}$$

where

$$\mathcal{V}_\varepsilon^{Bulk}(\mathbf{r}) = \mathcal{V}_\varepsilon(\mathbf{r})|_{Bulk} = \begin{cases} V(\mathbf{r}) - f(\varepsilon)\dfrac{(\mu+\Delta)(\tilde{V}(\mathbf{r})+\Delta)}{\mu+3\Delta/2} & \text{if} \quad \tilde{V}(\mathbf{r}) < \mu + \Delta/2 \\ 0 \quad \text{elsewhere} \end{cases} \tag{3.41}$$

and

$$\mathcal{V}_\varepsilon^{Depl}(\mathbf{r}) = \mathcal{V}_\varepsilon(\mathbf{r})|_{Depl} = \begin{cases} 0 & \text{if} \quad \tilde{V}(\mathbf{r}) < \mu + \Delta/2 \\ V(\mathbf{r}) - f(\varepsilon)(\mu+\Delta) \quad \text{elsewhere} \end{cases} \tag{3.42}$$

In the bulk, the disorder (3.41) seen by an excitation, $\mathcal{V}_\varepsilon^{Bulk}(\mathbf{r})$, may be approximated by $(V(\mathbf{r}) - f(\varepsilon)\tilde{V}(\mathbf{r}))|_{Bulk}$, provided we neglect the quantity Δ, which is valid for low impurity density, $\rho\sigma_{\rm R}^d \ll 1$. Due to the screening of the bare potential by the smoothed one, this so-called *bulk contribution* yields a nonmonotonic contribution to $k_\varepsilon l_{\rm B}$ similar to case A (see Fig. 3.6), up to very slight differences. A first one is that the overall magnitude of this contribution, which we will denote $V_{\rm R}^{B\,2}$, is no longer $V_{\rm R}^2$ but the square amplitude of $\mathcal{V}_\varepsilon^{Bulk}(\mathbf{r})$, which is smaller due to the truncation around the positive impurities. The second one is that since $\mathcal{V}_\varepsilon^{Bulk}(\mathbf{r})$ has a non zero average value, this introduces a shift in k_ε; the latter is nevertheless negligible for weak impurity density, except at very small energy.

In the depleted regions, the disorder (3.42) seen by an excitation, $\mathcal{V}_\varepsilon^{Depl}(\mathbf{r})$, is nothing but the bare disorder, up to a homogeneous shift. In this field, no screening occurs and the excitations thus behave as free particles, yielding a monotonic contribution to $k_\varepsilon l_{\rm B}$ (see

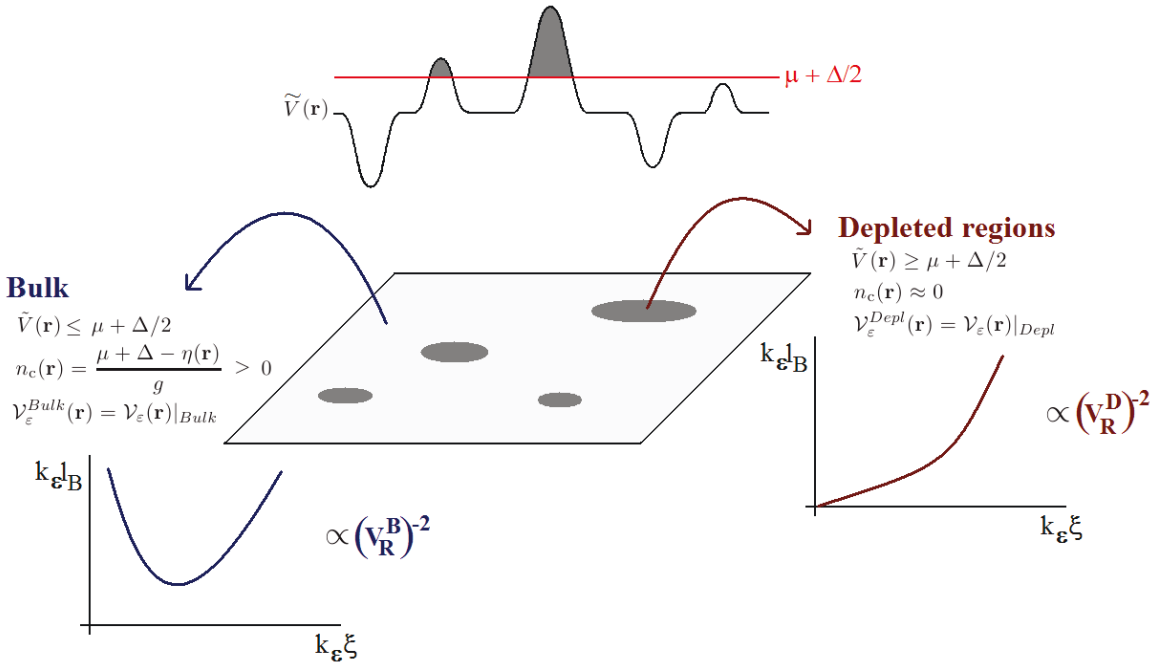

Figure 3.6: Contributions to the IDP of the bulk and depleted regions. Each contribution is characterized by a precise energy dependence for the IDP (decreasing-increasing for the bulk, monotonously increasing for the depleted regions), and by its overall magnitude ($V_R^{B\,2}$ or $V_R^{D\,2}$), which measures the typical disorder strength of the contribution. Neglecting the correlations between those two contributions, the full IDP is dominated by the smallest contribution : therefore, depending on their relative importance, it can exhibit several behaviours, as observed on Fig. 3.5.

Fig. 3.6). In the white-noise limit ($k_\varepsilon \sigma_R \ll 1$), this contribution is $k_\varepsilon l_B \sim (k_\varepsilon \xi)^{4-d}$, while at high energy, $k_\varepsilon l_B \sim (k_\varepsilon \xi)^5$. Here again, its overall magnitude, which we will denote $V_R^{D\,2}$, is smaller than V_R^2 since this *depleted contribution* only comes from a residual disorder, made of the truncated part of the positive impurities. We again do not include the negligible shift of k_ε due to the nonzero average value of $\mathcal{V}_\varepsilon^{Depl}(\mathbf{r})$.

To interpret the various behaviors of the IDP observed in Fig. 3.5, we will neglect the correlations between those two contributions, which amounts to approximate $\mathcal{C}_\varepsilon(\mathbf{q})$ by $\mathcal{C}_\varepsilon(\mathbf{q})|_{Bulk} + \mathcal{C}_\varepsilon(\mathbf{q})|_{Depl}$ [5]. Within this approximation, the disorder parameter $(k_\varepsilon l_B)^{-1}$ is then the sum of the bulk and depleted contributions. Its inverse (the IDP $k_\varepsilon l_B$) is thus dominated by the smallest corresponding contribution. This is clearly visible on Fig. 3.5, where the bulk and depleted contributions have been respectively represented by dashed and dotted lines. Moreover, we are now in a position to understand the various behaviours of the IDP. To obtain the full IDP, one has to compare the bulk and depleted contributions, each one being roughly characterized by a specific energy dependence of the IDP (decreasing-increasing for the bulk, monotonously increasing for the depleted regions), and by its overall magnitude ($V_R^{B\,2}$ or $V_R^{D\,2}$)

[5] Let us emphasize that bulk and depleted contributions *are* in principle correlated; for instance, if $\mathcal{V}_\varepsilon^{Depl}(\mathbf{r}_0) \neq 0$ at some point $\mathbf{r}_0$ (near the center of one impurity), then $\mathcal{V}_\varepsilon^{Bulk}$ will necessarily be non zero close to $\mathbf{r}_0$ (in the non truncated part of the same impurity); therefore, although this approximation holds very well when one contribution clearly dominates the second one, it may become quantitatively inaccurate when both are of the same order of magnitude.

(see Fig. 3.6).

At low energy, the energy dependances of the two contributions differ dramatically : because of the screening in the bulk, the contribution of the depleted region always dominates if it exists, and captures the increasing behavior of $k_\varepsilon l_{\rm B}$.

At intermediate and high energy, where both contributions are finite, the behavior of $k_\varepsilon l_{\rm B}$ crucially depends on the relative magnitudes of the two contributions. When $V_0^+\tilde{h}(0)-\overline{V}\gtrsim\mu$ (case B), only the very upper fraction of the positive impurities is truncated, so that $V_{\rm R}^D \ll V_{\rm R}^B$. Therefore, the bulk starts to dominate at moderate energy. It results in a turning point $k_\varepsilon^{\max}$ where bulk and depleted regions equally contribute to the IDP, yielding there a local maximum. Above it, the high-energy behaviour is dominated by the bulk, and is characterized by the presence of a local minimum. The IDP curve is therefore of type B. When V_0^+ further increases (case C), an increasing part of the positive impurities depletes the density, so that the depleted regions dominate in a wider energy range. As a consequence, $k_\varepsilon^{\max}$ moves to higher values. At some point, it eventually merges with the local minimum $k_\varepsilon^{\min}$, which does not significantly depend on V_0^+. The curve then becomes monotonic. In the limit $V_0^+\tilde{h}(0)-\overline{V}\gg\mu$, the positive impurities are almost entirely truncated. In this case, and for the particular case of the balanced impurity model, bulk and depleted regions exactly equally contribute to the IDP in the high-energy limit.

Therefore, the diversity of behaviours for the IDP arises from the interplay between screening in the bulk and density depletion. While the disorder is efficiently screened in the bulk by the density background, enhancing transport, no screening can arise in the depleted regions, where the excitations thus behave as free particles in a bare residual disorder. This mechanism strongly modifies the universal low-energy behaviour of Goldstone modes. It suggests that depletion alters the very nature of the excitations, which are no longer pure Goldstone modes but locally behave as free particles.

3.2.3 Localization diagram

We now turn to the localization properties of the collective bosonic excitations, focusing on the 3D case where mobility edges appear at the localization threshold $k_\varepsilon l_{\rm B}\sim 1$. Using this criterion, the latter are easily determined from IDP curves as those of Fig. 3.5. At variance with the free-particle case where the IDP increases monotonously with energy, giving rise to one single mobility edge, the case of collective excitations is much more involved. Due to its nonmonotonic energy dependence, the IDP can cross the localization threshold several times. Moreover, due to the non trivial interplay between screening and density depletion, the IDP curves depend on the impurity amplitudes V_0^+ and V_0^- in a very complex way. As a consequence, the resulting localization diagram, shown on Fig. 3.7 as a function of positive (V_0^+) and negative (V_0^-) impurity amplitudes, displays a rich variety of scenarii with up to three mobility edges in the excitation spectrum. The various regions are characterized by the number of mobility edges in the excitation spectrum, which is entirely determined by three conditions.

Firstly, the existence of depleted regions results in a band of localized states at low energy, with one upper mobility edge. Those states are qualitatively similar to free-particle localized states, since localization is dominated here by the propagation of excitations in the depleted regions and subjected to the bare disorder. The condition for having depleted regions defines the roughly vertical left boundary on the diagram. It is given by

$$V_0^+\tilde{h}(0)-\overline{V}=\mu,$$

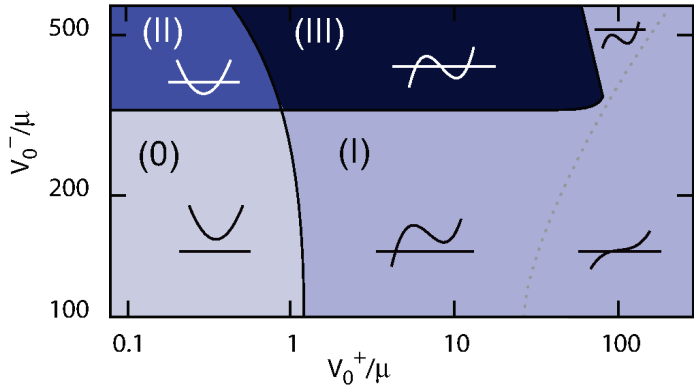

Figure 3.7: Localization diagram of pair excitations in the 3D impurity model, plotted as a function of the amplitudes of positive (V_0^+) and negative (V_0^-) impurities, for $\sigma_R = \xi$ and $\rho\sigma_R^3 = 2 \times 10^{-4}$. It exhibits four classes of mobility spectra, characterized by zero (0), one (I), two (II), or three (III) mobility edges. Note the different scales on the two axes.

i.e. $V_0^+\tilde{h}(0) + \rho(\sqrt{2\pi}\sigma_R)^d V_0^-/2 \simeq \mu$ in the limit of small impurity density, $\rho\sigma_R^d \ll \tilde{h}(0)$. The IDP curve is of type A on the left part and of type B or C on the right part.

Secondly, depending on the position of the local minimum of the IDP, $(k_\varepsilon l_B)^{\min}$, relatively to the localization thresehold, a band of localized states can also arise at mid-energy with two additional mobility edges, which is more specific to many-body localization. As long as $V_0^+ \ll V_0^-$ and the contribution of the depleted regions is weak enough, this local minimum is governed by the bulk contribution. Its position, $k_\varepsilon^{\min}$, is nearly independent of the disorder strength [see Eq. (3.39)] and the value of the IDP at the minimum is proportional to the overall magnitude of the bulk contribution, $(k_\varepsilon l_B)^{\min} \propto 1/(V_0^-)^2$. This yields the nearly horizontal boundary on the diagram, above which a band of localized middle-energy states exists in the excitation spectrum. Therefore, on the left part of the first boundary, there is no mobility edge on the bottom part (0) and two mobility edges on the top part (II). On the right side, there is one mobility edge on the bottom part (I) and three on the top part (III).

On the top part of the diagram, when V_0^+ further increases, the contribution of the depleted regions increases and the band of low-energy localized states grows up; at some point, it merges with the band of middle-energy localized states, and the intermediate band of extended states disappears, yielding only one mobility edge left in the spectrum. The corresponding condition, which defines the nearly vertical boundary on the top right of the diagram, is governed by the position of the local maximum relatively to the threshold (when V_0^+ increases and crosses this boundary, the maximum goes below the threshold and only one mobility edge is left). It thus results from the competition between depleted and bulk contributions. Its inclination is due to the fact that an increase of the depleted contribution (via V_0^+) has to be compensated by a decrease of the bulk contribution (via V_0^-) to keep $(k_\varepsilon l_B)^{\max} \sim 1$.

Conversely, on the bottom part of the diagram, when V_0^+ further increases, the IDP curves turn monotonic at higher V_0^+ (as indicated by the dotted line), but this does not affect the number of mobility edges, which remains one.

3.2.4 Beyond the impurity model

Although obtained in the frame of the impurity model, we expect this diagram to be very generic. As discussed before, the diversity of scenarii for mobility spectra generically arises from the interplay between screening in the bulk and density depletion. However, this interplay is strongly nonuniversal, in the sense that it depends on the precise statistics of the disorder. More precisely, the statistics of the disorder is involved at two different levels :

- The two-point correlations (correlation length σ_{R} and shape of the correlation function $\tilde{c_2}(\mathbf{q})$) govern the screening process and the behaviour of the bulk contribution, as already discussed. A more detailed study of the influence of disorder correlations will be found in Sec. 3.3, showing that the energy dependance of the IDP can be tailored by designing the shape of the correlation function.

- The one-point statistics of the disorder in involved via density depletion in a non trivial way. Indeed, the full probability distribution of the one-point amplitude governs the onset of depletion and the statistics of depleted regions. In particular, the disorder strengh does not only act as an overall magnitude V_{R}^2 as in the weak disorder case [see Sec 3.2.2]. For instance, a blue-detuned and a red-detuned speckle with same amplitude V_{R}^2 will lead to completely different mobility spectra since only in the first case, depleted regions are always present.

Therefore, although the previous localization diagram displays the generic picture, the details of such a diagram, notably the shape of the boundaries, are specific to each model of disorder. Furthermore, a given model of disorder does not necessary display all possibilities. The imbalanced impurity model with a finite correlation length is actually the simplest disorder we found that does.

For instance, for only positive impurities (x-axis of the localization diagram) or in the balanced case (first bisector of the diagram), the only possibilities are (0) or (I) because the minimum of the IDP cannot be controlled independently of the density depletion.

Conversely, for only negative impurities (y-axis of the localization diagram), the depleted region is absent and the only possibilities are (0) or (II).

The case of a white-noise disorder is also limited because the smoothed impurity potential diverges in the center, $\tilde{h}(\mathbf{r}) = \mathrm{e}^{-r/\xi}/4\pi\xi^2 r$. In this case, depleted regions appear as soon as $V_0^+ \neq 0$ and the only left possibilities are (I) and (III). The same situation is encountered with a blue-detuned speckle.

3.3 Influence of the disorder correlations

In this section, we analyse the influence of disorder correlations on the disorder parameter and the localization diagram. In particular, we show that while standard correlation functions lead to very similar results as those of the impurity model, tailored correlations can lead to more complex IDP curves and richer localization diagrams. They can thus eventually be used to enhance either transport or localization at a specific energy. However, we will also show that the effect of disorder correlations is generally expected to be less marked when the spatial dimension increases.

For the sake of simplicity, we will perform this analysis in the weak disorder case without density depletion [6]. The onset of density depletion being mostly governed by the disorder one-point statistics, it can, in a first approximation, be conceptually dissociated from the correlations [7]. In this regime, we recall that the IDP is given in $d > 1$ by Eq. (3.34), which may be rewritten as a function of dimensionless parameters

$$\frac{1}{k_\varepsilon l_{\rm B}} \simeq \left(\frac{V_R}{\mu}\right)^2 \left(\frac{\sigma_R}{\xi}\right)^d \frac{\pi}{8} \frac{1}{(k_\varepsilon \xi)^{4-d}} \int (1-\cos\theta) S^2(k_\varepsilon \xi, \cos\theta) \tilde{c_2}(|2k_\varepsilon \sigma_R \sin(\theta/2)|) \frac{d\Omega_d}{(2\pi)^d}. \quad (3.43)$$

In 1D, Eq. (3.35) should be used, which is rewritten in a dimensionless form

$$\frac{1}{k_\varepsilon l_{\rm B}} \sim \frac{\pi}{8} \left(\frac{V_R}{\mu}\right)^2 \left(\frac{\sigma_R}{\xi^4 k_\varepsilon^3}\right) S^2(k_\varepsilon \xi, \cos\pi) \tilde{c_2}(|2k_\varepsilon \sigma_R|). \quad (3.44)$$

We recall that a detailed analytical inspection of those formulas is provided in the supplement at the end of the chapter, Sec. 3.6.

In both cases, the IDP explicitely depends on the dimensionless power spectrum c_2, which encodes the shape of the disorder correlations. In experiments carried out with speckle potentials, the latter can be precisely designed via the shape and transmission properties of the diffusive plate. More precisely, as shown in Sec. 1.3.2, the power spectrum of the disorder is the autoconvolution of the pupil function (i.e. the intensity distribution within the diffusive plate).

3.3.1 Generic case : Gaussian autocorrelation function

In many ultracold-atom experiments, the autocorrelation function c_2 is Gaussian. Such a case can for instance be achieved with speckle potentials if the pupil function is Gaussian, or with Gaussian impurity disorders. Note that our previous impurity model falls into this category. In this case, the correlation function reads

$$C(\mathbf{r}) = V_R^2 e^{-r^2/\sigma_R^2} \qquad \text{i.e.} \qquad \tilde{c_2}(\mathbf{q}) = \pi^{d/2} e^{-q^2/4}.$$

Figure 3.8(a) shows the disorder parameter $1/k_\varepsilon l_B$ as a function of excitation energy and correlation length in the 3D case. Very similar curves are found in 1D and 2D.

The IDP admits one and only one local minimum, which clearly obeys the general scaling $k_\varepsilon^{min} \propto min(1/\xi, 1/\sigma_{\rm R})$. The absolute minimum of the IDP in the $(k_\varepsilon\xi, \sigma_{\rm R}/\xi)$ plane is obtained in the limit $k_\varepsilon\xi \propto \sigma_{\rm R}/\xi \to 0$. Interestingly, if one looks at the quantity l_B (see Fig 3.8(b) in 1D), the absolute minimum is now reached at finite correlation length and finite energy. In 1D, where $l_B \propto$ Ł$_{loc}$, this yields an absolute localization maximum at finite correlation length, an effect that was already reported in [13]. This effect however disappears in higher dimensions : in 2D for instance, using $\log(L_{\rm loc}/l_{\rm B}) \propto k_\varepsilon l_{\rm B}$, we find the absolute localization maximum in the limit $k_\varepsilon\xi \propto \sigma_{\rm R}/\xi \to 0$.

All those features are in fact very generic to any standard correlation function c_2, i.e. maximum and finite for $q = 0$, monotonously and rapidly decaying.

[6] In the presence of depletion, correlations will influence both the bulk and the depleted contribution, and possibly in different ways, which makes the full analysis very challenging.

[7] This is not rigorously true since depletion is actually governed by the one-point statistics of the *smoothed* disorder, which depends on disorder correlation via the mechanism of smoothing. Such effects are however expected to be relatively small.

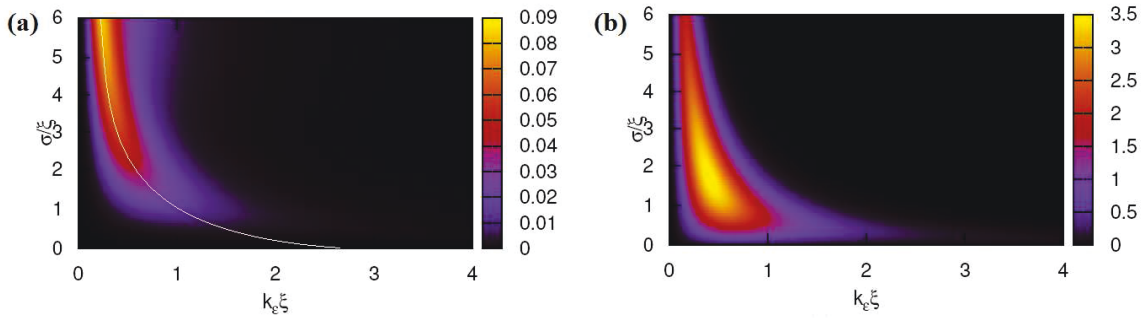

Figure 3.8: (a) Disorder parameter $1/k_\varepsilon l_B$ for a 3D Gaussian disorder, as a function of excitation energy and correlation length. The white solid line represents the local minimum k_ε^{min}, which scales as $k_\varepsilon^{min} \propto min(1/\xi, 1/\sigma_{\rm R})$. (b) Inverse transport length $1/l_B$ for the 1D Gaussian disorder, which gives the localization behaviour (we recall that $1/l_B \propto 1/L_{\rm loc}$ in 1D). An absolute localization maximum occurs at finite correlation length.

3.3.2 Speckle with uniform apertures

Very often in experiments with speckle potentials, the diffusive plane consists in an uniformly illuminated aperture. In this case, the pupil function is simply determined by the shape of the aperture. We will consider here the case of isotropic apertures, where $I(\mathbf{r}) = I_0\Theta(R-|\mathbf{r}|)$ with Θ denoting the Heaviside function. From Eq. (1.9), this yields the following correlation functions :

In 1D,

$$C(\mathbf{r}) = V_R^2 \mathrm{sinC}^2(r/\sigma_{\rm R}) \qquad \text{i.e.} \qquad \tilde{c_2}(\mathbf{q}) = \pi(1-q/2)\Theta(1-q/2).$$

In 2D,

$$C(\mathbf{r}) = V_R^2 \left(\frac{2J_1(r/\sigma_{\rm R})}{r/\sigma_{\rm R}} \right)^2 \qquad \text{i.e.} \qquad \tilde{c_2}(\mathbf{q}) = 8\left(\arccos(q/2) - q/2\sqrt{1-(q/2)^2} \right)\Theta(1-q/2),$$

with J_1 the first Bessel function.

In 3D,

$$C(\mathbf{r}) = V_R^2 \mathrm{sinC}^2(r/\sigma_{\rm R}) \qquad \text{i.e.} \qquad \tilde{c_2}(\mathbf{q}) = \frac{\pi^2}{q}\Theta(2-q).$$

The results for the IDP are shown on Fig. 3.9. They are very similar do the previous case, which should be of no surprise since the correlation function in Fourier space is again monotonously decaying from $q = 0$. All considerations about localization maxima still hold. A few differences should be emphasized.

In 1D, the existence of a cutoff at $q = 2$ in $\tilde{c_2}(\mathbf{q})$ creates an *effective mobility edge* (the IDP is infinite for $k_\varepsilon\sigma_{\rm R} > 1$, and no localization occurs), as represented by the red dashed line on Fig. 3.9(b). This specificity of 1D speckle potentials already appears in the non-interacting case.

In 3D, the divergence of $\tilde{c_2}(\mathbf{q})$ in $\mathbf{q} = 0$, which is responsible from the absence of white-noise limit, modifies the low-energy scaling of the IDP. As discussed in the supplement at the end of this chapter, this yields $k_\varepsilon l_{\rm B} \sim (k_\varepsilon\xi)^{-2}$, instead of $k_\varepsilon l_{\rm B} \sim (k_\varepsilon\xi)^{-3}$ for a model which admits a white-noise limit. Similar corrections to the general scalings of the IDP can also be encountered with speckle potentials exhibiting long-range (e.g. power-law) correlations (see supplement 3.6 at the end of this chapter).

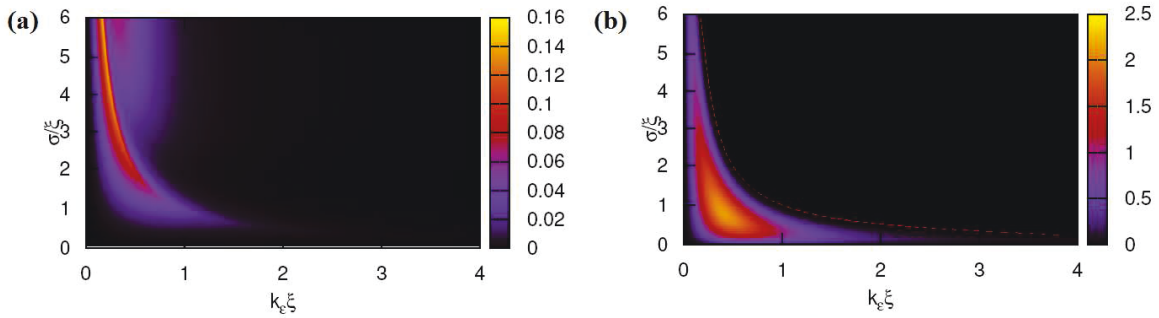

Figure 3.9: (a) Disorder parameter $1/k_\varepsilon l_B$ for a 3D speckle potential with a uniform aperture, as a function of excitation energy and correlation length. (b) Inverse transport length $1/l_B$ for a 1D speckle potential with a uniform aperture. An absolute localization maximum occurs at finite correlation length, and an effective mobility edge (red dashed line) shows up due to the cutoff in the power spectrum of the disorder.

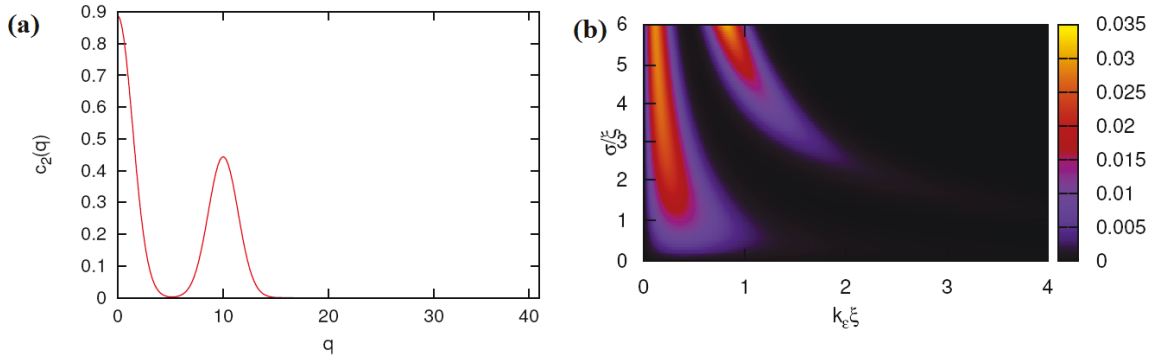

Figure 3.10: (a) Power spectrum of a 1D speckle obtained by crossing two Gaussian beams, Eq. (3.45), for $q_0 = 10$. (b) Disorder parameter $1/k_\varepsilon l_B$ for the 1D speckle disorder obtained by crossing two Gaussian beams, as a function of excitation energy and correlation length. Several localization maxima show up.

Altogether, compared to the previous standard situation, this leads only to minor quantitative changes in the IDP dependence (and therefore in the localization diagram, at fixed one-point statistics of the disorder.).

3.3.3 Tailored correlations

We now turn to major qualitative specificities in the IDP behaviour which can be achieved by tailoring exotic optical potentials. Exotic correlations have already been studied in the non-interacting case [180, 181], and have been shown to possibly modify the standard localization picture. We extend here this analysis to the interacting case.

Multiple localization maxima

As discussed above, the IDP generically displays one single localization maximum. It is however possible, as already observed for free-particles [178, 181], to have several, in particular by designing a non-monotonic correlation function $\tilde{c_2}(\mathbf{q})$.

Several experimental tools can be used to obtain non-monotonic correlation functions with speckle potentials. The 1D experimental configuration proposed in [47] consists in using two

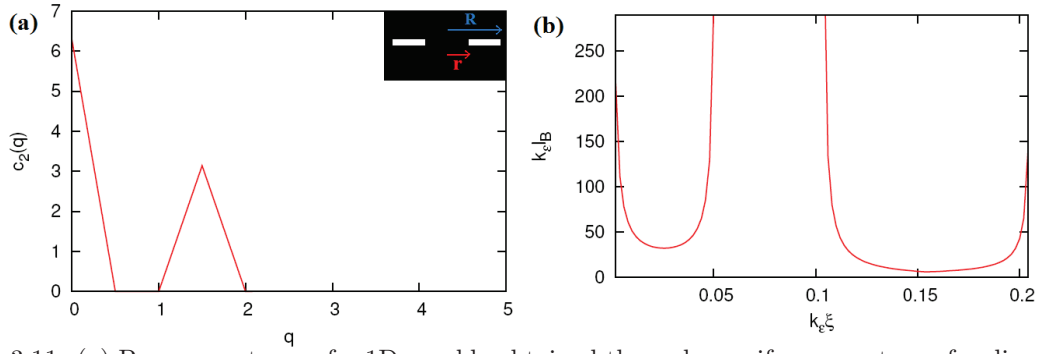

Figure 3.11: (a) Power spectrum of a 1D speckle obtained through a uniform aperture of radius R with a mask of radius r (in inset, the real space configuration), for $r/R = 0.5$. (b) Inverse disorder parameter $k_\varepsilon l_B$ for the 1D speckle obtained from a uniform aperture with a mask. Bands of energy are protected against localization due to vanishing correlations.

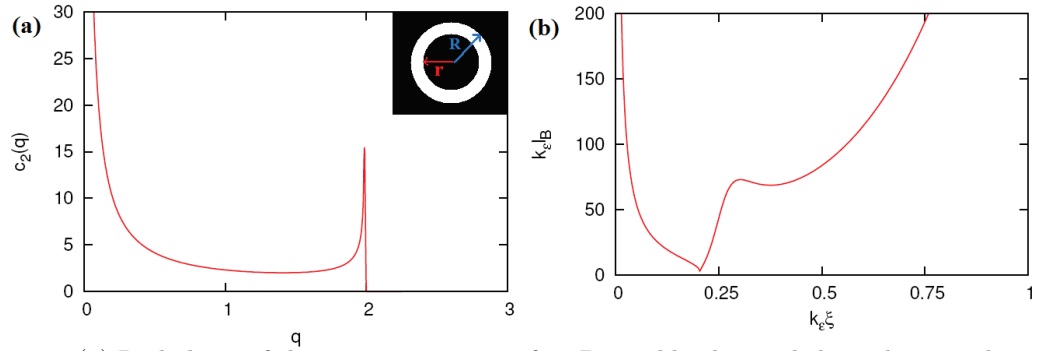

Figure 3.12: (a) Radial cut of the power spectrum of a 2D speckle obtained through a circular aperture of radius R with a mask of radius r (in inset, the real space configuration), for $r/R = 0.95$. (b) Inverse disorder parameter $k_\varepsilon l_B$ for the 2D speckle obtained from a circular aperture with a mask.

crossed Gaussian beams instead of just one, yielding

$$\tilde{c_2}(\mathbf{q}) = \frac{\pi}{4}\Big[e^{-(q-q_0)^2/4} + e^{-q^2/4} + e^{-(q+q_0)^2/4}\Big], \tag{3.45}$$

which is plotted in Fig. 3.10(a). Alternatively, one can send one single laser beam onto a diffusive plate made of a uniformly illuminated aperture partly masked by a dark diaphragm. In 1D and 2D, in the case where the mask is placed at the center of the aperture, this generates non-monotonic correlation functions. The corresponding power spectra are represented on Figs. 3.11(a) (2D) and 3.12(a) (1D).

In 1D, where the energy dependance of the IDP directly follows that of $\tilde{c_2}(q)$ by virtue of Eq. (3.44), such non-monotonic correlation functions always lead to multiple local extrema in the IDP curves [see for instance Fig. 3.10(b) for the 1D two-beam speckle case of Eq. (3.45), or Fig. 3.11(b) for the 1D speckle with a mask]. The example of the 2D speckle with a mask [see Fig. 3.12(b)] shows that it can also be the case in 2D, although the phenomenon is less marked due to the global attenuation by the onshell integral in Eq. (3.43).

Correlation-forbidden localization

We have seen previously that in 1D, a speckle potential can give rise to an effective mobility edge if it exhibits a high-momentum cut-off in its power spectrum. More generally, in 1D, it is straightforward to see from Eq. (3.35) that any power spectrum with zeros at a given momentum

q_0 will result in extended states at the energy $\varepsilon(q_0/2)$. This phenomenon, which was already reported for free particles, survives in the presence of interactions. The only difference is the dispersion relation $\varepsilon(q)$, which is the Bogoliubov one instead of the free-particle one. The case of the 1D speckle with a mask (see Fig. 3.11) offers a concrete example where two bands of extended states appear, localization being there forbidden by disorder correlations.

In higher dimensions, such an effect would require that $\tilde{c_2}(\mathbf{q})$ identically vanish below a certain momentum. The experimental realization of such correlations has remained so far an open challenge.

Correlation-enhanced localization

Conversely, using strongly-peaked correlation functions can enhance localization at a given energy.

In 1D, this is again obvious from Eq. (3.44).

Interestingly, this effect can be expected to survive in 2D. Indeed, the analytical calculation with an "idealized" delta-peaked ring power spectrum, $\tilde{c_2}(\mathbf{q}) \propto \delta(q - q_0)$, leads to a divergence in Eq. (3.43), yielding a vanishing IDP at $2k_\varepsilon\sigma_\mathrm{R} = q_0$. Although this case is purely ideal, highly-peaked off-centered power spectra may enable to reach arbitrarily low localization lengths in 2D. This effect should be all the more marked than any small reduction in the IDP is exponentially transmitted to the localization length in 2D. However, the experimental realization of highly-peaked off-centered power spectra seems more challenging. In particular, the correlation function in real space should have both positive and negative values (in the previous example of a delta-peaked ring, the Fourier transform is a Bessel function). For this reason, such a situation cannot be achieved with speckle configurations, where the real-space correlation function is the square modulus of the Fourier transform of the pupil function.

3.4 Beyond the Bogoliubov approximation- Observability and experimental perspectives

In this section, we show that the previously predicted behaviours for the localization of excitations and the existence of different mobility spectra can be observed in present-day ultracold-atom experiments. In particular, our results rely on the Bogoliubov approximation, which neglects all couplings between excitations and treats them as an ideal gas (see chapter 2). In fact, due to nonlinear couplings, Bogoliubov quasi-particles acquire a finite lifetime. Therefore, the observability of their transport and localization properties requires that this lifetime τ exceed the typical transport mean-free time $\tau_\mathrm{B} \equiv l_\mathrm{B}/w_\varepsilon$ (with w_ε the excitation group velocity). We will show here that this can be achieved experimentally in Sec. (3.4.1), before enlightening some experimental perspectives in Sec. (3.4.2).

3.4.1 Estimation of Beliaev lifetimes

Inhomogeneous Beliaev damping

For sufficiently low temperatures, the decay of Bogoliubov excitations is dominated by Beliaev processes [147,182,183][8]. In such a process, an excitation of momentum $\mathbf{k}$ spontaneously decays into two excitations of momenta $\mathbf{k}'$ and $\mathbf{k} - \mathbf{k}'$. To estimate the corresponding damping rate $\Gamma = 1/\tau$ in the presence of disorder, we will perform our analysis in the most general

[8] Landau damping being then negligible.

inhomogeneous situation. We recall that Γ arises from the cubic terms in the Bogoliubov expansion (see chapter 2), which read,

$$\hat{H}^{(3)} = g \int \sqrt{n_{\rm c}(\mathbf{r})} \hat{B}^\dagger(\mathbf{r}) [\hat{B}^\dagger(\mathbf{r}) + \hat{B}(\mathbf{r})] \hat{B}(\mathbf{r}) d^d\mathbf{r}, \tag{3.46}$$

with $\hat{B}$ the Bogoliubov operator (3.14). As routinely done in the homogeneous case, the idea is to use the Fermi golden rule to compute the decay rate Γ_ν of an excitation ν (initial state $|i\rangle \equiv \hat{b}^\dagger_\nu |0\rangle$) into two excitations ν_1 and ν_2 (final state $|f\rangle \equiv \hat{b}^\dagger_{\nu_1} \hat{b}^\dagger_{\nu_2} |0\rangle$). It yields

$$\Gamma_\nu = \frac{2\pi}{\hbar} \frac{g}{2} \sum_{\nu_1,\nu_2} \left| \int \sqrt{n_{\rm c}(\mathbf{r})} \langle 0 | \hat{b}_{\nu_2} \hat{b}_{\nu_1} \hat{B}^\dagger(\mathbf{r}) [\hat{B}^\dagger(\mathbf{r}) + \hat{B}(\mathbf{r})] \hat{B}(\mathbf{r}) \hat{b}^\dagger_\nu |0\rangle d^d\mathbf{r} \right|^2 \delta(E_f - E_i). \tag{3.47}$$

The matrix element appearing in the integral is then computed using the Wick theorem and is expressed as a function of the quantities $\langle \hat{b}\hat{B}\rangle, \langle \hat{b}\hat{B}^\dagger\rangle, \langle \hat{b}^\dagger\hat{B}\rangle, \langle \hat{b}^\dagger\hat{B}^\dagger\rangle$. Those quantities can then be expressed as a function of the excitation wavefunctions $u_\nu(\mathbf{r})$ and $v_\nu(\mathbf{r})$ only, by reinserting the Bogoliubov transform (3.15), which yields the exact expression

$$\Gamma_\nu = \frac{2\pi}{\hbar} \frac{g}{2} \sum_{\nu_1,\nu_2} \left| \int \sqrt{n_{\rm c}(\mathbf{r})} \mathcal{B}^\nu_{\nu_1,\nu_2}(\mathbf{r}) d^d\mathbf{r} \right|^2 \delta(E_f - E_i) \tag{3.48}$$

where

$$\begin{aligned} \mathcal{B}^\nu_{\nu_1,\nu_2}(\mathbf{r}) \quad = 2 \quad \Big(& u^*_{\nu_2}(\mathbf{r}) u^*_{\nu_1}(\mathbf{r}) u_\nu(\mathbf{r}) + u^*_{\nu_2}(\mathbf{r}) v^*_{\nu_1}(\mathbf{r}) u_\nu(\mathbf{r}) + u^*_{\nu_2}(\mathbf{r}) v^*_{\nu_1}(\mathbf{r}) v_\nu(\mathbf{r}) \\ & + v^*_{\nu_2}(\mathbf{r}) u^*_{\nu_1}(\mathbf{r}) u_\nu(\mathbf{r}) + v^*_{\nu_2}(\mathbf{r}) u^*_{\nu_1}(\mathbf{r}) v_\nu(\mathbf{r}) + v^*_{\nu_2}(\mathbf{r}) v^*_{\nu_1}(\mathbf{r}) v_\nu(\mathbf{r}). \Big) \end{aligned} \tag{3.49}$$

In the homogeneous case, where the $u_\nu(\mathbf{r})$ and $v_\nu(\mathbf{r})$ functions are given by Eq. (2.30), explicit analytical scalings can be obtained in both the phonon and the free-particle regimes. In the phonon regime, a low-energy expansion of the $u_\nu(\mathbf{r})$ and $v_\nu(\mathbf{r})$ functions yields the well-known result

$$\Gamma \simeq 3\hbar q^5 / 320\pi mn,$$

with n the average density of the gas. In the free-particle regime, we find similarly

$$\Gamma \simeq g^2 nmq / 2\pi\hbar.$$

Remarkably, both scalings coincide at the crossover $q \simeq 1/\xi$, yielding $\tau \simeq m/10\hbar n^{3/2} a_{\rm sc}^{5/2}$, where $a_{\rm sc} = mg/4\pi\hbar^2$ is the scattering length.

Local density approximation

In the presence of disorder, the excitations can be fairly described in the diffusive regime within a local density approximation. This amounts to write them as plane waves whose amplitudes are determined by the local value of the density. Each mode is therefore labelled by its momentum k and reads

$$\begin{aligned} u_k(\mathbf{r}) &= \frac{e^{ikr}}{\sqrt{\mathcal{V}}} U_k(\mathbf{r}) \\ v_k(\mathbf{r}) &= \frac{e^{ikr}}{\sqrt{\mathcal{V}}} V_k(\mathbf{r}) \end{aligned} \tag{3.50}$$

where

$$U_k(\mathbf{r}) = \sqrt{\frac{1}{2}\left[\frac{\epsilon_k + gn_{\rm c}(\mathbf{r})}{\sqrt{\epsilon_k(\epsilon_k + 2gn_{\rm c}(\mathbf{r}))}} + 1\right]}$$
$$V_k(\mathbf{r}) = \sqrt{\frac{1}{2}\left[\frac{\epsilon_k + gn_{\rm c}(\mathbf{r})}{\sqrt{\epsilon_k(\epsilon_k + 2gn_{\rm c}(\mathbf{r}))}} - 1\right]}, \tag{3.51}$$

similarly to the homogeneous case. In the same spirit of what we did in Sec. 3.2.2, we will now make a distinction between bulk and depleted regions.

In the depleted regions, $U_k \sim 1$ and $V_k \sim 0$, recovering a free-particle behaviour. Since $\mathcal{B}(\mathbf{r})$ is a regular function and $n_{\rm c}(\mathbf{r}) \approx 0$, the contribution of the depleted regions to the integral in Eq. (3.48) vanishes. Therefore, the depleted regions, where the excitations behave as free particles with infinite lifetime, very weakly contribute to Γ.

Conversely, in the bulk, the local contribution of position $\mathbf{r}$ to the integral is all the more higher than the local density is higher.

Therefore, a rigorous upper estimate (although very rough) for Γ is given by its homogeneous expression evaluated at the maximum density n_{max}, yielding $\tau \simeq m/10\hbar n_{max}^{3/2} a_{\rm sc}^{5/2}$. This in particular shows that the lifetime τ can always be increased by lowering the average density [9]. Furthermore, since all functions in Eq. (3.48) are regular as a function of density, a reasonable order of magnitude for Γ is expected to be obtained by evaluating the previous expression at the average density. For a typical excitation at the crossover between the phonon and the free-particle regime, $q \simeq 1/\xi$, it yields $\tau \simeq m/10\hbar n^{3/2} a_{\rm sc}^{5/2}$.

Validity of the linear approach

We now compare this lifetime to the transport mean-free time $\tau_{\rm B} = l_{\rm B}/w_\varepsilon$, for a typical excitation ($\varepsilon \sim \mu$) near the localization threshold $k_\varepsilon l_{\rm B} \sim 1$. On the one hand, we can roughly use for w_ε the value of the sound velocity in the phonon regime, $c = \sqrt{gn/m}$. On the other hand, $l_{\rm B} \sim 1/k_\varepsilon$ for excitations of interest. Altogether, one gets $\tau_{\rm B} \sim m/4\pi\hbar n a_{\rm sc}$. Therefore, the validity condition of our approach reads $\tau_{\rm B}/\tau \sim \sqrt{na_{\rm sc}^3} \ll 1$, which remarkably is nothing but the validity condition of the Bogoliubov approach. The latter is always verified in dilute-gas Bose-Einstein condensates. For instance, using the parameters of Ref. [42], we find $\tau \sim 6$s and $\tau_{\rm B} \sim 5$ms, making experimental observations of our predictions possible (we recall as well that a typical experiment can be a few seconds).

3.4.2 Experimental perspectives

The existence of several mobility spectra is particularly relevant to ultracold-atom experiments, especially as regards quench experiments. In these systems, out-of-equilibrium dynamics can be generated by a local quench, which produces collective excitations [120,123,124,184,185]. Their transport properties in the disorder and their ability to mediate long-range energy transfer are then determined by the four classes of mobility spectra of the localization diagram such as that of Fig. 3.7. In case (0), all excitations are protected against localization and can propagate to infinity, although with a diffusive (not ballistic) wave front, i.e. $\langle r^2 \rangle = 2D_{\rm B}t$, owing to the finite value of the transport mean-free path $l_{\rm B}$. In all other cases, energy can only be

[9] provided the disorder is bounded below, otherwise the density can locally remain very high.

partially transferred since some excitation modes are localized. In case (I), those are low-energy modes, which is qualitatively similar to the noninteracting case. In cases (II) and (III), this is (also) the case of intermediate-energy modes, which is specific to many-body localization. Energy-resolved quenches may thus provide experimental evidence of such mobility spectra in ultracold gases, since energy can or cannot be transferred throughout the system depending on the selected excitations. This feature would hardly be observable in condensed-matter systems, where the relevant energy generally lies around the Fermi level.

Moreover, ultracold gases offer a wide range of models of disorder, from impurities [108–110] to speckle potentials [3, 186, 187]. We stress again the possibility to tailor their statistical properties [47, 178, 179] (both correlations and one-point statistics) in order to observe richer localization diagrams. This could permit to design a large class of mobility spectra, which could eventually prove a precious tool to control quench experiments.

3.5 Conclusions

In this chapter, we have studied the transport and localization properties of collective excitations in disordered weakly-interacting Bose gases in the superfluid regime. Our formalism, based on the inhomogeneous Bogoliubov theory, enabled us to consider the problem in arbitrary dimension, and to treat both the weak and strong disorder cases, going beyond the previous studies. We briefly summarize here our results.

At the meanfield level, the disorder modulates the density background, and can possibly deplete it locally if it is strong enough. We developed an analytical description of the ground-state including density depletion at the mean-field level. The ground-state was however found to remain an extended delocalized superfluid.

As regards collective excitations, we followed then a two-step process. Firstly, we used the Bogoliubov theory to formulate the transport properties of collective excitations in terms of a two-wave scattering problem. This enabled to enlighten their *universal* features : while all excitations are localized in 1D and 2D, a localization transition occurs in 3D, determined by the criterion $k_\varepsilon l_\mathrm{B} \sim 1$. Secondly, to estimate the inverse disorder parameter (IDP) $k_\varepsilon l_\mathrm{B}$, we had to develop a microscopic theory. We found that the behaviour of the IDP results from the non-trivial competition between density depletion induced by strong disorder and screening induced by the interactions. As a consequence, it is strongly *non-universal*, in the sense that it depends on the model of disorder. Most importantly, we found that this non-universal competition can lead to a non-monotonic energy dependence of the IDP. In 3D where the IDP determines the onset of localization, the excitation spectrum can split into alternating bands of localized and extended states, with up to three mobility edges. A generic localization diagram was derived. We then investigated in more details the role of disorder correlations. Although their effect diminishes when the spatial dimension increases, they were shown to possibly lead to richer mobility spectra.

Finally, we discussed the experimental observability of our predictions. In particular, an estimation of Bogoliubov quasi-particles lifetimes permitted to conclude to the observability of our predictions. Experimental perspectives and implications on quench experiments were discussed.

3.6 SUPPLEMENT : Universal behaviour of the disorder parameter in the weak disorder case

In this section, we provide a detailed description of the behaviour of the IDP in the weak disorder case without density depletion. We recall that in this case (see Sec. 3.2.2), the IDP is given, in $d > 1$, by Eq. (3.34), which may be rewritten as a function of dimensionless parameters

$$\frac{1}{k_\varepsilon l_{\rm B}} \simeq \left(\frac{V_R}{\mu}\right)^2 \left(\frac{\sigma_R}{\xi}\right)^d \frac{\pi}{8} \frac{1}{(k_\varepsilon \xi)^{4-d}} \int (1-\cos\theta) S^2(k_\varepsilon \xi, \cos\theta) \tilde{c_2}(|2k_\varepsilon \sigma_R \sin(\theta/2)|) \frac{d\Omega_d}{(2\pi)^d}. \quad (3.52)$$

The 1D case is discussed later. The IDP is therefore uniquely determined by the correlation function of the disorder, since the screening function S is universal and the disorder amplitude trivially acts as an overall magnitude.

For any given correlation function $\tilde{c_2}$, the disorder parameter depends on only two parameters, namely the correlation length σ_R/ξ and the excitation energy $k_\varepsilon \xi$. As expressed by Eq. (3.52), it is determined by the angular integral of the product of two functions of the angle θ:

- The screening function $S^2(k_\varepsilon \xi, \cos\theta)$ encodes the effect of interactions. In Eq. (3.52), it is the only difference compared to the free-particle case. It is governed only by the excitation energy $k_\varepsilon \xi$. At low-energy ($k_\varepsilon \xi \ll 1$), $S^2(k_\varepsilon \xi, \cos\theta) \sim 4(k_\varepsilon \xi)^4 \cos^2(\theta)$ vanishes due to screening. At high-energy ($k_\varepsilon \xi \gg 1$), $S^2(k_\varepsilon \xi, \cos\theta) \sim 1$ for almost all θ, recovering the free-particle case.
- The on-shell correlation function $\tilde{c_2}(|2k_\varepsilon \sigma_R \sin(\theta/2)|)$ expresses that the IDP probes only the on-shell Fourier components of the disorder. It is governed only by the parameter $k_\varepsilon \sigma_R$.

Universal scalings in $d > 1$

Universal scalings in $d > 1$ can be inferred by inspection of Eq. (3.52). Four limiting cases can be considered.

(a) For $k_\varepsilon \sigma_R \ll 1$ and $k_\varepsilon \xi \ll 1$, one has $S^2(k_\varepsilon \xi, \cos\theta) \sim 4(k_\varepsilon \xi)^4 \cos^2(\theta)$ and $\tilde{c_2}(|2k_\varepsilon \sigma_R \sin(\theta/2)|) \sim \tilde{c_2}(0)$ for a potential which admits a white-noise limit (see appendix B). Therefore,

$$\frac{1}{k_\varepsilon l_{\rm B}} \sim \frac{V_{\rm R}^2}{\mu^2} \left(\frac{\sigma_{\rm R}}{\xi}\right)^d (k_\varepsilon \xi)^d. \quad (3.53)$$

More generally, if $\tilde{c_2}(q) \underset{q\to 0}{\sim} 1/q^\alpha$, one gets

$$\frac{1}{k_\varepsilon l_{\rm B}} \sim \frac{V_{\rm R}^2}{\mu^2} \left(\frac{\sigma_{\rm R}}{\xi}\right)^{d-\alpha} (k_\varepsilon \xi)^{d-\alpha}. \quad (3.54)$$

Notice that integrability of $\tilde{c_2}$ [10] necessarily imposes that $d > \alpha$. Therefore, the transport length always diverges at low energy.

[10] We recall that $\int \tilde{c_2}(\mathbf{q}) d^d\mathbf{q} = (2\pi)^d$.

(b) For $k_\varepsilon\sigma_R \ll 1$ and $k_\varepsilon\xi \gg 1$, one has $S^2(k_\varepsilon\xi, \cos\theta) \sim 1$. Assuming again a scaling of the form $\tilde{c_2}(q) \underset{q\to 0}{\sim} 1/q^\alpha$ (with $\alpha = 0$ if the potential has a white-noise limit), one gets

$$\frac{1}{k_\varepsilon l_{\rm B}} \sim \frac{V_{\rm R}^2}{\mu^2}\left(\frac{\sigma_{\rm R}}{\xi}\right)^{d-\alpha}\frac{1}{(k_\varepsilon\xi)^{4-d+\alpha}}. \tag{3.55}$$

Since $d > \alpha$, one can check that the transport length always diverges at high-energy [11].

(c) For $k_\varepsilon\sigma_R \gg 1$ and $k_\varepsilon\xi \gg 1$, one has $S^2(k_\varepsilon\xi, \cos\theta) \sim 1$; one the other hand, the effect of large $k_\varepsilon\sigma_R$ will be to select in the integral the angle $\theta = 0$ since the function $\tilde{c_2}$ generically vanishes at high momenta. To properly quantify this, we may change variables by posing $u \equiv 2k_\varepsilon\sigma_R \sin(\theta/2)$. This yields, in the limits we are considering

$$\frac{1}{k_\varepsilon l_{\rm B}} \sim \frac{V_{\rm R}^2\xi}{\mu^2\sigma_{\rm R}}\frac{1}{(k_\varepsilon\xi)^5}\int_0^{2k_\varepsilon\sigma_R} u^d\tilde{c_2}(u)du. \tag{3.56}$$

In most cases, the correlation function decreases rapidly enough so that $\int_0^\infty u^d\tilde{c_2}(u)du$ is finite, and one simply finds

$$\frac{1}{k_\varepsilon l_{\rm B}} \sim \frac{V_{\rm R}^2\xi}{\mu^2\sigma_{\rm R}}\frac{1}{(k_\varepsilon\xi)^5}. \tag{3.57}$$

The transport length diverges at high energy as $(k_\varepsilon\xi)^5$, in all dimension. Yet, long-range correlations (integrability of $\tilde{c_2}$ only requires that $\int_0^\infty u^{d-1}\tilde{c_2}(u)du$ be finite) may lead to corrections to this scaling. For instance, in 3D, if $\tilde{c_2}(q) \underset{q\to\infty}{\sim} 1/q^{7/2}$, one finds

$$\frac{1}{k_\varepsilon l_{\rm B}} \sim \frac{V_{\rm R}^2\xi}{\mu^2\sigma_{\rm R}}\frac{1}{(k_\varepsilon\xi)^{9/2}}.$$

(d) For $k_\varepsilon\sigma_R \gg 1$ and $k_\varepsilon\xi \ll 1$, one should similarly perform the same change of variables $u \equiv 2k_\varepsilon\sigma_R \sin(\theta/2)$. Using then $S^2(k_\varepsilon\xi, \cos\theta) \sim 4(k_\varepsilon\xi)^4\cos^2(\theta) \sim 4(k_\varepsilon\xi)^4[1 - 4(u/2k_\varepsilon\sigma_R)^2 + 4(u/2k_\varepsilon\sigma_R)^4]$, one finds for most correlation functions (i.e. such that $\int_0^\infty u^d\tilde{c_2}(u)du$ is finite)

$$\frac{1}{k_\varepsilon l_{\rm B}} \sim \frac{V_{\rm R}^2}{\mu^2}\frac{1}{k_\varepsilon\sigma_{\rm R}}. \tag{3.58}$$

Here as well, corrections can arise for long-range correlations.

Note - In the white-noise limits ($k_\varepsilon\sigma_R \ll 1$, cases (a) and (b)), we recover as expected the overall dependance on $V_{\rm R}^2\sigma^d$. In the free-particle limits ($k_\varepsilon\xi \gg 1$, cases (b) and (c)), the overall dependance on $\mu^2\xi^4$ makes the interactions disappear.

Specificities in $d = 1$

The previous scalings have been derived from Eq. (3.52), which is valid in dimension $d > 1$. In 1D, Eq. (3.35) should be used, which is rewritten in a dimensionless form

$$\frac{1}{k_\varepsilon l_{\rm B}} \sim \frac{\pi}{8}\left(\frac{V_R}{\mu}\right)^2\left(\frac{\sigma_R}{\xi^4 k_\varepsilon^3}\right)S^2(k_\varepsilon\xi, \cos\pi)\tilde{c_2}(|2k_\varepsilon\sigma_R|). \tag{3.59}$$

[11] This is strictly true for $\alpha > 0$ only, but the case $\alpha < 0$ seems very exotic.

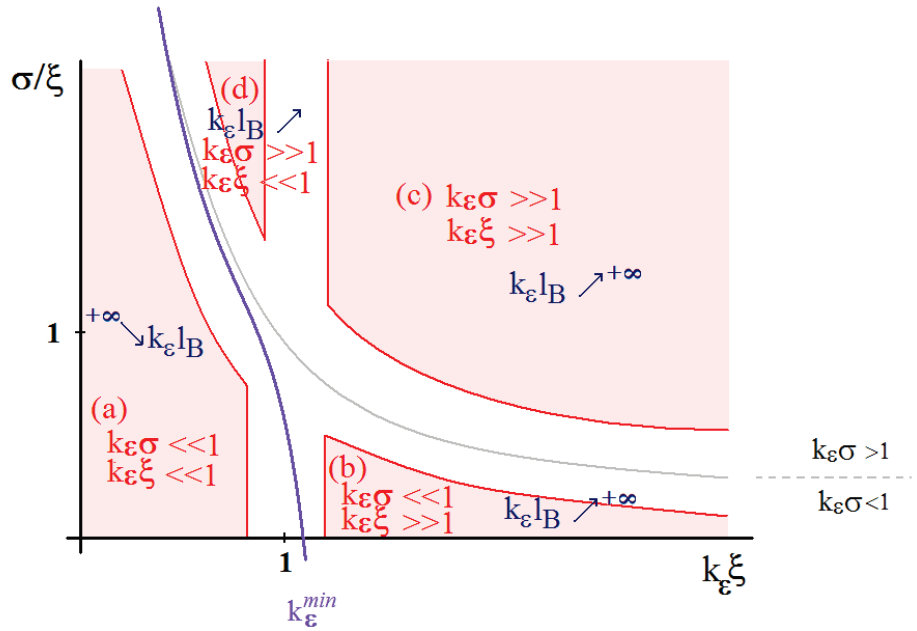

Figure 3.13: Universal behaviour of the IDP as a function of $k_\varepsilon\xi$ and $\sigma_{\rm R}/\xi$. The four areas in red correspond to the four limiting cases (a),(b),(c),(d) where a scaling for $k_\varepsilon l_B$ has been previously obtained. From those behaviours, it appears that the local minimum, represented by the purple line, obeys the general scaling $k_\varepsilon^{min} \propto min(1/\xi, 1/\sigma_{\rm R})$.

Notice that this expression is exactly the same as that of the Lyapunov exponent Γ found in Ref. [13] [12], in agreement with the fact that in 1D, $\Gamma = 1/L_{loc} \propto 1/l_{\rm B}$.

Universal scalings and limiting cases in 1D can then be found by inspection of Eq. (3.59). For $k_\varepsilon\sigma_R \ll 1$ (in both limits $k_\varepsilon\xi \ll 1$ and $k_\varepsilon\xi \gg 1$), one finds that the previous scalings in $d > 1$, Eqs. (3.54) and (3.55), still hold. Conversely, for $k_\varepsilon\sigma_R \gg 1$, Eq. (3.59) shows that the energy dependence of the IDP in 1D follows the momentum dependence of the power spectrum, yielding a scaling which is specific to each model of disorder. In particular, the previous scalings Eqs. (3.56) and (3.58) no longer hold in 1D.

Local minimum

The previous scalings (a), (b), (c) and (d), Eqs. (3.53) to (3.58), show that the transport length generically diverges at low-energy due to screening, and diverges as well at high-energy, hence recovering the free-particle behaviour. Therefore, it exhibits in-between a local minimum. According to the previous scaling laws, the latter may be located around $k_\varepsilon^{min} \propto min(1/\xi, 1/\sigma_{\rm R})$, as illustrated on Fig. 3.13. Its exact position however depends on the detailed shape of the correlation function (several minima can in principle exist for complicated correlations). Importantly, it does not depend on $V_{\rm R}$, since the disorder amplitude acts as a global multiplicative factor on the transport length.

White-noise limit

In the white-noise limit, $k_\varepsilon l_{\rm B}$ can be analytically computed in the full energy range. Indeed, since $c_2(\mathbf{r}) = \tilde{c}_2(0)\delta(\mathbf{r})$ in this case (see appendix A), $\tilde{c}_2(\mathbf{q}|) = \tilde{c}_2(0)$ is a constant. Therefore,

[12] There is a difference of a factor $\sqrt{2\pi}$ in [13], which arises from the different convention used for Fourier transforms.

Eq. (3.52) immediately yields

$$\frac{1}{k_\varepsilon l_{\rm B}(\varepsilon)} \simeq \frac{2\pi m^2 D}{\hbar^4 k_\varepsilon^{4-d}} F(k_\varepsilon \xi),$$

where $D = V_R^2 \sigma_R^d \tilde{c_2}(0)$, and $F(k_\varepsilon \xi) = \int \frac{d\Omega_d}{(2\pi)^d} S^2(k_\varepsilon \xi, \cos\theta)(1-\cos\theta)$ is a universal function of the unique parameter $k_\varepsilon \xi$ which can be analytically or numerically computed.

In 3D for instance, we find

$$\begin{aligned} F(k_\varepsilon \xi) = \quad & \frac{1}{(2\pi)^2}\left[2\left(1+2\frac{1-t^2}{t}\right) \quad +\left(\frac{2(1-t^2)(t-1)}{t} - \frac{(t^2-1)^2}{t^2}\right)\ln\left(\frac{t-1}{t+1}\right)\right. \\ & \left. -\left(\frac{(1-t^2)^2(1-t)}{t^2}\right)\left(\frac{2}{(1-t^2)}\right)\right] \end{aligned} \tag{3.60}$$

where $t = \dfrac{1+2(k_\varepsilon \xi)^2}{2(k_\varepsilon \xi)^2}$.

Chapter 4

Localization-delocalization transition of interacting bosons in one-dimensional quasiperiodic lattices

Grâce à presque et à quasi, plus d'un mensonge s'esquive.
(proverbe)

Quasiperdiodic potentials, which are formed of a small number of incommensurate sinusoidal components, have attracted over the past decades an increasing attention. They have proved relevant to describe the structure of incommensurate crystals, which are characterized by a superimposed periodic modulation of the atomic positions which is incommensurate with that of the main lattice. Such structures are naturally created during the growth of certain crystals [188] by Peierls instabilities or as a result of charge-density waves [189]. They can also be created on purpose in crystals by molecular epitaxy [190], or in ultracold gases loaded in optical potentials [3, 111, 191–193], using for instance a bichromatic setup as introduced in Sec. 1.3.2.

Quasiperiodic potentials constitute an appealing intermediate between disordered and periodic systems. On the one hand, their energy spectrum shows reminiscences of energy bands. On the other hand, the lack of translation invariance can induce the existence of localized states, similarly to the phenomenon of Anderson localization in truly disordered systems [2]. In this case however, the quasi-repetition of finite patterns radically changes the localization picture. For instance, in the non-interacting case in one dimension, while a truly disordered potential localises all states as soon as it is switched on, with an energy-dependent localization length [44, 194], there exists, in the case of a quasiperiodic potential made of a single incommensurate sinusoidal modulation, a critical potential strength above which localization occurs; below it, all states are extended Bloch-like waves, and above it, all states are localized with an energy-independent localization length [195–197].

Similarly to the case of purely disordered systems, taking into account interactions and many-body effects in quasiperiodic systems constitutes a very challenging question. Such issues

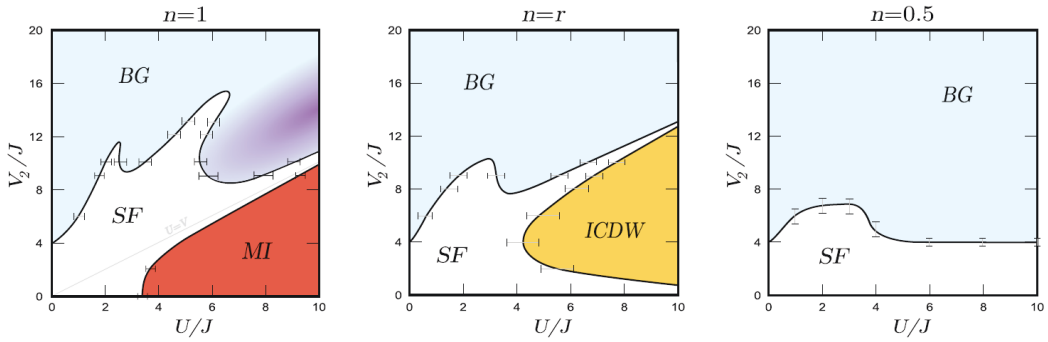

Figure 4.1: Phase diagrams of the bichromatic Bose-Hubbard model for densities $n = 1$, $n = r$ (the incommensurate ratio of the two lattices), and $n = 0.5$, as a function of interaction strength U and $V_2 = 2\Delta$, with Δ the quasiperiodic potential strength. Figure extracted from Ref. [208].

have been first investigated in disordered systems, as reviewed in Sec. 1.2, and extensions to quasiperiodic systems are just starting. So far, most studies have focused on the zero-temperature phase diagram of one-dimensional bosons in quasiperiodic lattices [1]. Indeed, what remains of the truly disordered phase diagrams presented in Sec. 1.2 (see Fig. 1.3) when considering a quasiperiodic potential is not obvious at all, since quasiperiodic potentials can be expected to display an intermediate behavior between commensurate and disordered ones.

Early studies considered first the case of a *commensurate* superlattice, where a Mott insulating state with fractional filling and a weakly superfluid phase were found [200–202]. As regards quasiperiodic superlattices, most analytical studies have relied so far on bosonization [203,204] and meanfield [205] approaches. Additionally, many numerical studies of the 1D quasiperiodic Bose-Hubbard model have been performed, based on exact diagonalization [206], quantum Monte-Carlo [207] or density-matrix renormalization group (DMRG) [208,209]. The latter were in particular combined with analytical considerations, which allowed for a rather complete description of the physics of such interacting quasiperiodic systems, as depicted on Fig. 4.1. As in the purely disordered case, the phase diagram exhibits a superfluid (SF)-Bose glass (BG) transition. For strong interactions, a Mott insulator (MI) is obtained if the density is commensurate with the main lattice, while a pinned incommensurate density wave (ICDW) is obtained if it is commensurate with the secondary lattice. For a filling incommensurate with both lattices, a superfluid phase is expected for all interaction strength. In particular, no Bose glass can arise in this region, at variance with the truly disordered case (see Fig. 1.3).

Besides this quest for phase diagrams, the question of the localization of collective excitations in quasiperiodic lattices remains largely open. As already pointed out, this issue is particularly relevant to understand most dynamical properties of correlated quantum systems [161], such as the propagation of correlations in recently-developed quench experiments [123, 124, 185]. Moreover, it is timely in view of current experiments performed on interacting Bose gases in bichromatic lattices [192].

In this chapter, we study the localization properties of collective excitations of a weakly-interacting Bose gas in the superfluid regime, subjected to a one-dimensional quasiperiodic potential [210]. As explained in Sec. 1.3.2, such a system can be realized with ultracold gases in a bichromatic configuration, i.e. by superimposing, on top of a main optical lattice, a weak

[1] More recent studies at finite [198] and infinite temperature [199] have been reported.

secondary lattice of incommensurate period. In the tight-binding limit, one can restrict to the lowest energy band of the main lattice and work in the basis of the corresponding Wannier states. The effect of the main lattice therefore reduces to a discretization of space, while the second lattice acts as an effective quasiperiodic potential,

$$V_j = \Delta \cos(2\pi r j + \varphi), \tag{4.1}$$

of amplitude Δ, phase φ, and with r the incommensurate ratio between the two lattice wavelengths. Such a system can thus be explicitely mapped onto a Bose-Hubbard model in the external potential (4.1), whose various parameters (Δ, φ, tunnelling rate...) can be extracted ab initio from the directly tunable parameters of the experiment (laser intensities and frequencies) [193].

This chapter is organized as follows. In Sec. 4.1, we first recall useful results about the localization properties of *non-interacting* particles in quasiperiodic lattices. We then turn to the interacting case. In Sec. 4.2, we briefly recall the meanfield theory for the weakly-interacting regime, and set the localization problem of the excitations. The latter is numerically solved in Sec. 4.3. In particular, we determine the localization diagram of collective excitations and show evidence of a sharp localization transition separating extended states at low energy and localized states at high energy. In Sec. 4.4, we develop an analytical treatment, which allows us to accurately reproduce and understand the numerical results. Our approach permits to quantitatively map the localization transition of interacting bosons onto that of an effective multi-harmonic quasiperiodic system, which is analytically solvable [210].

4.1 Localization of non-interacting particles in quasiperiodic lattices

Before addressing the question of interacting bosons, we study in this section the case of non-interacting particles in quasiperiodic lattices. In Sec. 4.1.1, we focus on the one-dimensional lattice with a single quasiperiodic modulation (the so-called *Aubry-André model*), and review the analytical prediction by Aubry and André [195] about the localization transition, as well as other useful analytical results. In Sec. 4.1.2, we discuss the numerical resolution of this problem, which will provide us the tools to numerically investigate more elaborate models. Indeed, in Sec. 4.1.3, we discuss the physics of more involved quasiperiodic potentials (*generalized Aubry-André models*) and present a perturbative approach developed by Sokolov [211] to qualitatively capture their localization behaviour.

4.1.1 Aubry-André model - Analytical results

The physics of a single particle in a one-dimensional lattice in the presence of the quasiperiodic potential (4.1) is described by the Schrödinger equation [2]

$$t(\psi_{j+1} + \psi_{j-1}) + \Delta \cos(2\pi r j + \varphi)\psi_j = E\psi_j \tag{4.2}$$

where ψ_j is the value of the wavefunction of energy E at site j, and where only nearest-neighbor hopping is considered, with a rate t. We recall that r is an irrational number to

[2] Consistently with Aubry and André convention, we do not put here a "-" sign in the kinetic term, so that our t actually denotes the opposite tunelling rate.

ensure incommensurability of the potential with the main lattice spacing (we will in fact see later that stronger requirements should be imposed on r).

Equation (4.2) defines the so-called *Aubry-André* or *Harper* model, which arises in several other contexts. For instance, for $\Delta = 2$, it describes the physics of an electron moving on a 2D square lattice in a perpendicular magnetic field [212, 213], the parameter $r = \Phi/\Phi_0$ corresponding then to the magnetic flux Φ per cell in units of the flux quantum $\Phi = h/e$. In the mathematical language, Eq. (4.2) defines the *almost Mathieu operator* [214]. It has been intensively studied in both physical [195, 215] and mathematical [216] contexts.

In the following, we will first derive Aubry and André argument for the localization transition, before enlightening a few properties of the energy spectrum.

The Aubry-André argument - Self-duality and localization transition

a/ Self-duality - The Aubry-André argument is based on the fundamental property that Eq. (4.2) is invariant under a suitable transformation. To show it, the idea introduced by Aubry and André [195] consists in writing ψ as a plane wave enriched with harmonics coming from the potential V. This defines the *duality transform*

$$\psi_j = e^{i\varphi j} \sum_{l=-\infty}^{l=\infty} \chi_l e^{il(2\pi r j+\varphi)} \tag{4.3}$$

Reinserting it into Eq. (4.2) yields

$$t(\chi_{l+1} + \chi_{l-1}) + \frac{4t^2}{\Delta}\cos(2\pi r l + \varphi)\chi_l = \frac{2tE}{\Delta}\chi_l \tag{4.4}$$

or equivalently

$$\frac{\Delta}{2}(\chi_{l+1} + \chi_{l-1}) + 2t\cos(2\pi r l + \varphi)\chi_l = E\chi_l \tag{4.5}$$

Equation (4.5) is called the dual equation of Eq. (4.2), and remarkably has the same form of the model equation (4.2). It shows that the dual wavefunction χ of the wavefunction ψ obeys the same equation as ψ, with an interversion of tunnelling and quasiperiodic amplitudes. The Aubry-André model is therefore said to be *self-dual*.

Moreover, it should be noticed that the duality transform Eq. (4.3) exchanges the localization and extension properties of the wavefunctions, in the sense that if $\sum_j |\psi_j|^2 < \infty$ (as expected for an exponentially localized state) and Eq. (4.3) converges, then $\sum_l |\chi_l|^2 = \infty$ (as expected for an extended state). By combining this observation with the duality between Eqs. (4.4) and (4.2), Aubry and André were able to infer the localization properties of their model, i.e. which states are extended and which are localized, as we explain now.

First of all, using the duality between Eqs. (4.4) and (4.2), one can immediately infer a relation for the integrated density of states per unit volume of the model equation. The latter, denoted $N_{a,b}(E)$, is defined as the number of eigenstates of energy lower than E, divided by the total number of sites [3], for the model equation Eq. (4.2) with tunneling a and quasiperiodic amplitude b. With this notation, duality straightforwardly yields

$$N_{t,\Delta}(E) = \frac{2t}{\Delta} N_{t,4t^2/\Delta}\Big(\frac{2tE}{\Delta}\Big) \tag{4.6}$$

[3] We recall that in all this chapter, the cell spacing is assumed to be 1.

Although very intuitive, this relation hides some subtleties, and requires in particular that r be an irrational number. This distinction between commensurate and incommensurate cases is detailed in Ref. [195].

b/ Lyapunov exponent and Thouless formula - The localization behaviour of a state at energy E can then be captured by inspection of its *characteristic exponent* $\gamma(E)$. The latter, also known as the Lyapunov exponent, is defined by

$$\gamma(E) = -\lim_{j\to\infty} \frac{\log(|\psi_j|^2)}{2j} \tag{4.7}$$

with ψ the wavefunction of energy E. It measures the exponential decay rate of the wavefunction at large distance. For an exponentially localized state, $\gamma(E)$ coincides with the inverse localization length (in unit of the lattice cell spacing), while it vanishes for an extented state. Moreover, the characteristic exponent $\gamma(E)$ can advantageously be calculated by using the *Thouless formula* [217]. The latter establishes a relation, for a one-dimensional *random* system with nearest-neighbor hopping, between $\gamma(E)$ and the density of states per unit volume $\rho(E) = dN(E)/dE$, according to

$$\gamma(E) = \int_{-\infty}^{\infty} \log \frac{|E-E'|}{t} \rho(E')dE'. \tag{4.8}$$

There exist several proofs for this formula [194], and we give one in the note below [4]. In particular, it enlightens what are the crucial hypotheses for the Thouless formula to hold :

- Firstly, since it relies on the iteration of Eq. (4.2), the Thouless formula is restricted to one-dimensional systems with nearest-neighbor hopping. Extensions of the formula to other situations exist [218].

- Secondly, replacing the discrete sum by an integral in the thermodynamic limit requires regularity properties of the density of states, which is guaranteed if the system is truly disordered. It is also valid for a quasiperiodic disorder such as the one used here, provided r is not only an irrationnal, but as well a Diophantine number (i.e. the solution of a polynomial equation with integer coefficients).

Using the Thouless formula and the duality equation for the density of states (4.6), we immediately obtain the duality equation for the characteristic exponents

$$\gamma_{t,\Delta}(E) = \gamma_{t,4t^2/\Delta}\Big(\frac{2tE}{\Delta}\Big) + \log(\Delta/2t). \tag{4.9}$$

[4] To prove the Thouless formula, let us fix a site j and study $\psi_j(E)$ as a function of the energy E. To do so, we consider the differential problem defined on $[0; j]$ by Eq. (4.2) with the boundary conditions $\psi_0/\psi_{-1} = cste$ (Von Neumann) and $\psi_j = 0$ (Dirichlet). We can in fact assume that both the values of ψ_0 and ψ_{-1} are fixed, since ψ_0 is fixed by the global normalization of the wavefunction. Let us call $E_i, i = 1, 2, ..., j$ the eigenvalues of the considered differential problem. By definition, $\psi_j(E)$ has zeros for all energies $E = E_i, i = 1, 2, ..., j$. Then, for any arbitrary energy E, one can iteratively compute from ψ_{-1} and ψ_0 the values of $\psi_1(E)$, $\psi_2(E)$,... by iterating the second-order recursion relation Eq. (4.2). One immediately finds than $\psi_j(E)$ is a polynomial in E of order j, and of dominant coefficient $1/t^j$. Since its zeros are known, one can therefore explicitely write that $\psi_j(E) = (1/t^j)\prod_{i=1}^{j}(E - E_i)$. Hence, $\log(|\psi_j|^2)/2j = (1/j)\sum_{i=1}^{j} \log|(E - E_i)/t| = \int \log|(E - E')/t|\rho(E')dE'$ in the thermodynamic limit $j \to \infty$, yielding the Thouless formula.

c/ Localization transition - The localization behaviour can now be straightforwardly inferred from Eq. (4.9), if one recalls that a characteristic exponent is always non-negative [see definition (4.7)].

If $\Delta > 2t$, one necessarily has $\gamma_{t,\Delta}(E) > 0$ from Eq. (4.9), whatever the energy E, corresponding to localized states at all energies. Such localized states are associated to extended dual states χ, characterized thus by $\gamma_{t,4t^2/\Delta}\Big(\dfrac{2tE}{\Delta}\Big) = 0$. Therefore, one gets $\gamma_{t,\Delta}(E) = \log(\Delta/2t)$, stating that all states are localized with the same energy-independent localization length, $L_{\rm loc} = 1/\log(\Delta/2t)$.

Conversely, if $\Delta < 2t$, all states ψ_j are extended. Indeed, the existence of an exponentially localized state [5] would imply an extended dual state, yielding simultaneously $\gamma_{t,\Delta}(E) > 0$ and $\gamma_{t,4t^2/\Delta}\Big(\dfrac{2tE}{\Delta}\Big) = 0$, violating Eq. (4.9).

Therefore, one gets an *energy-independent* localization transition at $\Delta = 2t$ (all states localize simultaneously at this quasiperiodic amplitude), characterized by an *energy-independent* localization length in the localized regime. This strikingly contrasts with the case of a one-dimensional true disorder where all states are localized for any disorder strength, with an energy-dependent localization length. This transition also differs from the Anderson transition in 3D, which is energy-dependent and occurs for any disorder strength.

This localization transition also translates into the dynamics [205], as numerically studied by measuring the time evolution of the width $w(t) \sim t^\gamma$ of a wavepacket. Three different asymptotic regimes were then found :
- for $\Delta < 2t$, a ballistic regime, $\gamma = 1$;
- for $\Delta = 2t$, a sub-diffusive regime, $\gamma \sim 0.5$;
- for $\Delta > 2t$, a localized regime, $\gamma = 0$.

d/ Finite-size systems - Commensurate or incommensurate ? - As seen above, a necessary and sufficient mathematical condition to observe a sharp transition in the Aubry-André model is that r be a Diophantine number. In practice however, experiments are always carried out on a finite system and r can always be known up to a finite number of digits. For this reason, there is in fact no sharp distinction between commensurate and incommensurate cases, and the condition is more subtle. In practice, to observe a sharp transition, one requires to have many lattice sites per period of the quasiperiodic potential, and a system size which does not exceed too much the period of the quasiperiodic potential (in order to avoid periodic replicas). This defines a so-called effective *degree of commensurability*, which depends on whether r is close to a simple ratio or not, and on the relation between the period of the potential and the system size. Studies with tunable degree of commensurability have been reported [193] and revealed a broadening of the transition for values of r that are close to simple rational ratio.

In that case, the mechanism for the transition has been more precisely described by Aubry and André [195]. When increasing the quasiperiodic amplitude, what happens in fact is that states corresponding to wavevectors that are commensurate with r localize first, yielding dense localized states in the spectrum. When the quasiperiodic amplitude further increases, localization spreads out from those points before invading the whole spectrum. Therefore, the transition as a function of Δ/t is broadened compared to the ideal incommensurate case. Such an effect however decreases exponentially fast when the degree of commensurability is increased.

[5] As pointed out by Aubry and André, there might exist non-exponentially localized states, but those are expected to have a zero measure.

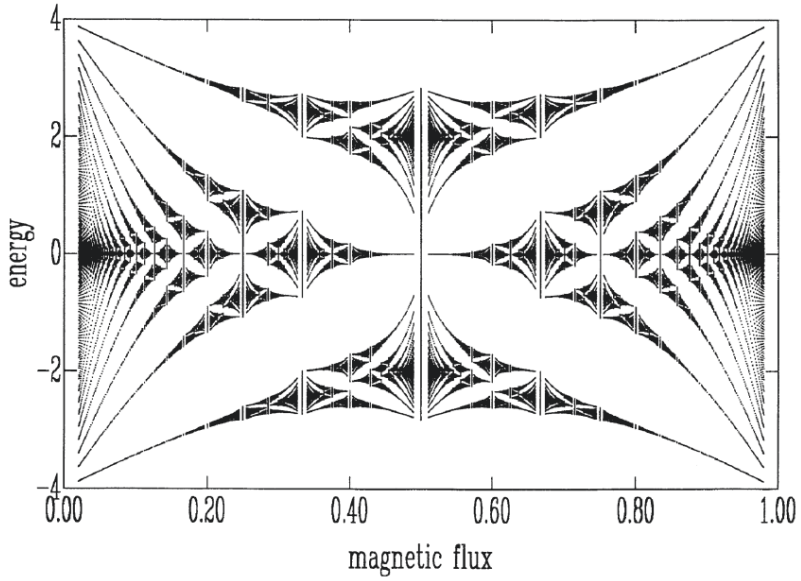

Figure 4.2: Hofstadter butterfly. Energy spectrum of an electron moving on a 2D square lattice as a function of the perpendicular magnetic flux. This system can be mapped onto the Aubry-André model at $\Delta = 2t$, with r representing the magnetic flux. The spectrum displays a rich fractal structure.

Energy spectrum of the Aubry-André model

The energy spectrum of the Aubry-André model (4.2) has been the object of numerous studies [195, 196, 213, 219] and was found to exhibit a very different structure in the extended and localized regimes.

In the extended regime, $\Delta < 2t$, the spectrum is independent of the phase φ [195]. Each eigenvalue has a twofold degeneracy. More interestingly, the energy spectrum is made of several narrow energy bands separated by gaps (also referred to as minigaps in the litterature) [196]. When $\Delta = 0$, there is no gap and the spectrum consists in a unique energy band of width $4t$. When Δ increases, more and more minigaps open, and then broaden. The spectrum is therefore uncountable, and its total measure decreases when Δ increases, until vanishing at the transition point $\Delta = 2t$. In particular, Aubry and André found that the total Lebesgue measure of the spectrum, $B(\Delta)$, obeys the empiric law $B(\Delta) = 4t - 2\Delta$.

In the localized regime $\Delta > 2t$, the structure changes drastically. First, the energy spectra obtained for two different phases φ and φ' are fully disconnected, except if the latter are related by a commensurability relation $\varphi = \varphi' + 2\pi r\mathbb{Z} \pmod{2\pi}$, in which case the energy spectra are the same. The energy spectrum is then made of pointlike energy levels and has a fractal structure : in particular, it is of zero measure, and has no ground state.

The critical case $\Delta = 2t$ has been intensively studied in another context, since it describes the physics of an electron moving on a 2D square lattice in a perpendicular magnetic field [212, 213]. In particular, much attention has been devoted to understanding the spectrum as a function of the parameter $r = \Phi/\Phi_0$, which in this context corresponds to the magnetic flux Φ per cell in units of the flux quantum $\Phi = h/e$. For irrational values of r, it was found to be a singular and fractal set of zero measure, in agreement with the previous results, and to form a

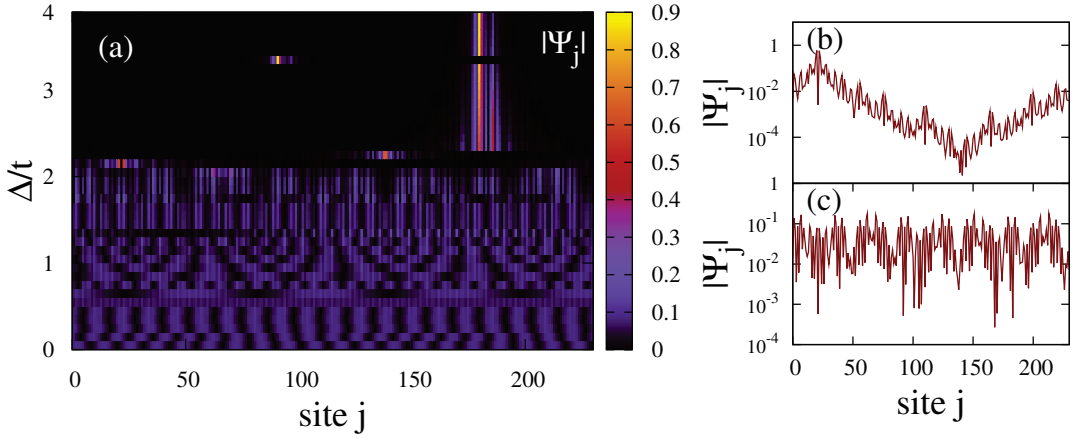

Figure 4.3: (a) Colorplot of the onsite coefficients of the tenth eigenstate, obtained by exact diagonalization of the Aubry-André model, for increasing quasiperiodic amplitudes Δ/t. A localization transition clearly appears for $\Delta = 2t$. (b)-(c) Semilog profiles of the same eigenstate for $\Delta/t = 2.1$ [localized regime, (b)]) and $\Delta/t = 1.9$ [extended regime, (c)].

Cantor set in the thermodynamic limit. Conversely, for rational values of $r = p/q$, it is made of q energy subbands. This rich and complex structure is depicted on Fig. (4.2), referred to as the Hofstadter butterfly.

4.1.2 Numerical results

In this section, we discuss the numerical resolution of the Aubry-André model (4.2). The objectives are twofold. On the one hand, it will enable us to reproduce the previous theoretical predictions. More importantly on the second hand, the same tools will be advantageously applied in the next section to the case of generalized quasiperiodic potentials, which will play an important role in the remainder of this chapter.

The numerical resolution is performed by exact diagonalization of Eq. (4.2). Notice that the quasiperiodic potential that we consider here can in principle be replaced by any external potential, so that the same procedure can be used to investigate the case of more elaborate potentials (see Sec. 4.1.3).

We make the common choice of a maximally incommensurate ratio, $r \approx (\sqrt{5}-1)/2$, known to display a sharp transition in the non-interacting case [193, 197, 216]. A subtle point arises here [197]. In principle, any Diophantine number would be suitable. However, numerical calculations are performed on a finite system, and periodic boundary conditions should be imposed to avoid undesirable boundary effects. Therefore, the periodic potential cannot be truly incommensurate, but has to be in fact *commensurate* with the system size to fulfill the periodic boundary conditions ! To do so, one has to choose not only a Diophantine number, but also a number which can be very closely approximated by rational numbers (a so-called *Liouville number*). In this respect, the golden ratio $(\sqrt{5}-1)/2$ is a good choice. Since it is very well approximated by the ratio of two successive Fibonacci numbers F_{p-1}/F_p, we choose for the number of lattice sites a Fibonacci number F_p, and perform our simulations with $r = F_{p-1}/F_p$, simultaneously fulfilling the appearently contradicting requirements of incommensurability and periodic boundary conditions.

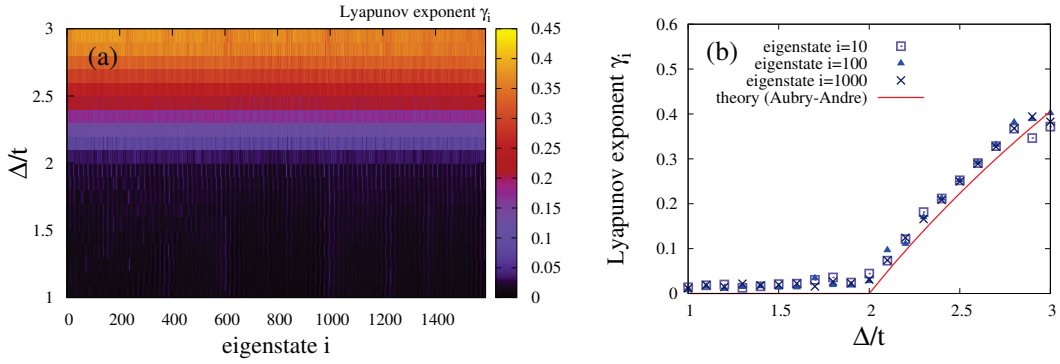

Figure 4.4: (a) Colorplot of the Lyapunov exponent of all eigenstates of the spectrum and for an increasing quasiperiodic amplitude. It shows that the transition at $\Delta = 2t$ is energy-independent. The dependence of the Lyapunov exponent on the quasiperiodic amplitude is essentially the same for all eigenstates (as exemplified in (b) for three eigenstates), and well captured by Aubry-André formula (red line in (b)).

Exact diagonalization of Eq. (4.2) gives access to the energy spectrum and wavefunctions of the Aubry-André model. The numerical results are presented on Figs. 4.3 and 4.4. Figure 4.3(a) displays the behaviour of a given eigenstate (here, the tenth) when increasing the quasiperiodic amplitude. While it is extended over the whole system for $\Delta < 2t$, it turns localized on a very few number of sites as soon as $\Delta > 2t$, recovering Aubry-André localization transition. Semilog profiles are shown on Fig. 4.3(b) and (c) in the extended and localized regimes, featuring in particular a neat exponential localization for $\Delta > 2t$.

Several observables can then be considered to more accurately describe the localization properties. The *participation ratio* PR, defined by

$$PR^{-1} = \frac{\Sigma|\psi_j|^4}{(\Sigma|\psi_j|^2)^2},$$

measures the typical number of sites significantly contributing to a given eigenstate. From its definition, it can be checked that it is 1 for a state localized on one single site, and N for a state extending over the whole system. It is a good qualitative indicator of the localization behaviour, but intermediate values are often difficult to interpret [6].

Therefore, to quantitatively characterize the localization transition, we will consider the localization length, or equivalently its inverse, the Lyapunov exponent γ. The latter can be extracted from a linear fit of the semilog tail of the wavefunction [see Eq. (4.7)]. Figure 4.4(a) displays the behaviour of γ for all eigenstates of the spectrum and as a function of the quasiperiodic amplitude Δ. All states feature the same localization transition at $\Delta = 2t$, which is therefore energy-independent. The behaviour of γ when increasing the quasiperiodic amplitude is plotted for a few eigenstates on Fig. 4.4(b) : all states exhibit the same energy-independent localization length, which is accurately described by the Aubry-André formula (red line).

[6] For instance, a PR of 2 can be obtained from a state localized over two sites, but also from an extended state with two distant main peaks.

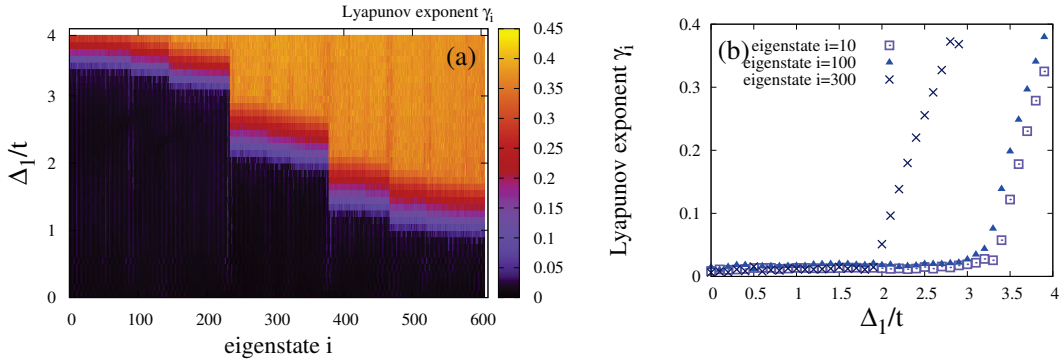

Figure 4.5: (a) Colorplot of the Lyapunov exponent of all eigenstates of the spectrum for the Soukoulis and Economou model, for an increasing main quasiperiodic amplitude Δ_1 at fixed secondary amplitude $\Delta_2 = 0.5t$. When increasing Δ_1, high-energy modes localize first. Therefore, three regimes appear : for $\Delta_1 \lesssim t$, all states are extended ('ext' regime); for $t \lesssim \Delta_1 \lesssim 3.5t$, low-energy states are extended while high-energy ones are localized ('ext-loc' regime); for $\Delta_1 \gtrsim 3.5t$, all states are localized ('loc' regime). The occasional abrupt changes in the Lyapunov exponent when going from an eigenstate to the following correspond to the minigaps of the spectrum, where the excitation energy between consecutive modes varies abruptly. (b) Dependence of the Lyapunov exponent on the main quasiperiodic amplitude Δ_1 for three eigenstates.

4.1.3 Generalized quasiperiodic potentials - Locator perturbation theory

We now turn to more elaborate incommensurate potentials, which are not made of one single sinusoidal component. Such generalized quasiperiodic potentials are very interesting in their own right. On the one hand, they are expected to be very general in nature, since quasiperiodic structures are rarely described by a single purely sinusoidal modulation. On the other hand, we shall see that they display a very different physics and a richer localization behaviour, owing to the fact that they generally do not exhibit duality. From a practical point of view, their study in this manuscript is motivated by the fact that they will naturally emerge when considering the interacting case in the next section.

Non self-dual models

A first extension to the Aubry-André model was studied by Soukoulis and Economou, who considered a two-harmonic quasiperiodic potential [220]

$$t(\psi_{j+1} + \psi_{j-1}) + \Big[\Delta_1 \cos(2\pi r j) + \Delta_2 \cos(4\pi r j)\Big]\psi_j = E\psi_j. \tag{4.10}$$

It can be checked that such model is no longer invariant under the duality transform (4.3) and that the Aubry-André argument cannot be applied. For their parameters, Soukoulis and Economou found a mobility edge, separating extended states in the lowest part of the spectrum from localized states in the highest part.

Using the numerical tools developed in the previous section, we were able to study this model for a wide range of parameters. In particular, we have studied the localization transition when increasing the main quasiperiodic amplitude Δ_1 in the presence of a fixed (small) secondary modulation of amplitude Δ_2. Our results are plotted on Fig. 4.5, for $\Delta_2 = 0.5t$. At variance with the Aubry-André case where all eigenstates localize *simultaneously* at $\Delta_1 = 2t$, high-energy eigenstates here localize first. Therefore, three regimes show up : for $\Delta_1 \lesssim t$, all

states are extended ('ext' regime); for $t \lesssim \Delta_1 \lesssim 3.5t$, low-energy states are extended while high-energy ones are localized ('ext-loc' regime); for $\Delta_1 \gtrsim 3.5t$, all states are localized ('loc' regime).

Another extension of the Aubry-André model was then studied by Riklund *et al.* [221], who kept the form of a single harmonic quasiperiodic potential, but added tunelling terms up to the next-nearest neighbors,

$$t_1(\psi_{j+1} + \psi_{j-1}) + t_2(\psi_{j+2} + \psi_{j-2}) + \Delta \cos(2\pi r j)\psi_j = E\psi_j \tag{4.11}$$

Such a model is again not self-dual. However, it can be checked that the duality transform (4.3) converts it into the Soukoulis and Economou model (4.10), with $t = \Delta/2$, $\Delta_1 = 2t_1$, and $\Delta_2 = \Delta t_2/t_1$. Consistently, Riklund *et al.* found, when increasing the quasiperiodic amplitude Δ, that the system should go from a situation where all states are extended to a situation where all are localized, but through a 'loc-ext' regime for intermediate quasiperiodic amplitude [7]. Interestingly, the system can have localized states for a quasiperiodic amplitude $\Delta < 2t_1$, where the Aubry-André model has only extended states, yielding the somehow paradoxal conclusion that increasing the hopping range in incommensurate systems can generate localized states.

Those results suggested to combine the two previous models [222] and study the model

$$t_1(\psi_{j+1} + \psi_{j-1}) + t_2(\psi_{j+2} + \psi_{j-2}) + \Big[\Delta_1 \cos(2\pi r j) + \Delta_2 \cos(4\pi r j)\Big]\psi_j = E\psi_j \tag{4.12}$$

Interestingly, such a model is invariant under the duality transform Eq. (4.3), provided the disorder amplitudes and hopping coefficients are related by the relations $\Delta_1 = 2t_1$ (as in the Aubry-André model) and $\Delta_2/\Delta_1 = t_2/t_1$. As in the Aubry-André model, self-duality was found to result here in an energy-independent metal-insulator transition. However in this precise case, the localization length in the localized regime was found to depend on the energy, due to an additional energy-dependent term in the Thouless formula. Indeed, due to the introduction of non-nearest-neighbor hopping, the Thouless formula cannot be used here in its original form and needs to be generalized.

More generally, it was shown that all models of the form

$$\sum_l t_l \psi_{j+l} + \Delta v_j \psi_j = E\psi_j \tag{4.13}$$

exhibit self-duality [195, 218], provided the hopping coefficients t_l are related to the harmonics of the on-site potential by the formula $v_j = \sum_l t_l e^{il(2\pi r j+\varphi)}$. In this case, a localization transition at which all eigenstates localize simultaneously is expected to occur for a critical value of the disorder strength Δ_c, which is the fixed point of the duality transform [8]. However, the localization length can depend on the energy due to the more complex form of the Thouless formula when including non-nearest-neighbor hopping.

[7] Note that the intermediate regime in Riklund model is indeed 'loc-ext', while it is 'ext-loc' in the Soukoulis and Economou model, consistently with the fact that localization properties are inverted when going to the dual space.

[8] Interestingly, there exists self-dual models which are not of the form of Eq. (4.13), for instance with infinite-range hopping, and for which energy-dependent mobility edges have been predicted [218].

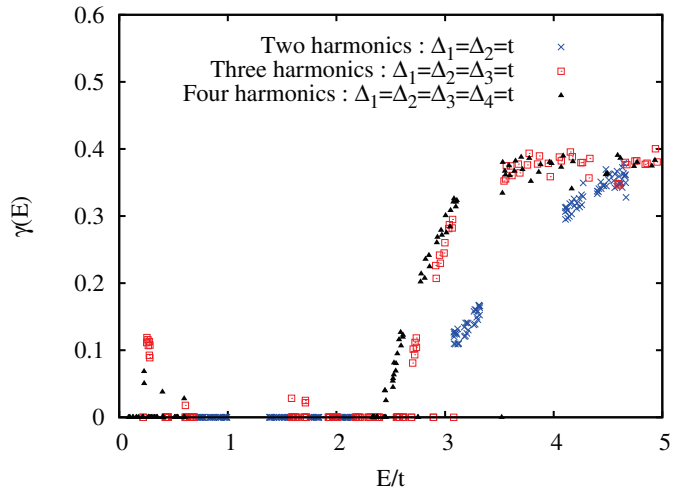

Figure 4.6: Lyapunov exponent as a function of excitation energy for the multiharmonic model (4.14) with two (blue crosses), three (red squares), and four (dark triangles) harmonics included, and in the case where all included harmonics have the same amplitude $\Delta_i = t$. All cases display a similar localization transition, and the position of the mobility edge weakly depends on the number of harmonics included.

Conversely, for non-dual quasiperiodic models, mobility edge(s) generically appears in the spectrum for intermediate disorder strength, since all states do not localize simultaneously. We have performed numerical simulations with multiharmonic quasiperiodic potentials, i.e. models of the form

$$t(\psi_{j+1} + \psi_{j-1}) + \Big[\Delta_1 \cos(2\pi r j) + \Delta_2 \cos(4\pi r j) + \Delta_3 \cos(6\pi r j) + ...\Big]\psi_j = E\psi_j. \qquad (4.14)$$

As soon as two harmonic at least are present, we found very similar conclusions to the two-harmonic case studied by Soukoulis and Economou, and the three regimes 'ext', 'ext-loc' and 'loc' generically show up. The results for the Lyapunov exponent, obtained in the same way as in the previous section 4.1.2, are displayed on Fig. 4.6 for a various number of harmonics in the model. Interestingly, in the 'ext-loc' regime, the position of the mobility edge weakly depends on the number of harmonics included. All those multiharmonic models therefore fall into the same universality class, except the particular one where only a single harmonic is present, which exhibits duality and falls into Aubry-André universality class.

Locator perturbation theory

To systematically study localization in incommensurate lattice potentials, a general formulation based on locator perturbation theory was developed by Sokoloff [196, 211]. The latter can be applied to any lattice model, and can advantageously be used in any dimension and for any incommensurate on-site potential, i.e. for any model of the form

$$\sum_{\vec{a}} t\psi(\vec{r}+\vec{a}) + \psi(\vec{r})V(\vec{r}) = E\psi(\vec{r}). \qquad (4.15)$$

The general idea [211] consists in writing a standard perturbation theory for the self-energy and examining the possibility of divergence in it. A divergence at energy E indeed reveals an extended state, whereas no divergences appear for localized states. In the thermodynamic limit

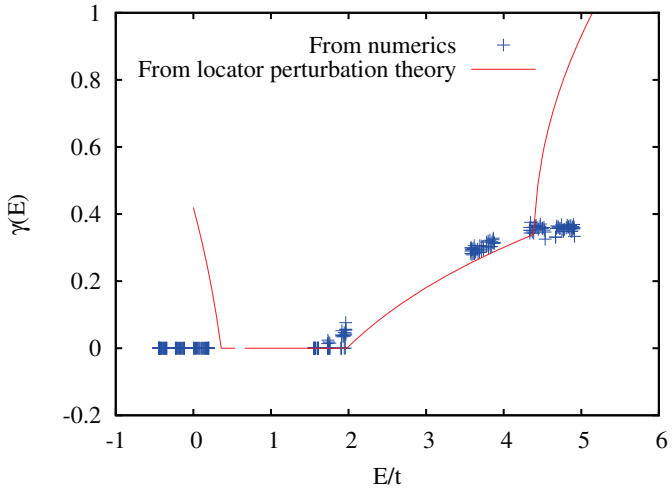

Figure 4.7: Lyapunov exponent as a function of excitation energy, for the two-harmonic case with $\Delta_1 = 1.9t$ and $\Delta_2 = t$, as obtained from exact diagonalization (blue) and locator perturbation theory Eq. (4.16) (red). Locator perturbation theory gives a fair estimation of the localization behaviour and of the mobility edge.

and for incommensurate potentials, it was shown by Sokoloff [211] that the convergence of the self-energy, which involves products of denominators of the form $E - V(\vec{r} + \vec{a_1} + \vec{a_2} + ...)$, can be tested by examining the convergence of the geometric series whose ratio $D(E)$ is the geometric mean of an energy denominator,

$$D(E) = \exp\left(\frac{1}{\mathcal{V}} \int \log \left| \frac{E - V(\vec{r})}{t} \right| d^d \vec{r} \right). \tag{4.16}$$

Indeed, it can be shown that the self-energy converges provided the so-called localization function $D(E)$ is larger than K, where K^n is the number of self-avoiding paths of n steps in the considered lattice geometry. For instance, in a one-dimensional lattice with only nearest-neighbor hopping, $K = 1$, so that a simple localization criterion reads $D(E) > 1$, with $D(E)$ given by Eq. (4.16). Such a criterion can hence be applied to any quasiperiodic potential. Since this result relies on perturbation theory, it is asymptotically valid near the center of the band ($E \to 0$). As discussed by Sokoloff [196], the localization function can as well be used as an estimate for the localization length. In the limit of sharply localized states, the latter is roughly given by $L_{loc}(E) \approx 1/\log(D(E))$.

As an example, let us apply this criterion to the Aubry-André model. In this case, the localization function reads

$$D(E) = \exp\left(\frac{1}{2\pi} \int_0^{2\pi} \log \left| \frac{E - \Delta\cos(x)}{t} \right| dx \right).$$

It can be analytically calculated and remarkably yields the value $\Delta/2t$ independently of E (provided $|E| < \Delta$, explicitely giving here the upper bound for the validity of the approach). Therefore, one recovers the localization transition at $\Delta = 2t$ as predicted by Aubry and André, as well as the energy-independent localization length $L_{loc} = 1/\log(\Delta/2t)$.

For more elaborate multiharmonic potentials, we can compare this formula to the previous numerical results [see for instance Fig. 4.7 for the two-harmonic case]. Although quite an approximative formula for L_{loc}, the mobility edge is rather fairly estimated.

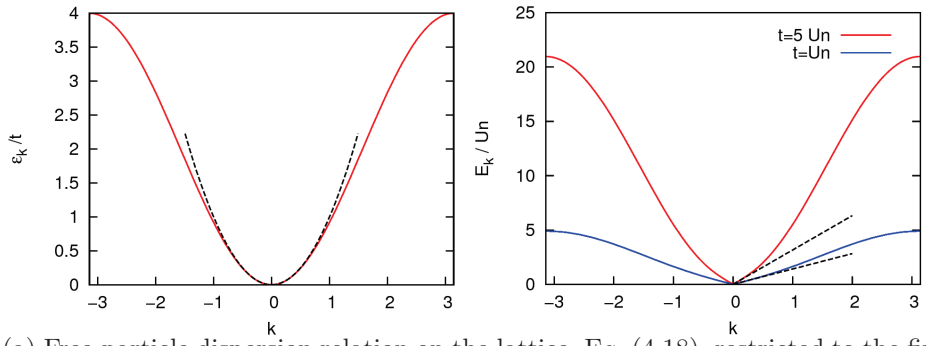

Figure 4.8: (a) Free-particle dispersion relation on the lattice, Eq. (4.18), restricted to the first Brillouin zone $k \in [-\pi; \pi]$. The low-k limit coincides with the quadratic free-particle dispersion relation on the continuum, $\varepsilon = tk^2$ (dashed line). The total bandwidth is $4t$. (b) Bogoliubov dispersion relation on the homogeneous lattice, Eq. (4.25), for two different parameters, $t = Un$ and $t = 5Un$. Similarly to the continuous case, it is linear at low momenta (dashed line) and free-particle-like at high momenta.

4.2 The weakly-interacting Bose gas on the quasiperiodic lattice

We now turn to the interacting case. In this section, we briefly set the model and use the mean-field theory to formulate the problem of the localization of collective excitations.

4.2.1 The model

The low-energy physics of interacting bosons in one-dimensional quasiperiodic lattices is governed by the single-band Aubry-André-Hubbard Hamiltonian,

$$\hat{H} = -\sum_{j,l} T_{j,l}\hat{a}_j^\dagger \hat{a}_l + \sum_j V_j \hat{a}_j^\dagger \hat{a}_j + \frac{U}{2}\sum_j \hat{a}_j^\dagger \hat{a}_j^\dagger \hat{a}_j \hat{a}_j, \tag{4.17}$$

where $\hat{a}_j$ and $\hat{a}_j^\dagger$ are the bosonic annihiliation and creation operators at the lattice site j. The first term in Eq. (4.17) represents quantum tunneling with the hopping matrix $\hat{T}$ chosen to include only nearest-neighbor tunnelling, $T_{j,j\pm1} = t$ and $T_{j,l} = 0$ for $|j - l| > 1$, and where we include the homogeneous on-site term $T_{j,j} = -2t$ for convenience. With this convention, the clean free-particle spectrum,

$$\varepsilon_k = 2t[1 - \cos(k)], \tag{4.18}$$

is centered on $\varepsilon = 2t$ with the band edges $\varepsilon = 0$ and $\varepsilon = 4t$ [see Fig.4.8(a)]. The second term represents the on-site quasiperiodic potential modulation,

$$V_j = \Delta \cos(2\pi r j + \varphi), \tag{4.19}$$

where r is an irrational number to ensure incommensurability of the modulation with the spacing of the main lattice, φ is a phase, and Δ the quasiperiodic amplitude. Here again, we make the common choice of a maximally incommensurate ratio, $r \approx (\sqrt{5} - 1)/2$. Finally, the third term represents onsite repulsive interactions with the two-particle interaction energy $U > 0$.

4.2.2 Mean-field theory

In the weakly-interacting superfluid regime we are interested in, characterized by a high occupation number per lattice site ($n \gg U/t$, with n the mean density), we can rely on meanfield theory [223,224]. In this case, the discreteness of the particle number on each site indeed plays no role and one can perform a continuous treatment of the extended condensate. The approach for lattice systems is very similar to that of continuous systems, which was presented in details in chapter 2.

Gross-Pitaevskii equation

The first step is to determine the meanfield density background n_j, which is achieved by minimizing the classical energy functional obtained by replacing the operator $\hat{a}_j$ by the real-valued field $\phi_j \equiv \sqrt{n_j}$ in Eq. (4.17). This yields the Gross-Pitaevskii equation (GPE)

$$\mu\phi_j = -\hat{T}\phi_j + V_j\phi_j + U\phi_j^3 \tag{4.20}$$

where the term $\hat{T}\phi_j$ is a shortcut for the hopping matrix contribution $t(\phi_{j+1} - 2\phi_j + \phi_{j-1})$ and μ is the chemical potential. The latter is adjusted to fulfill the constraint of a fixed particle number, $N = \Sigma_j|\phi_j|^2$.

Bogoliubov equations

Given the density background n_j, we write $\delta\hat{a}_j = \hat{a}_j - \phi_j \equiv \delta\hat{n}_j/2\sqrt{n_j} + i\sqrt{n_j}\delta\hat{\theta}_j$, where $\delta\hat{n}_j$ and $\delta\hat{\theta}_j$ are the density and phase fluctuations. Hamiltonian (4.17) is then expanded up to second order in this Bogoliubov operator, yielding

$$H^{(II)} = \sum_j \left[\hat{X}_j \frac{\hat{T}\phi_j}{\phi_j}\hat{X}_j - \hat{X}_j\hat{T}\hat{X}_j + 2Un_j\hat{X}_j^2\right] + \sum_j \left[\hat{P}_j \frac{\hat{T}\phi_j}{\phi_j}\hat{P}_j - \hat{P}_j\hat{T}\hat{P}_j\right] \tag{4.21}$$

where we have introduced the standard operators $\hat{X}_j = \delta\hat{n}_j/2\phi_j$ et $\hat{P}_j = \delta\hat{\theta}_j\phi_j$. The collective excitations, characterized by their energy E and represented by two fields u_j and v_j, are then determined by diagonalizing the quadratic Hamiltonian (4.21), and are found to be the solutions of the Bogoliubov de-Gennes equations (BdGEs)

$$\begin{bmatrix} -\hat{T}+V_j-\mu+2Un_j & Un_j \\ -Un_j & \hat{T}-V_j+\mu-2Un_j \end{bmatrix} \begin{bmatrix} u_j \\ v_j \end{bmatrix} = E \begin{bmatrix} u_j \\ v_j \end{bmatrix}. \tag{4.22}$$

Note that both the Gross-Pitaevskii (4.20) and the Bogoliubov (4.22) equations on the lattice are straightforwardly deducible form the continuous case [Eqs. (2.13) and (2.20)] by applying the following substitutions : $g \to U$, $\hbar^2/2m\nabla^2 \to t(._{x+1} + ._{x-1} - 2._x) \equiv \hat{T}$. In Fourier space, the latter amounts to replace the free-particle quadratic dispersion relation by that of the clean lattice, $\hbar^2k^2/2m \to \varepsilon_k$.

In particular, in the homogeneous case $V_j = 0$, one has $\mu = Un$ so that the Bogoliubov equations rewrite

$$\begin{pmatrix} -\hat{T}+Un & Un \\ -Un & \hat{T}-Un \end{pmatrix} \begin{pmatrix} u_j \\ v_j \end{pmatrix} = E \begin{pmatrix} u_j \\ v_j \end{pmatrix} \tag{4.23}$$

In this case, translation invariance allows to search the excitations under the form $u_j = u_p \tilde{u}_j^{(p)}$ and $v_j = v_p \tilde{v}_j^{(p)}$ where $\tilde{u}_j^{(p)}$ and $\tilde{v}_j^{(p)}$ are Bloch waves of quasi-momentum p, and u_p and v_p are complex amplitudes. The eigenproblem (4.23) then reduces to diagonalizing a 2×2 matrix,

$$\begin{pmatrix} \varepsilon_p + Un & Un \\ -Un & -\varepsilon_p - Un \end{pmatrix} \begin{pmatrix} u_p \\ v_p \end{pmatrix} = E_p \begin{pmatrix} u_p \\ v_p \end{pmatrix}, \tag{4.24}$$

yielding the Bogoliubov spectrum

$$E_p = \sqrt{\varepsilon_p(\varepsilon_p + 2Un)}. \tag{4.25}$$

This expression, which is plotted on Fig. 4.8(b), is similar to what is obtained in the continuous case, except that ε_p is given by the free-particle dispersion relation on the lattice, Eq. (4.18), instead of $\varepsilon_p = p^2/2m$.

The GPE for the density background (4.20) together with the BdGEs (4.22) form a complete set which determines the localization problem of collective excitations.

4.3 Numerical resolution

In this section, we first consider the numercial resolution of this problem, Eqs. (4.20) and (4.22), on the 1D quasiperiodic lattice.

As already discussed in Sec. 4.1.2, the number of lattice sites is chosen to be a Fibonacci number F_p and r is approximated by the ratio F_{p-1}/F_p in order to use periodic boundary conditions with a good approximation of the incommensurate ratio r. In practice, we use $F_p = 610$, which yields $r = (\sqrt{5}-1)/2 \pm 0.000002$.

Firstly, the density background is computed by solving the GPE (4.20) using imaginary time propagation with a Crank-Nicolson scheme [225]. The good numerical convergence of the imaginary-time propagation of the GPE is a delicate point for the later determination of the collective excitations using the BdGEs, in which the density background n_j computed numerically is incorporated. As a convergence criterion, we fix a precision threshold on the effective, imaginary time-dependent chemical potential

$$\mu(\tau) \equiv -\frac{\hbar}{2}\frac{d}{d\tau} \log\left(\sum_j n_j\right).$$

We have checked that the density profile is practically unchanged when the precision threshold varies from 10^{-8} to 10^{-15}. The same holds when the imaginary time step $\Delta\tau$ used in the propagation varies from $t\Delta\tau = 0.01$ to 0.5 [9]. Moreover, the density profile precisely agrees with the perturbative expansion of the GPE solution (see Sec. 4.4.1) implemented up to order 50. Altogether, the precision on the density profile n_j is estimated of the order of 10^{-8} for all results presented here.

Secondly, using this precisely determined density field, the excitations are computed by exact diagonalization of the BdGEs. (4.22) using the Lanczos algorithm for sparse non-Hermitian eigenproblems [225].

[9] Above this value, the Crank-Nicolson scheme can become unstable.

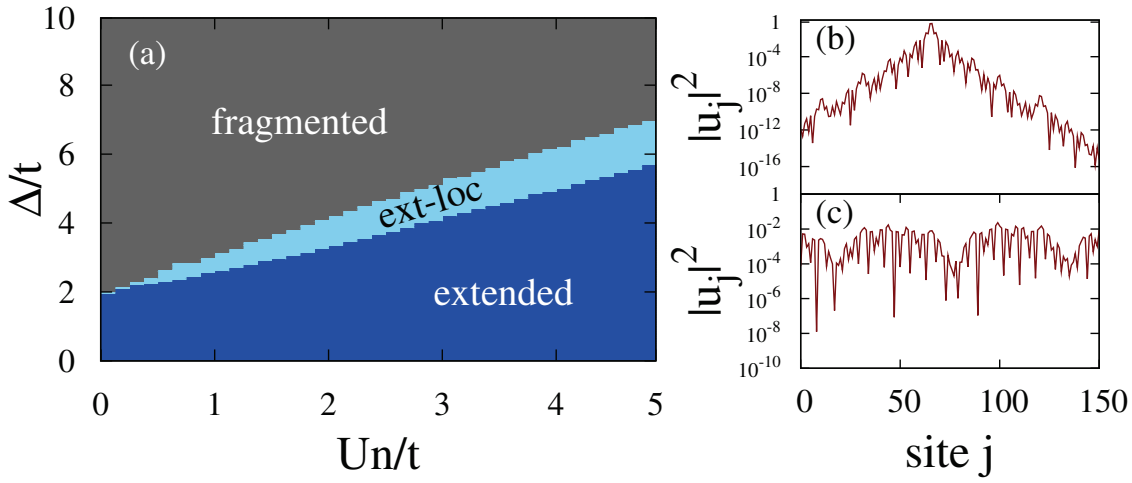

Figure 4.9: Numerical results. (a) Localization diagram as a function of the interaction strength and the quasiperiodic amplitude. It displays three regimes: (i) 'Extended regime' where the density background is connected and all excitations are extended; (ii) 'Fragmented regime' where the density background is fragmented; (iii) 'Extended-localized regime' where the density background is connected and the excitation spectrum shows a delocalization-localization transition with exponentially localized high-energy states and extended low-energy states. (b)-(c) Typical excitation wavefunction u in the localized (b) and extended (c) regimes, plotted in semi-log scale and for the 150 first lattice sites (similar plots are found for the v wavefunctions). The two panels correspond to two excitations with consecutive energies in the spectrum, above (b) and below (c) the mobility edge, for $Un/t = 1.75$ and $\Delta/t = 3.3$.

The numerical results are summarized on the diagram of Fig. 4.9(a). It displays three different regimes. For weak quasiperiodic amplitude Δ, the density background is fully connected and all excitations are extended ('extended regime'). For a given interaction strength U and tunneling t, the density modulations increase with the quasiperiodic amplitude Δ. Above a critical value of Δ_c, the density profile gets fragmented ('fragmented regime'), which yields the upper boundary on the diagram. The fragmentation condition is chosen to be the minimal value of Δ such that at least one lattice site has a density lower than 0.01 atom per site. We have checked that varying this arbitrary threshold down to 0.001 yields insignificant changes of the fragmentation boundary. Moreover the latter is in good agreement with the experimental observation of Ref. [192]. In the fragmented regime, the density profile is cut in disconnected pieces. It corresponds to trivial localization, a case that we disregard in the following. Notice that in the limit $U \to 0$, we recover the critical value $\Delta_c = 2t$, that is the localization transition of the non-interacting Aubry-André model. The most interesting regime appears for intermediate quasiperiodic amplitude ('ext-loc regime'). In this regime, although the density background is fully connected, we find a localization transition of the collective excitations. Remarkably enough, they are the high-energy excitations that are exponentially localized over a few lattice sites [see Fig. 4.9(b)] while the low-energy excitations are extended over the whole system [see Fig. 4.9(c)]. This transition is sharp as exemplified on Figs. 4.9(b) and (c), which correspond to two consecutive excitations in the spectrum, for $Un = 1.75t$ and $\Delta = 3.3t$. Such results are consistent with the observed behaviour of the participation ratio [226], although the latter remains a qualitative indicator which does not allow for a precise characterization of the localization transition.

In order to characterize the delocalization-localization transition, we compute two Lyapunov

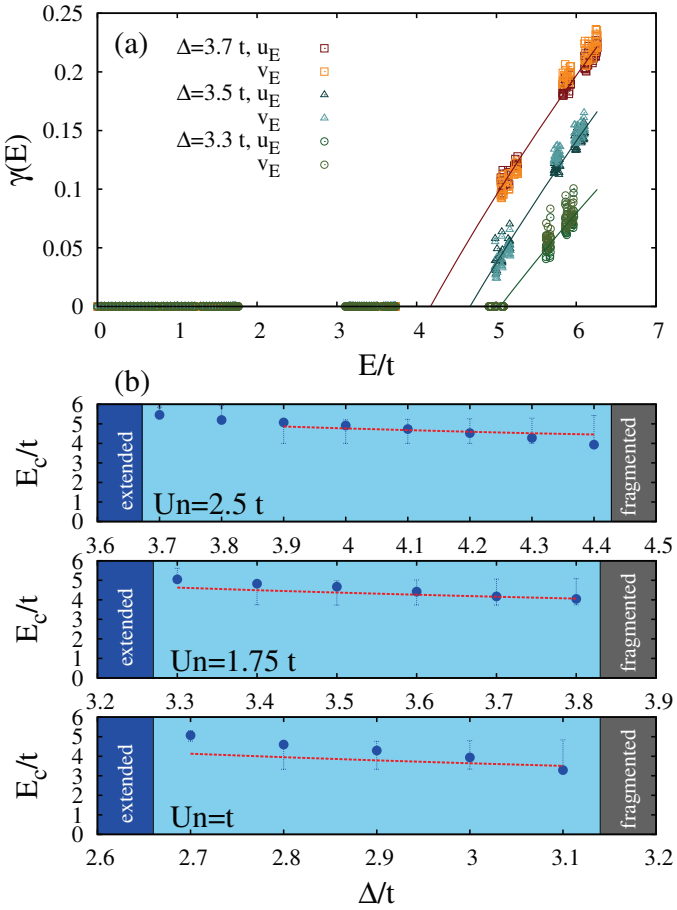

Figure 4.10: (a) Lyapunov exponents of the Bogoliubov wavefunctions u and v, for $Un/t = 1.75$ and $\Delta/t = 3.3, 3.5, 3.7$. The excitation spectrum is banded and displays a sharp localization transition separating extended ($\gamma = 0$) and localized ($\gamma > 0$) states. (b) Mobility edge as a function of the quasiperiodic amplitude Δ/t as extracted from power-law fits to the numerical $\gamma(E)$ curves [solid lines on panel (a)]. Error-like bars correspond to the edges of the minigap containing the mobility edge. The dotted, red line shows the analytical prediction of the locator perturbation theory applied to the effective model (4.45) with the potential (4.49).

exponents for the excitations corresponding to the two Bogoliubov wavefunctions,

$$\gamma_u(E) \equiv -\lim_{j\to\infty} \log|u_j|/j \qquad \text{and} \qquad \gamma_v(E) \equiv -\lim_{j\to\infty} \log|v_j|/j.$$

They are extracted from linear fits of the tails of the logarithm of the wavefunctions u and v. Figure 4.10(a) displays those Lyapunov exponents versus the excitation energy, for fixed interaction and disorder strengths. The Lyapunov exponents γ_u and γ_v are indistinguishable and herafter we omit the wavefunction index u or v. In the 'ext-loc' regime the Lyapunov exponent curves clearly show the transition, separating extended ($\gamma = 0$) and localized ($\gamma > 0$) states. As already discussed, the excitation spectrum splits into several bands separated by minigaps, a general feature in quasiperiodic systems [196, 197, 211, 218, 220, 222], and we find that the transition generally lies into one of the minigaps. Therefore, to precisely determine the position of the mobility edge, we rely on fits of the $\gamma(E)$ curves wih several fitting functionals [linear, $\gamma(E) \sim E - E_c$; power-law, $\gamma(E) \sim E^\alpha - E_c^\alpha$; and logarithmic, $\gamma(E) \sim \log(E/E_c)$]. The result is found to be almost independent of the fitting functional and thus provides a reliable

estimate of the mobility edge. Figure 4.10(b) shows the mobility edge versus the quasiperiodic amplitude for various interaction strengths. The error-like bars represent the edges of the minigap containing the mobility edge. The uncertainty on the fitted mobility edge is smaller than these bars. The red-dotted line is the result of the analytical effective model developed in the next section.

4.4 Analytical approach : building an effective model

In order to interpret those results, we now turn to an analytical treatment of the localization problem. The main difficulty lies on the fact that localization in quasiperiodic systems occurs for strong quasiperiodic amplitude Δ [195]. For this reason, lowest-order perturbation theory, which proved successful for 1D disordered systems [13, 79, 170], fails here [10]. To overcome this issue, we will develop in the following an approach based on a generic expansion in harmonics of the quasiperiodic potential. In Sec. 4.4.1, we analytically determine the density background n_j and show that it takes the form of a series of harmonics of the quasiperiodic potential. As we detail then in Sec. 4.4.2, this permits to map the localization problem for the excitations onto that of an effective multiharmonic quasiperiodic system. The latter is solved in Sec. 4.4.3 using locator perturbation theory, providing analytical estimates of the localization transition.

4.4.1 Harmonic expansion of the density background

In this section, we determine the density background n_j, and show that it takes the form of as a series of harmonics of the quasiperiodic potential which, remarkably, can be analytically computed.

General series expansion of the density background

To determine the density background $n_j \equiv \phi_j^2$, one has to solve the GPE (4.20) together with the normalization condition

$$n = \frac{1}{L}\Sigma_j n_j, \tag{4.26}$$

where L is the number of sites and n is the averaged density. To do so, we perform a series expansion in powers of the quasiperiodic potential V_j. In the absence of an external potential, we have $\phi_j = \sqrt{n}$ and the chemical potential $\mu = Un$. In the presence of an external potential, we then write

$$\phi_j = \sqrt{n}\left(\phi_j^{(0)} + \phi_j^{(1)} + \phi_j^{(2)} ...\right) \tag{4.27}$$

$$\mu = Un\left(\mu^{(0)} + \mu^{(1)} + \mu^{(2)} + ...\right) \tag{4.28}$$

$$n_j = n\left(n_j^{(0)} + n_j^{(1)} + n_j^{(2)} ...\right) \tag{4.29}$$

where the superscripts denote increasing orders in the quasiperiodic amplitude Δ, and $\phi_j^{(0)} = 1$, $n_j^{(0)} = 1$, $\mu^{(0)} = 1$. Notice that the chemical potential has to be expanded also to fulfill the

[10] We have found that lowest-order perturbation theory as used for 1D disordered, interacting Bose gases in Refs. [13,79,170] is both quantitatively and qualitatively incorrect here. In particular, it predicts a diagram that is inconsistent with that of Fig. 4.9 and it is not able to predict the localization transition. We will come back on this point later.

normalization condition (4.26). Inserting the expansions (4.27) and (4.28) in the GPE (4.20), and the expansion (4.29) in the normalization condition (4.26), we get

$$\begin{aligned} Un\left(\mu^{(0)}+\mu^{(1)}+...\right)\left(\phi_j^{(0)}+\phi_j^{(1)}+...\right) &= -\hat{T}\left(\phi_j^{(0)}+\phi_j^{(1)}+...\right)+V_j\left(\phi_j^{(0)}+\phi_j^{(1)}+...\right) \\ &\quad +Un\left(\phi_j^{(0)}+\phi_j^{(1)}+...\right)^3 \end{aligned} \tag{4.30}$$

and

$$\frac{1}{L}\sum_j\left(\phi_j^{(0)}+\phi_j^{(1)}+...\right)^2=1. \tag{4.31}$$

Then, collecting all the terms of same order p in the quasiperiodic amplitude yields

$$\left(1-\frac{1}{2Un}\hat{T}\right)\phi_j^{(p)}=-\frac{V_j}{2Un}\phi_j^{(p-1)}-\frac{1}{2}\sum_{\substack{k+\ell+m=p\\0\leq k,\ell,m\leq p-1}}\phi_j^{(k)}\phi_j^{(\ell)}\phi_j^{(m)}+\frac{1}{2}\sum_{1\leq k\leq p-1}\mu^{(k)}\phi_j^{(p-k)}+\frac{\mu^{(p)}}{2} \tag{4.32}$$

and

$$\sum_j\left(2\phi_j^{(0)}\phi_j^{(p)}+\sum_{1\leq k\leq p-1}\phi_j^{(k)}\phi_j^{(p-k)}\right)=0. \tag{4.33}$$

Equations (4.32) and (4.33) can then be used to iteratively compute all $\phi_j^{(p)}$ and $\mu^{(p)}$, at any required order p. The iteration process works as follows. Given all $\phi_j^{(k)}$ and $\mu^{(k)}$ at orders $k<p$, we calculate $\phi_j^{(p)}$ as a function of $\mu^{(p)}$ from Eq. (4.32) by inverting the operator $1-\hat{T}/2Un$. The quantity $\mu^{(p)}$ is then found by inserting this expression for $\phi_j^{(p)}$ into Eq. (4.33). Having determined $\phi_j^{(p)}$, we then find the density field using Eq. (4.29), whose expansion in powers of the quasiperiodic amplitude writes

$$n_j^{(p)}=\sum_{\substack{k+\ell=p\\0\leq k,\ell\leq p}}\phi_j^{(k)}\phi_j^{(\ell)}. \tag{4.34}$$

This procedure is completely general and can be applied to any external potential V_j. In particular, it can easily be numercically implemented in a recursive way. In the case of a quasiperiodic potential $V_j=\Delta\cos(2\pi rj+\varphi)$, we have implemented it up to order 50 and found excellent agreement with the direct numerical solution of the GPE (4.20) obtained by imaginary time propagation (see Fig. 4.11). It provides a cross-check of the precision of the numerical solution and of the convergence of the present analytical expansion. Additionally, Fig. 4.11 shows that in the regime of interest ('ext-loc regime' of Fig. 4.11), first-order terms are generally not sufficient to accurately capture the density profile. Therefore, one needs a priori to take into account the full series to accurately describe this regime.

Analytical expansion in the case of a quasiperiodic potential

We now show that in the case of the quasiperiodic potential $V_j=\Delta\cos(2\pi rj+\varphi)$, the above iterative process remarkably becomes fully algebraic, since the operator $1-\hat{T}/2Un$ in Eq. (4.32) can be analytically inverted at any order. This will in particular allow us to give explicit analytical formulas for the lowest-order terms, and enlighten the harmonic structure of

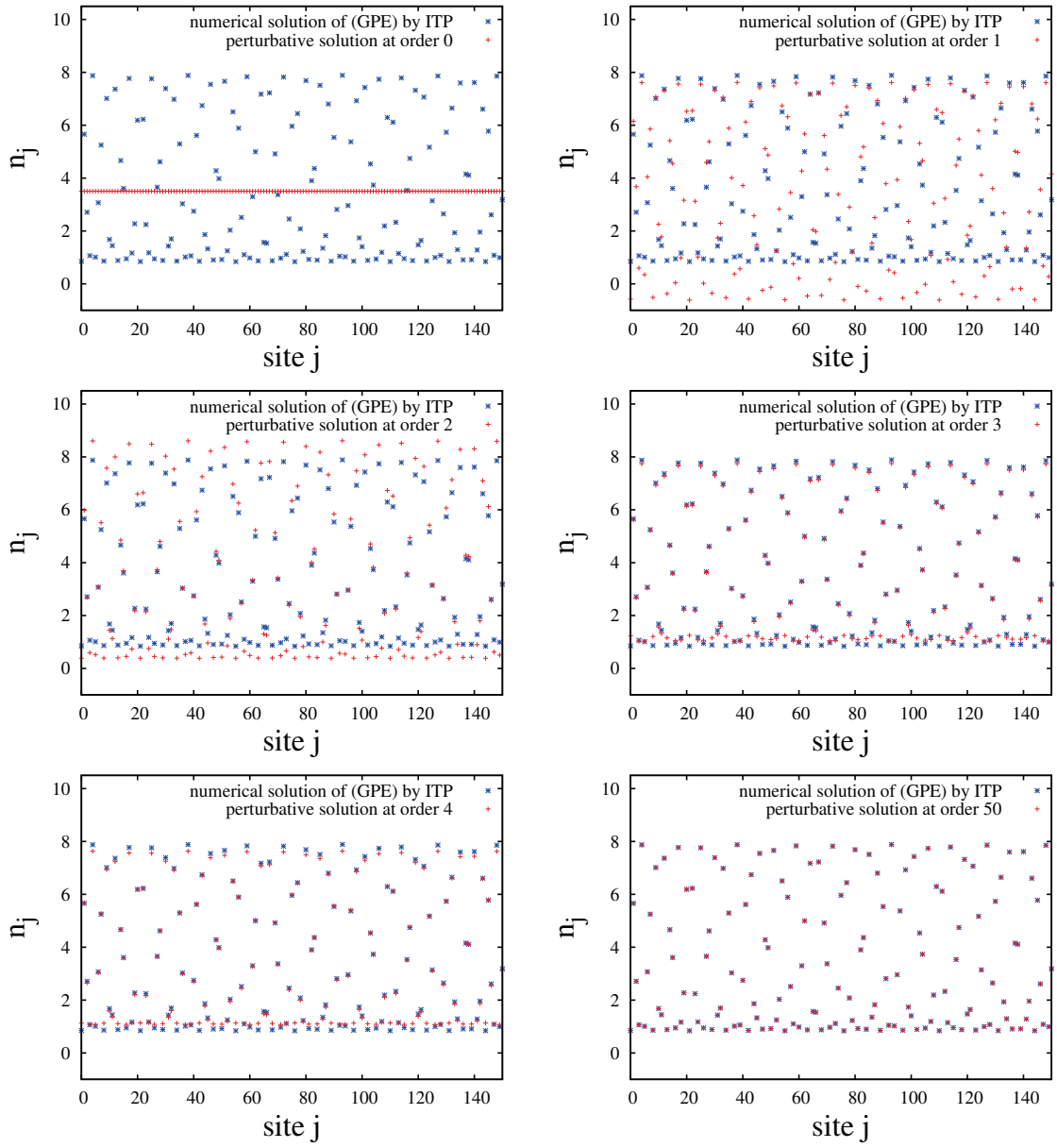

Figure 4.11: Comparison between the density profile as numerically obtained by imaginary time propagation (blue), and as obtained from the above perturbative procedure (red), iteratively implemented at various orders (from left to right and top to bottom : 0, 1, 2, 3, 4, 50). The used parameters ($Un/t = 1.75$ and $\Delta/t = 3.7$) correspond to a regime 'ext-loc' in the localization diagram). When going to increasing orders, the agreement gets better and better. This provides a cross-check of both the precision of the numerical solution and the convergence of the analytical expansion.

the density background n_j. In the following, it will prove convenient to write the density field in the form

$$n_j = \frac{\mu - \tilde{V}_j}{U}, \tag{4.35}$$

where the field $\tilde{V}$ includes corrections of all orders to the homogeneous density profile.

At first order, Eq. (4.32) reduces to $-\hat{T}\phi_j^{(1)} + 2Un\phi_j^{(1)} = -V_j + Un\mu^{(1)}$. It is straightforward

to solve it in Fourier space where the operator $\hat{T}$ is diagonal. It yields

$$\phi_k^{(1)} = -\frac{V_k - Un\mu^{(1)}\delta_{k,0}}{\varepsilon_k + 2Un},$$

where we recall that the free-particle dispersion relation is $\varepsilon_k = 4t\sin^2(k/2)$ [see Eq. (4.18)]. Inserting the previous expression for $\phi_k^{(1)}$ into Eq. (4.33), we find $\mu^{(1)} = V_{k=0}/Un = 0$ and

$$\phi_k^{(1)} = -\frac{V_k}{\varepsilon_k + 2Un}.$$

Remarkably, since the quasiperiodic potential contains only the spatial frequency r (in Fourier space, $V_k = \Delta(e^{i\varphi}\delta_{k,+2\pi r} + e^{-i\varphi}\delta_{k,-2\pi r})/2$), one can immediately get back to real space and write

$$\phi_j^{(1)} = -\frac{\Delta}{2Un} f_r \cos(2\pi r j + \varphi), \tag{4.36}$$

where $f_r = \dfrac{1}{1 + \varepsilon_{2\pi r}/2Un}$.

Hence, to lowest order, the density profile is a quasiperiodic field. It exactly follows the modulations of the quasiperiodic potential, although with a reduced amplitude since $f_r < 1$ [11]. The factor f_r is a remainder of the nonlocal operator $1-\hat{T}/2Un$ in the l.h.s. of Eq. (4.32), which reduces to an algebraic operation in the case of a quasiperiodic potential. Then, Eqs. (4.34) and (4.35) yield the first order term of the field $\tilde{V}_j$. It reads $\tilde{V}_j^{(1)} = -2Un\phi_j^{(1)}$ where $\phi_j^{(1)}$ is given by Eq. (4.36), i.e.

$$\tilde{V}_j^{(1)} = \Delta f_r \cos(2\pi r j + \varphi). \tag{4.37}$$

The next orders are found following the same process, which remains algebraic to any order in the case of the quasiperiodic potential. To second order, it yields the term

$$\phi_j^{(2)} = \left(\frac{\Delta}{2Un}\right)^2 \left[-\frac{f_r^2}{4} + \left(f_r - \frac{3}{2}f_r^2\right) f_{2r} \frac{\cos[2(2\pi r j + \varphi)]}{2} \right], \tag{4.38}$$

and a negative shift on the chemical potential,

$$\mu^{(2)} = -\left(\frac{\Delta}{2Un}\right)^2 (f_r - f_r^2). \tag{4.39}$$

The field $\tilde{V}_j$ is then given at second order by $\tilde{V}_j^{(2)} = Un[\mu^{(2)} - n_j^{(2)}] = Un[\mu^{(2)} - (2\phi_j^{(2)} + \phi_j^{(1)2})]$ where $\phi^{(1)}$, $\phi^{(2)}$ and $\mu^{(2)}$ are given by Eqs. (4.36), (4.38), and (4.39), i.e.

$$\tilde{V}_j^{(2)} = -\frac{\Delta^2}{4Un} \left\{ f_r - f_r^2 + \left[\frac{f_r^2}{2} + \left(f_r - \frac{3}{2}f_r^2\right) f_{2r} \right] \cos[2(2\pi r j + \varphi)] \right\}. \tag{4.40}$$

Hence, the second-order terms $\phi_j^{(2)}$ and $\tilde{V}_j^{(2)}$ contain a constant term and the second harmonics of the quasiperiodic potential. Those terms are generated by the nonlinear term of the GPE.

[11] The presence of the factor f_r is closely linked to the smoothing effect occurring in the continuous case and discussed in chapter 3. However, since the bare quasiperiodic potential contains only one frequency, smoothing simply amounts here to a reduction of its amplitude (instead of smoothing out its short-wavelength variations, as generically expected).

Indeed, since the first order term contains only the first harmonic, $\phi_j^{(1)} \propto \cos(2\pi r j + \varphi)$, the product terms $\phi_j^{(1)}\phi_j^{(1)}\phi_j^{(0)}$ appearing in Eq. (4.32) contain only the zeroth and second harmonics.

More generally, it is straightforward to show recursively that the terms of order p, $\phi_j^{(p)}$ and $\tilde{V}_j^{(p)}$, contain the p-th harmonics of the quasiperiodic potential, $\cos[p(2\pi r j + \varphi)]$, as well as all lower harmonics of same parity. In particular, a constant term in ϕ_j and a correction to the chemical potential μ appear only at even orders. Hence, $\tilde{V}_j$ takes the form of a multi-harmonic quasiperiodic field

$$\tilde{V}_j = \sum_p A_p \cos[p(2\pi r j + \varphi)], \tag{4.41}$$

where the amplitude A_p of the p-th harmonics is a power series of order p, $A_p \sim \alpha_p(\Delta/2Un)^p + \alpha_{p+2}(\Delta/2Un)^{p+2} + ...$ The amplitudes A_p can be analytically obtained iteratively following the above procedure.

4.4.2 A multi-harmonic effective model for the excitations

Knowing the density field, we now turn to the localization problem for the excitations, as defined by the BdGEs (4.22). Using the energy-dependent linear transformation [13, 79]

$$g_j^{\pm} = \pm\rho_E^{\pm 1/2}(u_j - v_j) + \rho_E^{\mp 1/2}(u_j + v_j) \tag{4.42}$$

where $\rho_E = \sqrt{1 + (\mu/E)^2} + \mu/E$, the BdGEs (4.22) exactly rewrite

$$-(\rho_E^{-1}E + \hat{T})g_j^+ + \left[V_j - \frac{3+\rho_E^2}{1+\rho_E^2}\tilde{V}_j\right]g_j^+ = \frac{2\rho_E\tilde{V}_j}{1+\rho_E^2}g_j^- \tag{4.43}$$

$$(\rho_E E - \hat{T})g_j^- + \left[V_j - \frac{1+3\rho_E^2}{1+\rho_E^2}\tilde{V}_j\right]g_j^- = \frac{2\rho_E\tilde{V}_j}{1+\rho_E^2}g_j^+. \tag{4.44}$$

The solution of these equations is significantly simplified by noticing that the real-space Green function of the operator $-\hat{T} + \rho_E E$ is of width $\sqrt{t/\rho_E E}$ and amplitude $1/(\rho_E E + 2t)\sqrt{1 - [2t/(\rho_E E + 2t)]^2}$. Hence, for $\rho_E E \gg t$, this operator can be replaced by the local operator $\rho_E E + 2t$ in Eq. (4.44). It is then straightforward from Eq. (4.44) to write the expression of g_j^- as a function of g_j^+ and of the potentials V_j and $\tilde{V}_j$. Inserting this expression into Eq. (4.43) we find a closed equation for g_j^+,

$$-\hat{T}g_j^+ + \mathcal{V}_j^E g_j^+ = E\rho_E^{-1}g_j^+, \tag{4.45}$$

with the effective potential [12]

$$\mathcal{V}_j^E \simeq V_j - \frac{3+\rho_E^2}{1+\rho_E^2}\tilde{V}_j - \frac{\left(\frac{2\rho_E}{1+\rho_E^2}\right)^2\tilde{V}_j^2}{\rho_E E + 2t + V_j - \frac{1+3\rho_E^2}{1+\rho_E^2}\tilde{V}_j}. \tag{4.46}$$

Equation (4.45) with the potential (4.46) shows that the localization problem of an excitation at energy E can be mapped onto that of a single particle in an effective potential $\mathcal{V}_j^E$. As

[12] Notice that in the non-fragmented regime, the denominator in Eq. (4.46) is always strictly positive.

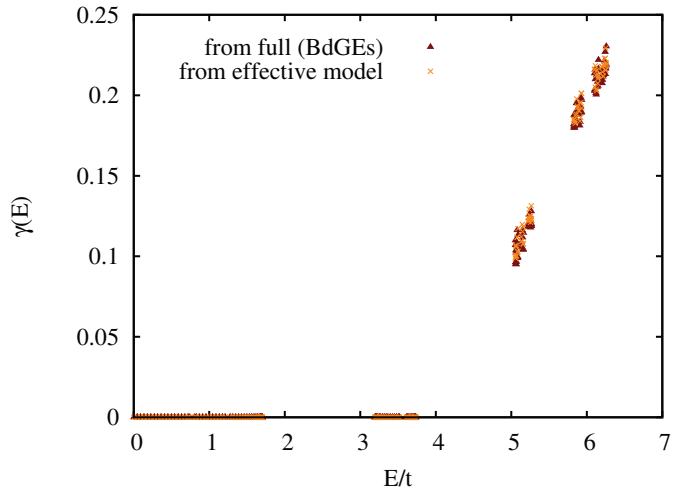

Figure 4.12: Lyapunov exponent as obtained from the full numerical resolution (dark red triangles, same curve as on Fig. 4.10), and from the numerical diagonalization of the effective model (4.45) (orange crosses), for parameters $Un/t = 1.75$ and $\Delta/t = 3.7$. The effective model qualitatively and quantitatively reproduces the localization transition and the behaviour of the Lyapunov exponent.

an additional cross-check, we have performed an exact diagonalization of Eq. (4.45) with the potential (4.46) around energy E (taking for $\tilde{V}_j$ the (exact) numerical density profile). The results are displayed on Fig. 4.12, and show that the Lyapunov exponents and the localization transition given by this effective model coincide with those found using direct diagonalization of the BdGEs (4.22). It validates the effective model (4.45)-(4.46) and the approximation $-\hat{T} + \rho_E E \simeq 2t + \rho_E E$ used above.

More importantly, this effective model qualitatively explains the localization transition of the collective excitations. Indeed, the quantity $\mathcal{V}_j^E$ is a multiharmonic periodic potential whose period $1/r$ is incommensurate with that of the main lattice, which is unity. As discussed in Sec. 4.1.3, multiharmonic quasiperiodic potentials are known to exhibit in general an energy-dependent mobility edge with low-energy extended states and high-energy localized states [211, 218, 220, 222]. This holds except in the particular case of self-dual models, where the localization transition is generally energy-independent. This is however not the case of our effective model, since self-duality requires a specific relation between the amplitudes of the p-th harmonics and of the tunelling rate to the p-th neighbors, while tunelling is strictly restricted here to the first neighbors. Therefore, the mapping onto a multi-harmonic quasiperiodic potential provides an interpretation of the energy-dependent localization transition observed numerically [13]. Importantly, it should be noticed that interactions change here the universality class of the transition, which differs from that of the non-interacting Aubry-André case. This contrasts with the purely disordered case discussed in the previous chapter, where all excitations remain localized in one-dimension, similarly to the non-interacting case [79].

One now understands as well why lowest-order perturbation theory fails here to reproduce the localization transition. At lowest order, the effective potential $\mathcal{V}_j^E$ would artificially be truncated to its first-order term, and would become a pure quasiperiodic potential

[13] Rigourously speaking, the energy dependance of the effective potential $\mathcal{V}_j^E$ could yield a more complex energy dependence of the localization behaviour, but we find that it is not the case.

$\Delta_E^{(1)} \cos(2\pi r j + \varphi)$. This would unphysically restore duality in the effective model, which would fall into the very particular universality class of the Aubry-André model. More precisely, a discussion of the effective model based on the simple Aubry-André criterion, $\Delta_E^{(1)} > 2J$, predicts a completely wrong localization diagram.

4.4.3 Localization behaviour

Localization properties can be further inferred using locator perturbation theory [211], as presented in Sec. 4.1.3. In particular, the latter provides a localization criterion, which roughly corresponds to the convergence of the self-energy in the thermodynamic limit. This criterion reads $D(E) > 1$, where $D(E)$ is the so-called localization function. In the case of the effective model Eq. (4.45), the latter reads

$$D(E) = \exp\left(r \int_0^{1/r} dx \, \ln \left| \frac{E\rho_E^{-1} - 2t - \mathcal{V}^E(x)}{t} \right| \right). \tag{4.47}$$

Indeed, this straightforwardly comes from the general definition Eq. (4.16), by noticing that the integral can be restricted to one period of the potential, and that the effective energy of the equivalent model, $E\rho_E^{-1}$ (and not E !), should be shifted by $-2t$ to correct for the position of the center of the band (we recall that locator perturbation theory is formulated for an energy band centered on the zero of energies). Equation (4.47) can in principle be applied to the full effective potential $\mathcal{V}^E(x)$. In order to obtain analytical results, it is however worth truncating the infinite series of harmonics in $\mathcal{V}^E$. As mentionned previously, keeping only one harmonic is not sufficient to capture the physics even qualitatively, since it would artificially restore duality and change the universality class of the localization transition. On the other hand, beyond two, the number of harmonics does not change the universality class and very weakly affects the position of the mobility edge, as discussed in Sec .4.1.3. We may thus restrict ourselves to the two lowest-order harmonics, which are generated in first instance in second-order perturbation theory. As this order, one immediately gets from Eq. (4.46)

$$\mathcal{V}_j^E \simeq V_j - \frac{3+\rho_E^2}{1+\rho_E^2}\tilde{V}_j^{(1)} - \frac{3+\rho_E^2}{1+\rho_E^2}\tilde{V}_j^{(2)} - \frac{\left(\frac{2\rho_E}{1+\rho_E^2}\right)^2}{\rho_E E + 2t}\left(\tilde{V}_j^{(1)}\right)^2, \tag{4.48}$$

where $\tilde{V}^{(1)}$ and $\tilde{V}^{(2)}$ are given in Eqs. (4.37) and (4.40). It yields the two-harmonic effective potential

$$\mathcal{V}_j^E \simeq \Delta_E^{(0)} + \Delta_E^{(1)} \cos(2\pi r j + \varphi) + \Delta_E^{(2)} \cos[2(2\pi r j + \varphi)] \tag{4.49}$$

with the amplitudes

$$\Delta_E^{(0)} = \frac{3+\rho_E^2}{1+\rho_E^2}\frac{\Delta^2}{4Un}(f_r - f_r^2) - \frac{2\rho_E^2}{(1+\rho_E^2)^2}\frac{\Delta^2 f_r^2}{\rho_E E + 2t} \tag{4.50}$$

$$\Delta_E^{(1)} = \Delta\left[1 - \frac{3+\rho_E^2}{1+\rho_E^2} f_r\right] \tag{4.51}$$

$$\Delta_E^{(2)} = \frac{3+\rho_E^2}{1+\rho_E^2}\frac{\Delta^2}{4Un}\left[\frac{f_r^2}{2} + \left(f_r - \frac{3}{2}f_r^2\right) f_{2r}\right] - \frac{2\rho_E^2}{(1+\rho_E^2)^2}\frac{\Delta^2 f_r^2}{\rho_E E + 2t}, \tag{4.52}$$

and $f_r = \dfrac{1}{1 + 2t \sin^2(\pi r)/Un}$. The result of locator perturbation theory applied to the two-harmonic potential (4.49) is shown on Fig 4.10(b). It correctly predicts a localization transition where collective excitations are extended at low energy and localized at high energy. Moreover, its estimation of the position of the mobility edge is in very good agreement with the full numerical results.

Perturbation theory beyond second order generates higher-order harmonics in the effective potential and renormalizes the amplitudes $\Delta^{(0)}$, $\Delta^{(1)}$ and $\Delta^{(2)}$. For $U \lesssim 3t$, we find that they induce negligible effects and do not significantly affect the prediction for the mobility edge. For higher values of U, however, second-order perturbation theory is not sufficient to accurately estimate the density background, and higher-order terms should be included.

4.5 Conclusions

In summary, we have shown that the collective excitations of lattice Bose superfluids subjected to a single-harmonic quasiperiodic potential undergo a localization transition with extended low-energy states and localized high-energy states. In particular, it should be emphasized that the interactions change here the universality class of the localization transition. This is in striking contrast with the purely disordered case [13, 79, 170], where even in the presence of interactions, all excitations remain localized in one dimension. In the quasiperiodic case, the transition can be understood as the result of the scattering of collective excitations by the potential and the density background, which contains an infinite series of harmonics of the potential.

It could be observed in ultracold-atom experiments, using for instance spectroscopy techniques, which give direct access to the excitations [227–229]. Alternatively, it could be observed in quench dynamics, where the abrupt change of some physical parameter generates collective excitations that govern the propagation of experimentally-observable correlations [119, 120, 123, 124, 184, 185].

Chapter 5

Two-component Bose gases with one-body and two-body couplings

Mais je n'ai plus trouvé qu'un horrible mélange.
Jean Racine, Athalie, Acte II, scène 5

Multi-component (spinor) quantum fluids underlie a variety of physical systems, such as ^{3}He-^{4}He mixtures in three-fluid models [230], Bose-condensed spin-polarized Hydrogen gases in the two lowest-energy states [231–233], optically-excited excitons in high-quality Cu_20 crystals [234, 235], as well as gaseous Bose-Einstein condensates either in two overlaped atomic hyperfine states [236–238] or in adjacent traps coupled by tunnel effect [239]. In particular, in the context of ultracold gases, manipulating the internal states of alkali atoms via the combination of optical and magnetic fields offers numerous possibilities to accurately engineer multi-component quantum fluids. The dynamics of such spinor gases sparks a variety of physical effects, including quantum phase transitions, topological defects and spin domains, governed by the complex interplay between particle-particle interaction, exchange coupling, magnetic-like ordering, and temperature effects. Early studies focused on the possibility of observing Bose-Einstein condensation [240], as well as stability conditions [230, 241, 242], phase separation [237, 243–249], and spontaneous symmetry breaking mechanisms [250–253] in two-component Bose-Einstein condensates. Two-component Bose gases have also been used to study phase coherence [254], Josephson-like physics [255–259], spin texture dynamics [260–263], and twin quantum states for quantum information processing [264–266].

Among the main challenges in the field of two-component Bose gases lies the question of disorder. As for single component Bose gases, disorder in interacting Bose systems is indeed expected to induce nontrivial effects [3]. More interestingly however, multi-component gases have been shown to display more intriguing features, among which *random-field-induced order (RFIO)* effects [126–129], i.e. long-range order induced by a random field, which are attracting a growing attention.

Random-field-induced order effects were originally predicted in the context of spin systems [126]. In low-dimensional spin systems with continous symmetry, long-range order is a priori forbidden by virtue of the Mermin-Wagner-Hohenberg theorem. However, a small

amount of disorder can break the continuous symmetry of the system and make it magnetize, hence restoring long-range order. This is for instance the case of the classical XY model on a 2D lattice in a uniaxial random field, which spontaneously magnetizes at T = 0 in the direction perpendicular to the magnetic field axis, as well as at low temperatures. An analogous effect has be identified in two-component Bose gases [127] submitted to a random Raman coupling, the latter inducing at the meanfield level a relative phase of $\pi/2$ between the two Bose-Einstein condensates. This effect has been proved in 1D, 2D and 3D at zero temperature, but understanding how finite temperature affects it remains an open question.

More generally, disorder can be introduced in multi-component ultracold gases in several other ways, which would be worth studying. First, disordered potentials have been shown to induce Anderson localization of Bogoliubov excitations in single-component Bose gases [13, 79, 172, 267] [see chapters (3) and (4)], but the extension to the case of coupled Bose gases is an open question. Secondly, since disorder can be included in interaction terms using inhomogeneous Feshbach resonances [268], it could be interesting to study the effects of random inter-species couplings.

To systematically study disorder-induced effects at zero and finite temperature, one needs to develop a unified formalism for inhomogeneous two-component Bose gases, going beyond the meanfield level. For single-component Bose gases, this is achieved by the Bogoliubov theory [see chapter (2)], which has been successfully used to study the influence of disorder in various contexts, as presented in the previous chapters (3) and (4). In this chapter, we extend the Bogoliubov theory to the case of a two-component Bose gas, in the most general inhomogeneous framework. We then apply this formalism to the case of a homogeneous gas, which in particular allows for the determination of collective excitations, as well as correlation functions and fluctuations of the two-component Bose gas at zero and finite temperature [269]. Although technically simpler, the homogeneous case already features many non-trivial physical effects. Therefore, its understanding constitutes to some extent a necessary step before addressing the question of disorder.

All along this chapter, we will consider a two-component Bose gas with both one-body (field-field) and two-body (density-density) couplings, and formulate our theory in the most general case, where both one-body and two-body couplings are position-dependent and the fluid is subjected to a state-dependent external potential. This can be realized in ultracold-atom gases by using a mixture of atoms in two different internal hyperfine states (noted 1 and 2) of the same atomic species. The two-body interaction with coupling constant g_{12} results from short-range particle-particle interactions between atoms in different internal states, while the one-body interaction can be implemented by two-photon Raman optical coupling, which transfers atoms from one internal state to the other (see schematic view on Fig. 5.1). In Sec. 5.1, we present the model and derive the meanfield theory of the coupled two-component Bose fluid for both ground state and low-energy pair excitations. The use of the phase-density Bogoliubov-Popov approach permits to treat true condensates and quasi-condensates on an equal footing [156, 270]. General formulas for phase and density correlations are derived. In Sec. 5.2, we focus on the case of homogeneous systems. After rewriting the general meanfield equations for homogeneous systems (5.2.1), we discuss the pair-excitation spectrum and the corresponding fields (5.2.2), and use them to calculate the correlation functions including both quantum and thermal fluctuation terms (5.2.3).

5.1 Mean-field theory of a two-component Bose gas

We consider a two-component Bose-Bose mixture at thermodynamic equilibrium at temperature T, and in the weakly interacting regime. We assume that the two components (labelled by $\sigma \in \{1,2\}$) interact with each other and can exchange atoms to maintain chemical equilibrium. The average total number of atoms, $N = N_1 + N_2$, is conserved but the average number of atoms in each component, N_σ, is not. The physics of this system is governed by the grand-canonical Hamiltonian

$$\hat{H} \equiv \hat{\mathcal{H}} - \mu\hat{N} = \hat{H}_1 + \hat{H}_2 + \hat{H}_{12}\,, \tag{5.1}$$

where $\hat{\mathcal{H}}$ is the many-body Hamiltonian and $\hat{N} = \hat{N}_1 + \hat{N}_2$ is the total number operator, with $\hat{N}_\sigma = \int \mathrm{d}\mathbf{r}\ \hat{\psi}^\dagger_\sigma(\mathbf{r})\hat{\psi}_\sigma(\mathbf{r})$ and $\hat{\psi}_\sigma(\mathbf{r})$ the (bosonic) field operator of component σ. Assuming two-body contact interactions, the Hamiltonian associated the the sole component σ (written in the grand-canonical form for the chemical potential μ of the mixture) is

$$\hat{H}_\sigma = \int \mathrm{d}\mathbf{r}\ \hat{\psi}^\dagger_\sigma \left[-\frac{\hbar^2\nabla^2}{2m} + V_\sigma - \mu + \frac{g_\sigma(\mathbf{r})}{2}\hat{\psi}^\dagger_\sigma\hat{\psi}_\sigma\right]\hat{\psi}_\sigma \tag{5.2}$$

and the coupling Hamiltonian is

$$\hat{H}_{12} = \int \mathrm{d}\mathbf{r}\left[\, g_{12}(\mathbf{r})\hat{\psi}^\dagger_1\hat{\psi}^\dagger_2\hat{\psi}_1\hat{\psi}_2 + \left(\frac{\hbar\Omega(\mathbf{r})}{2}\hat{\psi}^\dagger_2\hat{\psi}_1 + \mathrm{H.c.}\right)\right]. \tag{5.3}$$

The single-component Hamiltonian $\hat{H}_\sigma$ contains (i) a kinetic term (m is the atomic mass), (ii) a potential term, $V_\sigma(\mathbf{r})$, both associated with single-particle dynamics, and (iii) an intra-component interaction term of coupling parameter g_σ. The coupling Hamiltonian, $\hat{H}_{12}$, contains (i) a term originating from elastic contact interaction between two atoms in different components characterized by the inter-component coupling constant g_{12}, and (ii) an exchange term proportional to Ω, which transfers atoms from one component to the other and in particular permits chemical equilibrium. In ultracold-atom systems, the exchange one-body term can be realized by two-photon Raman or radio-frequency coupling [236] or by Josephson coupling between two adjacent traps [255, 259, 271–273], whereas the two-body coupling can be controlled by Feshbach resonance techniques [274]. In the most general case, all coupling terms g_1, g_2,

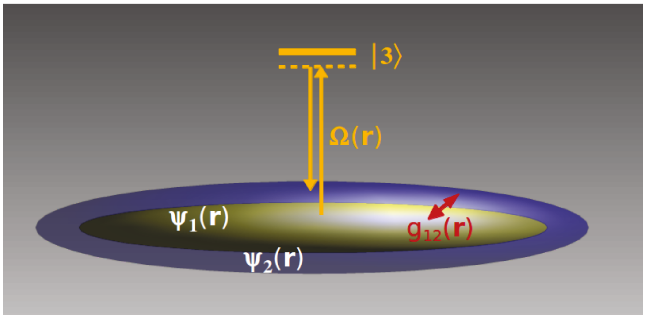

Figure 5.1: Coupled two-component Bose gas. The gas is made of bosonic particles of a single atomic species, which can be in two different internal states (labeled 1 and 2). It is described by the two field operators $\hat{\psi}_1(\mathbf{r})$ and $\hat{\psi}_2(\mathbf{r})$, corresponding to each component. We assume that the two components are coupled by one-body and/or two-body interactions of respective coupling constants Ω and g_{12}, which can be position dependent in the most general case.

g_{12}, and Ω can be position-dependent. Hereafter, we write $\Omega(\mathbf{r}) \equiv \Omega_0(\mathbf{r})\mathrm{e}^{-i\alpha(\mathbf{r})}$, with $\Omega_0 = |\Omega|$ and $\alpha(\mathbf{r})$ the phase of the exchange coupling, for convenience.

In the following, we first reformulate the above Hamiltonians into the phase-density formalism, which is more appropriate for our study. We then apply the Gross-Pitaevskii approach, which describes the meanfield quasicondensate background of the two-component Bose-Bose mixture, and develop the Bogoliubov-de Gennes theory for the mixture, which provides the spectrum of collective excitations and can be used to describe finite-temperature effects. We finally write down the general expressions for the density and phase correlation functions, which will be calculated in the next sections.

5.1.1 Phase-density formalism

The complete grand-canonical Hamiltonian $\hat{H}$ is invariant under the gauge transformation $\{\hat{\psi}_1(\mathbf{r}), \hat{\psi}_2(\mathbf{r})\} \to \mathrm{e}^{i\theta_0}\{\hat{\psi}_1(\mathbf{r}), \hat{\psi}_2(\mathbf{r})\}$ for any value of $\theta_0 \in \mathbb{R}$, as can be easily checked in Eqs. (5.2) and (5.3). More precisely, if $\Omega(\mathbf{r}) \equiv 0$, the phases of the two components are independent and $\hat{H}$ is invariant under the more general transformation $\{\hat{\psi}_1(\mathbf{r}), \hat{\psi}_2(\mathbf{r})\} \to \{\mathrm{e}^{i\theta_0^1}\hat{\psi}_1(\mathbf{r}), \mathrm{e}^{i\theta_0^2}\hat{\psi}_2(\mathbf{r})\}$ for any values of $\theta_0^1, \theta_0^2 \in \mathbb{R}$. If however $\Omega(\mathbf{r}) \not\equiv 0$, the phases of the two components are coupled via the last term in Eq. (5.3) and the relative phase is a determined quantity. In both cases, the phases of the field operators $\hat{\psi}_\sigma(\mathbf{r})$ are not fully determined and it is useful to turn to the phase-density formalism. The latter has been successfully used for a long time [270, 275] and was recently developed in a lattice formulation, which allows for a precise definition of the phase operator [154]. We write the field operator for each component in the form

$$\hat{\psi}_\sigma(\mathbf{r}) = \mathrm{e}^{i\hat{\theta}_\sigma(\mathbf{r})}\sqrt{\hat{n}_\sigma(\mathbf{r})}, \tag{5.4}$$

where the density ($\hat{n}_\sigma$) and phase ($\hat{\theta}_\sigma$) operators satisfy the Bose commutation rule $[\hat{n}_\sigma(\mathbf{r}), \hat{\theta}_{\sigma'}(\mathbf{r}')] = i\delta_{\sigma\sigma'}\delta(\mathbf{r}-\mathbf{r}')$. Replacing $\hat{\psi}_\sigma$ by expression (5.4) into Eqs. (5.2) and (5.3), we find

$$\hat{H}_\sigma = \int \mathrm{d}\mathbf{r}\ \sqrt{\hat{n}_\sigma}\Big[\frac{-\hbar^2}{2m}\left(\nabla^2 - |\nabla\hat{\theta}_\sigma|^2\right) + V_\sigma - \mu + \frac{g_\sigma}{2}\hat{n}_\sigma\Big]\sqrt{\hat{n}_\sigma} \tag{5.5}$$

and

$$\hat{H}_{12} = \int \mathrm{d}\mathbf{r}\ \Big[g_{12}\hat{n}_1\hat{n}_2 + \Big\{\frac{\hbar\Omega}{2}\sqrt{\hat{n}_2}\mathrm{e}^{i(\hat{\theta}_1-\hat{\theta}_2)}\sqrt{\hat{n}_1} + \mathrm{H.c.}\Big\}\Big]. \tag{5.6}$$

Expressions (5.5) and (5.6) determine the complete Hamiltonian (5.1) in terms of density and phase operators [1]. This form is particularly suitable for perturbative expansion in the condensate or quasi-condensate regime, where the density fluctuations are suppressed by strong-enough repulsive interactions but the phase fluctuations can be large [154, 156, 158, 270, 276].

5.1.2 Meanfield background: Gross-Pitaevskii theory

The zeroth-order term in quantum and thermal fluctuations corresponds to the meanfield background. The latter is determined using the Gross-Pitaevskii approach [147, 277], adapted to the two-component mixture. It amounts to minimize the grand-canonical energy functional $E_{\mathrm{MF}} \equiv \langle\psi_{\mathrm{MF}}|\hat{H}|\psi_{\mathrm{MF}}\rangle$ with the two-component Hartree-Fock ansatz

$$|\psi_{\mathrm{MF}}\rangle = \frac{(\hat{a}_1^\dagger)^{N_1}}{\sqrt{N_1!}}\ \frac{(\hat{a}_2^\dagger)^{N_2}}{\sqrt{N_2!}}\ |\mathrm{vac}\rangle\,, \tag{5.7}$$

[1] Note that we have dropped a constant term arising from the commutation relation of $\hat{\psi}_\sigma(\mathbf{r})$ and $\hat{\psi}_\sigma^\dagger(\mathbf{r})$ in the intra-component interaction term of Eq. (5.2). The latter can be absorbed in a renormalization of the chemical potential μ.

where $\hat{a}_\sigma^\dagger$ creates an atom in component σ with a spatial wave function $\psi_\sigma(\mathbf{r}) \equiv \mathrm{e}^{i\theta_\sigma(\mathbf{r})}\sqrt{n_\sigma(\mathbf{r})}$. At this stage, the number of atoms in each component, N_σ, and the corresponding phase $[\theta_\sigma(\mathbf{r})]$ and density $[n_\sigma(\mathbf{r})]$ fields are unknown variational quantities. Here, we use the normalization condition $\int \mathrm{d}\mathbf{r}\; n_\sigma(\mathbf{r}) = N_\sigma$ and we recall that the chemical potential μ is determined implicitly by the relation $\int \mathrm{d}\mathbf{r}\; [n_1(\mathbf{r}) + n_2(\mathbf{r})] = N$.

Proceeding in the standard way, we evaluate the complete grand-canonical Hamiltonian (5.1) within the Hartree-Fock ansatz (5.7) and find

$$E_{\mathrm{MF}} = \langle \hat{H}_1 \rangle_{\mathrm{MF}} + \langle \hat{H}_2 \rangle_{\mathrm{MF}} + \langle \hat{H}_{12} \rangle_{\mathrm{MF}} \tag{5.8}$$

where $\langle \hat{H}_\sigma \rangle_{\mathrm{MF}}$ and $\langle \hat{H}_{12} \rangle_{\mathrm{MF}}$ are given by Eqs. (5.5) and (5.6) with the phase $\hat{\theta}_\sigma(\mathbf{r})$ and density $\hat{n}_\sigma(\mathbf{r})$ operators replaced by the corresponding Hartree-Fock fields $\theta_\sigma(\mathbf{r})$ and $n_\sigma(\mathbf{r})$. Then, minimizing E_{MF} with respect to $\theta_\sigma(\mathbf{r})$ and $n_\sigma(\mathbf{r})$ yields the following coupled Euler-Lagrange equations:

$$0 = -\frac{\hbar^2}{2m}\left(\frac{\nabla^2\sqrt{n_\sigma}}{\sqrt{n_\sigma}} - |\nabla\theta_\sigma|^2\right) + V_\sigma - \mu + g_\sigma n_\sigma + g_{12} n_{\bar{\sigma}} + \frac{\hbar\Omega_0}{2}\sqrt{\frac{n_{\bar{\sigma}}}{n_\sigma}}\cos(\theta - \alpha) \tag{5.9}$$

$$0 = \frac{\hbar^2}{m}\nabla(n_\sigma \nabla\theta_\sigma) \pm \hbar\Omega_0\sqrt{n_1 n_2}\sin(\theta - \alpha)\,, \tag{5.10}$$

where $\theta(\mathbf{r}) \equiv \theta_1(\mathbf{r}) - \theta_2(\mathbf{r})$ is the relative phase between the two components, $\bar{\sigma}$ is the conjugate of σ [i.e. $\bar{\sigma} = 2$ (resp. 1) for $\sigma = 1$ (resp. 2)], and the $\pm$ sign in Eq. (5.10) is $+$ (resp. $-$) for $\sigma = 1$ (resp. 2).

5.1.3 Excitations: Bogoliubov-de Gennes theory

The low-energy spectrum of the collective excitations of the two-component Bose gas is then determined using the Bogoliubov-de Gennes approach [131, 156, 270, 278, 279], which amounts to perform a perturbative expansion of Hamiltonian (5.1) in phase and density fluctuations. We write $\hat{n}_\sigma = n_\sigma + \delta\hat{n}_\sigma$ and $\hat{\theta}_\sigma = \theta_\sigma + \delta\hat{\theta}_\sigma$, with $n_\sigma(\mathbf{r})$ and $\theta_\sigma(\mathbf{r})$ given by the mean-field Gross-Pitaevskii theory, and

$$|\delta\hat{n}_\sigma| \ll n_\sigma \quad \text{and} \quad |\nabla\delta\hat{\theta}_\sigma| \ll mc/\hbar \tag{5.11}$$

where $c = \sqrt{\mu/m}$ is the velocity of sound in a single-component Bose-Einstein (quasi-)condensate of chemical potential μ. These conditions are usually well verified in weakly-interacting ultracold, two-component gases [236–238, 280].

Weak-fluctuation expansion of the Hamiltonian

Proceeding up to second order in phase and density fluctuations, it is convenient to define the position-dependent operators

$$\hat{X}_\sigma(\mathbf{r}) \equiv \frac{\delta\hat{n}_\sigma(\mathbf{r})}{2\sqrt{n_\sigma(\mathbf{r})}} \tag{5.12}$$

and

$$\hat{P}_\sigma(\mathbf{r}) \equiv \sqrt{n_\sigma(\mathbf{r})}\,\delta\hat{\theta}_\sigma(\mathbf{r})\,, \tag{5.13}$$

which are canonical conjugates (up to a multiplying factor of 1/2), i.e. $\left[\hat{X}_\sigma(\mathbf{r}), \hat{P}_{\sigma'}(\mathbf{r}')\right] = i\delta_{\sigma,\sigma'}\delta(\mathbf{r}-\mathbf{r}')/2$. Then, inserting $\sqrt{\hat{n}_\sigma} \simeq \sqrt{n_\sigma} + \hat{X}_\sigma - \hat{X}_\sigma^2/2\sqrt{n_\sigma}$ and $\hat{\theta}_\sigma = \theta_\sigma + \hat{P}/\sqrt{n_\sigma}$ into Eqs. (5.5) and (5.6), we find

$$\hat{H} \simeq E_{\rm MF} + \hat{H}_1^{(2)} + \hat{H}_2^{(2)} + \hat{H}_{12}^{(2)} \,. \tag{5.14}$$

The zeroth-order term, $E_{\rm MF}$, coincides with the mean-field energy (5.8) where the fields n_σ and θ_σ are substituted to the solutions of the coupled Euler-Lagrange equations (5.9) and (5.10). The first-order term, $\hat{H}^{(1)} = \sum_\sigma \left\{ \delta\hat{n}_\sigma \cdot \frac{\partial \hat{H}}{\partial \hat{n}_\sigma}\Big|_{\psi_{\rm MF}} + \delta\hat{\theta}_\sigma \cdot \frac{\partial \hat{H}}{\partial \hat{\theta}_\sigma}\Big|_{\psi_{\rm MF}} \right\}$, vanishes since the zeroth-order term minimizes $\langle\psi_{\rm MF}|\hat{H}|\psi_{\rm MF}\rangle = E_{\rm MF}$. The second-order terms, $\hat{H}_1^{(2)}, \hat{H}_2^{(2)}$ and $\hat{H}_{12}^{(2)}$, are found after some straightforward algebra, which yields

$$\begin{aligned}
\hat{H}_\sigma^{(2)} &= \int {\rm d}\mathbf{r}\ \hat{X}_\sigma \left[-\frac{\hbar^2}{2m}\left(\nabla^2 - \frac{\nabla^2\sqrt{n_\sigma}}{\sqrt{n_\sigma}} \right) + 2g_\sigma n_\sigma \right] \hat{X}_\sigma + \int {\rm d}\mathbf{r}\ \hat{P}_\sigma \left[-\frac{\hbar^2}{2m}\left(\nabla^2 - \frac{\nabla^2\sqrt{n_\sigma}}{\sqrt{n_\sigma}} \right) \right] \hat{P}_\sigma \\
&\quad + \int {\rm d}\mathbf{r}\ \frac{2\hbar^2}{m} \nabla\theta_\sigma \cdot \left(\sqrt{n_\sigma}\hat{X}_\sigma \right) \nabla \left(\hat{P}_\sigma/\sqrt{n_\sigma} \right) ,
\end{aligned} \tag{5.15}$$

where some irrelevant constant terms have been dropped, and

$$\begin{aligned}
\hat{H}_{12}^{(2)} &= -\sum_\sigma \int {\rm d}\mathbf{r}\ \frac{\hbar\Omega_0}{2} \sqrt{\frac{n_{\bar\sigma}}{n_\sigma}} \cos(\theta-\alpha) \left[\hat{X}_\sigma^2 + \hat{P}_\sigma^2 \right] + \int {\rm d}\mathbf{r}\ \left[4g_{12}\sqrt{n_1 n_2} + \hbar\Omega_0 \cos(\theta-\alpha) \right] \hat{X}_1\hat{X}_2 \\
&\quad + \int {\rm d}\mathbf{r}\ \hbar\Omega_0 \cos(\theta-\alpha) \hat{P}_1\hat{P}_2 + \int {\rm d}\mathbf{r}\ \hbar\Omega_0 \sin(\theta-\alpha) \left[\hat{X}_1\hat{P}_2 - \hat{X}_2\hat{P}_1 \right] \\
&\quad - \int {\rm d}\mathbf{r}\ \hbar\Omega_0 \sin(\theta-\alpha) \left[\frac{\sqrt{n_2}}{\sqrt{n_1}}\hat{X}_1\hat{P}_1 - \frac{\sqrt{n_1}}{\sqrt{n_2}}\hat{X}_2\hat{P}_2 \right] .
\end{aligned} \tag{5.16}$$

We now apply the canonical transformation [2] to our quadratic Hamiltonian [3]

$$\hat{B}_\sigma \equiv \hat{X}_\sigma + i\hat{P}_\sigma \,, \tag{5.17}$$

such that the operators $\hat{B}_\sigma$ satisfy the Bose commutation rules

$$[\hat{B}_\sigma(\mathbf{r}), \hat{B}_{\sigma'}(\mathbf{r}')] = 0 \tag{5.18}$$

$$[\hat{B}_\sigma(\mathbf{r}), \hat{B}_{\sigma'}^\dagger(\mathbf{r}')] = \delta_{\sigma\sigma'}\delta(\mathbf{r}-\mathbf{r}') \,. \tag{5.19}$$

Then, summing all contributions of Eq. (5.15) for $\sigma = 1$ and $\sigma = 2$ and those of Eq. (5.16), we find

$$\begin{aligned}
\hat{H}^{(2)} &= \frac{1}{2}\sum_\sigma \int {\rm d}\mathbf{r}\ \left[\hat{B}_\sigma^\dagger \mathbf{A}_\sigma \hat{B}_\sigma + \hat{B}_\sigma \mathbf{A}_\sigma^* \hat{B}_\sigma^\dagger + \left\{ g_\sigma n_\sigma \hat{B}_\sigma\hat{B}_\sigma + {\rm H.c.} \right\} \right] \\
&\quad + \int {\rm d}\mathbf{r}\ \left[g_{12}\sqrt{n_1 n_2}\hat{B}_1\hat{B}_2 + {\rm H.c.} \right] + \int {\rm d}\mathbf{r}\ \left[\left\{ g_{12}\sqrt{n_1 n_2} + \frac{\hbar\Omega}{2}e^{i\theta} \right\} \hat{B}_2^\dagger\hat{B}_1 + {\rm H.c.} \right]
\end{aligned} \tag{5.20}$$

[2] This transformation simply arises by analogy with the annihilation operator of the harmonic oscillator. Here, the density fluctuation operator $\delta\hat{n}_\sigma/2\sqrt{n_\sigma}$ plays the same role as the position operator $\hat{X}_\sigma$ and the phase fluctuation operator $\sqrt{n_\sigma}\delta\hat{\theta}$ plays the same role as the momentum operator $\hat{P}_\sigma$ of the quantum harmonic oscillator [281].

[3] In the case of a pure condensate with macroscopic occupation of a unique single-particle state, ψ_σ (assumed to be real-valued), the operator $\hat{B}_\sigma$ represents the fluctuations of the field operator: $\hat{\psi}_\sigma \simeq \psi_\sigma + \hat{B}_\sigma$.

where we have used the coupled Euler-Lagrange equation (5.9) to simplify a couple a terms, and have introduced the super-operator

$$\mathbf{A}_\sigma = -\frac{\hbar^2}{2m}\left(\nabla^2 + 2i\nabla\theta_\sigma\cdot\nabla - |\nabla\theta_\sigma|^2\right) + V_\sigma - \mu + 2g_\sigma n_\sigma + g_{12}n_{\bar\sigma}\,. \tag{5.21}$$

Finally, the Hamiltonian (5.20) can be written in a more compact form by introducing the four-component operators

$$\bar{\mathcal{B}} \equiv \left[\hat{B}_1^\dagger, -\hat{B}_1, \hat{B}_2^\dagger, -\hat{B}_2\right] \quad \text{and} \quad \mathcal{B} \equiv \begin{bmatrix} \hat{B}_1 \\ \hat{B}_1^\dagger \\ \hat{B}_2 \\ \hat{B}_2^\dagger \end{bmatrix} \tag{5.22}$$

so that

$$\hat{H}^{(2)} = \frac{1}{2}\int \mathrm{d}\mathbf{r}\ \bar{\mathcal{B}}(\mathbf{r})\mathbf{M}(\mathbf{r})\mathcal{B}(\mathbf{r}) + \text{const} \tag{5.23}$$

where $\mathbf{M}(\mathbf{r})$ is the 4×4 super-operator defined by

$$\mathbf{M} \equiv \begin{bmatrix} \mathcal{L}_1^{\mathrm{GP}} & \Gamma \\ \Gamma^* & \mathcal{L}_2^{\mathrm{GP}} \end{bmatrix} \tag{5.24}$$

with

$$\mathcal{L}_\sigma^{\mathrm{GP}} = \begin{bmatrix} +\mathbf{A}_\sigma & +g_\sigma n_\sigma \\ -g_\sigma n_\sigma & -\mathbf{A}_\sigma^* \end{bmatrix} \tag{5.25}$$

and

$$\Gamma = \begin{bmatrix} +g_{12}\sqrt{n_1 n_2} + \frac{\hbar\Omega^*}{2}e^{-i\theta} & +g_{12}\sqrt{n_1 n_2} \\ -g_{12}\sqrt{n_1 n_2} & -g_{12}\sqrt{n_1 n_2} - \frac{\hbar\Omega}{2}e^{+i\theta} \end{bmatrix}. \tag{5.26}$$

Bogoliubov transformation

The second-order term (5.23) in the expansion of the many-body Hamiltonian (5.1) governs the low-energy excitations of the two-component Bose gas. Its quadratic form is convenient for diagonalization via the usual Bogoliubov method [131, 156, 270, 278], adapted to the two-component Bose gas. Here, we extend previous approaches [241, 255] to the most general case where the coupling terms can be position-dependent. Inserting the modal expansion

$$\mathcal{B}(\mathbf{r}) = \sum_\nu \left(\begin{bmatrix} u_{1\nu}(\mathbf{r}) \\ v_{1\nu}(\mathbf{r}) \\ u_{2\nu}(\mathbf{r}) \\ v_{2\nu}(\mathbf{r}) \end{bmatrix} \hat{b}_\nu + \begin{bmatrix} v_{1\nu}^*(\mathbf{r}) \\ u_{1\nu}^*(\mathbf{r}) \\ v_{2\nu}^*(\mathbf{r}) \\ u_{2\nu}^*(\mathbf{r}) \end{bmatrix} \hat{b}_\nu^\dagger \right), \tag{5.27}$$

with $\hat{b}_\nu$ the annihilation operator of an elementary excitation of the coupled two-component Bose gas, into Eq. (5.23), we find

$$\hat{H}^{(2)} = \frac{1}{2}\sum_\nu E_\nu \left(\hat{b}_\nu^\dagger \hat{b}_\nu + \hat{b}_\nu \hat{b}_\nu^\dagger\right), \tag{5.28}$$

provided that the wave functions fulfill the so-called coupled Bogoliubov equations:

$$\begin{bmatrix} \mathcal{L}_1^{\mathrm{GP}} & \Gamma \\ \Gamma^* & \mathcal{L}_2^{\mathrm{GP}} \end{bmatrix} \begin{bmatrix} u_{1\nu} \\ v_{1\nu} \\ u_{2\nu} \\ v_{2\nu} \end{bmatrix} = E_\nu \begin{bmatrix} u_{1\nu} \\ v_{1\nu} \\ u_{2\nu} \\ v_{2\nu} \end{bmatrix} \tag{5.29}$$

and the bi-orthogonality conditions

$$\sum_\sigma \int \mathrm{d}\mathbf{r}\, \Big[u_{\sigma\nu}(\mathbf{r})u^*_{\sigma\nu'}(\mathbf{r}) - v_{\sigma\nu}(\mathbf{r})v^*_{\sigma\nu'}(\mathbf{r})\Big] = \delta_{\nu\nu'} \tag{5.30}$$

$$\sum_\sigma \int \mathrm{d}\mathbf{r}\, \Big[u_{\sigma\nu}(\mathbf{r})v_{\sigma\nu'}(\mathbf{r}) - v_{\sigma\nu}(\mathbf{r})u_{\sigma\nu'}(\mathbf{r})\Big] = 0\,. \tag{5.31}$$

These modes (indexed by ν), being of bosonic nature, satisfy the Bose commutation rules $[\hat{b}_{\sigma\nu}, \hat{b}^\dagger_{\sigma'\nu'}] = \delta_{\sigma\sigma'}\delta_{\nu\nu'}$ and $[\hat{b}_{\sigma\nu}, \hat{b}_{\sigma'\nu'}] = 0$.

Notice that we disregard here the contribution of the zero-mode terms in the modal expansion (5.27). As discussed in Sec. 2.2.2, they arise from the non conservation of the particle number in the approach the use. They induce quantum phase diffusion [153] and fluctuations of the numbers of particles [154]. A proper particle-number conserving approach could be performed. However (see Sec. 2.2.2), the non-conserving approach is sufficient if one is only interested in the quasi-particle part of the Bogoliubov spectrum.

Orthogonal field operator

Yet, the only subtle issue [see Sec. 2.2.2 and Ref. [154, 282]] when using such an approach is that the field operators $\hat{B}_\sigma(\mathbf{r})$ should be properly orthogonalized with respect to the (quasi-)condensate wave function $\psi_\sigma(\mathbf{r}) \equiv \mathrm{e}^{i\theta_\sigma}\sqrt{n_\sigma}$, which amounts to apply the substitution $\hat{B}_\sigma(\mathbf{r}) \to \hat{\Lambda}_\sigma(\mathbf{r})$ with

$$\hat{\Lambda}_\sigma(\mathbf{r}) \equiv \hat{B}_\sigma(\mathbf{r}) - \frac{\psi_\sigma(\mathbf{r})}{N_\sigma}\int \mathrm{d}\mathbf{r}'\ \hat{B}_\sigma(\mathbf{r}')\psi^*_\sigma(\mathbf{r}')\,. \tag{5.32}$$

We then have

$$\hat{\Lambda}_\sigma(\mathbf{r}) = \sum_\nu \Big[u^\perp_{\sigma\nu}(\mathbf{r})\hat{b}_\nu + v^{\perp *}_{\sigma\nu}(\mathbf{r})\hat{b}^\dagger_\nu\Big] \tag{5.33}$$

with

$$u^\perp_{\sigma\nu} \equiv u_{\sigma\nu} - \frac{\psi_\sigma(\mathbf{r})}{N_\sigma}\int \mathrm{d}\mathbf{r}'\ u_{\sigma\nu}(\mathbf{r}')\psi^*_\sigma(\mathbf{r}') \tag{5.34}$$

$$v^\perp_{\sigma\nu} \equiv v_{\sigma\nu} - \frac{\psi^*_\sigma(\mathbf{r})}{N_\sigma}\int \mathrm{d}\mathbf{r}'\ v_{\sigma\nu}(\mathbf{r}')\psi_\sigma(\mathbf{r}')\,. \tag{5.35}$$

According to Eqs. (5.18) and (5.19), the orthogonal field operators $\hat{\Lambda}_\sigma$ satisfy the modified commutation rules

$$[\hat{\Lambda}_\sigma(\mathbf{r}), \hat{\Lambda}_{\sigma'}(\mathbf{r}')] = 0 \tag{5.36}$$

$$[\hat{\Lambda}_\sigma(\mathbf{r}), \hat{\Lambda}^\dagger_{\sigma'}(\mathbf{r}')] = \delta_{\sigma\sigma'}\left[\delta(\mathbf{r}-\mathbf{r}') - \frac{\psi_\sigma(\mathbf{r})\psi^*_\sigma(\mathbf{r}')}{N_\sigma}\right]. \tag{5.37}$$

The solutions of the non-Hermitian eigenvalue problem (5.29), together with the bi-orthogonality conditions (5.30)-(5.31) and the orthogonalization process (5.34)-(5.35), determine the excitation spectrum of the two-component Bose gas in the weakly-interacting regime. A mode ν describes a coupled two-component elementary excitation (Bogoliubov quasiparticle) of the mixture. The energy and wave functions of these excitations are E_ν and $\{u^\perp_{1\nu}(\mathbf{r}), v^\perp_{1\nu}(\mathbf{r}), u^\perp_{2\nu}(\mathbf{r}), v^\perp_{2\nu}(\mathbf{r})\}$, respectively. They can be determined numerically, or analytically in certain cases. All physical observables can then be constructed by expansion on the corresponding basis.

5.1.4 Correlation functions

We now consider the correlation properties of observable quantities, namely the phases and the densities of the two-component Bose gas. These quantities can be measured independently for each component in experiments with ultracold atoms, using a gaseous mixture of a single bosonic atom prepared in two different internal states [236–238, 280] and internal-state dependent imaging techniques [137]. The density profiles, fluctuations and correlation functions of each component are then found directly from the images [283, 284]. The phase fluctuations and correlation functions of each component are found by time-of-flight [285, 286] or Bragg spectroscopy [229, 287, 288] techniques. The total and relative density profiles are then obtained by addition or subtraction of those of each component, which also provides their fluctuations and correlation functions. Finally, the correlation function of the relative phase, $\theta = \theta_1 - \theta_2$, can be found using matter-wave interference techniques [238, 259].

For each component σ, the phase correlation function is

$$\begin{aligned} G_\theta^\sigma(\mathbf{r},\mathbf{r}') &\equiv \langle\hat\theta_\sigma(\mathbf{r})\hat\theta_\sigma(\mathbf{r}')\rangle - \langle\hat\theta_\sigma(\mathbf{r})\rangle\langle\hat\theta_\sigma(\mathbf{r}')\rangle \\ &= -\frac{\langle: (\hat\Lambda_\sigma - \hat\Lambda_\sigma^\dagger)(\hat\Lambda'_\sigma - \hat\Lambda_\sigma^{\dagger\prime}) :\rangle}{4\sqrt{n_\sigma\, n'_\sigma}}\,, \end{aligned} \tag{5.38}$$

where the bare (resp. primed) quantities are evaluated at point $\mathbf{r}$ (resp. $\mathbf{r}'$). The operator : : represents normal ordering with respect to the orthogonal field operators $\hat\Lambda$ and $\hat\Lambda^\dagger$, which is used to avoid unphysical divergences [154]. Similarly, the density correlation function is

$$\begin{aligned} G_n^\sigma(\mathbf{r},\mathbf{r}') &\equiv \langle n_\sigma(\mathbf{r})n_\sigma(\mathbf{r}')\rangle - \langle n_\sigma(\mathbf{r})\rangle\langle n_\sigma(\mathbf{r}')\rangle \\ &= \sqrt{n_\sigma\, n'_\sigma}\,\langle: (\hat\Lambda_\sigma + \hat\Lambda_\sigma^\dagger)(\hat\Lambda'_\sigma + \hat\Lambda_\sigma^{\dagger\prime}) :\rangle\,. \end{aligned} \tag{5.39}$$

Using the expansion of the orthogonal field operator into the basis of orthogonal Bogoliubov modes, Eq. (5.33), and the usual auxiliary wave functions [4]

$$f^{\rm p}_{\sigma\nu}(\mathbf{r}) = u^\perp_{\sigma\nu}(\mathbf{r}) - v^\perp_{\sigma\nu}(\mathbf{r})\,, \tag{5.40}$$

$$f^{\rm m}_{\sigma\nu}(\mathbf{r}) = u^\perp_{\sigma\nu}(\mathbf{r}) + v^\perp_{\sigma\nu}(\mathbf{r})\,, \tag{5.41}$$

we then get the following explicit expressions after some algebraic calculations:

$$G_\theta^\sigma(\mathbf{r},\mathbf{r}') = \frac{1}{2\sqrt{n_\sigma n'_\sigma}}\sum_\nu \mathcal{R}e\Big[f^{\rm p}_{\sigma\nu}f^{\rm p\prime *}_{\sigma\nu}N_\nu - f^{\rm p}_{\sigma\nu}v^{\perp\prime *}_{\sigma\nu}\Big] \tag{5.42}$$

and

$$G_n^\sigma(\mathbf{r},\mathbf{r}') = 2\sqrt{n_\sigma n'_\sigma}\sum_\nu \mathcal{R}e\Big[f^{\rm m}_{\sigma\nu}f^{\rm m\prime *}_{\sigma\nu}N_\nu + f^{\rm m}_{\sigma\nu}v^{\perp\prime *}_{\sigma\nu}\Big], \tag{5.43}$$

where

$$N_\nu = \frac{1}{\exp(E_\nu/k_{\rm B}T) - 1} \tag{5.44}$$

is the thermal population of mode ν, according to the Bose-Einstein statistical distribution. Note that expressions (5.42) and (5.43) are symmetric in $(\mathbf{r},\mathbf{r}')$. This can be checked by

[4] Here, we use the notations $f^{\rm p;m}_{\sigma\nu}$ instead of the more usual notations $f^{\pm}_{\sigma\nu}$ because the $\pm$ sign below labels a different quantity (the two branches of the spectra).

noting that the commutation rule $[\hat{\Lambda}_\sigma(\mathbf{r}), \hat{\Lambda}_\sigma(\mathbf{r}')] = 0$ [see Eq. (5.36)] implies the relation $\sum_\nu u^\perp_{\sigma\nu}(\mathbf{r}) v^{\perp *}_{\sigma\nu}(\mathbf{r}') = \sum_\nu u^\perp_{\sigma\nu}(\mathbf{r}') v^{\perp *}_{\sigma\nu}(\mathbf{r})$.

The two-point correlation function of the relative phase is defined by the same formula as Eq. (5.38) with θ_σ replaced by $\theta = \theta_1 - \theta_2$. The same calculation strategy yields

$$G_\theta(\mathbf{r}, \mathbf{r}') = \frac{1}{2} \sum_\nu \mathcal{R}e\Big[\Big(\frac{f^{\rm p}_{1\nu}}{\sqrt{n_1}} - \frac{f^{\rm p}_{2\nu}}{\sqrt{n_2}} \Big) \Big(\frac{f^{\rm p'}_{1\nu}}{\sqrt{n'_1}} - \frac{f^{\rm p'}_{2\nu}}{\sqrt{n'_2}} \Big)^* N_\nu - \Big(\frac{f^{\rm p}_{1\nu}}{\sqrt{n_1}} - \frac{f^{\rm p}_{2\nu}}{\sqrt{n_2}} \Big) \Big(\frac{v^{\perp\prime}_{1\nu}}{\sqrt{n'_1}} - \frac{v^{\perp\prime}_{2\nu}}{\sqrt{n'_2}} \Big)^* \Big] . \tag{5.45}$$

Having developed a general formalism for calculating the excitation modes of the two-component Bose gas with arbitrary one- and two-body couplings, and established general formulas for the density and phase correlation functions, we explicitly calculate these quantities in the homogeneous case in the next section.

5.2 Homogeneous systems

In this section, we consider a homogeneous system, where all potentials (V_1 and V_2) and coupling terms (g_1, g_2, g_{12} and Ω) in Hamiltonians (5.2) and (5.3) are independent of the position. Assuming that the potentials V_1 and V_2 are equal [5], it can be assumed without loss of generality that $V_1 = V_2 = 0$. This case allows for analytical calculations and contains the main physical effects discussed below. Hereafter, we first rewrite the formalism of Sec. 5.1 in a form adapted to the homogeneous case (Sec. 5.2.1). We then solve it in the most general situation where both one-body and two-body couplings coexist to discuss the excitation spectrum and wavefunctions (5.2.2), as well as density, phase, and relative-phase fluctuations of the two-component gas (5.2.3).

5.2.1 Meanfield equations

Since all derivative terms in the Euler-Lagrange equations (5.9) and (5.10) vanish in the homogeneous case, it immediately follows from Eq. (5.10) that $\theta - \alpha = 0$ or π if $\Omega = \Omega_0 e^{-i\alpha} \neq 0$. Inserting these two solutions into the meanfield version of Eq. (5.6), we find that $\theta = \alpha$ is a maximum of $E_{\rm MF}$ and is thus an unstable solution. The stable solution is $\theta = \alpha + \pi$, which is a minimum of $E_{\rm MF}$. For instance, the two components are in phase (resp. out of phase) when $\Omega \in \mathbb{R}^-$ (resp. $\Omega \in \mathbb{R}^+$). If $\Omega = 0$, the relative phase θ is not a determined quantity as already discussed in the first paragraph of Sec. 5.1.1. Inserting the stable solution into Eq. (5.9), we then find

$$g_1 n_1 + g_{12} n_2 - \mu - \frac{\hbar\Omega_0}{2} \sqrt{\frac{n_2}{n_1}} = 0 \tag{5.46}$$

$$g_2 n_2 + g_{12} n_1 - \mu - \frac{\hbar\Omega_0}{2} \sqrt{\frac{n_1}{n_2}} = 0 \tag{5.47}$$

and $n_1 + n_2 = n = N/\mathcal{V}$ with N the total number of particles and $\mathcal{V}$ the volume of the system. We will assume that the parameters are such that the two components are miscible, i.e. there exists a homogeneous solution of Eqs. (5.46) and (5.47) of minimal energy with $n_1 > 0$ and $n_2 > 0$.

[5] In the case where $V_1 \neq V_2$, the densities n_1 and n_2 would be modified compared to the following calculations. It is expected to lead to similar effects as those due to a modification of the coupling parameters g_1, g_2 and g_{12}.

Translation invariance ensures that the Bogoliubov modes are the plane waves

$$u_{\sigma\mathbf{k}}(\mathbf{r}) = \frac{1}{\sqrt{\mathcal{V}}}\tilde{u}_{\sigma\mathbf{k}}e^{i\mathbf{k}.\mathbf{r}} \tag{5.48}$$

$$v_{\sigma\mathbf{k}}(\mathbf{r}) = \frac{1}{\sqrt{\mathcal{V}}}\tilde{v}_{\sigma\mathbf{k}}e^{i\mathbf{k}.\mathbf{r}}\,, \tag{5.49}$$

$$f^{p/m}_{\sigma\mathbf{k}}(\mathbf{r}) = \frac{1}{\sqrt{\mathcal{V}}}\tilde{f}^{p/m}_{\sigma\mathbf{k}}e^{i\mathbf{k}.\mathbf{r}}\,, \tag{5.50}$$

where we label the modes by the wave vector $\mathbf{k}$ (instead of ν). In the following, we omit the tilde sign to simplify the notations. Then, the amplitudes $u_{1\mathbf{k}}$, $v_{1\mathbf{k}}$, $u_{2\mathbf{k}}$, and $v_{2\mathbf{k}}$ are the solutions of the eigenproblem (5.29) for the diagonal blocks

$$\mathcal{L}^{GP}_{\sigma} = \begin{bmatrix} +\mathbf{A}_{\sigma\mathbf{k}} & +g_\sigma n_\sigma \\ -g_\sigma n_\sigma & -\mathbf{A}_{\sigma\mathbf{k}} \end{bmatrix}, \tag{5.51}$$

with $\mathbf{A}_{\sigma\mathbf{k}} = \epsilon_{\mathbf{k}} + 2g_\sigma n_\sigma + g_{12}n_{\bar{\sigma}} - \mu$ where $\epsilon_{\mathbf{k}} = \hbar^2\mathbf{k}^2/2m$ is the free-particle dispersion relation, and for the off-diagonal blocks

$$\Gamma = \begin{bmatrix} +g_{12}\sqrt{n_1 n_2} - \hbar\Omega_0/2 & +g_{12}\sqrt{n_1 n_2} \\ -g_{12}\sqrt{n_1 n_2} & -g_{12}\sqrt{n_1 n_2} + \hbar\Omega_0/2 \end{bmatrix}. \tag{5.52}$$

The biorthogonality conditions (5.30) and (5.31) reduce to

$$\sum_{\sigma=1,2}\left(|u_{\sigma\mathbf{k}}|^2 - |v_{\sigma\mathbf{k}}|^2\right) = 1 \tag{5.53}$$

or equivalently

$$f^m_{1\mathbf{k}}f^p_{1\mathbf{k}} + f^m_{2\mathbf{k}}f^p_{2\mathbf{k}} = 1. \tag{5.54}$$

since the $f^{\mathrm{p/m}}_{\sigma\mathbf{k}}$ functions can be chosen to be real. Note that since the classical fields ϕ_σ is homogeneous and the Bogoliubov wave function $u_{\sigma\mathbf{k}}$ and $v_{\sigma\mathbf{k}}$ are plane waves, the orthogonalization procedure of Eqs. (5.30) and (5.31) is irrelevant for $\mathbf{k} \neq 0$.

Finally, the correlation functions introduced in Sec. 5.1.4 are found by inserting Eqs. (5.48) and (5.49) into Eq. (5.42) and (5.43), which yields the following explicit formulas. For the phase correlation function of component σ,

$$G^{\sigma}_{\theta}(\mathbf{r},\mathbf{r}') = \frac{1}{2n_\sigma\mathcal{V}}\sum_{\mathbf{k}\neq 0}\left[|f^p_{\sigma\mathbf{k}}|^2 N_{\mathbf{k}} - f^p_{\sigma\mathbf{k}}v^*_{\sigma\mathbf{k}}\right]\cos\left[\mathbf{k}.(\mathbf{r}-\mathbf{r}')\right]; \tag{5.55}$$

For the density correlation function of component σ,

$$G^{\sigma}_{n}(\mathbf{r},\mathbf{r}') = \frac{2n_\sigma}{\mathcal{V}}\sum_{\mathbf{k}\neq 0}\left[|f^m_{\sigma\mathbf{k}}|^2 N_{\mathbf{k}} + f^m_{\sigma\mathbf{k}}v^*_{\sigma\mathbf{k}}\right]\cos\left[\mathbf{k}.(\mathbf{r}-\mathbf{r}')\right]. \tag{5.56}$$

Similarly, the correlation function of the relative phase is

$$G_{\theta}(\mathbf{r},\mathbf{r}') = \frac{1}{2\mathcal{V}}\sum_{\mathbf{k}\neq 0}\left[\left|\frac{f^p_{1\mathbf{k}}}{\sqrt{n_1}} - \frac{f^p_{2\mathbf{k}}}{\sqrt{n_2}}\right|^2 N_{\mathbf{k}} - \left(\frac{f^p_{1\mathbf{k}}}{\sqrt{n_1}} - \frac{f^p_{2\mathbf{k}}}{\sqrt{n_2}}\right)\left(\frac{v_{1\mathbf{k}}}{\sqrt{n_1}} - \frac{v_{2\mathbf{k}}}{\sqrt{n_2}}\right)^*\right]\cos\left[\mathbf{k}.(\mathbf{r}-\mathbf{r}')\right]. \tag{5.57}$$

Notice that, for simplicity, we have indicated only $\mathbf{k} \neq 0$ below the sum symbols of Eqs. (5.55), (5.56) and (5.57). As a matter of fact, we will see that in general the Bogoliubov spectrum displays two branches, over which the sums should be performed.

5.2.2 Excitation spectrum and wavefunctions

We now study the excitation spectrum of the homogeneous two-component Bose gas. Detailed calculations in the most general case are provided in the supplement at the end of this chapter 5.4. In brief, we generically find that the excitation spectrum is composed of two branches (see Fig. 5.2), one being gapped provided $\Omega_0 \neq 0$, and the other one being ungapped and of Bogoliubov type. Both are particle-like at high energy. The two branches are found to be always distinct except if $\Omega_0 = g_{12} = 0$, in which case they both coincide with the usual Bogoliubov spectrum, $E_{\mathbf{k}} = \sqrt{\epsilon_{\mathbf{k}}\,(\epsilon_{\mathbf{k}} + 2\mu)}$. This holds for any positive values of g_1 and g_2. For the sake of simplicity, we will restrict in the following to the case where the two intra-component couplings are equal, $g_1 = g_2$, which captures the main physics of the problem and is technically simpler. We will assume that $g_{12} < g$, which is the miscibility condition for $\Omega_0 = 0$ [243].

Meanfield background and Bogoliubov spectrum

In the case $g_1 = g_2 \equiv g$, the meanfield densities of the two components are equal, $n_1 = n_2$, and Eqs. (5.46) and (5.47) yield the chemical potential

$$\mu = (g + g_{12})n/2 - \hbar\Omega_0/2, \tag{5.58}$$

with $n = n_1 + n_2$ the total density. The excitation spectrum is computed in the supplement at the end of this chapter 5.4.2 [see Eq. (5.98) together with Eqs. (5.96) and (5.97)]. As mentioned above, it is composed of two branches, which explicitly read

$$E^{\rm in}_{\mathbf{k}} = \sqrt{\epsilon_{\mathbf{k}}\,(\epsilon_{\mathbf{k}} + gn + g_{12}n)} \tag{5.59}$$

$$E^{\rm off}_{\mathbf{k}} = \sqrt{(\epsilon_{\mathbf{k}} + \hbar\Omega_0)\,(\epsilon_{\mathbf{k}} + \hbar\Omega_0 + (g - g_{12})n)}\,. \tag{5.60}$$

as a function of the problem parameters. The meaning of the labels "in" and "off" used to distinguish the two branches will become clear later. The spectrum is plotted in Fig. 5.2. The "in" branch shows the usual (ungapped) Bogoliubov-like dispersion relation : it is phonon-like for $\epsilon_{\mathbf{k}} \ll gn, g_{12}n$ and $E^{\rm in}_{\mathbf{k}} \simeq c\hbar k$ with $c = \sqrt{(g + g_{12})n/2m}$ the sound velocity; it is free-particle-like for $\epsilon_{\mathbf{k}} \gg gn, g_{12}n$ and $E^{\rm in}_{\mathbf{k}} \simeq \epsilon_{\mathbf{k}} + (g + g_{12})n/2$. Conversely, the "off" branch is gapped, and free-particle-like in both low and high-energy limits, provided $\Omega_0 \neq 0$: for $\epsilon_{\mathbf{k}} \ll (g - g_{12})n, \hbar\Omega_0$, we have $E^{\rm off}_{\mathbf{k}} \simeq E_{\rm gap} + \frac{2\hbar\Omega_0 + (g-g_{12})n}{2\sqrt{\hbar\Omega_0(\hbar\Omega_0 + (g-g_{12})n)}}\epsilon_{\mathbf{k}}$ where $E_{\rm gap} = \sqrt{\hbar\Omega_0(\hbar\Omega_0 + (g - g_{12})n)}$; for $\epsilon_{\mathbf{k}} \gg (g - g_{12})n, \hbar\Omega_0$, we have $E^{\rm off}_{\mathbf{k}} \simeq \epsilon_{\mathbf{k}} + \hbar\Omega_0 + (g - g_{12})n/2$. Thus, at low energy, the "off" branch is always above the "in" branch. At higher energy though, it depends on the strengths of the two couplings, since the two branches are separated by an energy $\Delta = \lim_{k\to\infty}(E^{\rm off}_{\mathbf{k}} - E^{\rm in}_{\mathbf{k}}) = \hbar\Omega_0 - g_{12}n$. For attractive two-body coupling, $g_{12} < 0$, we have $E^{\rm in}_{\mathbf{k}} < E^{\rm off}_{\mathbf{k}}$ for any momentum $\mathbf{k}$, and the separation $E^{\rm off}_{\mathbf{k}} - E^{\rm in}_{\mathbf{k}}$ increases with both Ω_0 and g_{12}. Therefore, attractive two-body coupling cooperates with one-body coupling. In contrast, repulsive two-body coupling, $g_{12} > 0$, competes with one-body coupling and tends to decrease the separation between the branches. If the repulsive interactions are strong enough, $g_{12}n > \hbar\Omega_0$, the two curves exhibit a crossing point, above which $E^{\rm in}_{\mathbf{k}} > E^{\rm off}_{\mathbf{k}}$. This happens at the energy $\epsilon^c_{\mathbf{k}} \equiv (\hbar k^c)^2/2m = \hbar\Omega_0[\hbar\Omega_0 + (g - g_{12})n]/2(g_{12}n - \hbar\Omega_0)$. When increasing the repulsive inter-component interactions, this crossing first appears at high momentum $k \approx \infty$, and then moves to lower momenta.

In the particular case where $\Omega_0 = 0$, the "off" branch as well turns to be Bogoliubov-like; it is ungapped and phonon-like at low energy and $E^{\rm off}_{\mathbf{k}} \simeq c\hbar k$ with $c = \sqrt{(g - g_{12})n/2m}$ the sound velocity. In this case, which can be viewed as the limiting situation where the crossing of the two branches takes place at $k = 0$, the "off" branch entirely lies above the "in" branch for $g_{12} < 0$, and entirely below for $g_{12} > 0$.

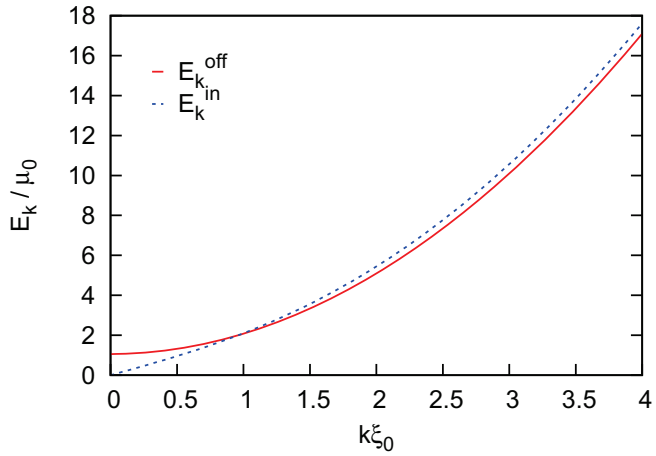

Figure 5.2: Bogoliubov spectrum of the coupled excitations in a homogeneous two-component Bose gas with $g_{12} \neq 0$ and $\Omega \neq 0$. Plotted are the two energy branches $E_{\mathbf{k}}^{\mathrm{in/off}}$ [Eqs. (5.59) and (5.60)] in the case $g_1 = g_2$, for $g_{12} = 0.7 g_1$ and $\hbar\Omega_0 = 0.4 g_1 n$. This corresponds to a situation where $g_{12} n > \hbar\Omega_0$ and the two branches cross at a certain momentum k^c (see text). For $g_{12} n < \hbar\Omega_0$, there is no crossing point and the "off" branch is always above the "in" branch . Here, $\mu_0 = g_1 N/2\mathcal{V}$ is the chemical potential in the absence of any coupling, and $\xi_0 = \hbar/\sqrt{2m\mu_0}$ is the corresponding healing length.

Bogoliubov excitations

Let us come back to arbitrary values of Ω_0. The computation of Bogoliubov wavefunctions is performed in the general case in the supplement (5.4) at the end of this chapter. Their expressions in the case $g_1 = g_2$ follow from the procedure indicated there [see Eqs. (5.92) to (5.95)] and read

$$f_{1\mathbf{k}}^{\mathrm{m,in}} = f_{2\mathbf{k}}^{\mathrm{m,in}} = \left[\frac{\epsilon_{\mathbf{k}}}{2E_{\mathbf{k}}^{\mathrm{in}}}\right]^{1/2} \tag{5.61}$$

$$f_{1\mathbf{k}}^{\mathrm{p,in}} = f_{2\mathbf{k}}^{\mathrm{p,in}} = \left[\frac{E_{\mathbf{k}}^{\mathrm{in}}}{2\epsilon_{\mathbf{k}}}\right]^{1/2} \tag{5.62}$$

for the "in" branch , and

$$f_{1\mathbf{k}}^{\mathrm{m,off}} = -f_{2\mathbf{k}}^{\mathrm{m,off}} = \left[\frac{\epsilon_{\mathbf{k}} + \hbar\Omega_0}{2E_{\mathbf{k}}^{\mathrm{off}}}\right]^{1/2} \tag{5.63}$$

$$f_{1\mathbf{k}}^{\mathrm{p,off}} = -f_{2\mathbf{k}}^{\mathrm{p,off}} = \left[\frac{E_{\mathbf{k}}^{\mathrm{off}}}{2\epsilon_{\mathbf{k}} + 2\hbar\Omega_0}\right]^{1/2} . \tag{5.64}$$

for the "off" branch. In the following, we will omit the branch labels ("in"/"off") in the functions $f_{\sigma\mathbf{k}}^{\mathrm{p/m}}$ for simplicity, except when necessary. The moduli of the $f_{\sigma\mathbf{k}}^{\mathrm{p/m}}$ functions, which do not depend on the component σ in the case $g_1 = g_2$ considered here, are plotted on Fig. 5.3. For the "in" branch , each component behaves as an effective single-component Bose gas with renormalized effective parameters, since the previous Bogoliubov spectrum and wavefunctions are similar to those of a single-component gas. Notice in particular the divergence of the $f_{\sigma\mathbf{k}}^{\mathrm{p}}$ functions. In contrast, the gapped dispersion relation of the "off" branch yields a different behavior for the $f_{\sigma\mathbf{k}}^{\mathrm{p/m}}$ functions. They do not depend much on $\mathbf{k}$ as soon as $\hbar\Omega_0$ and gn are of

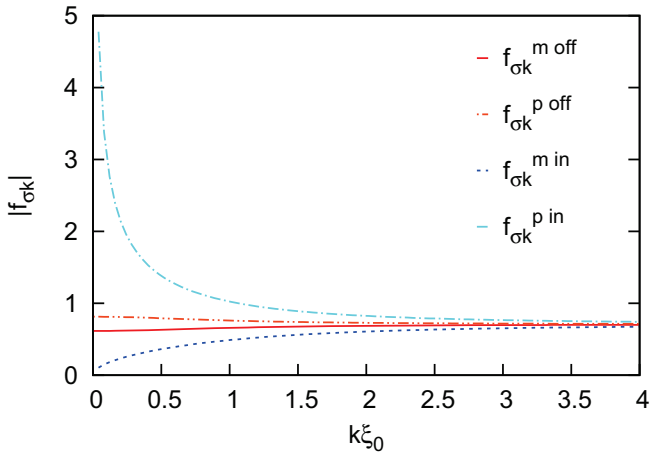

Figure 5.3: Amplitudes of the wavefunctions $f^{\mathrm{p/m}}_{\sigma\mathbf{k}}$ of the coupled Bogoliubov excitations for a homogeneous two-component Bose gas with $g_{12} \neq 0$ and $\Omega \neq 0$. Plotted are the absolute values, $|f^{\mathrm{p/m}}_{\sigma\mathbf{k}}|$ [see Eqs. (5.61) to (5.64)] for the same parameters as in Fig. 5.2. Since $g_1 = g_2$, the absolute values are independent of the component σ. The excitations are in phase in the "in" branch ($E^{\mathrm{in}}_{\mathbf{k}}$) and off phase for the "off" branch ($E^{\mathrm{off}}_{\mathbf{k}}$).

the same order, and in particular, the $f^{\mathrm{p}}_{\sigma\mathbf{k}}$ functions no longer diverge at low energy, since the gap acts as a low-momentum cut-off.

It follows as well from Eqs. (5.61) to (5.64) that, for a given component σ, the $f^{\mathrm{m}}_{\sigma}(\mathbf{r})$ and $f^{\mathrm{p}}_{\sigma}(\mathbf{r})$ wavefunctions are always in phase [i.e. $f^{\mathrm{m}}_{\sigma\mathbf{k}} f^{\mathrm{p}}_{\sigma\mathbf{k}} > 0$]. Conversely, the modes associated to the components 1 ($f^{\mathrm{m}}_{1\mathbf{k}}, f^{\mathrm{p}}_{1\mathbf{k}}$) and 2 ($f^{\mathrm{m}}_{2\mathbf{k}}, f^{\mathrm{p}}_{2\mathbf{k}}$) are off phase in the "off" branch and in phase in the "in" branch, hence the denomination used to label the two branches. More precisely, since the separation $E^{\mathrm{off}}_{\mathbf{k}} - E^{\mathrm{in}}_{\mathbf{k}}$ increases with Ω_0, we find that the one-body coupling $\Omega(\mathbf{r})$ tends to favor fluctuations of the phases of the components that are in phase, independently of its sign and more generally independently of its phase α. This contrasts with the behavior of the mean-field phases θ_1 and θ_2, the difference of which is imposed by the phase of $\Omega(\mathbf{r})$ (see Sec. 5.2.1). Indeed, the behavior of the fluctuations can by understood from the fact that the one-body coupling tends to impose the difference between the total phases of the two components. Since it is realized at the meanfield level, the phase fluctuations tend to be in phase, whatever the phase of $\Omega(\mathbf{r})$. As regards two-body coupling, we find that $E^{\mathrm{off}}_{\mathbf{k}} - E^{\mathrm{in}}_{\mathbf{k}}$ decreases with g_{12}, so that for $g_{12} > 0$, the two-body coupling favors off-phase density fluctuations whereas for $g_{12} < 0$, it favors in-phase density fluctuations. This can be traced to the fact that for repulsive inter-component interactions ($g_{12} > 0$), off-phase density fluctuations ($f^{\mathrm{m}}_{1\mathbf{k}} f^{\mathrm{m}}_{2\mathbf{k}} < 0$) cost less interaction energy than in-phase density fluctuations (and the other way round for $g_{12} < 0$). Therefore, for attractive two-body coupling, in-phase fluctuations are energetically favored, cooperatively by one-body and two-body couplings. Conversely, if the two-body coupling is repulsive and strong enough to compete with the one-body coupling ($g_{12} n > \hbar\Omega_0$), so that the two branches cross, they compete with the following result : for low-energy excitations ($\epsilon_{\mathbf{k}} < \epsilon^{c}_{\mathbf{k}}$), in-phase fluctuations cost less energy than off-phase fluctuations, whereas it is the opposite for high energy excitations ($\epsilon_{\mathbf{k}} > \epsilon^{c}_{\mathbf{k}}$).

5.2.3 Fluctuations and correlations

Phase and density correlations

The phase and density correlations in each component σ are determined by the $f^{\rm p}_{\sigma\mathbf{k}}$ and $f^{\rm m}_{\sigma\mathbf{k}}$ functions [see Eqs. (5.55) and (5.56)]. Due to the similarity, in the in-phase branch, of the dispersion relation and formulas for the $f^{p/m}_{\sigma\mathbf{k}}$ functions with those of a single-component Bose gas, each component behaves as an effective single-component gas. The effective parameters however depend on all coupling parameters g_1, g_2 and g_{12} and are in general different for the two components (if $g_1 \neq g_2$). Then, the density fluctuations remain small for strong-enough interaction parameters and low temperatures in any dimension. In contrast, the behavior of the phase fluctuations strongly depends on the dimension, owing to the $1/\sqrt{|\mathbf{k}|}$ divergence of the $f^{\rm p,in}_{\sigma\mathbf{k}}$ functions. In three dimensions, the two components form true Bose-Einstein condensates with intra-component phase coherence. In lower dimensions, they form quasi-condensates with strong intra-component phase fluctuations driven by the ungapped Bogoliubov-like spectrum of the in-phase branch.

Relative phase correlations and fluctuations

Let us turn to the relative phase correlations. Equation (5.57) shows that in the case $g_1 = g_2$ that we consider here, only the off-phase branch contributes to the sum. The correlation function for the relative phase can thus be rewritten

$$G_\theta(\mathbf{r},\mathbf{r}') = \frac{1}{2\mathcal{V}n}\sum_{\mathbf{k}\neq 0}\left\{2N_{\mathbf{k}} + \left(1 - \frac{\epsilon_{\mathbf{k}}+\hbar\Omega_0}{E^{\rm off}_{\mathbf{k}}}\right)\right\}\left|f^{\rm p,off}_{1\mathbf{k}} - f^{\rm p,off}_{2\mathbf{k}}\right|^2 \cos\left[\mathbf{k}.(\mathbf{r}-\mathbf{r}')\right], \tag{5.65}$$

making appear the thermal and quantum contributions. Owing to the gap in the off-phase branch, its contribution remains finite, which ensures mutual phase coherence between the two Bose gases, in any dimension. This is however not true in the particular case $\Omega_0 = 0$ where the off-phase branch is ungapped : there, the two components are mutually phase coherent only in three dimensions, but show no true long-range mutual phase coherence in lower dimensions. Therefore, a finite one-body coupling suppresses the fluctuations of the relative phase, in agreement with the previous discussion according to which it tends to impose the phase at the meanfield level, favoring in-phase fluctuations of the phase. To be more quantitative, we can rewrite Eq. (5.65) into the form

$$G_\theta(\mathbf{r},\mathbf{r}') = \frac{1}{n\mathcal{V}}\sum_{\mathbf{k}\neq 0}\left[\sqrt{\frac{\epsilon_{\mathbf{k}}+(g-g_{12})n+\hbar\Omega_0}{\epsilon_{\mathbf{k}}+\hbar\Omega_0}}\coth\left(\frac{E^{\rm off}_{\mathbf{k}}}{2k_{\rm B}T}\right) - 1\right]\times\cos[\mathbf{k}.(\mathbf{r}-\mathbf{r}')]\,. \tag{5.66}$$

Since $E^{\rm off}_{\mathbf{k}}$ increases with Ω_0 and both $\coth(E^{\rm off}_{\mathbf{k}}/2k_{\rm B}T)$ and $\sqrt{(\epsilon_{\mathbf{k}}+(g-g_{12})n+\hbar\Omega_0)/(\epsilon_{\mathbf{k}}+\hbar\Omega_0)}$ decrease when Ω_0 increases, the relative phase fluctuations $G_\theta(\mathbf{r},\mathbf{r})$ indeed decrease when the intensity of the one-body coupling increases. The influence of the two-body coupling on relative phase fluctuations is more involved. On the one hand, $\coth\left(\frac{E^{\rm off}_{\mathbf{k}}}{2k_{\rm B}T}\right)$ is an increasing function of g_{12} since $E^{\rm off}_{\mathbf{k}}$ decreases when g_{12} increases [see Eq. (5.60)]. Indeed, an increase of the two-body coupling lowers the contributing off-phase branch, increasing its thermal occupancy. On the other hand, the amplitude of phase fluctuations in the off-phase branch, $\sqrt{\frac{\epsilon_{\mathbf{k}}+(g-g_{12})n+\hbar\Omega_0}{\epsilon_{\mathbf{k}}+\hbar\Omega_0}} = E^{\rm off}_{\mathbf{k}}/(\epsilon_{\mathbf{k}}+\hbar\Omega_0) \propto (f^{\rm p,off}_{\mathbf{k}})^2$,

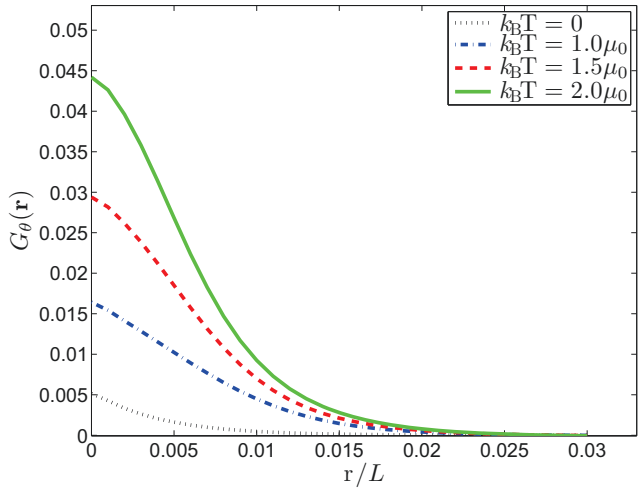

Figure 5.4: Correlation function of the relative phase for a one-dimensional two-component Bose gas with one-body ($\Omega_0 \neq 0$) and two-body ($g_{12} \neq 0$) couplings, plotted for various temperatures ($k_B T/\mu_0 =$ 0, 1, 1.5, 2) in the case where $g_1 = g_2 \equiv g$. The parameters here correspond to $N = 10^4$ atoms of ^{87}Rb ($m \simeq 144 \times 10^{-27}$kg) in a 1D box of size $2L = 10^{-4}$m, and interacting via the scattering length $a_1 = a_2 = 5.95$nm. It corresponds in the absence of any coupling to the chemical potential $\mu_0 = gn = 7.88 \times 10^{-31}$J, which we choose as the energy unit. In these units, we use the parameters $\hbar\Omega_0 = 1\mu_0$ and $g_{12}n = 0.75\mu_0$.

is a decreasing function of g_{12}, which is intimately linked to the previously discussed observation that an increasing g_{12} enhances the amplitude of off-phase density fluctuations. To determine the overall behavior of the relative phase fluctuations, it is worth replacing $\sqrt{(\epsilon_{\mathbf{k}} + (g - g_{12})n + \hbar\Omega_0)/(\epsilon_{\mathbf{k}} + \hbar\Omega_0)}$ by $E^{\rm off}_{\mathbf{k}}/(\epsilon_{\mathbf{k}} + \hbar\Omega_0)$ in Eq. (5.66). Then, since $u\coth(u)$ is an increasing function of u (for $u > 0$) and $E^{\rm off}_{\mathbf{k}}$ is a decreasing function of g_{12}, we conclude that the relative phase fluctuations decrease when the two-body coupling increases. In particular, the relative phase fluctuations are maximally suppressed when $g_{12} > 0$ approaches g from below. In other words, in a homogeneous two-component Bose gas, repulsive inter-component interactions reduce relative phase fluctuations while attractive inter-component interactions enhance relative phase fluctuations.

Let us mention that the physics of the general case $g_1 \neq g_2$ can be expected to be slightly different. Indeed, in this case, the contribution of the in-phase branch to the relative phase correlation function is non zero [see Eq. (5.57)] and the divergence of the $f^{\rm p,in}_{\sigma\mathbf{k}}$ functions in this branch can lead to large fluctuations in low dimensions. Therefore, a small difference between g_1 and g_2 suppresses mutual phase coherence on large scales.

Temperature dependence of relative phase correlations

Let us discuss as well the behavior of the relative phase correlation function $G_\theta(\mathbf{r}, \mathbf{r}')$ versus temperature, in the case $g_1 = g_2$. Equation (5.66) is plotted on Fig. 5.4 as a function of $|\mathbf{r} - \mathbf{r}'|$ for various temperatures, in the 1D case. The function $G_\theta(\mathbf{r}, \mathbf{r}')$ generically decreases with $|\mathbf{r} - \mathbf{r}'|$ and goes to zero at large separations. Furthermore, it increases with the temperature T, as is easily checked from Eq. (5.66), since the thermal contribution gets more and more important.

a/ At zero temperature, the relative-phase correlation function reads

$$G_\theta(\mathbf{r}) = \frac{1}{n}\int \frac{d\mathbf{k}}{(2\pi)^d}\left[\frac{E^{\rm off}_{\mathbf{k}}}{\epsilon_{\mathbf{k}}+\hbar\Omega_0}-1\right]\cos(\mathbf{k}.\mathbf{r}), \tag{5.67}$$

which is found by replacing the discrete sum in Eq. (5.66) by an integral. It can be seen from Eq. (5.60) that this function identically vanishes in the limit $g_{12} = g$. For $(g-g_{12})n \ll \hbar\Omega_0$, we can approximate $\frac{E^{\rm off}_{\mathbf{k}}}{\epsilon_{\mathbf{k}}+\hbar\Omega_0}-1$ by $\frac{(g-g_{12})n}{2(\epsilon_{\mathbf{k}}+\hbar\Omega_0)}$ and analytically calculate the integral in Eq. (5.67). In 1D, it yields the exponentially decaying correlation function

$$G^{\rm 1D}_\theta(\mathbf{r}) = \frac{m(g-g_{12})n}{2n\hbar^2 L_\theta^{-1}} e^{-|\mathbf{r}|/L_\theta}, \quad \text{for } T=0, \tag{5.68}$$

where the correlation length is

$$L_\theta = \sqrt{\frac{\hbar}{2m\Omega_0}}. \tag{5.69}$$

Equation (5.68) accurately reproduces the exact formula (5.67) plotted on Fig. 5.4, which corresponds to $(g-g_{12})n = 0.25\hbar\Omega_0$. In 3D, we find

$$G^{\rm 3D}_\theta(\mathbf{r}) = \frac{m(g-g_{12})n}{4\pi n\hbar^2|\mathbf{r}|} e^{-|\mathbf{r}|/L_\theta}, \quad \text{for } T=0, \tag{5.70}$$

which exhibits a divergence in $r = 0$ and decreases over the same characteristic length L_θ as in 1D, Eq. (5.69). For larger values of $(g-g_{12})n$, a formal expansion in powers of $(g-g_{12})n/\hbar\Omega_0$ of the term inside the brackets in Eq. (5.67) shows that the main dependence of the relative phase correlation function in $e^{-|\mathbf{r}|/L_\theta}$ is preserved, with a multiplicative correction that is polynomial in $|\mathbf{r}|/L_\theta$. We numerically checked that the previous analytical formulas continue to hold up to this polynomial correction in both 1D and 3D. They predict in particular the correct correlation length, which therefore very weakly depends on the two-body coupling, although they tend to slightly overestimate the value of $G_\theta(0)$.

b/ At finite temperature, the behavior of $G_\theta(\mathbf{r})$ at large separations $|\mathbf{r}|$ can as well be obtained analytically. To do so, we replace in Eq. (5.66) the discrete sum by an integral and use Eq. (5.60), which yields

$$G_\theta(\mathbf{r}) = \frac{1}{n}\int \frac{d\mathbf{k}}{(2\pi)^d}\left[\frac{E^{\rm off}_{\mathbf{k}}}{\epsilon_{\mathbf{k}}+\hbar\Omega_0}\coth\left(\frac{E^{\rm off}_{\mathbf{k}}}{2k_{\rm B}T}\right)-1\right]\cos(\mathbf{k}.\mathbf{r}). \tag{5.71}$$

The behavior at large $|\mathbf{r}|$ is dominated by the components of momentum k smaller than $1/r$. Thus, for $k_T|\mathbf{r}| \gg 1$, where k_T is defined by $E^{\rm off}_{k_T} = k_{\rm B}T$, we have $k_{\rm B}T \gg E^{\rm off}_{\mathbf{k}}$ for all contributing terms of the integral. Then, if $k_{\rm B}T \gg (\epsilon_{\mathbf{k}}+\hbar\Omega_0)$, Eq. (5.71) can be simplified into

$$G_\theta(\mathbf{r}) \;\simeq\; \frac{1}{n}\int \frac{d\mathbf{k}}{(2\pi)^d}\frac{2k_{\rm B}T}{\epsilon_{\mathbf{k}}+\hbar\Omega_0}\cos(\mathbf{k}.\mathbf{r}). \tag{5.72}$$

Notice that the previous condition requires that $k_{\rm B}T \gg E_{\rm gap}$, $\hbar\Omega_0$, Eq. (5.72) thus being valid in a large-separation and high-temperature regime. For $k_T|\mathbf{r}| \gg 1$, the integral in Eq. (5.72) can be calculated, yielding

$$G^{\rm 1D}_\theta(\mathbf{r}) \simeq \frac{2mk_{\rm B}T}{n\hbar^2 L_\theta^{-1}} e^{-|\mathbf{r}|/L_\theta}, \tag{5.73}$$

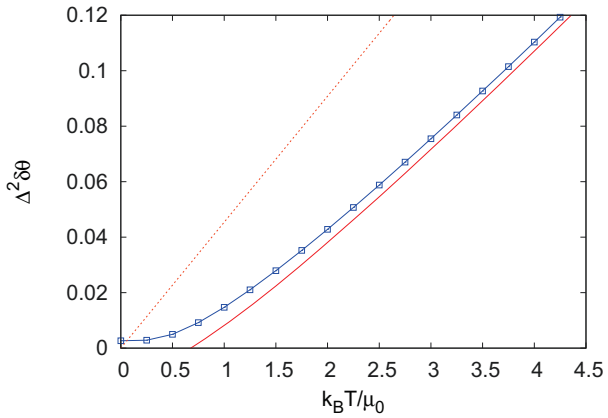

Figure 5.5: Relative phase fluctuations as a function of temperature for a one-dimensional two-component Bose gas with one-body ($\Omega_0 \neq 0$) and two-body ($g_{12} \neq 0$) couplings, plotted for the same parameters as in Fig. 5.4. The solid blue line with dots is the exact calculation, corresponding to Eq. (5.71) in $\mathbf{r} = 0$. The solid red line is the expansion (5.81) and the dotted red line corresponds to the first left-hand-side term in Eq.(5.81). While the quantum fluctuations are small, the thermal contribution increases with temperature. At high temperature, the exact calculation is accurately reproduced by the high-temperature expansion (5.81), whereas the linear dominant term proves insufficient to do so.

in one dimension, and

$$G_\theta^{\rm 3D}(\mathbf{r}) \simeq \frac{m k_{\rm B} T}{\pi n \hbar^2 |\mathbf{r}|} e^{-|\mathbf{r}|/L_\theta}, \tag{5.74}$$

in three dimensions. Remarkably, we find the same expression for the correlation length of the relative phase Eq. (5.69), as for zero temperature. In 1D, this result recovers that of Ref. [255] and extends it to the case where one-body and two-body couplings coexist. The correlation length of the relative phase then weakly depends on the two-body coupling and decreases when the one-body coupling increases. For smaller separations, the previous formulas no longer hold. A cut-off at $\mathbf{k}_T$ in the integral would have to be taken into account, which in particular would solve the apparent divergence found in Eq. (5.74) for $\mathbf{r} = 0$.

Temperature dependence of relative phase fluctuations

We finally discuss the relative phase fluctuations, which are given by

$$G_\theta(0) \;=\; \frac{1}{n\pi} \int_0^\infty dk \left[\frac{E_{\mathbf{k}}^{\rm off}}{\epsilon_{\mathbf{k}} + \hbar\Omega_0} \coth\left(\frac{E_{\mathbf{k}}^{\rm off}}{2 k_{\rm B} T} \right) - 1 \right] \tag{5.75}$$

with $E_{\mathbf{k}}^{\rm off} = \sqrt{(\epsilon_{\mathbf{k}} + \hbar\Omega_0)\,(\epsilon_{\mathbf{k}} + \hbar\Omega_0 + (g - g_{12})n)}$, see Eqs. (5.60) and (5.71).

As already pointed out, the relative phase fluctuations always decrease with the one-body coupling Ω_0, which thus favors mutual phase coherence between the two condensates. Moreover, repulsive two-body coupling ($g_{12} > 0$) tends to reduce the fluctuations of the relative phase while attractive two-body coupling enhance them.

We will focus here on the temperature dependence of those fluctuations, which is shown in Fig. 5.5, for the 1D case. The zero-temperature fluctuations, which are given by their quantum contribution, are smaller than those of a single condensate [255]. The fluctuations

then unsurprisingly increase with temperature. At high temperature, the dominant term commonly found in literature [255] is linear in T and reads $2mk_{\rm B}T/n\hbar^2 L_\theta^{-1}$, which coincides with the prefactor in Eq. (5.73). In particular, the one-body coupling favors local mutual phase coherence between the two components. However, the dominant contribution is generally not sufficient to accurately reproduce the exact calculations as shown in Fig. 5.5. In order to get a better accuracy, we perform here a high-temperature expansion of the relative phase fluctuations in the 1D case, valid for $k_{\rm B}T \gg \hbar\Omega_0, (g-g_{12})n$, which recovers the linear dominant term and goes beyond it by capturing the next-order correction.

High-temperature expansion - Introducing k_T such that $E^{\rm off}_{k_T} = k_{\rm B}T$, we can split the integral in Eq. (5.75) into two parts, corresponding to $k < k_T$ and to $k > k_T$, respectively. For $k \gg k_T$, $\coth\left(\frac{E^{\rm off}_{\mathbf{k}}}{2k_{\rm B}T}\right) \approx 1$ up to some exponentially decaying terms. Hence, we can safely approximate the first part of the integral by $\frac{1}{n\pi}\int_{k_T}^{\infty} dk \left(\frac{E^{\rm off}_{\mathbf{k}}}{\epsilon_{\mathbf{k}}+\hbar\Omega_0} - 1\right)$, the leading-order term of which scales as $1/k_T \propto 1/\sqrt{T}$ in the high-temperature limit. We can thus disregard this contribution. For $k \ll k_T$, we have $E^{\rm off}_{k_T} \ll 2k_{\rm B}T$ so that we can use the expansion $\coth(x) \approx_{x\to 0} 1/x + x/3 - x^3/45 + ...$, yielding the contribution

$$\frac{1}{n\pi}\int_0^{k_T} dk \left[\frac{2k_{\rm B}T}{\epsilon_{\mathbf{k}}+\hbar\Omega_0} + \frac{\epsilon_{\mathbf{k}}+\hbar\Omega_0+(g-g_{12})n}{6k_{\rm B}T} - ... - 1\right], \tag{5.76}$$

where we have retained the first two contributions. At high temperature, the first term is linear in T and reads $\frac{2mk_{\rm B}T}{n\hbar^2 L_\theta^{-1}}$, where $L_\theta = \sqrt{\frac{\hbar}{2m\Omega_0}}$. Then, all terms coming from the expansion of the coth function are of order $\sqrt{T}$ and more, and the last term coming from the -1 is constant. Therefore, at high temperature, one recovers the well-known linear dominant term

$$G_\theta(\mathbf{r}=0) \simeq \frac{2mk_{\rm B}T}{n\hbar^2 L_\theta^{-1}} + O(\sqrt{T}) \tag{5.77}$$

Obtaining the next correcting terms, scaling as $\sqrt{T}$, from Eq. (5.76) is not straightforward since one would have to evaluate all terms of the integral and resum them. Furthermore, with this approach, each term would depend on k_T, which was introduced as a typical bound to split the integral and is thus somehow defined up to an arbitrary constant of the order of one. It would prevent us to extract the correct numerical prefactor of the $\sqrt{T}$ term.

In order to overcome this issue, we resort to an alternative method. As can be checked from Eq. (5.76), the term in $(g-g_{12})n = 0$ contributes to the expansion only in terms of order $1/\sqrt{T}$ and more. We can thus neglect it here. With this approximation, we have $E^{\rm off}_{\mathbf{k}} \simeq \epsilon_{\mathbf{k}} + \hbar\Omega_0$, so that we can simply rewrite Eq. (5.75) in the form

$$G_\theta(0) \;=\; \frac{1}{\pi}\sqrt{\frac{2k_{\rm B}T}{\hbar^2 n^2/2m}}\int_0^{\infty} du\, \left[\coth\left(u^2+\eta\right) - 1\right] \tag{5.78}$$

where we defined the small parameter $\eta = \hbar\Omega_0/2k_{\rm B}T$. We now split the integral into two parts. For $u \ll \sqrt{\eta}$, $u^2+\eta \ll 1$ so that we can use the previous expansion of the coth function, and obtain

$$\frac{1}{\pi}\sqrt{\frac{2k_{\rm B}T}{\hbar^2 n^2/2m}}\int_0^{\sqrt{\eta}} du \left(\frac{1}{u^2+\eta} + \frac{u^2+\eta}{3} + ... - 1\right) \tag{5.79}$$

Each term can then be exactly integrated. The first term gives a contribution linear in temperature, which reads $\frac{mk_{\rm B}T}{n\hbar^2 L_\theta^{-1}}$. Notice that, comparing to Eq. (5.77), it yields only one half of the leading-order term linear in T. All the other terms are of orders 1, $1/T$, $1/T^2$,..., thus strictly smaller than the $\sqrt{T}$ term we are looking for. For $u \gg \sqrt{\eta}$, we can use the expansion $\coth\left(u^2+\eta\right) \approx \coth(u^2)+\eta\coth^{(1)}(u^2)+...$, where $\coth^{(n)}$ is the n-th derivative of coth, which yields

$$\frac{1}{\pi}\sqrt{\frac{2k_{\rm B}T}{\hbar^2 n^2/2m}}\int_{\sqrt{\eta}}^{\infty} du \qquad \left\{ \left[\coth(u^2)-1\right] + \sum_{n\geq 1}\frac{\eta^n}{n!}\coth^{(n)}(u^2)\right\}. \tag{5.80}$$

Notice first that each term contains a contribution that is linear in T. Indeed, their respective equivalents in 0 are non integrable and read $(\coth(u^2)-1) \sim_{u\to 0} 1/u^2$ and $\coth^{(n)}(u^2) \sim_{u\to 0} n!(-1)^n/u^{2n+2}$, so that all the terms in Eq. (5.80) scale once integrated as $1/\sqrt{\eta}$. Together with the global prefactor $\sqrt{2k_{\rm B}T}$, it yields a linear scaling. The latter can be explicitly calculated by integrating the previous equivalents, which yields $\frac{4mk_{\rm B}T}{n\pi\hbar^2 L_\theta^{-1}} \times (1-1/3+1/5-1/7+...) = \frac{mk_{\rm B}T}{n\hbar^2 L_\theta^{-1}}$, that is one half of Eq. (5.77). Together with the contribution of the first part of the integral, we thus recover exactly the same linear term as in the above subsection. Then, coming back to Eq. (5.80), we can find the next order terms by subtracting to each term its equivalent in $u=0$. The first correction reads $\frac{1}{\pi}\sqrt{\frac{2k_{\rm B}T}{\hbar^2 n^2/2m}}\int_{\sqrt{\eta}}^{\infty} du\ [\coth(u^2)-1-1/u^2]$. The latter scales as $\sqrt{T}$ when $\eta \to 0$ since the function $u \to \coth(u^2)-1-1/u^2$ is integrable. One can then check that the contributions of the other terms will respectively scale as $1/\sqrt{T}$, $1/T^{3/2}$,... We hence find the final expansion

$$G_\theta(\mathbf{r}=0) \simeq \frac{2mk_{\rm B}T}{n\hbar^2 L_\theta^{-1}} - \frac{I_1}{\pi}\sqrt{\frac{2k_{\rm B}T}{\hbar^2 n^2/2m}} + {\rm O}(1), \tag{5.81}$$

where $I_1 = \int_0^\infty du\ [1/u^2 - \coth(u^2) - 1] \simeq 1.82$.

The first correction to the linear term, which scales as $\sqrt{T}$, is remarkably independent from the couplings. As can be seen in Fig. 5.5, Eq. (5.81) provides a fair approximation to the exact calculations. In particular, we find that the $\sqrt{T}$ correction significantly lowers the relative phase fluctuations.

5.3 Conclusions

In this chapter, we have derived a general meanfield theory for a two-component Bose gas in the presence of both one-body and two-body couplings. We considered the most general situation where both one-body and two-body couplings can be position dependent, and where the gas can experience a component-dependent external potential. Our formulation uses the phase-density formalism, which applies to both true condensates and quasi-condensates with large phase fluctuations. We have written the coupled Gross-Pitaevskii equations, which determine the ground-state background, as well as the Bogoliubov equations, which determine the pair-excitation spectrum of the mixture. We obtained general formulas for phase and density correlation functions within each component, as well as for their relative phase, at zero and finite temperature.

We have then applied our formalism to a homogeneous case where both one-body and two-body couplings coexist (Sec. 5.2). Our discussion then focused on the excitation spectrum and the relative phase fluctuations in the case of equal intra-component interactions, which captures the main physics. We summarize our main results in the following.

The excitation spectrum is composed of two branches, which are distinct provided at least one of the couplings is present. The first branch, which corresponds to in-phase fluctuations of the two Bose gases, is of Bogoliubov type. It depends only on the two-body coupling while being unaffected by one-body coupling. The second branch, which corresponds to off-phase fluctuations, is gapped as soon as the one-body coupling is non zero. The two branches cross each other at a given momentum if the two-body coupling is repulsive and exceeds the one-body coupling.

As regards phase and density fluctuations, each component behaves as an effective single-component Bose gas with coupling parameters that are renormalized by the inter-species two-body coupling. In particular, while the density fluctuations remain small in all dimensions, the two components exhibit strong intra-component phase fluctuations in low dimensions, driven by the ungapped Bogoliubov-like spectrum of the in-phase branch.

The behavior of the relative phase is more involved. At the meanfield level, it is imposed by the one-body coupling, in particular by its phase. Then, the fluctuations of the relative phase depend only on the modulus of the one-body coupling and on the two-body coupling. At variance with the phase and density fluctuations within each component, the relative-phase fluctuations are mostly determined by the off-phase branch of the spectrum, provided that the intra-species interaction strengths are not too different. This is strictly the case where they are equal ($g_1 = g_2$). Then, the two components are mutually phase coherent in any dimension, due to the gap in the contributing off-phase branch (provided the one-body coupling does not vanish, $\hbar\Omega_0 \neq 0$). Therefore, the one-body coupling always favors relative-phase coherence of the two Bose gases, independently of its phase. As regards the two-body coupling, two mechanisms compete. On the one hand, an increasing g_{12} tends to lower the contributing off-phase branch, hence increasing its thermal occupancy. On the other hand, it enhances the amplitude of off-phase density fluctuations, and therefore reduces the amplitude of phase fluctuations in the contributing off-phase branch. We found that the latter effect always dominates. Therefore, repulsive inter-component interactions suppress relative phase fluctuations while attractive inter-component interactions enhance relative phase fluctuations. Then, repulsive two-body coupling cooperates with one-body coupling and further suppresses relative-phase fluctuations, while attractive two-body coupling competes with one-body coupling and enhances relative-phase fluctuations. Closed analytical forms were eventually found for the relative-phase correlation function, in the high-temperature and large-separation regime. This enabled us to identify a correlation length for the relative phase, which was found to decrease when the one-body coupling increases, and to be roughly independent on the two-body coupling.

Moreover, the general formalism we have developped in this chapter is ready to be used in the case of inhomogeneous gases, and many direct applications can be envisionned.

For instance, one can study the effect of inhomogeneous (e.g. harmonic, and possibly component-dependent) trapping. This would be particularly relevant to describe ultracold-atom experiments. In this case, one may resort to numerical solutions of the Gross-Pitaevskii and Bogoliubov equations.

Other interesting applications of this formalism include the study of the effects of dis-

order and random couplings, among which random-field-induced-order at finite temperature, Anderson localization of Bogoliubov excitations of coupled Bose gases, random interatomic couplings... Here again, resorting to numerical solutions or combining our formalism with well-established methods developed for single-component disordered gases could efficiently lead to promising advances.

5.4 SUPPLEMENT : General formulas for the homogeneous two-component Bose gas

In this supplement, we compute the excitation spectrum and wavefunctions of the homogeneous two-component Bose gas in the most general situation where both one-body and two-body couplings are present.

5.4.1 General case, $g_1 \neq g_2$

In principle, the first step is to solve the meanfield background, Eqs. (5.46) and (5.47). However, in the most general case with $g_1 \neq g_2$, $\Omega_0 \neq 0$, and $g_{12} \neq 0$, we did not find a simple closed solution [6], [7]. Thus, in the following, we will write directly the Bogoliubov equations as a function of n_1, n_2 and μ.

Given the meanfield solution n_1, n_2 and μ, one has to solve the homogeneous Bogoliubov equations (5.29) together with (5.51) and (5.52). By taking the sum and difference of the first two rows on the one hand, and of the last two rows of the other hand, we can rewrite those Bogoliubov equations in terms of the $f^{\rm p,m}_{\sigma\mathbf{k}}$ functions :

$$E_{\mathbf{k}} f^{\rm m}_{\sigma\mathbf{k}} = \left(\epsilon_{\mathbf{k}} + \frac{\hbar\Omega_0}{2}\sqrt{\frac{n_{\bar\sigma}}{n_\sigma}}\right) f^{\rm p}_{\sigma\mathbf{k}} - \frac{\hbar\Omega_0}{2} f^{\rm p}_{\bar\sigma\mathbf{k}} \tag{5.82}$$

$$E_{\mathbf{k}} f^{\rm p}_{\sigma\mathbf{k}} = \left(\epsilon_{\mathbf{k}} + \frac{\hbar\Omega_0}{2}\sqrt{\frac{n_{\bar\sigma}}{n_\sigma}} + 2g_\sigma n_\sigma\right) f^{\rm m}_{\sigma\mathbf{k}} + \left(2g_{12}\sqrt{n_1 n_2} - \frac{\hbar\Omega_0}{2}\right) f^{\rm m}_{\bar\sigma\mathbf{k}}, \tag{5.83}$$

where $\bar\sigma$ is the conjugate of component σ [$\bar\sigma = 2$ (resp. 1) for $\sigma = 1$ (resp. 2)]. Using the normalization condition (5.54), it yields

$$E^2_{\mathbf{k}} f^{\rm p}_{\sigma\mathbf{k}} = (\epsilon_{\sigma\mathbf{k}} + 2U_\sigma)\left(\epsilon_{\sigma\mathbf{k}} f^{\rm p}_{\sigma\mathbf{k}} - \frac{\hbar\Omega_0}{2} f^{\rm p}_{\bar\sigma\mathbf{k}}\right) + \left(2U_{12} - \frac{\hbar\Omega_0}{2}\right)\left(-\frac{\hbar\Omega_0}{2} f^{\rm p}_{\sigma\mathbf{k}} + \epsilon_{\bar\sigma\mathbf{k}} f^{\rm p}_{\bar\sigma\mathbf{k}}\right) \tag{5.84}$$

$$E_{\mathbf{k}} = f^{\rm p}_{1\mathbf{k}}\left(\epsilon_{1\mathbf{k}} f^{\rm p}_{1\mathbf{k}} - \frac{\hbar\Omega_0}{2} f^{\rm p}_{2\mathbf{k}}\right) + f^{\rm p}_{2\mathbf{k}}\left(\epsilon_{2\mathbf{k}} f^{\rm p}_{2\mathbf{k}} - \frac{\hbar\Omega_0}{2} f^{\rm p}_{1\mathbf{k}}\right), \tag{5.85}$$

where we have defined $\epsilon_{\sigma\mathbf{k}} \equiv \epsilon_{\mathbf{k}} + \frac{\hbar\Omega_0}{2}\sqrt{\frac{n_{\bar\sigma}}{n_\sigma}}$, $U_\sigma \equiv g_\sigma n_\sigma$, and $U_{12} \equiv g_{12}\sqrt{n_1 n_2}$. By defining as well

$$A_{\mathbf{k}\sigma} = \epsilon_{\sigma\mathbf{k}}(\epsilon_{\sigma\mathbf{k}} + 2U_\sigma) - \frac{\hbar\Omega_0}{2}\left(2U_{12} - \frac{\hbar\Omega_0}{2}\right) \tag{5.86}$$

$$B_{\mathbf{k}\sigma} = \epsilon_{\bar\sigma\mathbf{k}}\left(2U_{12} - \frac{\hbar\Omega_0}{2}\right) - \frac{\hbar\Omega_0}{2}(\epsilon_{\sigma\mathbf{k}} + 2U_\sigma) \tag{5.87}$$

we can rewrite Eq. (5.84) separating the terms in $f^{\rm p}_{\sigma\mathbf{k}}$ from those in $f^{\rm p}_{\bar\sigma\mathbf{k}}$

$$f^{\rm p}_{\bar\sigma\mathbf{k}} B_{\mathbf{k}\sigma} = f^{\rm p}_{\sigma\mathbf{k}}[E^2_{\mathbf{k}} - A_{\mathbf{k}\sigma}] \tag{5.88}$$

[6] In the case $g_1 = g_2 \equiv g$, we have $n_1 = n_2 = N/2\mathcal{V}$, with N the total number of atoms, by symmetry of the two components. Equations (5.46) and (5.47) are then identical and yield the simple solution $\mu = (g + g_{12})N/2\mathcal{V} - \hbar\Omega_0/2$.

[7] In the case $\Omega_0 = 0$, Equations (5.46) and (5.47) reduce to a linear problem whose solution reads $n_\sigma = \frac{N}{\mathcal{V}}\frac{g_{\bar\sigma} - g_{12}}{g_1 + g_2 - 2g_{12}}$ and $\mu = \frac{N}{\mathcal{V}}\frac{g_1 g_2 - g_{12}^2}{g_1 + g_2 - 2g_{12}}$ with $\bar\sigma = 2$ (resp. 1) for $\sigma = 1$ (resp. 2)

The Bogoliubov energies are then found from the ratio of the two avatars of Eq. (5.88) corresponding to $\sigma = 1$ and $\sigma = 2$ respectively. It yields

$$E_{\mathbf{k}}^{\pm} = \sqrt{\frac{1}{2}(A_{\mathbf{k}1} + A_{\mathbf{k}2}) \pm \sqrt{(A_{\mathbf{k}1} - A_{\mathbf{k}2})^2/4 + B_{\mathbf{k}1}B_{\mathbf{k}2}}}. \tag{5.89}$$

The excitation spectrum is composed of two branches, the one labelled by (+) always being above the one labelled by (−). Their low/high-momentum behaviors are easily found from a low/high-momentum expansion of the $A_{k\sigma}$ and $B_{k\sigma}$. At low momentum, the (−) branch is ungapped and phonon-like; conversely, the (+) branch exhibits a finite gap as soon as $\Omega_0 \neq 0$, given by

$$E_{\rm gap} = \left[\frac{\hbar^2\Omega_0^2}{4}\left(2 + \frac{n_1}{n_2} + \frac{n_2}{n_1}\right) + \hbar\Omega_0\sqrt{n_1 n_2}(g_1 + g_2 - 2g_{12})\right]^{1/2}. \tag{5.90}$$

At high energy, both branches are particle-like, and separated by an energy

$$\Delta = \left[\left(\frac{\hbar\Omega_0}{2}\frac{n_2 - n_1}{\sqrt{n_1 n_2}} + g_1 n_1 - g_2 n_2\right)^2 + (2g_{12}\sqrt{n_1 n_2} - \hbar\Omega_0)^2\right]^{1/2}. \tag{5.91}$$

In between, the two branches can possibly coincide at a specific $\mathbf{k}$ provided the equation $(A_{\mathbf{k}1} - A_{\mathbf{k}2})^2/4 + B_{\mathbf{k}1}B_{\mathbf{k}2} = 0$ has a solution (see Sec. 5.2.2 for a precise example in the case $g_1 = g_2$).

In the particular case where $\Omega_0 = g_{12} = 0$, and only in this case [8], the two branches are identical and correspond to the usual single-particle Bogoliubov spectrum, $E_{\mathbf{k}}^{\pm} = \sqrt{\epsilon_{\mathbf{k}}\,(\epsilon_{\mathbf{k}} + 2\mu)}$. Notice that this holds even for $g_1 \neq g_2$ because the meanfield background is identical for the two Bose gases, i.e. $g_1 n_1 = g_2 n_2 = \mu$ [see Eqs. (5.46) and (5.47) with $\Omega_0 = g_{12} = 0$]. In this case, the spectrum shows twofold degeneracy (there is also a trivial $+\mathbf{k} \leftrightarrow -\mathbf{k}$ degeneracy, which we disregard here).

Given the excitation spectrum, we can then compute the Bogoliubov wavefunctions $f_{\sigma\mathbf{k}}^{\rm p,m}$. To do so, we use Eq. (5.88) and express $f_{2\mathbf{k}}^{\rm p}$ as a function of $f_{1\mathbf{k}}^{\rm p}$. Inserting this expression into Eq. (5.85), we find

$$f_{1\mathbf{k}}^{\rm p} = \sqrt{\frac{E_{\mathbf{k}}}{\epsilon_{1\mathbf{k}} - \hbar\Omega_0\dfrac{E_{\mathbf{k}}^2 - A_{\mathbf{k}1}}{B_{\mathbf{k}1}} + \epsilon_{1\mathbf{k}}\left(\dfrac{E_{\mathbf{k}}^2 - A_{\mathbf{k}1}}{B_{\mathbf{k}1}}\right)^2}} \tag{5.92}$$

up to an arbitrary phase that we set to zero. Using again Eq. (5.88), we find :

$$f_{2\mathbf{k}}^{\rm p} = \frac{E_{\mathbf{k}}^2 - A_{\mathbf{k}1}}{B_{\mathbf{k}1}}\sqrt{\frac{E_{\mathbf{k}}}{\epsilon_{1\mathbf{k}} - \hbar\Omega_0\dfrac{E_{\mathbf{k}}^2 - A_{\mathbf{k}1}}{B_{\mathbf{k}1}} + \epsilon_{1\mathbf{k}}\left(\dfrac{E_{\mathbf{k}}^2 - A_{\mathbf{k}1}}{B_{\mathbf{k}1}}\right)^2}}. \tag{5.93}$$

Notice that although $f_{2\mathbf{k}}^{\rm p}$ could also be expressed by a symmetric expression as Eq. (5.92), this would not be sufficient to determine its relative phase with respect to $f_{1\mathbf{k}}^{\rm p}$. We finally deduce

[8] For the two branches to be identical, one necessarily have $\Omega_0 = 0$ to make the (+) branch ungapped [see Eq. (5.90)], and then $g_{12} = 0$ to make the two branches coincide at high energy [see Eq. (5.91)].

the $f^{\rm m}_{\sigma\mathbf{k}}$ waves from the $f^{\rm p}_{\sigma\mathbf{k}}$ using Eq. (5.82). It yields

$$f^{\rm m}_{1\mathbf{k}} = \frac{\epsilon_{1\mathbf{k}} - \hbar\Omega_0(E^2_{\mathbf{k}} - A_{\mathbf{k}1})/2B_{\mathbf{k}1}}{\sqrt{E_{\mathbf{k}}\left[\epsilon_{1\mathbf{k}} - \hbar\Omega_0\dfrac{E^2_{\mathbf{k}} - A_{\mathbf{k}1}}{B_{\mathbf{k}1}} + \epsilon_{1\mathbf{k}}\left(\dfrac{E^2_{\mathbf{k}} - A_{\mathbf{k}1}}{B_{\mathbf{k}1}}\right)^2\right]}} \tag{5.94}$$

and

$$f^{\rm m}_{2\mathbf{k}} = \frac{\epsilon_{2\mathbf{k}}(E^2_{\mathbf{k}} - A_{\mathbf{k}1})/B_{\mathbf{k}1} - \hbar\Omega_0/2}{\sqrt{E_{\mathbf{k}}\left[\epsilon_{1\mathbf{k}} - \hbar\Omega_0\dfrac{E^2_{\mathbf{k}} - A_{\mathbf{k}1}}{B_{\mathbf{k}1}} + \epsilon_{1\mathbf{k}}\left(\dfrac{E^2_{\mathbf{k}} - A_{\mathbf{k}1}}{B_{\mathbf{k}1}}\right)^2\right]}}. \tag{5.95}$$

5.4.2 Symmetric case, $g_1 = g_2$

In the case discussed in Sec. 5.2.2 where the intra-component couplings are equal, $g_1 = g_2$, we have by symmetry of the two components $n_1 = n_2$, $A_{\mathbf{k}1} = A_{\mathbf{k}2} \equiv A_{\mathbf{k}}$ and $B_{\mathbf{k}1} = B_{\mathbf{k}2} \equiv B_{\mathbf{k}}$ with

$$A_{\mathbf{k}} = \left(\epsilon_{\mathbf{k}} + \frac{\hbar\Omega_0}{2}\right)\left(\epsilon_{\mathbf{k}} + \frac{\hbar\Omega_0}{2} + gn\right) - \frac{\hbar\Omega_0}{2}\left(ng_{12} - \frac{\hbar\Omega_0}{2}\right) \tag{5.96}$$

$$B_{\mathbf{k}} = \left(\epsilon_{\mathbf{k}} + \frac{\hbar\Omega_0}{2}\right)\left(ng_{12} - \frac{\hbar\Omega_0}{2}\right) - \frac{\hbar\Omega_0}{2}\left(\epsilon_{\mathbf{k}} + \frac{\hbar\Omega_0}{2} + gn\right). \tag{5.97}$$

Equation (5.89) then reads $E^{\pm}_{\mathbf{k}} = \sqrt{A_{\mathbf{k}} \pm |B_{\mathbf{k}}|}$. Therefore, the two energies corresponding to a given momentum $\mathbf{k}$, irrespective to the branches, are nothing but $\sqrt{A_{\mathbf{k}} \pm B_{\mathbf{k}}}$. This allows for redefining the two branches of the spectrum in a different way :

$$E^{\rm in/off}_{\mathbf{k}} = \sqrt{A_{\mathbf{k}} \pm B_{\mathbf{k}}} \tag{5.98}$$

Although none of the branches is now systematically above or below the other one, this convention for the "in" branch and the "off" branch will prove more convenient in Sec. 5.2.2, especially while computing the Bogoliubov wavefunctions. Indeed, notice that $(E^2_{\mathbf{k}} - A_{\mathbf{k}1})/B_{\mathbf{k}1} = 1$ for the "in" branch and -1 for the "off" branch . This enables us to considerably simplify Eqs. (5.92) to (5.95) for the Bogoliubov wavefunctions in the case $g_1 = g_2$.

Conclusions and perspectives

La bêtise consiste à vouloir conclure.
Gustave Flaubert

In this manuscript, we have studied the collective localization transitions of disordered weakly-interacting Bose superfluids in various contexts. Such an issue is essential to understand the dynamics of disordered many-body systems and is for instance directly relevant to quench experiments, where energy and information transfer within the fluid are mediated by the ability of collective excitations to propagate throughout the system. Additionally, since collective excitations govern most finite-temperature properties of Bose gases, understanding their behaviour in the presence of disorder can constitute a promising step in the quest for the phase diagram of disordered bosons at finite temperature.

By the systematic use of both analytical and numerical methods, we have addressed this question in different contexts, which remarkably led to a rich and original physics in each case.

In the case of a Bose gas in continuous space subjected to a true disorder, presented in chapter 3, we have shown that the propagation of collective excitations displays both universal and non-universal features. Similarly to the free-particle case, we found a universal localization behaviour, stating that all excitations are localized in 1D and 2D while a mobility edge shows up in 3D. Conversely, the energy dependence of the localization length and the position of the mobility edge(s) are strongly non-universal and depend on the interplay, at the microscopic scale, between disorder and interactions. On the one hand, interactions screen the disorder, protecting the transport of low-energy excitations in contrast with the free-particle case. On the other hand, density depletion induced by strong disorder alters the very nature of collective excitations, which may locally behave as free particles. This competition yields a nontrivial localization diagram, with possibly several mobility edges in the spectrum.

The case of a one-dimensional quasiperiodic lattice, presented in chapter 4, is very different. For non-interacting particles, it is characterized by an energy-independent localization transition. Our study in the interacting case, supported by both numerical and analytical calculations, has revealed that interactions dramatically alter this picture. An intermediate regime, where low-energy extended states and high-energy localized states coexist in the excitation spectrum, appears for intermediate quasiperiodic strength. Therefore, interactions change in this case the universality class of the transition. To explain it, we have developed an analytical treatment of the problem, which allowed us to map the problem onto an effective free-particle problem in a multi-harmonic field. Both analytics and numerics are in quantitative agreement, and a full localization diagram was obtained.

Finally, in chapter 5, we have set the formalism to address the case of two-component Bose gases. Our approach, based on the Bogoliubov theory, gives access to collective excitations, as well as fluctuations and correlation functions of the coupled Bose gas, in the most general inhomogeneous situation. Applying it to a homogeneous gas, we have worked out the non-trivial physics of this case, which already displays a great diversity of regimes, and derived explicit formulas for the relative phase correlation function, which may be useful for experiments. Therefore, the route is now opened to the investigation of disorder in this context.

Outlook

The experimental activity in the field of disordered and quasiperiodic ultracold gases is currently very active. On the one hand, disordered, quasiperiodic, and multi-component Bose gases are today commonly realized. On the other hand and although more recent, so are now quantum-quench experiments, sparked by the increasing interest for many-body dynamics. Therefore, the experimental observation of collective localization transitions can be expected to come soon, yielding fruitful comparison with our works. In the case of a Bose superfluid subjected to a true disorder (chapter 3), the main challenge would be the experimental observation of the various classes of mobility spectra. Our analysis has shown that this should be within the reach of current experiments. In the case of a one-dimensional Bose superfluid on a quasiperiodic lattice (chapter 4), our localization diagram is consistent with the reported observations of the superfluid-Bose glass transition. As regards the localization transition for collective excitations, the latter lies in a very typical range of parameters, and could therefore be observed. Additionally, recent transport measurements with BECs in quasiperiodic lattices, as well as observations of the superfluid to Bose glass transition at finite temperature, could be related to the localization properties of collective excitations that we have described. As regards multi-component Bose gases (chapter 5), experiments with disorder could start in the coming years. Our general formalism, which already provides a successful quantitative description of the homogeneous case, for instance as regards relative phase fluctuations, could thus be promisingly applied to the coming experiments with disorder.

As regards theoretical perspectives, one can envision several extensions to our work.

In the case of a true disorder (chapter 3), we have predicted the existence of several classes of mobility spectra. Since our approach mostly amounts to characterizing a diffusive motion by retaining the leading disordered terms, relying then on the criterion $k_\varepsilon l_\mathrm{B} \sim 1$ for localization, it would be fruitful to resort to an independent method to corroborate such predictions, especially in the strongly disordered regime. For instance, transport properties of collective excitations could be studied by a dynamical treatment of the problem, via large scale numerical simulations of the time-dependent Gross-Pitaevskii equation in a disordered potential. The diffusive or localization behaviour of collective excitations, as well as their propagation in both depleted and non depleted regions, could then be explicitely monitored.

In the case of a 1D Bose superfluid on a quasiperiodic lattice (chapter 4), two main extensions could be envisioned. On the one hand, investigating the 2D and 3D cases could be particularly promising, especially for non-separable systems (i.e. which cannot be split into several one-dimensional systems). In such case, since the single-particle physics already differs from the 1D case (locator perturbation theory predicts in higher dimensions an energy-dependent localization transition), one should expect for collective excitations a rich behaviour. Moreover, our methods, be it the numerical resolution (imaginary time propagation and ex-

act diagonalization) or the analytical treatment (derivation of an effective model and locator perturbation theory), are completely general and can be applied in higher dimensions as well. On the other hand, one could stay in 1D but consider the case of two weak incommensurate optical lattices on the continuous space (instead of having one deep lattice discretizing space). From a theoretical point of view, the absence of duality in such a model should give rise to an richer physics, although presumably reminiscent of the case we have studied. Moreover, such a configuration could be promisingly realized in future experiments, and would considerably help reduce heating, which is always important in the presence of deep lattices.

In the case of a two-component Bose gas (chapter 5), our work opens the way to the investigation of disorder. The latter can be introduced in several ways (random external potential, random couplings,...) and one can therefore expect a rich physics. For instance, combining our inhomogeneous formalism with the techniques developed in the previous chapters, it would be interesting to study the collective localization transitions of excitations of the coupled condensates. In view of the diversity of scenarii that we have enlightened in the homogeneous case, a rich behaviour can be anticipated. Another promising appplication of our work would be the study of random-field-induced order (RFIO) at finite temperature, which so far remains an open question.

Version française

Dans ce mémoire, nous nous sommes intéressés à la question des transitions de localisation collective dans les superfluides de Bose désordonnés. C'est une question essentielle pour mieux appréhender les phénomènes de dynamique à N corps dans les systèmes désordonnés, et qui est par exemple directement pertinente pour décrire les expériences de *quench*, dans lesquelles c'est précisément la capacité des excitations collectives à se propager au sein du fluide qui détermine la manière dont l'information est véhiculée à travers le système. De plus, dans la mesure où les excitations collectives déterminent aussi la plupart des propriétés du gaz à température finie, comprendre leur comportement en présence de désordre peut constituer une avancée majeure dans la quête du diagramme de phases de bosons désordonnés à température finie.

En combinant systématiquement approches analytiques et méthodes numériques, nous avons étudié cette question dans différents contextes, conduisant, d'une façon très remarquable, à une physique riche et originale dans chacun des cas étudiés.

Dans le cas d'un gaz de Bose dans l'espace continu et soumis à un vrai potentiel de désordre, étudié au chapitre 3, nous avons montré que la propagation des excitations présente à la fois des propriétés universelles de transport et des caractéristiques non universelles. En effet, les excitations collectives présentent le même comportement universel de localisation que les particules libres, à savoir qu'elles sont toujours localisées en 1D et 2D, alors qu'une transition de localisation apparaît en 3D. En revanche, la dépendance en énergie des longueurs de localisation, et la position du/des éventuel(s) seuil(s) de mobilité sont fortement non universels et résultent de la compétition, à l'échelle microscopique, entre le désordre et les interactions. D'une part, les interactions ont tendance à écranter le désordre, protégeant le transport des excitations de basse énergie. D'une part, un fort désordre peut conduire à une dépletion locale du profil de densité du condensat, altérant la nature même des excitations collectives qui, localement, se comportent alors comme des particules libres. De cette compétition résulte en particulier un diagramme de localisation non trivial, caractérisé par la présence éventuelle de plusieurs seuils de mobilité dans le spectre des excitations.

Le cas d'un réseau quasi-périodique unidimensionnel, présenté au chapitre 4, est très différent. Pour des particules libres, un tel système est caractérisé par une transition de localisation indépendante de l'énergie. Notre étude du problème avec interactions, menée à l'aide d'outils analytiques et numériques, révèle que les interactions modifient radicalement cette image. Elles se traduisent en effet par l'apparition d'un régime intermédiaire caractérisé par la coexistence, dans le spectre d'excitation, d'états étendus de basse énergie et d'états localisés de haute énergie, et changent donc de ce fait la classe d'universalité de la transition. L'approche analytique que nous avons développée nous a permis d'expliquer ce comportement en termes de localisation dans un modèle effectif multiharmonique. Nos méthodes, numérique et analytique, sont quantitativement en accord, et nous présentons un diagramme complet de localisation.

Enfin, au chapitre 5, nous avons établi le formalisme de base pour étudier le cas d'un gaz de Bose à deux composants. Ce formalisme, basé sur la théorie de Bogoliubov, donne accès aux excitations collectives du gaz, ainsi qu'à ses fluctuations et fonctions de corrélation, dans la situation inhomogène la plus générale. L'appliquant dans un second temps au cas homogène,

nous avons mis en lumière la physique du gaz à deux composants, qui présente une grande diversité de régimes, et dérivé des formules analytiques explicites pour les fluctuations de sa phase relative, qui pourraient s'avérer utiles aux expériences en cours sur ces systèmes. D'une certaine manière, ce travail ouvre ainsi la voie à l'étude des effets du désordre dans ces systèmes.

Perspectives

Le domaine des gaz d'atomes froids désordonnés est aujourd'hui extrêmement actif sur le plan expérimental. D'une part, les gaz de Bose désordonnés, quasi-périodiques, ou à plusieurs composants sont couramment réalisés dans un grand nombre de groupes expérimentaux. D'autre part, depuis quelques années maintenant, il en va désormais de même des expériences de *quench*, motivées par l'intérêt grandissant pour les questions de dynamique des systèmes à N corps. Par conséquent, on peut espérer être en mesure d'observer expérimentalement, d'ici quelques années, les comportements de localisation collective décrits dans ce mémoire. Dans le cas d'un gaz de Bose soumis à un vrai désordre (chapitre 3), le principal objectif serait l'observation des multiples seuils de mobilité prédits dans le spectre d'excitation. Notre analyse a montré à cet égard que ce régime intéressant était à la portée des expériences actuelles d'atomes froids. Dans le cas d'un réseau quasi-périodique unidimensionnel (chapitre 4), il faut d'abord souligner que notre diagramme de localisation est tout à fait cohérent avec les observations expérimentales de la transition superfluide-verre de Bose. En ce qui concerne la transition de localisation des excitations collectives, celle-ci se trouve précisément dans la même gamme de paramètres que les expériences actuelles, et pourrait donc être observée. Qui plus est, de récentes expériences de transport d'un condensat dans un potentiel quasi-périodique, ainsi que certaines observations de la transition superfluide-verre de Bose à température finie, pourraient être directement reliées aux propriétés de localisation des excitations collectives que nous avons décrites. En ce qui concerne les gaz de Bose à deux composants (chapitre 5), les expériences en présence de désordre pourraient débuter dans un futur très proche. L'application de notre formalisme, qui fournit déjà une description quantitative du cas homogène, par exemple en ce qui concerne les fluctuations de phase relative, pourrait alors être très prometteuse.

Sur le plan théorique, notre travail ouvre également de nombreuses perspectives.

Dans le cas d'un vrai désordre (chapitre 3), nous avons conclu à l'existence possible de plusieurs seuils de mobilité dans le spectre. Dans la mesure où notre approche repose essentiellement sur la caractérisation, à l'ordre le plus bas en désordre, d'un mouvement diffusif, et s'appuie dans un second temps sur le critère de localisation $k_\varepsilon l_\mathrm{B} \sim 1$, il serait particulièrement prometteur de la tester au moyen d'une méthode totalement indépendante, en particulier dans le régime de fort désordre. Une possibilité pourrait consister à effectuer un traitement dynamique du problème, et étudier le transport des excitations par des simulations numériques de grande échelle basées sur l'équation de Gross-Pitaevskii dépendant du temps, en présence d'un potentiel désordonné. Le comportement, diffusif ou localisé, des excitations pourrait alors être directement observé, ainsi que la manière dont celles-ci se propagent localement, en présence et en l'absence de dépletion du profil de densité.

Dans le cas d'un gaz de Bose quasi-périodique (chapitre 4), on peut envisager deux extensions principales à notre travail. D'une part, il serait intéressant d'étudier le cas des dimensions supérieures, en particulier pour des systèmes non séparables (i.e. qui ne se découplent pas en plusieurs systèmes unidimensionnels). Dans la mesure où le comportement des particules libres est déjà très différent en dimensions 2 et 3 (la théorie de locateur prédit en effet une

transition de localisation dépendant de l'énergie), on peut s'attendre pour les excitations collectives à une physique très riche. De plus, toutes les méthodes que nous avons utilisées, qu'elles soient numériques (propagation en temps imaginaire, diagonalisation exacte) ou analytiques (dérivation du modèle effectif, théorie de locateur), sont complètement générales et directement transposables au cas de dimensions supérieures. D'autre part, il serait intéressant de rester en dimension 1 mais d'étudier le cas de deux réseaux optiques incommensurables et d'amplitudes voisines, dans l'espace continu (au lieu d'avoir un réseau principal profond qui discrétise l'espace). En effet dans ce cas-là, l'absence de dualité du modèle devrait conduire à une physique plus riche, possédant toutefois un certain nombre de réminiscences du cas que nous avons étudié. De plus, une telle configuration pourrait être particulièrement prometteuse pour les expériences futures, dans la mesure où elle contribuerait à réduire les problèmes de chauffage, qui sont toujours importants en présence de réseaux optiques profonds.

Dans le cas d'un gaz de Bose à deux composants (chapitre 5), notre travail ouvre la voie à l'étude du désordre dans ces systèmes. Ce dernier peut être introduit de nombreuses façons (potentiel extérieur, couplages désordonnés...) et on peut donc s'attendre à une physique très riche. Par exemple, la combinaison de notre formalisme inhomogène et des méthodes développées dans les chapitres précédents pourrait permettre d'étudier les propriétés de localisation des excitations collectives dans les condensats couplés. Au vu de la diversité de scénarios rencontrés dans le cas homogène, on peut pressentir une grande variété de comportements. Une autre application prometteuse de notre travail pourrait être l'étude des effets d'ordre induit par le désordre (RFIO) à température finie, qui demeure à ce jour une question ouverte.

Appendices

Appendix A

Statistical properties of random potentials

Un beau désordre est un effet de l'art.
Nicolas Boileau

A random potential $V(\mathbf{r})$ is a random function of position $\mathbf{r}$ (i.e. for each point $\mathbf{r}$, $V(\mathbf{r})$ is a random variable). A given *realization* of the potential corresponds then to a given function of position $\mathbf{r}$. In principle, to completely characterize a random potential, one needs to know all the n-point probability distributions :

- $P_{\mathbf{r}}(V)$ (the one-point probabilty distribution) for all $\mathbf{r}$;
- $P_{\mathbf{r},\mathbf{r}'}(V,V')$ (the joint probabilty distribution) for all $\mathbf{r},\mathbf{r}'$;

...etc.

In most cases, to completely describe a random potential, it is however sufficient to know all the n-point correlation functions

$$C_n(\mathbf{r}_1,\mathbf{r}_2,...\mathbf{r}_n) = \langle V(\mathbf{r}_1)V(\mathbf{r}_2)...V(\mathbf{r}_n)\rangle, \tag{A.1}$$

where $\langle ...\rangle$ denotes statistical averaging (i.e. ensemble averaging over all realizations of the potential).

A.1 General properties

Homogeneity- A random potential is assumed to be spatially homogeneous, which means that its statistical properties are translation-invariant (for instance, the one-point probability distribution is independent of the position). As a consequence, all n-point correlators $C_n(\mathbf{r}_1,\mathbf{r}_2,...\mathbf{r}_n)$ satisfy

$$C_n(\mathbf{r}_1+\rho,\mathbf{r}_2+\rho,...\mathbf{r}_n+\rho) = C_n(\mathbf{r}_1,\mathbf{r}_2,...\mathbf{r}_n), \tag{A.2}$$

and depend only on $n-1$ relative coordinates.

Vanishing correlations at infinity- Another key assumption is the disappearance of statistical correlations at large separations, as expressed by

$$\langle V(\mathbf{r}_1)...V(\mathbf{r}_n)V(\mathbf{r}_{n+1}+\rho)...V(\mathbf{r}_m+\rho)\rangle \underset{|\rho|\to\infty}{\longrightarrow} \langle V(\mathbf{r}_1)...V(\mathbf{r}_n)\rangle\langle V(\mathbf{r}_{n+1})...V(\mathbf{r}_m)\rangle \tag{A.3}$$

Properties of the first correlation functions- In most problems, the physics is efficiently described by the single-point and two-point properties of the disordered potential. Let us briefly review their main properties, which come from the previous general assumptions.

- Single-point properties are determined by the probability distribution $P(V)$, and do not depend on position due to spatial homogeneity. In particular, one can assume without loss of generality a vanishing statistical average, $\langle V \rangle = 0$. The standard deviation therefore reads $V_{\mathrm{R}}^2 = \langle V^2 \rangle$.

- Due to spatial homogeneity, the two-point correlation function, or *autocorrelation function*, depends only on one relative coordinate $C_2(\mathbf{r}) = \langle V(\mathbf{r}')V(\mathbf{r}+\mathbf{r}')\rangle$. Homogeneity implies as well the relations

$$C_2(\mathbf{r}) = C_2(-\mathbf{r}) \qquad \text{and} \qquad \tilde{C}_2(\mathbf{q}) = \tilde{C}_2(-\mathbf{q}),$$

  where the Fourier transform of the two-point correlation function, also referred to as the *power spectrum* of the disorder, is defined by $\tilde{C}_2(\mathbf{q}) = \int C_2(\mathbf{r}) e^{-i\mathbf{q}.\mathbf{r}} d^d\mathbf{r}$.

  Due to the disappearance of correlations at infinity, the autocorrelation function drops to zero at large separations, on a typical length-scale called the *correlation length*, σ_{R}. The latter can be used to define a dimensionless autocorrelation function $c_2(\mathbf{r})$ by $C_2(\mathbf{r}) = V_{\mathrm{R}}^2 c_2(\mathbf{r}/\sigma_{\mathrm{R}})$, or equivalently in Fourier space $\tilde{C}(\mathbf{q}) = V_{\mathrm{R}}^2 \sigma_{\mathrm{R}}^d \tilde{c_2}(\mathbf{q}\sigma_{\mathrm{R}})$.

  In many cases, the disorder is further assumed to be *isotropic*, which means that $C_2(\mathbf{r}) = C_2(r)$ is a radial function (and so is its Fourier transform).

A.2 Standard examples

Gaussian disorder

A Gaussian disorder is a random potential whose all n-point correlation functions can be expanded into products of two-point correlators using Wick's theorem. In other words, all cumulants of order $n > 2$ identically vanish [1]. Since $\langle V \rangle = 0$, this implies that all correlation functions of odd order vanish identically, while correlation functions of even order expand into products of two-point correlation functions C_2. For instance, the four-point correlator of a Gaussian potential reads

$$C_4(\mathbf{r}_1, \mathbf{r}_2, \mathbf{r}_3) = C_2(\mathbf{r}_1)C_2(\mathbf{r}_2 - \mathbf{r}_3) + C_2(\mathbf{r}_2)C_2(\mathbf{r}_3 - \mathbf{r}_1) + C_2(\mathbf{r}_3)C_2(\mathbf{r}_1 - \mathbf{r}_2) \tag{A.4}$$

Therefore, all statistical properties of a Gaussian random potential are entirely determined by its two-point correlator C_2.

Notice that the expression "Gaussian" disorder is sometimes misleadingly used to refer to a disorder whose one-point probability distribution is a Gaussian, or to a disorder whose two-point correlation function is Gaussian. Such disorders are however not necessarily Gaussian in the sense of the previous definition. For example, a Gaussian speckle is a speckle potential whose autocorrelation function C_2 is Gaussian, but it is not a Gaussian disorder (a speckle potential is actually never Gaussian since it always has non-vanishing cumulants of order higher than 2.)

[1] We recall that the cumulants are obtained from the moments C_n by substracting all possible factorized contributions.

White-noise disorder

A white-noise (or uncorrelated) disorder is a Gaussian disorder whose autocorrelation function is delta-correlated,

$$C_2(\mathbf{r}) = D\delta(\mathbf{r}). \tag{A.5}$$

The coefficient D characterizes the disorder strength and has the dimension of $(energy)^2(length)^d$, where d is the dimensionality.

White-noise disorders are widely used, mostly because at low-energy, many continuous random potentials can be replaced by a white-noise potential. Indeed, when the correlation length σ_{R} of a random potential becomes much smaller than all the relevant length scales present in the problem, the physics can be well-described within the so-called *white-noise limit*, which amounts to let $\sigma_{\mathrm{R}} \to 0$ at fixed $V_{\mathrm{R}}^2\sigma_{\mathrm{R}}^d$. In this limit, the autocorrelation function of the potential reads

$$C_2(\mathbf{r}) = \tilde{c_2}(0)V_{\mathrm{R}}^2\sigma_{\mathrm{R}}^d\delta(\mathbf{r})$$

and the potential can be described by a white-noise potential with $D = \tilde{c_2}(0)V_{\mathrm{R}}^2\sigma_{\mathrm{R}}^d$.

This applies to all random potentials for which $\tilde{c_2}(0) < \infty$. The others, among which some speckle potentials, do not have a white-noise limit.

Appendix B

Elements of quantum transport theory

It is notoriously difficult to obtain reliable results for quantum mechanical scattering problems [...] any simple uncontrolled approximation is not worth more than the weather forecast.
W. Thirring

In this appendix, we briefly review the basics of quantum transport theory. Although it does not aim at providing an exhaustive presentation, which would hardly fit into the present format, this short summary outlines the main ideas and gives a justification of all the results used in this manuscript. We refer to [17, 18, 289, 290] for a more detailed presentation [1].

We will consider the general situation of a single particle propagating in a disordered medium defined by a disordered potential, in arbitrary dimension d. The Hamiltonian can be typically written

$$\hat{H} = \hat{H}_0 + \hat{V} \tag{B.1}$$

where $\hat{H}_0 = \hat{p}^2/2m$ describes the disorder-free, translation-invariant, Hamiltonian and $\hat{V}$ the time-independent disordered potential, which breaks translation invariance.

Diagrammatic perturbation theory is a perturbative approach in $\hat{V}$, which roughly consists in an expansion of $\hat{H}$ in powers of $\hat{V}$. It is therefore expected to be valid in the weak-disorder regime.

B.1 Quantum propagator

The time evolution of the particle wavefunction $|\psi\rangle$ obeying the Schrödinger equation, $i\hbar\partial_t|\psi\rangle = \hat{H}|\psi\rangle$, is determined by $|\psi(t)\rangle = G^R(t)|\psi(0)\rangle$, where $G^R(t)$ denotes the forward time evolution operator defined by $G^R(t) = -\frac{i}{\hbar}\Theta(t)\exp(-i\hat{H}t/\hbar)$ (with $\Theta(t)$ the Heaviside function).

[1] Figures of this appendix are extracted or based on [289, 290].

The *retarded Green function*, also referred to as the *field propagator*, is the Fourier transform of the forward time evolution operator $G^R(t)$ [2],

$$G^R(E) = \int G^R(t) e^{i(E+i0^+)t/\hbar} dt = \frac{1}{E - \hat{H} + i0^+} \tag{B.2}$$

For notational brievity, we will in the following omit the superscript R, except when necessary. From Eq. (B.2), one immediately gets

$$G(E) = G_0(E) + G_0(E) V G(E) \tag{B.3}$$

where $G_0(E)$ denotes the disorder-free Green function. The latter is diagonal in momentum space and writes

$$\langle k'|G_0(E)|k\rangle = (2\pi)^d \delta(k-k') G_0(E,k) = \frac{(2\pi)^d \delta(k-k')}{E - \varepsilon_0(k) + i0^+} \tag{B.4}$$

where $\varepsilon_0(k) = \hbar^2 k^2/2m$ is the free-disorder dispersion relation.

Iterating Eq. (B.3) yields the so-called *Born series*

$$G = G_0 + G_0 V G_0 + G_0 V G_0 V G_0 + ... \tag{B.5}$$

where we have omitted the energy arguments for brievity. Explicitely rewriting Eq. (B.5) as a function of all matrix elements proves very tedious

$$\begin{aligned} \langle k'|G(E)|k\rangle &= \delta(k-k') G_0(E,k) + G_0(E,k') V_{k'-k} G_0(E,k) \\ &\quad + \sum_{k''} G_0(E,k') V_{k'-k''} G_0(E,k'') V_{k''-k} G_0(E,k) + ... \end{aligned} \tag{B.6}$$

but can be simply represented by the Feynman diagram

$\langle k'|G(E)|k\rangle = \delta_{kk'}$ 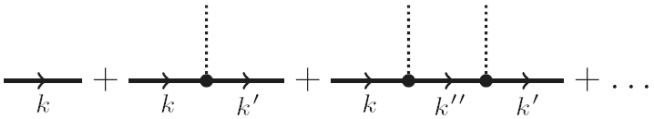

$+ \ldots$

Here, solid lines supported by k represent the disorder-free propagator $G_0(E,k)$ while scattering by the disordered potential is repreented by a dotted line. Labelling the latter is useless since it is automatically determined by the incident and scattered momenta. Finally, in such diagrams, all internal momenta, such as k'' here, have to be summed over.

B.2 Ensemble averaging and self-energy

Dyson equation

Although the Born series (B.5) permits to compute the full propagator, the result will be different for each particular realization of the disorder, and so will be the calculation of any observable quantity. In fact, relevant quantities are only obtained after statistical averaging over realizations of the disorder, and what one has to consider is the averaged propagator. The latter expresses

$$\overline{G} = G_0 + G_0 \overline{V G_0 V} G_0 + G_0 \overline{V G_0 V G_0 V} G_0 + ... \tag{B.7}$$

[2] The regularisation term $i0^+$ in Eq. (B.2) guarantees the causality of the forward time evolution operator.

where we have used the fact that $\overline{V} = 0$ to drop the first term $G_0\overline{V}G_0$. Equation (B.7) can be advantageously represented using Feynman diagrams

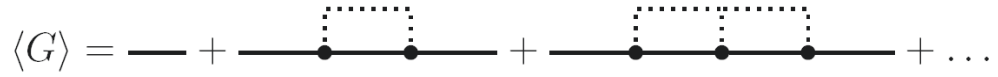

Remarkably, averaging over disorder restores translation invariance, and $\overline{G}$ is diagonal in momentum space. It appears as well that the average propagator involves correlations of the potential of all orders, as represented by the connected dotted lines between disordered vertex. Equation (B.7) can be rewritten in the most compact form

$$\overline{G} = G_0 + G_0\Sigma\overline{G}, \tag{B.8}$$

known as the *Dyson equation*, which defines the *self-energy* Σ, one of the most fundamental objects in diagrammatic perturbation theory. Indeed, by iterating the Dyson equation, one gets

$$\overline{G} = G_0 + G_0\Sigma G_0 + G_0\Sigma G_0\Sigma G_0 + ..., \tag{B.9}$$

conveniently rewritten in the form

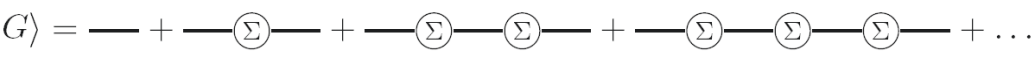

Therefore, since no disorder correlations appear here *between* the different self-energy blocks, it appears that the self-energy contains exactly all the correlations that cannot be split into products of independent factors by suppressing a single propagator line (referred to as the *one-particle irreducible* contributions). In some sense, the self-energy is the simplest object containing all relevant disorder correlations.

Physical meaning of the self-energy

The Dyson equation can be formally solved into $\overline{G} = [G_0^{-1} - \Sigma]^{-1}$. Since translation-invariance is restored by disorder-averaging, the matrix elements of $\overline{G}$ are diagonal in momentum space and read

$$\langle k'|\overline{G}(E)|k\rangle = (2\pi)^d\delta(k-k')\overline{G}(E,k) = \frac{(2\pi)^d\delta(k-k').}{E - \varepsilon_0(k) - \Sigma(E,k) + i0^+} \tag{B.10}$$

From the knowledge of the average propagator, one can calculate many physical quantities. In particular, information about the dressed eigenstates of the problem are encoded in the *spectral function*

$$A(E,k) \equiv -2\mathrm{Im}(\overline{G}(E,k)) = \frac{-2\mathrm{Im}\Sigma(E,k)}{(E - \varepsilon_0(k) - \mathrm{Re}\Sigma(E,k))^2 + (\mathrm{Im}\Sigma(E,k))^2}, \tag{B.11}$$

which represents the probability distribution for an excitation k to have the energy E. In the free-disorder case, $A(E,k) = 2\pi\delta[E - \varepsilon_0(k)]$, describing eigenstates at energies $E = \varepsilon_0(k)$ and of infinite lifetime. In the disordered case [see Eq. (B.11)], the self-energy encodes how the disorder affects the free dispersion relation :

- One the one hand, its real-part shifts the energy levels, the disordered ones, E_k, being given by the implicit equation $E_k = \varepsilon_0(k) + \mathrm{Re}\Sigma(E_k, k)$.

- One the other hand, since plane waves of momentum k are no longer eigenstates of the disordered problem, they acquire a finite spectral width, defining the elastic scattering rate $\Gamma_k = -2\mathrm{Im}\Sigma(E_k, k)$, and a corresponding elastic scattering lifetime $\tau_S(k) = \hbar\Gamma_k^{-1}$.

Further physical quantities can be computed from the spectral function, such as the density of states

$$N(E) = \frac{1}{2\pi}\int A(E,k)\frac{d^dk}{(2\pi)^d} \tag{B.12}$$

More generally, the spectral function is a central quantity in quantum transport theory, which regularly appears in calculations. Very often, calculations rely on the *on-shell approximation*, which amounts to replace it by its disorder-free expression, $2\pi\delta[E-\varepsilon_0(k)]$, and is sufficient at the lowest order in disorder.

Born approximation

To compute physical quantities, one therefore needs to know how to calculate the self-energy. This can in principle be achieved by applying the Feynman rules to evaluate and sum up all irreducible diagrams entering the self-energy. However, since Σ contains diagrams with correlations of all orders, an exact calculation is impossible. In practice, a frequent approximation, which proves correct for weak disorder, consists in taking into account only the lowest-order term. Within this *Born approximation*, the only contributing diagram

$\Sigma(k,E) =$ 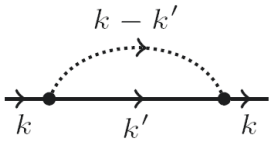

is easily evaluated as

$$\Sigma^{(2)}(E,k) = \int C(k-k')G_0(E,k')\frac{d^dk'}{(2\pi)^d} \tag{B.13}$$

with $C(k)$ the power spectrum of the disorder potential.

We are now in a position to apply the previous tools to compute the most fundamental quantities of quantum transport theory.

B.3 Scattering mean-free path

The *scattering mean-free path* l_S, i.e. the average distance travelled by a wave k without being scattered, is a central quantity to characterize the disordered transport. It is directly related to the elastic scattering lifetime $\tau_S(k)$ by $l_S = \tau_S(k)\hbar k/m = -\hbar^2 k/2m\mathrm{Im}\Sigma^{(2)}(E_k,k)$. At lowest order in disorder, one can use the on-shell approximation, which amounts here to replace $\Sigma^{(2)}(E_k,k)$ by $\Sigma^{(2)}[\varepsilon_0(k),k]$. The latter can be straightforwardly evaluated within the Born approximation using Eq. (B.13). Recalling that $\mathrm{Im}G_0(E,k') = -\pi\delta[E-\varepsilon_0(k')]$, one gets the final result

$$\frac{1}{kl_S} = \frac{2\pi m^2}{\hbar^4 k^{4-d}}\int \frac{d\Omega_d}{(2\pi)^d} C[2k\sin(\theta/2)], \tag{B.14}$$

where $d\Omega_d$ is the infinitesimal solid angle in dimension d, and the correlation function of the disorder, $C[2k\sin(\theta/2)]$, is probed on the energy shell $\varepsilon = \varepsilon_0(k)$.

B.4 Intensity transport

So far, our analysis has been based on the field propagator $\overline{G}$, since we have considered properties related to the wavefunction of the particle. However, some fundamental observables in quantum transport theory, such as the spatial density, are not directly linked to $\overline{G}$ and require a more elaborate formalism.

Bethe-Salpeter equation

Whereas the wavefunction evolves as $|\psi(t)\rangle = G^R(t)|\psi(0)\rangle$, the one-body density matrix $\rho(t)$ evolves as $\rho(t) = \Theta(t)\exp(-i\hat{H}t/\hbar)\rho(0)\exp(+i\hat{H}t/\hbar)$. Therefore, we need a theory not only for the average field propagator $\overline{G^R(E)}$, but for the average *intensity propagator* $\Phi \equiv \overline{G^R(E)G^A(E')}$, with $G^A(E)$ the advanced Green function. This intensity propagator includes all correlations between advanced and retarded amplitudes (referred to as *particle*- and *hole*-channels in condensed matter), and can be diagrammatically represented by a four-point vertex. In the same way than we derived a theory for the field propagator, a theory for the intensity propagator is needed. We will not enter into the detailed derivation of such a theory, which requires more elaborate tools, but the idea works as follows.

By complete analogy with the approach used for the average field propagator $\overline{G^R(E)}$, leading to the Dyson equation (B.8), the idea is to construct a structurally similar equation for the intensity propagator, known as the Bethe-Salpeter equation

$$\overline{G^R G^A} = \overline{G^R} \otimes \overline{G^A} + \overline{G^R} \otimes \overline{G^A} U \overline{G^R G^A} \tag{B.15}$$

The first term corresponds to the known evolution where the propagations of the field and of its conjugate in the effective medium are uncorrelated. All scattering events coupling those amplitudes are encoded in the intensity scattering operator U, as diagrammatically represented by

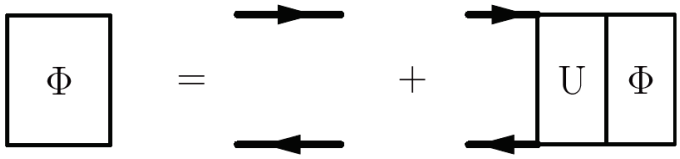

Note that the Bethe-Salpeter equation defines U, in the same way that the Dyson equation defines Σ. The precise form of U depends on the model of disorder but it has the general structure

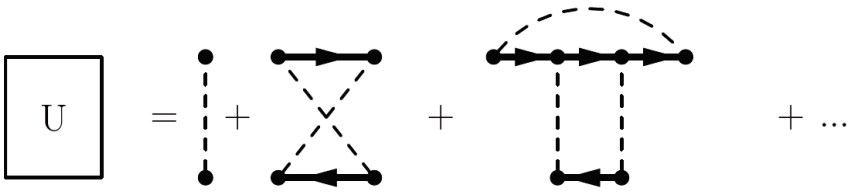

Using elaborate tools of quantum kinetic theory, one can formally solve the Bethe-Salpeter equation and generically show that on long times and over long distances, the motion is diffu-

sive [3], in the sense that the intensity propagator exhibits a diffusion pole,

$$\Phi(k,q,\omega) = \frac{1}{-i\omega + D(k)q^2}. \tag{B.16}$$

In real space, it is the solution of the diffusion equation $[\partial_t - D(k)\nabla^2]\Phi(k,r,t) = \delta(r,t)$. This diffusive motion is characterized by the momentum-dependent diffusion constant $D(k)$, or equivalently a transport time $\tau(k)$, which is given by

$$\frac{1}{\tau(k)} = \int \frac{dE}{2\pi}\frac{A(E,k)}{2\pi N(E)} \int A(E,k')A(E,k'')(1-\mathbf{k}'.\mathbf{k}'')U(E,k',k'')\frac{d^dk'd^dk''}{(2\pi)^{2d}}. \tag{B.17}$$

Since the latter depends on U, one should in principle take into account all possible correlations between retarded and advanced amplitudes (i.e. sum up all diagrams in U) to exactly characterize this diffusive/localized motion.

Boltzmann diffusion

Since generally, U cannot be calculated exactly, a first approximation consists in truncating U after its lowest-order contribution. In this so-called *Boltzmann approximation*, which is very similar to the Born approximation for the self-energy, one simply keeps for U the first diagram, which is evaluated as $U_B(E,k,k') = C(k-k')$. From Eq.(B.15), it yields for the intensity propagator the well-known *ladder diagram* structure,

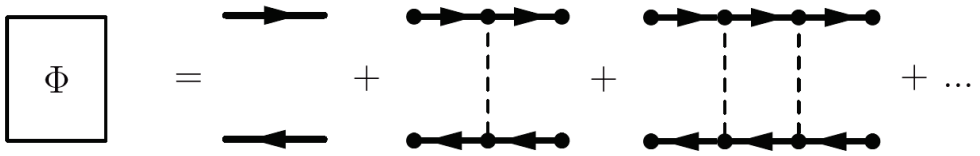

which describes an infinte series of independent scattering events. Such *diffuson* contribution depicts the situation where retarded and advanced amplitudes travel along the same paths, discarding all interference effects between them. It can more rigorously be shown that retaining only those ladder diagrams leads to Drude-like diffusion for the intensity propagator, with a diffusive constant which is directly evaluated by replacing in Eq. (B.17) U by its Boltzmann expression. Equivalently, one can write a corresponding *transport length* $l_{\rm B}$ defined by $D_B = kl_{\rm B}/d$. Within the on-shell approximation, which amounts to replace in Eq. (B.17) the spectral function by its disorder-free expression $2\pi\delta[E-\varepsilon_0(k)]$, one gets the final result

$$\frac{1}{kl_{\rm B}} = \frac{2\pi m^2}{\hbar^4 k^{4-d}} \int \frac{d\Omega_d}{(2\pi)^d}(1-\cos\theta)C[2k\sin(\theta/2)]. \tag{B.18}$$

The transport length $l_{\rm B}$ can be viewed as the typical length travelled by the particle before it loses the memory of its initial direction. Remarkably, it differs from the scattering length expression Eq. (B.14) only via the *anisotropy factor* $1-\cos\theta$. Indeed, for fully isotropic scattering, the latter is zero and $l_{\rm B} = l_S$, consistently with the fact that in this case, one scattering event is sufficient to completely blur the initial direction. Conversely, in most cases with correlated disorder, the anisotropy factor is finite and a large number of scattering events is required to significantly deflect the particle trajectory.

[3] or eventually localized if the diffusive constant vanishes.

B.5 Localization corrections

Weak Localization

Corrections to Boltzmann transport can be taken into account by including interference effects between retarded and advanced amplitudes. Such interferences arise when the correlated scattering events do not occur in the same order for the propagation of the advanced and the retarded amplitudes, as expressed diagrammatically by crossed correlation lines between the advanced and the retarded channels.

A first correction can be obtained considering the case where the advanced and retarded amplitudes travel along reversed trajectories, no matter how long they are. This so-called *Cooperon* contribution is diagrammatically represented by the *maximally-crossed diagrams*

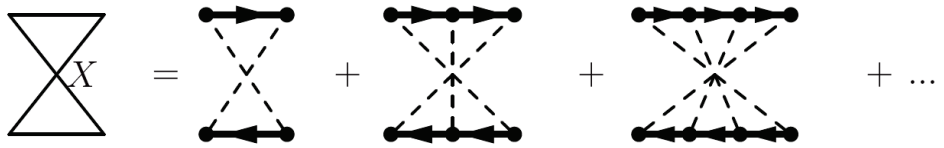

Remarkably, using a time-reversal argument, this contribution can be expressed in terms of the diffuson contribution. Its effect can thus be exactly taken into account, yielding the corrected diffusion constant

$$\frac{1}{D} = \frac{1}{D_B}\left[1 + \frac{1}{\pi N(\varepsilon_0(k))}\int \frac{1}{D_B q^2 - i0^+}\frac{d^d q}{(2\pi)^d}\right]. \tag{B.19}$$

The Cooperon correction, corresponding to the second term, makes $D < D_B$, providing a microscopic justification of weak localization.

Strong Localization

Due to its perturbative character, quantum diagrammatic theory cannot describe the strongly-disordered regime. To obtain a quantitative theory for strong localization, one would have in principle to take into account the contributions of all diagrams in U and resum all of them, which so far remains inextricable.

The self-consistent theory of localization [45] circumvents this problem by replacing in the denominator of Eq. (B.19) the Boltzmann diffusion constant D_B by the corrected one D itself, which is then self-consistently determined. This amounts to a self-consistent resummation of the diagrammatic series, including a whole class of diagrams of all orders (although not all), and provides qualitative estimates for the Anderson transition.

Alternatively, at variance with the diagrammatic perturbation theory, several approaches start from the opposite limit where $\hat{H}_0$ is small and develop weak-coupling perturbative methods. It is for instance the case of Anderson *locator perturbation theory* (see Sec. 4.1.3).

Bibliography

[1] N. Goldenfeld and L. P. Kadanov. Simple lessons from complexity. *Science*, **284** 87, 1999.

[2] P. W. Anderson. Absence of diffusion in certain random lattices. *Phys. Rev.*, **109** 1492–1505, 1958.

[3] L. Sanchez-Palencia and M. Lewenstein. Disordered quantum gases under control. *Nature Phys.*, **6** 87–95, 2010.

[4] B. C. Crooker, B. Hebral, E. N. Smith, Y. Takano, and J. D. Reppy. Superfluidity in a dilute Bose gas. *Phys. Rev. Lett.*, **51** 666–669, 1983.

[5] P. A. Crowell, F. W. Van Keuls, and J. D. Reppy. Onset of superfluidity in ^4He films adsorbed on disordered substrates. *Phys. Rev. B*, **55** 12620–12634, 1997.

[6] A. A. Abrikosov and L. P. Gorkov. *Sov. Phys. JETP*, **9** 220, 1959.

[7] P. A. Lee and T. V. Ramakrishnan. Disordered electronic systems. *Rev. Mod. Phys.*, **57** 287–337, 1985.

[8] P. W. Anderson. Local moments and localized states. In S. Lundqvist, editor, *Nobel lectures, Physics 1971-1980*. World Scientific Publishing Co., Singapore, 1992.

[9] D. M. Basko, I. L. Aleiner, and B. L. Altshuler. Metal-insulator transition in a weakly interacting many-electron system with localized single-particle states. *Ann. Phys.*, **321** 1126–1205, 2006.

[10] I. L. Aleiner, B. L. Altshuler, and G. V. Shlyapnikov. A finite-temperature phase transition for disordered weakly interacting bosons in one dimension. *Nature Phys.*, **6** 900–904, 2010.

[11] T. Giamarchi and H. J. Schulz. Anderson localization and interactions in one-dimensional metals. *Phys. Rev. B*, **37** 325–340, 1988.

[12] M. P. A. Fisher, P. B. Weichman, G. Grinstein, and D. S. Fisher. Boson localization and the superfluid-insulator transition. *Phys. Rev. B*, **40** 546–570, 1989.

[13] P. Lugan and L. Sanchez-Palencia. Localization of Bogoliubov quasiparticles in interacting Bose gases with correlated disorder. *Phys. Rev. A*, **84** 013612, 2011.

[14] V. Gurarie and J. T. Chalker. Bosonic excitations in random media. *Phys. Rev. B*, **68** 134207, 2003.

[15] J. Bardeen, N. L. Cooper, and J. R. Schrieffer. Theory of superconductivity. *Phys. Rev.*, **108** 1175, 1957.

[16] P. Kapitza. Viscosity of liquid helium below the lambda-point. *Nature*, page 74, 1938.

[17] J. Rammer. *Quantum Transport Theory.* Perseus Books, Reading, Mass., 1998.

[18] R. C. Kuhn, O. Sigwarth, C. Miniatura, D. Delande, and C. A. Müller. Coherent matter wave transport in speckle potentials. *New J. Phys.*, **9** 161, 2007.

[19] G. Bergmann. Weak localization in thin films. *Phys. Rep.*, **107**, 1984.

[20] M. E. Gershenson, B. I. Altshuler, A. G. Aronov, and Y. V. Sharvin. Quantum effects in disordered metal films. *Phys. Rev., Sov. Sc. Rev.*, **9** 225, 1987.

[21] I. A. Kuga, Y. Retroreflectance from a dense distribution of spherical particles. *J. Opt. Soc. Am.*, **1** 831, 1984.

[22] M. G. Wolf, P. E. Weak localization and coherent backscattering of photons in disordered media. *Phys. Rev. Lett.*, **55** 2696–2699, 1985.

[23] A. L. Van Albada, M. P. Observation of weak localization of light in a random medium. *Phys. Rev. Lett.*, **74** 4193, 1985.

[24] G. Labeyrie, F. De Tomasi, J.-C. Bernard, C. A. Mueller, C. Miniatura, and K. R. Coherent backscattering of light by cold atoms. *Phys. Rev. Lett.*, **83** 5266, 1999.

[25] F. Jendrzejewski, K. Müller, J. Richard, A. Date, T. Plisson, V. Josse, A. Aspect, and P. Bouyer. Coherent backscattering of ultracold atoms. *Phys. Rev. Lett.*, **109** 195302, 2012.

[26] G. Labeyrie, T. Karpiuk, J.-F. Schaff, B. Grémaux, C. Miniatura, and D. Delande. Enhanced backscattering of a dilute bose-einstein condensate. *Europhys. Lett.*, **100** 66001, 2012.

[27] A. Lagendijk, B. A. van Tiggelen, and D. Wiersma. Fifty years of Anderson localization. *Phys. Today*, **62** 24–29, 2009.

[28] R. Dalichaouch, J. P. Armstrong, S. Schultz, P. M. Platzman, and S. L. McCall. Microwave localization by 2-dimensional random scattering. *Nature (London)*, **354** 53 – 55, 1991.

[29] A. A. Chabanov, M. Stoytchev, and A. Z. Genack. Statistical signatures of photon localization. *Nature (London)*, **404** 850–853, 2000.

[30] D. S. Wiersma, P. Bartolini, A. Lagendijk, and R. Righini. Localization of light in a disordered medium. *Nature (London)*, **390** 671–673, 1997.

[31] M. Störzer, P. Gross, C. M. Aegerter, and G. Maret. Observation of the critical regime near Anderson localization of light. *Phys. Rev. Lett.*, **96** 063904, 2006.

[32] T. Schwartz, G. Bartal, S. Fishman, and M. Segev. Transport and Anderson localization in disordered two-dimensional photonic lattices. *Nature (London)*, **446** 52–55, 2007.

[33] Y. Lahini, A. Avidan, F. Pozzi, M. Sorel, R. Morandotti, D. N. Christodoulides, and Y. Silberberg. Anderson localization and nonlinearity in one-dimensional disordered photonic lattices. *Phys. Rev. Lett.*, **100** 013906, 2008.

[34] R. L. Weaver. *Wave Motion*, **12** 129, 1990.

[35] S. Faez, A. Strybulevych, J. H. Page, A. Lagendijk, and B. A. van Tiggelen. Observation of multifractality in Anderson localization of ultrasound. *Phys. Rev. Lett.*, **103** 155703, 2009.

[36] H. Hu, A. Strybulevych, J. H. Page, S. E. Skipetrov, and B. A. van Tiggelen. Localization of ultrasound in a three-dimensional elastic network. *Nature Phys.*, **4** 845–848, 2008.

[37] E. Larose, L. Margerin, B. A. van Tiggelen, and M. Campillo. Weak localization of seismic waves. *Phys. Rev. Lett.*, **93** 048501, 2004.

[38] J. Billy, V. Josse, Z. Zuo, A. Bernard, B. Hambrecht, P. Lugan, D. Clément, L. Sanchez-Palencia, P. Bouyer, and A. Aspect. Direct observation of Anderson localization of matter waves in a controlled disorder. *Nature (London)*, **453** 891–894, 2008.

[39] G. Roati, C. D'Errico, L. Fallani, M. Fattori, C. Fort, M. Zaccanti, G. Modugno, M. Modugno, and M. Inguscio. Anderson localization of a non-interacting Bose-Einstein condensate. *Nature (London)*, **453** 895–898, 2008.

[40] J. Chabé, G. Lemarié, B. Grémaud, D. Delande, P. Szriftgiser, and J. C. Garreau. Experimental observation of the Anderson metal-insulator transition with atomic matter waves. *Phys. Rev. Lett.*, **101** 255702, 2008.

[41] S. S. Kondov, W. R. McGehee, J. J. Zirbel, and B. DeMarco. Three-dimensional Anderson localization of ultracold fermionic matter. *Science*, **334** 66–68, 2011.

[42] F. Jendrzejewski, A. Bernard, K. Müller, P. Cheinet, V. Josse, M. Piraud, L. Pezzé, L. Sanchez-Palencia, A. Aspect, and P. Bouyer. Three-dimensional localization of ultracold atoms in an optical disordered potential. *Nature Phys.*, **8** 398–403, 2012.

[43] A. F. Ioffe and A. R. Regel. Non crystalline, amorphous, and liquid electronic semiconductors. *Prog. Semicond.*, **4** 237 – 291, 1960.

[44] E. Abrahams, P. W. Anderson, D. C. Licciardello, and T. V. Ramakrishnan. Scaling theory of localization: Absence of quantum diffusion in two dimensions. *Phys. Rev. Lett.*, **42** 673–676, 1979.

[45] D. Vollhardt and P. Wölfle. Anderson localization in $d \leq 2$ dimensions: A self-consistent diagrammatic theory. *Phys. Rev. Lett.*, **45** 842–846, 1980.

[46] D. Vollhardt and P. Wölfle. Diagrammatic, self-consistent treatment of the Anderson localization problem in $d \leq 2$ dimensions. *Phys. Rev. B*, **22** 4666–4679, 1980.

[47] M. Piraud, L. Pezzé, and L. Sanchez-Palencia. Matter wave transport and Anderson localization in anisotropic three-dimensional disorder. *Europhys. Lett.*, **99** 50003, 2012.

[48] D. Delande and G. Orso. Mobility edge for cold atoms in laser speckle potentials. *Phys. Rev. Lett.*, **113** 060601, 2014.

[49] B. Kramer and A. MacKinnon. Localization: theory and experiment. *Rep. Prog. Phys.*, **56** 1469, 1993.

[50] N. Mott. The basis of the electron theory of metals, with special reference to the transition metals. *Proc. Phys. Soc.*, **A 62** 416, 1949.

[51] N. F. Mott. Metal-insulator transition. *Rev. Mod. Phys.*, **40** 677–683, 1968.

[52] G. Mahan. *Many Particle Physics*. Springer, New York, 2000.

[53] A. T. Fiory and A. F. Hebard. Electron mobility, conductivity, and superconductivity near the metal-insulator transition. *Phys. Rev. Lett.*, **52** 2057, 1984.

[54] D. Belitz and T. R. Kirkpatrick. The Anderson-Mott transition. *Rev. Mod. Phys.*, **66** 261–380, 1994.

[55] B. L. Altshuler and A. G. Aronov. *Electron-electron interactions in disordered systems*. A. L. Efros and M. Pollak (North-Holland, Amsterdam), 1985.

[56] P. Lugan, D. Clément, P. Bouyer, A. Aspect, M. Lewenstein, and L. Sanchez-Palencia. Ultracold Bose gases in 1D disorder: From Lifshits glass to Bose-Einstein condensate. *Phys. Rev. Lett.*, **98** 170403, 2007.

[57] M. A. Cazalilla, R. Citro, T. Giamarchi, E. Orignac, and M. Rigol. One dimensional bosons: From condensed matter systems to ultracold gases. *Rev. Mod. Phys.*, **83** 1405, 2011.

[58] T. Giamarchi and H. J. Schulz. Localization and interactions in one-dimensional quantum fluids. *Europhys. Lett.*, **3** 1287, 1987.

[59] U. S. S. Rapsch and W. Zwerger. Density matrix renormalization group for disordered bosons in one dimension. *Europhys. Lett.*, **46** 559, 1999.

[60] E. Altman, Y. Kafri, A. Polkovnikov, and G. Refael. Superfluid-insulator transition of disordered bosons in one dimension. *Phys. Rev. B*, **81** 174528, May 2010.

[61] U. S. S. Rapsch and W. Zwerger. Density matrix renormalization group for disordered bosons in one dimension. *Europhys. Lett.*, **46** 559, 1999.

[62] G. M. Falco, T. Nattermann, and V. L. Pokrovsky. Localized states and interaction-induced delocalization in Bose gases with quenched disorder. *Europhys. Lett.*, **85** 30002, 2009.

[63] L. Fontanesi, M. Wouters, and V. Savona. Superfluid to Bose-glass transition in a 1d weakly interacting Bose gas. *Phys. Rev. Lett.*, **103** 030403, 2009.

[64] G. G. Batrouni and R. T. Scalettar. World-line quantum monte carlo algorithm for a one-dimensional bose model. *Phys. Rev. B*, **46** 9051, 1992.

[65] V. Gurarie, L. Pollet, N. V. Prokof'ev, B. V. Svistunov, and M. Troyer. Phase diagram of the disordered Bose-hubbard model. *Phys. Rev. B*, **80** 214519, 2009.

[66] I. F. Herbut. Dual theory of the superfluid-bose-glass transition in the disordered bose-hubbard model in one and two dimensions. *Phys. Rev. B*, **57** 13729, 1998.

[67] B. V. Svistunov. Superfluid-Bose-glass transition in weakly disordered commensurate one-dimensional system. *Phys. Rev. B*, **54** 16131–16134, 1996.

[68] L. Pollet, N. V. Prokof'ev, B. V. Svistunov, and M. Troyer. Absence of a direct superfluid to Mott insulator transition in disordered Bose systems. *Phys. Rev. Lett.*, **103** 140402, 2009.

[69] V. Gurarie, G. Refael, and J. T. Chalker. Excitations of one-dimensional Bose-Einstein condensates in a random potential. *Phys. Rev. Lett.*, **101** 170407, 2008.

[70] C. Monthus and T. Garel. Many-body localization transition in a lattice model of interacting fermions: Statistics of renormalized hoppings in configuration space. *Phys. Rev. B*, **81** 134202, 2010.

[71] A. Pal and D. A. Huse. Many-body localization phase transition. *Phys. Rev. B*, **82** 174411, 2010.

[72] V. Oganesyan and D. A. Huse. Localization of interacting fermions at high temperature. *Phys. Rev. B*, **75** 155111, 2007.

[73] C. Gogolin, M. P. Müller, and J. Eisert. Absence of thermalization in nonintegrable systems. *Phys. Rev. Lett.*, **106** 040401, 2011.

[74] E. Canovi, D. Rossini, R. Fazio, G. E. Santoro, and A. Silva. Quantum quenches, thermalization, and many-body localization. *Phys. Rev. B*, **83** 094431, 2011.

[75] J. von Neumann. Beweis des ergodensatzes und des h-theorems. *Z. Phys.*, **57** 30, 1929.

[76] J. von Neumann. Proof of the ergodic theorem and the h-theorem in quantum mechanics. *Eur. Phys. J. H*, **35** 201, 2010.

[77] S. Ziraldo and G. E. Santoro. Relaxation and thermalization after a quantum quench: Why localization is important. *Phys. Rev. B*, **87** 064201, 2013.

[78] G. Carleo, F. Becca, M. Schiró, and M. Fabrizio. Localization and glassy dynamics of many-body quantum systems. *Sci. Rep.*, **2** 243, 2012.

[79] P. Lugan, D. Clément, P. Bouyer, A. Aspect, and L. Sanchez-Palencia. Anderson localization of Bogolyubov quasiparticles in interacting Bose-Einstein condensates. *Phys. Rev. Lett.*, **99** 180402, 2007.

[80] K. Sacha, C. A. Müller, D. Delande, and J. Zakrzewski. Anderson localization of solitons. *Phys. Rev. Lett.*, **103** 210402, 2009.

[81] D. Delande, K. Sacha, M. Plodzien, S. K. Avazbaev, and J. Zakrzewski. Many-body Anderson localization in one-dimensional systems. *New J. Phys.*, **15** 45021–45031, 2013.

[82] E. Khatami, M. Rigol, A. Relaño, and A. M. Garcia-Garcia. Quantum quenches in disordered systems: Approach to thermal equilibrium without a typical relaxation time. *Phys. Rev. E*, **85** 050102, 2012.

[83] S. Ziraldo, A. Silva, and G. E. Santoro. Relaxation dynamics of disordered spin chains: Localization and the existence of a stationary state. *Phys. Rev. Lett.*, **109** 247205, 2012.

[84] M. H. Anderson, J. R. Ensher, M. R. Matthews, C. E. Wieman, and E. A. Cornell. Observation of Bose-Einstein condensation in a dilute atomic vapor. *Science*, **269** 198–201, 1995.

[85] K. B. Davis, M. O. Mewes, M. R. Andrews, N. J. Van Druten, D. S. Durfee, D. M. Kurn, and W. Ketterle. Bose-Einstein condensation in a gas of sodium atoms. *Phys. Rev. Lett.*, **75** 3969–3973, 1995.

[86] C. C. Bradley, C. A. Sackett, J. J. Tollett, and R. G. Hulet. Evidence of Bose-Einstein condensation in an atomic gas with attractive interactions. *Phys. Rev. Lett.*, **75** 1687–1690, 1995.

[87] H. J. Miesner, D. S. Durfee, D. M. Kurn, W. Ketterle, M. R. Andrews, and C. Townsend. Observation of interference between two bose condensates. *Science*, **285** 637, 1997.

[88] F. Schreck, L. Khaykovich, K. L. Corwin, G. Ferrari, T. Bourdel, J. Cubizolles, and C. Salomon. Quasipure Bose-Einstein condensate immersed in a Fermi sea. *Phys. Rev. Lett.*, **87** 4, 2001.

[89] B. DeMarco and D. S. Jin. Onset of Fermi degeneracy in a trapped atomic gas. *Science*, **285** 1703–1706, 1999.

[90] M. Greiner, O. Mandel, T. Esslinger, T. W. Hänsch, and I. Bloch. Quantum phase transition from a superfluid to a Mott insulator in a gas of ultracold atoms. *Nature (London)*, **415** 39–44, 2002.

[91] R. Jördens, N. Strohmaier, K. Günter, H. Moritz, and T. Esslinger. A Mott insulator of fermionic atoms in an optical lattice. *Nature (London)*, **455** 204–207, 2008.

[92] U. Schneider, L. Hackermüller, S. Will, T. Best, I. Bloch, T. A. Costi, R. W. Helmes, D. Rasch, and A. Rosch. Metallic and insulating phases of repulsively interacting fermions in a 3d optical lattice. *Science*, **322** 1520–1525, 2008.

[93] T. Kinoshita, T. Wenger, and D. S. Weiss. Observation of a one-dimensional Tonks-Girardeau gas. *Science*, **305** 1125–1128, 2004.

[94] B. Paredes, A. Widera, V. Murg, O. Mandel, S. Fölling, I. Cirac, G. V. Shlyapnikov, T. W. Hänsch, and I. Bloch. Tonks-Girardeau gas of ultracold atoms in an optical lattice. *Nature (London)*, **429** 277–281, 2004.

[95] Z. Hadzibabic, P. Krüger, M. Cheneau, B. Battelier, and J. Dalibard. Berezinskii-Kosterlitz-Thouless crossover in a trapped atomic gas. *Nature (London)*, **441** 1118–1121, 2006.

[96] D. Clément, A. F. Varón, J. A. Retter, L. Sanchez-Palencia, A. Aspect, and P. Bouyer. Experimental study of the transport of coherent interacting matter-waves in a 1D random potential induced by laser speckle. *New J. Phys.*, **8** 165, 2006.

[97] J. W. Goodman. *Speckle Phenomena in Optics: Theory and Applications*. Roberts and Co, Englewood, 2007.

[98] M. Robert-de Saint-Vincent, J. P. Brantut, B. Allard, T. Plisson, L. Pezzé, L. Sanchez-Palencia, A. Aspect, T. Bourdel, and P. Bouyer. Anisotropic 2d diffusive expansion of ultracold atoms in a disordered potential. *Phys. Rev. Lett.*, **104** 220602, 2010.

[99] M. White, M. Pasienski, D. McKay, S. Q. Zhou, D. Ceperley, and B. DeMarco. Strongly interacting bosons in a disordered optical lattice. *Phys. Rev. Lett.*, **102** 055301, 2009.

[100] T. Schulte, S. Drenkelforth, J. Kruse, W. Ertmer, J. Arlt, K. Sacha, J. Zakrzewski, and M. Lewenstein. Routes towards Anderson-like localization of Bose-Einstein condensates in disordered optical lattices. *Phys. Rev. Lett.*, **95** 170411, 2005.

[101] J. E. Lye, L. Fallani, M. Modugno, D. S. Wiersma, C. Fort, and M. Inguscio. Bose-Einstein condensate in a random potential. *Phys. Rev. Lett.*, **95** 070401, 2005.

[102] C. Fort, L. Fallani, V. Guarrera, J. E. Lye, M. Modugno, D. S. Wiersma, and M. Inguscio. Effect of optical disorder and single defects on the expansion of a Bose-Einstein condensate in a one-dimensional waveguide. *Phys. Rev. Lett.*, **95** 170410, 2005.

[103] D. Clément, A. F. Varón, M. Hugbart, J. A. Retter, P. Bouyer, L. Sanchez-Palencia, D. M. Gangardt, G. V. Shlyapnikov, and A. Aspect. Suppression of transport of an interacting elongated Bose-Einstein condensate in a random potential. *Phys. Rev. Lett.*, **95** 170409, 2005.

[104] M. Pasienski, D. McKay, M. White, and B. DeMarco. A disordered insulator in an optical lattice. *Nature Phys.*, **6** 677–680, 2010.

[105] D. Dries, S. E. Pollack, J. M. Hitchcock, and R. G. Hulet. Dissipative transport of a Bose-Einstein condensate. *Phys. Rev. A*, **82** 033603, 2010.

[106] B. Allard, T. Plisson, M. Holzmann, G. Salomon, A. Aspect, P. Bouyer, and T. Bourdel. Effect of disorder close to the superfluid transition in a two-dimensional Bose gas. *Phys. Rev. A*, **85** 033602, 2012.

[107] M. C. Beeler, M. E. W. Reed, T. Hong, and S. L. Rolston. Disorder-driven loss of phase coherence in a quasi-2D cold atom system. *New J. Phys.*, **14** 073024, 2012.

[108] U. Gavish and Y. Castin. Matter-wave localization in disordered cold atom lattices. *Phys. Rev. Lett.*, **95** 020401, 2005.

[109] B. Paredes, F. Verstraete, and J. I. Cirac. Exploiting quantum parallelism to simulate quantum random many-body systems. *Phys. Rev. Lett.*, **95** 140501, 2005.

[110] B. Gadway, D. Pertot, J. Reeves, M. Vogt, and D. Schneble. Glassy behavior in a binary atomic mixture. *Phys. Rev. Lett.*, **107** 145306, 2011.

[111] A. Aspect and M. Inguscio. Anderson localization of ultracold atoms. *Phys. Today*, **62** 30–35, 2009.

[112] B. Deissler, M. Zaccanti, G. Roati, C. D'Errico, M. Fattori, M. Modugno, G. Modugno, and M. Inguscio. Delocalization of a disordered bosonic system by repulsive interactions. *Nature Phys.*, **6** 354–358, 2010.

[113] B. Deissler, E. Lucioni, M. Modugno, G. Roati, L. Tanzi, M. Zaccanti, M. Inguscio, and G. Modugno. Correlation function of weakly interacting bosons in a disordered lattice. *New J. Phys.*, **13** 023020, 2011.

[114] E. Lucioni, B. Deissler, L. Tanzi, G. Roati, M. Zaccanti, M. Modugno, M. Larcher, F. Dalfovo, M. Inguscio, and G. Modugno. Observation of subdiffusion in a disordered interacting system. *Phys. Rev. Lett.*, **106** 230403, 2011.

[115] G. Lemarié, H. Lignier, D. Delande, P. Szriftgiser, and J. C. Garreau. Critical state of the anderson transition: Between a metal and an insulator. *Phys. Rev. Lett.*, **105** 090601, 2010.

[116] F. L. Moore, J. C. Robinson, C. Bharucha, P. E. Williams, and M. G. Raizen. Observation of dynamical localization in atomic momentum transfer: A new testing ground for quantum chaos. *Phys. Rev. Lett.*, **73** 2974 – 2977, 1994.

[117] F. L. Moore, J. C. Robinson, C. Bharucha, B. Sundaram, and M. G. Raizen. Atom optics realization of the quantum delta-kicked rotor. *Phys. Rev. Lett.*, **75** 4598, 1995.

[118] M. Lopez, J.-F. Clément, P. Szriftgiser, J. C. Garreau, and D. Delande. Experimental test of universality of the Anderson transition. *Phys. Rev. Lett.*, **108** 095701, 2012.

[119] P. Calabrese and J. Cardy. Time dependence of correlation functions following a quantum quench. *Phys. Rev. Lett.*, **96** 136801, 2006.

[120] G. Carleo, F. Becca, L. Sanchez-Palencia, S. Sorella, and M. Fabrizio. Light-cone effect and supersonic correlations in one- and two-dimensional bosonic superfluids. *Phys. Rev. A*, **89** 031602(R), 2014.

[121] S. Bravyi, M. B. Hastings, and F. Verstraete. Lieb-Robinson bounds and the generation of correlations and topological quantum order. *Phys. Rev. Lett.*, **97** 050401, 2006.

[122] S. R. Manmana, S. Wessel, R. M. Noack, and A. Muramatsu. Time evolution of correlations in strongly interacting fermions after a quantum quench. *Phys. Rev. B*, **79** 155104, 2009.

[123] M. Cheneau, P. Barmettler, D. Poletti, M. Endres, P. Schauss, T. Fukuhara, C. Gross, I. Bloch, C. Kollath, and S. Kuhr. Light-cone-like spreading of correlations in a quantum many-body system. *Nature (London)*, **481** 484–487, 2012.

[124] S. Trotzky, Y.-A. Chen, A. Flesch, I. P. McCulloch, U. Schollwöck, J. Eisert, and I. Bloch. Probing the relaxation towards equilibrium in an isolated strongly correlated one-dimensional Bose gas. *Nature Phys.*, **8** 325–330, 2012.

[125] A. Sanpera, A. Kantian, L. Sanchez-Palencia, J. Zakrzewski, and M. Lewenstein. Atomic Fermi-Bose mixtures in inhomogeneous and random lattices: From Fermi glass to quantum spin glass and quantum percolation. *Phys. Rev. Lett.*, **93** 040401, 2004.

[126] J. Wehr, A. Niederberger, L. Sanchez-Palencia, and M. Lewenstein. Disorder versus the Mermin-Wagner-Hohenberg effect: From classical spin systems to ultracold atomic gases. *Phys. Rev. B*, **74** 224448, 2006.

[127] A. Niederberger, T. Schulte, J. Wehr, M. Lewenstein, L. Sanchez-Palencia, and K. Sacha. Disorder-induced order in two-component Bose-Einstein condensates. *Phys. Rev. Lett.*, **100** 030403, 2008.

[128] A. Niederberger, J. Wehr, M. Lewenstein, and K. Sacha. Disorder-induced phase control in superfluid Fermi-Bose mixtures. *Europhys. Lett.*, **86** 26004, 2009.

[129] A. Niederberger, M. M. Rams, J. Dziarmaga, F. M. Cucchietti, J. Wehr, and M. Lewenstein. Disorder-induced order in quantum xy chains. *Phys. Rev. A*, **82** 013630, 2010.

[130] A. Einstein. Quantum theory of ideal monoatomic gases. *Sitzber. Preuss. Akad. Wiss.*, **23** 3, 1925.

[131] N. N. Bogolyubov. *J. Phys. USSR*, **11** 23, 1947.

[132] D. G. Fried, T. C. Killian, L. Willmann, D. Landhuis, S. Moss, D. Kleppner, and T. J. Greytak. Bose-Einstein condensation of atomic hydrogen. *Phys. Rev. Lett.*, **81** 3811, 1998.

[133] S. L. Cornish, N. R. Claussen, J. L. Roberts, E. A. Cornell, and C. E. Wieman. Stable ^{85}Rb Bose-Einstein condensates with widely tunable interactions. *Phys. Rev. Lett.*, **85** 1795–1798, 2000.

[134] G. Modugno, G. Ferrari, G. Roati, R. J. Brecha, A. Simoni, and M. Inguscio. Bose-Einstein condensation of potassium atoms by sympathetic cooling. *Science*, **294** 1320, 2001.

[135] A. Robert, O. Sirjean, A. Browaeys, J. Poupard, S. Nowak, D. Boiron, C. Westbrook, and A. Aspect. A Bose-Einstein condensate of metastable atoms. *Science*, **292** 461, 2001.

[136] A. Griesmaier, J. Werner, J. Hensler, S ans Stuhler, and T. Pfau. *Phys. Rev. Lett.*, **94** 160401, 2005.

[137] M. Greiner, C. A. Regal, and D. S. Jin. Emergence of a molecular Bose-Einstein condensate from a fermi gas. *Nature (London)*, **426** 537–540, 2003.

[138] S. Jochim, M. Bartenstein, A. Altmeyer, G. Hendl, S. Riedl, C. Chin, J. Hecker Denschlag, and R. Grimm. Bose-Einstein condensation of molecules. *Science*, **302** 2101–2103, 2003.

[139] M. W. Zwierlein, C. A. Stan, C. H. Schunck, S. M. F. Raupach, S. Gupta, Z. Hadzibabic, and W. Ketterle. Observation of Bose-Einstein condensation of molecules. *Phys. Rev. Lett.*, **91** 4, 2003.

[140] T. Nikuni, M. Oshikawa, A. Oosawa, and H. Tanaka. Bose-Einstein condensation of dilute magnons in $TlCuCl_3$. *Phys. Rev. Lett.*, **84** 5868, 2000.

[141] S. O. Demokritov, V. E. Demidov, O. Dzyapko, G. A. Melkov, A. A. Serga, B. Hillebrands, and A. N. Slavin. Bose-Einstein condensation of quasi-equilibrium magnons at room temperature under pumping. *Nature*, **443** 430, 2006.

[142] H. Deng, G. Weihs, C. Santori, J. Bloch, and Y. Yamamoto. Condensation of semiconductor microcavity exciton polaritons. *Science*, **298** 199, 2002.

[143] J. Kasprzak, M. Richard, S. Kundermann, A. Baas, P. Jeambrun, J. M. J. Keeling, F. M. Marchetti, M. H. Szymanska, R. Andre, J. L. Staehli, V. Savona, P. B. Littlewood, B. Deveaud, and L. S. Dang. Bose-Einstein condensation of exciton polaritons. *Nature*, **443** 409, 2006.

[144] J. Klaers, J. Schmitt, F. Vewinger, and M. Weitz. Bose-Einstein condensation of photons in an optical microcavity. *Nature*, **468** 545, 2010.

[145] C. N. Yang. Concept of off-diagonal long-range order and the quantum phases of liquid he and of superconductors. *Rev. Mod. Phys.*, **34** 694, 1962.

[146] O. Penrose and L. Onsager. Bose-Einstein condensation and liquid helium. *Phys. Rev.*, **104** 576, 1956.

[147] L. P. Pitaevskii and S. Stringari. *Bose-Einstein Condensation*. Clarendon press, Oxford, 2004.

[148] E. Gross. Structure of a quantized vortex in boson systems. *Il Nuovo Cimento (1955-1965)*, **20** 454, 1961.

[149] E. Gross. Hydrodynamics of a superfluid condensate. *J. Math. Phys.*, **4** 1703944, 1963.

[150] L. P. Pitaevskii. *Votex lines in an imperfect Bose gas*, volume 13. 1961. 451 pp.

[151] Y. Castin. *Coherent Atomic Matter Waves, R. Kaiser, C. Westbrook and F. David eds., Proceedings of the Les Houches Summer School of Theoretical Physics, Vol. LXXII*, chapter "Bose-Einstein condensates in atomic gases: simple theoretical results". EDP Sciences/Springer-Verlag, Berlin, 2001.

[152] D. V. Skryabin. Instabilities of vortices in a binary mixture of trapped Bose-Einstein condensates: Role of collective excitations with positive and negative energies. *Phys. Rev. A*, **63** 013602, 2000.

[153] M. Lewenstein and L. You. Quantum phase diffusion of a Bose-Einstein condensate. *Phys. Rev. Lett.*, **77** 3489–3493, 1996.

[154] C. Mora and Y. Castin. Extension of Bogoliubov theory to quasicondensates. *Phys. Rev. A*, **67** 053615, 2003.

[155] J. Armijo. *Density fluctuations in quasi one-dimensional ultracold bosonic gases*. PhD Thesis, Ecole doctorale de Physique de la région parisienne, 2011.

[156] V. M. Popov. *Functional Integrals in Quantum Field Theory and Statistical Physics*. Reidel, Dordrecht, 1983.

[157] A. I. Safonov, S. A. Vasilyev, I. S. Yasnikov, I. I. Lukashevich, and S. Jaakkola. Observation of quasicondensate in two-dimensional atomic hydrogen. *Phys. Rev. Lett.*, **81** 4545–4548, 1998.

[158] D. S. Petrov, G. V. Shlyapnikov, and J. T. M. Walraven. Regimes of quantum degeneracy in trapped 1d gases. *Phys. Rev. Lett.*, **85** 3745–3749, 2000.

[159] Y. Kagan, N. V. Prokof'ev, and B. V. Svistunov. Supercurrent stability in a quasi-one-dimensional weakly interacting bose gas. *Phys. Rev. A*, **61** 045601, 2000.

[160] D. S. Petrov. *Bose-Einstein condensation in low-dimensional trapped gases.* PhD Thesis, University of Amsterdam, 2003.

[161] A. Polkovnikov, K. Sengupta, A. Silva, and M. Vengalattore. *Colloquium*: Nonequilibrium dynamics of closed interacting quantum systems. *Rev. Mod. Phys.*, **83** 863–883, 2011.

[162] Nature Physics Insight on Quantum Simulation. *Nature Phys.*, **8** 263–299, 2012.

[163] E. Abrahams. World Scientific, Singapore, 2010.

[164] R. T. Scalettar, G. G. Batrouni, and G. T. Zimanyi. Localization in interacting, disordered, Bose systems. *Phys. Rev. Lett.*, **66** 3144–3147, 1991.

[165] W. Krauth, N. Trivedi, and D. Ceperley. Superfluid-insulator transition in disordered boson systems. *Phys. Rev. Lett.*, **67** 2307–2310, 1991.

[166] F. Evers and A. D. Mirlin. Anderson transitions. *Rev. Mod. Phys.*, **80** 1355–1417, 2008.

[167] C. W. J. Beenakker. Random-matrix theory of quantum transport. *Rev. Mod. Phys.*, **69** 731–808, 1997.

[168] A. Altland and M. R. Zirnbauer. Nonstandard symmetry classes in mesoscopic normal-superconducting hybrid structures. *Phys. Rev. B*, **55** 1142–1161, 1997.

[169] V. Gurarie and J. T. Chalker. Some generic aspects of bosonic excitations in disordered systems. *Phys. Rev. Lett.*, **89** 136801, 2002.

[170] N. Bilas and N. Pavloff. Anderson localization of elementary excitations in a one-dimensional Bose-Einstein condensate. *Eur. Phys. J. D*, **40** 387–397, 2006.

[171] L. Sanchez-Palencia. Smoothing effect and delocalization of interacting Bose-Einstein condensates in random potentials. *Phys. Rev. A*, **74** 053625, 2006.

[172] C. Gaul and C. A. Müller. Anisotropic scattering of bogoliubov excitations. *Europhys. Lett.*, **83** 10006, 2008.

[173] G. Casati, L. Molinari, and F. Izrailev. Scaling properties of band random matrices. *Phys. Rev. Lett.*, **64** 1851–1854, 1990.

[174] Y. V. Fyodorov and A. D. Mirlin. Analytical derivation of the scaling law for the inverse participation ratio in quasi-one-dimensional disordered systems. *Phys. Rev. Lett.*, **69** 1093–1096, 1992.

[175] J. D. Bodyfelt, T. Kottos, and B. Shapiro. One-parameter scaling theory for stationary states of disordered nonlinear systems. *Phys. Rev. Lett.*, **104** 164102, 2010.

[176] D. J. Thouless. Electron in disordered systems and the theory of localization. *Phys. Rep.*, **13** 93, 1974.

[177] S. Kotani and S. Taniguchi. In *Proc. Int. Symp. Kyoto*, page 225. Mathematical Library, Vol. 32, North-Holland, Amsterdam, 1984.

[178] M. Płodzień and K. Sacha. Matter-wave analog of an optical random laser. *Phys. Rev. A*, **84** 023624, 2011.

[179] M. Piraud, A. Aspect, and L. Sanchez-Palencia. Anderson localization of matter waves in tailored disordered potentials. *Phys. Rev. A*, **85** 063611, 2012.

[180] M. Piraud, L. Pezzé, and L. Sanchez-Palencia. Quantum transport of atomic matter waves in anisotropic two-dimensional and three-dimensional disorder. *New J. Phys.*, **15** 075007, 2013.

[181] M. Piraud, P. Lugan, P. Bouyer, A. Aspect, and L. Sanchez-Palencia. Localization of a matter wave packet in a disordered potential. *Phys. Rev. A*, **83** 031603(R), 2011.

[182] S. Beliaev. *Sov. Phys. JETP*, **7** 289, 1958.

[183] S. Beliaev. *Sov. Phys. JETP*, **7** 299, 1958.

[184] A. M. Lauchli and C. Kollath. Spreading of correlations and entanglement after a quench in the one-dimensional Bose-Hubbard model. *J. Stat. Mech*, **2008** P05018, 2008.

[185] T. Langen, R. Geiger, M. Kuhnert, B. Rauer, and J. Schmiedmayer. Local emergence of thermal correlations in an isolated quantum many-body system. *Nature Phys.*, **9** 640–643, 2013.

[186] G. Modugno. Anderson localization in Bose-Einstein condensates. *Rep. Prog. Phys.*, **73** 102401, 2010.

[187] B. Shapiro. Cold atoms in the presence of disorder. *J. Phys. A: Math. Theor.*, **45** 143001, 2012.

[188] D. Shechtman, I. Blech, D. Gratias, and J. W. Cahn. Metallic phase with long-range orientational order and no translational symmetry. *Phys. Rev. Lett.*, **53** 1951–1953, 1984.

[189] J. Wilson, F. Di Salvo, and S. Mahajan. Charge-density waves and superlattices in the metallic layered transition metal dichalcogenides. *Adv. Phys.*, **24** 117–201, 1975.

[190] R. Merlin, K. Bajema, R. Clarke, F. Y. Juang, and P. K. Bhattacharya. Quasiperiodic GaAs-AlAs heterostructures. *Phys. Rev. Lett.*, **55** 1768–1770, 1985.

[191] L. Fallani, J. E. Lye, V. Guarrera, C. Fort, and M. Inguscio. Ultracold atoms in a disordered crystal of light: Towards a Bose glass. *Phys. Rev. Lett.*, **98** 130404, 2007.

[192] L. Tanzi, E. Lucioni, S. Chaudhuri, L. Gori, A. Kumar, C. D'Errico, M. Inguscio, and G. Modugno. Transport of a Bose gas in 1D disordered lattices at the fluid-insulator transition. *Phys. Rev. Lett.*, **111** 115301, 2013.

[193] M. Modugno. Exponential localization in one-dimensional quasi-periodic optical lattices. *New J. Phys.*, **11** 033023, 2009.

[194] I. M. Lifshits, S. Gredeskul, and L. Pastur. *Introduction to the Theory of Disordered Systems*. Wiley, New York, 1988.

[195] S. Aubry and G. André. Analyticity breaking and Anderson localization in incommensurate lattices. *Ann. Israel Phys. Soc.*, **3** 133, 1980.

[196] J. Sokoloff. Band structure and localization in incommensurate lattice potentials. *Phys. Rev. B*, **23** 6422, 1981.

[197] C. Aulbach, A. Wobst, G.-L. Ingold, P. Hänggi, and I. Varga. Phase-space visualization of a metal-insulator transition. *New J. Phys.*, **6** 70, 2004.

[198] V. Michal, B. Altshuler, and G. Shlyapnikov. Delocalization of weakly interacting bosons in a 1D quasiperiodic potential. arXiv:1402.4796, 2014.

[199] S. Iyer, V. Oganesyan, G. Refael, and D. A. Huse. Many-body localization in a quasiperiodic system. *Phys. Rev. B*, **87** 134202, 2013.

[200] P. Buonsante and A. Vezzani. Phase diagram for ultracold bosons in optical lattices and superlattices. *Phys. Rev. A*, **70** 033608, 2004.

[201] P. Buonsante, V. Penna, and A. Vezzani. Fractional-filling mott domains in two-dimensional optical superlattices. *Phys. Rev. A*, **72** 031602, 2005.

[202] V. G. Rousseau, D. P. Arovas, M. Rigol, F. Hébert, G. G. Batrouni, and R. T. Scalettar. Exact study of the one-dimensional boson hubbard model with a superlattice potential. *Phys. Rev. B*, **73** 174516, 2006.

[203] D. M. J. Vidal and T. Giamarchi. Correlated fermions in a one-dimensional quasiperiodic potential. *Phys. Rev. Lett.*, **83** 3908, 1999.

[204] D. M. J. Vidal and T. Giamarchi. Interacting fermions in self-similar potentials. *Phys. Rev. B*, **65** 014201, 2001.

[205] F. D. M. Larcher and M. Modugno. Effects of interaction on the diffusion of atomic matter waves in one-dimensional quasiperiodic potentials. *Phys. Rev. A*, **80** 053606, 2009.

[206] R. Roth and K. Burnett. Phase diagram of bosonic atoms in two-color superlattices. *Phys. Rev. A*, **68** 023604, 2003.

[207] T. Roscilde. Bosons in one-dimensional incommensurate superlattices. *Phys. Rev. A*, **77** 063605, 2008.

[208] G. Roux, T. Barthel, I. P. McCulloch, C. Kollath, U. Schollwöck, and T. Giamarchi. Quasiperiodic Bose-Hubbard model and localization in one-dimensional cold atomic gases. *Phys. Rev. A*, **78** 023628, 2008.

[209] X. Deng, R. Citro, A. Minguzzi, and E. Orignac. Phase diagram and momentum distribution of an interacting Bose gas in a bichromatic lattice. *Phys. Rev. A*, **78** 013625, 2008.

[210] S. Lellouch and L. Sanchez-Palencia. Localization transition in weakly interacting Bose superfluids in one-dimensional quasiperdiodic lattices. *Phys. Rev. A*, **90** 061602(R), 2014.

[211] J. Sokoloff. Electron localization in crystals with quasiperiodic lattice potentials. *Phys. Rev. B*, **22** 5823, 1980.

[212] R. Peierls. Theory of the diamagnetism of conduction electrons. *Z. Phys.*, **80** 763, 1933.

[213] D. R. Hofstadter. Energy levels and wave functions of Bloch electrons in rational and irrational magnetic fields. *Phys. Rev. B*, **14** 2239–2249, 1976.

[214] H. L. Cycon, R. G. Froese, W. Kirsch, and B. Simon. *Schrodinger Operators*. Berlin Springer, 1987.

[215] P. G. Harper. Single band motion of conduction electrons in a uniform magnetic field. *Proc. Phys. Soc. London*, **A 68** 874–978, 1955.

[216] S. Y. Jitomirskaya. Metal-insulator transition for the almost mathieu operator. *Ann. Math.*, **105** 1159–1175, 1999.

[217] D. J. Thouless. Electron in disordered systems and the theory of localization. *J. Phys. C: Solid State Phys.*, **5** 77, 1972.

[218] B. W. J. Biddle, D.J. Priour Jr. and S. D. Sarma. Localization in one-dimensional lattices with non-nearest-neighbor hopping : Generalized anderson and aubry-andré models. *Phys. Rev. B*, **83** 075105, 2011.

[219] M. Y. Azbel. Quantum particle in one-dimensional potentials with incommensurate periods. *Phys. Rev. Lett.*, **43** 1954, 1979.

[220] C. Soukoulis and E. Economou. Localization in one-dimensional lattices in the presence of incommensurate potentials. *Phys. Rev. Lett.*, **48** 1043, 1982.

[221] R. Riklund, Y. Liu, G. Wahlstrom, and Z. Zheng. Extension of the hopping range in incommensurate systems can generate localised states. *J. Phys. C: Solid State Phys.*, **19** L705, 1986.

[222] M. Johansson and R. Riklund. Self-dual model for one-dimensional incommensurate crystals including next-nearest-neighbor hopping, and its relation to the hofstadter model. *Phys. Rev. B*, **43** 13468, 1991.

[223] D. Van Oosten, P. Van der Straten, and H. T. C. Stoof. Quantum phases in an optical lattice. *Phys. Rev. A*, **63** 3601, 2001.

[224] C. Gaul and C. A. Müller. Bogoliubov theory on the disordered lattice. *Eur. Phys. J. Special Topics*, **217** 69–78, 2013.

[225] W. H. Press, S. A. Teukolsky, W. T. Vetterling, and B. P. Flannery. *Numerical Recipes, 3rd Edition*. Cambridge University Press, Cambridge, 2007.

[226] G. Roux, A. Minguzzi, and T. Roscilde. Dynamic structure factor of one-dimensional lattice bosons in a disordered potential : a spectral fingerprint of the bose-glass phase. *New J. Phys.*, **15** 055003, 2013.

[227] J. Stenger, S. Inouye, A. P. Chikkatur, D. M. Stamper-Kurn, D. E. Pritchard, and W. Ketterle. Bragg spectroscopy of a Bose-Einstein condensate. *Phys. Rev. Lett.*, **82** 4569–4573, 1999.

[228] J. Steinhauer, R. Ozeri, N. Katz, and N. Davidson. Excitation spectrum of a Bose-Einstein condensate. *Phys. Rev. Lett.*, **88** 120407, 2002.

[229] S. Richard, F. Gerbier, J. H. Thywissen, M. Hugbart, P. Bouyer, and A. Aspect. Momentum spectroscopy of 1D phase fluctuations in Bose-Einstein condensates. *Phys. Rev. Lett.*, **91** 010405, 2003.

[230] A. F. Andreev and E. P. Bashkin. *Sov. Phys. JETP*, **42** 164, 1976.

[231] W. J. Mullin. Bose condensation of idealized spin-polarized atomic Hydrogen in equilibrium. *Phys. Rev. Lett.*, **44** 1420–1423, 1980.

[232] E. D. Siggia and A. E. Ruckenstein. Bose condensation in spin-polarized atomic Hydrogen. *Phys. Rev. Lett.*, **44** 1423–1426, 1980.

[233] B. W. Statt and A. J. Berlinsky. Theory of spin relaxation and recombination in spin-polarized atomic hydrogen. *Phys. Rev. Lett.*, **45** 2105–2109, 1980.

[234] D. W. Snoke and J. P. Wolfe. Picosecond dynamics of degenerate orthoexcitons in cu_2o. *Phys. Rev. B*, **42** 7876–7884, 1990.

[235] J. L. Lin and J. P. Wolfe. Bose-Einstein condensation of paraexcitons in stressed cu_2o. *Phys. Rev. Lett.*, **71** 1222–1225, 1993.

[236] M. R. Matthews, D. S. Hall, D. S. Jin, J. R. Ensher, C. E. Wieman, E. A. Cornell, F. Dalfovo, C. Minniti, and S. Stringari. Dynamical response of a Bose-Einstein condensate to a discontinuous change in internal state. *Phys. Rev. Lett.*, **81** 243–247, 1998.

[237] D. S. Hall, M. R. Matthews, J. R. Ensher, C. E. Wieman, and E. A. Cornell. Dynamics of component separation in a binary mixture of Bose-Einstein condensates. *Phys. Rev. Lett.*, **81** 1539–1542, 1998.

[238] D. S. Hall, M. R. Matthews, C. E. Wieman, and E. A. Cornell. Measurements of relative phase in two-component Bose-Einstein condensates. *Phys. Rev. Lett.*, **81** 1543–1546, 1998.

[239] T. Schumm, S. Hofferberth, L. M. Anderson, S. Wildermuth, S. Groth, J. Bar-Joeseph, I. Schmiedmayer, and P. Krüger. Matter-wave interferometry in a double well on an atom chip. *Nature Phys.*, **1** 57–62, 2005.

[240] H. Shi, H. Rastegar, and A. Griffin. Bose-Einstein condensation of a coupled two-component Bose gas. *Phys. Rev. E*, **51** 1075–1080, 1995.

[241] E. V. Goldstein and P. Meystre. Quasiparticle instabilities in multicomponent atomic condensates. *Phys. Rev. A*, **55** 2935–2940, 1997.

[242] P. Öhberg. Stability properties of the two-component Bose-Einstein condensate. *Phys. Rev. A*, **59** 634–638, 1999.

[243] T.-L. Ho and V. B. Shenoy. Binary mixtures of Bose condensates of alkali atoms. *Phys. Rev. Lett.*, **77** 3276–3279, 1996.

[244] C. K. Law, H. Pu, N. P. Bigelow, and J. H. Eberly. Stability signature in two-species dilute Bose-Einstein condensates. *Phys. Rev. Lett.*, **79** 3105–3108, 1997.

[245] E. P. Bashkin and A. V. Vagov. Instability and stratification of a two-component Bose-Einstein condensate in a trapped ultracold gas. *Phys. Rev. B*, **56** 6207–6212, 1997.

[246] T. Busch, J. I. Cirac, V. M. Pérez-García, and P. Zoller. Stability and collective excitations of a two-component Bose-Einstein condensed gas: A moment approach. *Phys. Rev. A*, **56** 2978–2983, 1997.

[247] E. Timmermans. Phase separation of Bose-Einstein condensates. *Phys. Rev. Lett.*, **81** 5718–5721, 1998.

[248] H. Pu and N. P. Bigelow. Properties of two-species Bose condensates. *Phys. Rev. Lett.*, **80** 1130–1133, 1998.

[249] H. Pu and N. P. Bigelow. Collective excitations, metastability, and nonlinear response of a trapped two-species Bose-Einstein condensate. *Phys. Rev. Lett.*, **80** 1134–1137, 1998.

[250] P. Öhberg and S. Stenholm. Hartree-fock treatment of the two-component bose-einstein condensate. *Phys. Rev. A*, **57** 1272–1279, 1998.

[251] D. Gordon and C. M. Savage. Excitation spectrum and instability of a two-species Bose-Einstein condensate. *Phys. Rev. A*, **58** 1440–1444, 1998.

[252] B. D. Esry and C. H. Greene. Spontaneous spatial symmetry breaking in two-component Bose-Einstein condensates. *Phys. Rev. A*, **59** 1457–1460, 1999.

[253] L. E. Sadler, J. M. Higbie, S. R. Leslie, M. Vengalattore, and D. M. Stamper-Kurn. Spontaneous symmetry breaking in a quenched ferromagnetic spinor Bose condensate. *Nature (London)*, **443** 312, 2006.

[254] J. Javanainen and S. M. Yoo. Quantum phase of a Bose-Einstein condensate with an arbitrary number of atoms. *Phys. Rev. Lett.*, **76** 161–164, 1996.

[255] N. K. Whitlock and I. Bouchoule. Relative phase fluctuations of two coupled one-dimensional condensates. *Phys. Rev. A*, **68** 053609, 2003.

[256] M.-S. Chang, Q. Qin, W. Zhang, L. You, and M. S. Chapman. *Nature Phys.*, **1** 111, 2005.

[257] H.-P. Stimming, N. J. Mauser, J. Schmiedmayer, and I. E. Mazets. Fluctuations and stochastic processes in one-dimensional many-body quantum systems. *Phys. Rev. Lett.*, **105** 015301, 2010.

[258] T. Zibold, E. Nicklas, C. Gross, and M. K. Oberthaler. Classical bifurcation at the transition from Rabi to Josephson dynamics. *Phys. Rev. Lett.*, **105** 204101, 2010.

[259] T. Betz, S. Manz, R. Bücker, T. Berrada, C. Koller, G. Kazakov, I. E. Mazets, H.-P. Stimming, A. Perrin, T. Schumm, and J. Schmiedmayer. Two-point phase correlations of a one-dimensional bosonic Josephson junction. *Phys. Rev. Lett.*, **106** 020407, 2011.

[260] K. Kasamatsu, M. Tsubota, and M. Ueda. Vortices in multicomponent Bose-Einstein condensates. *Int. J. Mod. Phys. B*, **19** 1835–1904, 2005.

[261] M. Vengalattore, S. R. Leslie, J. Guzman, and D. M. Stamper-Kurn. Spontaneously modulated spin textures in a dipolar spinor Bose-Einstein condensate. *Phys. Rev. Lett.*, **100** 170403, 2008.

[262] M. Vengalattore, J. Guzman, S. R. Leslie, F. Serwane, and D. M. Stamper-Kurn. Periodic spin textures in a degenerate $f = 1$ ^{87}Rb spinor Bose gas. *Phys. Rev. A*, **81** 053612, 2010.

[263] J. Guzman, G.-B. Jo, A. N. Wenz, K. W. Murch, C. K. Thomas, and D. M. Stamper-Kurn. Long-time-scale dynamics of spin textures in a degenerate $f = 1$ ^{87}Rb spinor Bose gas. *Phys. Rev. A*, **84** 063625, 2011.

[264] J. I. Cirac, M. Lewenstein, K. Mølmer, and P. Zoller. Quantum superposition states of Bose-Einstein condensates. *Phys. Rev. A*, **57** 1208–1218, 1998.

[265] C. Gross, H. Strobel, E. Nicklas, T. Zibold, N. Bar-Gill, G. Kurizki, and M. K. Oberthaler. *Nature (London)*, **480** 219, 2011.

[266] B. Lücke, M. Scherer, J. Kruse, L. Pezzé, F. Deuretzbacher, P. Hyllus, O. Topic, J. Peise, W. Ertmer, J. Arlt, L. Santos, A. Smerzi, and C. Klempt. *Science*, **334** 773, 2011.

[267] C. Gaul and C. A. Müller. Bogoliubov excitations of disordered Bose-Einstein condensates. *Phys. Rev. A*, **83** 063629, 2011.

[268] H. Gimperlein, S. Wessel, J. Schmiedmayer, and L. Santos. Ultracold atoms in optical lattices with random on-site interactions. *Phys. Rev. Lett.*, **95** 170401, 2005.

[269] S. Lellouch, T.-L. Dao, T. Koffel, and L. Sanchez-Palencia. Two-component Bose gases with one-body and two-body couplings. *Phys. Rev. A*, **88** 063646, 2013.

[270] V. M. Popov. *Theor. Math. Phys.*, **11** 72, 1972.

[271] S. Raghavan, A. Smerzi, S. Fantoni, and S. R. Shenoy. Coherent oscillations between two weakly coupled Bose-Einstein condensates: Josephson effects, π oscillations, and macroscopic quantum self-trapping. *Phys. Rev. A*, **59** 620–633, 1999.

[272] M. Albiez, R. Gati, J. Fölling, S. Hunsmann, M. Cristiani, and M. K. Oberthaler. Direct observation of tunneling and nonlinear self-trapping in a single bosonic Josephson junction. *Phys. Rev. Lett.*, **95** 010402, 2005.

[273] R. Gati, B. Hemmerling, J. Fölling, M. Albiez, and M. K. Oberthaler. Noise thermometry with two weakly coupled Bose-Einstein condensates. *Phys. Rev. Lett.*, **96** 130404, 2006.

[274] S. Inouye, M. R. Andrews, J. Stenger, H. J. Miesner, D. M. Stamper-Kurn, and W. Ketterle. Observation of Feshbach resonances in a Bose-Einstein condensate. *Nature (London)*, **392** 151–154, 1998.

[275] S. I. Shevchenko. *J. Sov. Low Temp. Phys.*, **18** 223, 1992.

[276] D. S. Petrov, G. D. M., and G. V. Shlyapnikov. Low-dimensional trapped gases. *J. Phys. IV (France)*, **116** 3, 2004.

[277] C. J. Pethick and H. Smith. *Bose-Einstein Condensation in Dilute Gases*. Cambridge University press, 2001.

[278] N. N. Bogolyubov. *Sov. Phys. JETP*, **7** 41, 1958.

[279] P.-G. de Gennes. *Superconductivity of Metals and Alloys*. Addison-Wesley, 1995.

[280] C. J. Myatt, E. A. Burt, R. W. Ghrist, E. A. Cornell, and C. E. Wieman. Production of two overlapping Bose-Einstein condensates by sympathetic cooling. *Phys. Rev. Lett.*, **78** 586–589, 1997.

[281] J.-L. Basdevant and J. Dalibard. *Quantum Mechanics*. Springer, Berlin, 2005.

[282] Y. Castin and R. Dum. Low-temperature Bose-Einstein condensates in time-dependent traps: Beyond the $u(1)$ symmetry-breaking approach. *Phys. Rev. A*, **57** 3008–3021, 1998.

[283] J. Estève, J.-B. Trebbia, T. Schumm, A. Aspect, C. I. Westbrook, and I. Bouchoule. Observations of density fluctuations in an elongated Bose gas: Ideal gas and quasicondensate regimes. *Phys. Rev. Lett.*, **96** 130403, 2006.

[284] J. Armijo, T. Jacqmin, K. V. Kheruntsyan, and I. Bouchoule. Probing three-body correlations in a quantum gas using the measurement of the third moment of density fluctuations. *Phys. Rev. Lett.*, **105** 230402, 2010.

[285] S. Dettmer, D. Hellweg, P. Ryytty, J. J. Arlt, W. Ertmer, K. Sengstock, D. S. Petrov, G. V. Shlyapnikov, H. Kreutzmann, L. Santos, and M. Lewenstein. Observation of phase fluctuations in elongated Bose-Einstein condensates. *Phys. Rev. Lett.*, **87** 160406, 2001.

[286] D. Hellweg, L. Cacciapuoti, M. Kottke, T. Schulte, K. Sengstock, W. Ertmer, and J. J. Arlt. Measurement of the spatial correlation function of phase fluctuating Bose-Einstein condensates. *Phys. Rev. Lett.*, **91** 010406, 2003.

[287] F. Gerbier, J. H. Thywissen, S. Richard, M. Hugbart, P. Bouyer, and A. Aspect. Momentum distribution and correlation function of quasicondensates in elongated traps. *Phys. Rev. A*, **67** 051602, 2003.

[288] L. Cacciapuoti, D. Hellweg, M. Kottke, T. Schulte, W. Ertmer, J. J. Arlt, K. Sengstock, L. Santos, and M. Lewenstein. Second-order correlation function of a phase fluctuating Bose-Einstein condensate. *Phys. Rev. A*, **68** 053612, 2003.

[289] C. A. Müller and D. Delande. *Ultracold Gases and Quantum Information, C. Miniatura et al. eds., Lecture Notes of the Les Houches Summer School in Singapore 2009: Vol. XCI*, chapter Disorder and interference: localization phenomena. Oxford University Press, Oxford, 2011.

[290] M. Piraud. *Anderson localization of matter waves in correlated disorder:from 1D to 3D*. PhD Thesis, UNIVERSITE PARIS-SUD, 2012.

Résumé

Ce mémoire présente une étude théorique des propriétés de localisation collective dans les superfluides de Bose désordonnés ou quasi-périodiques. S'il est connu depuis Anderson que le désordre peut localiser les particules libres, comprendre ses effets dans les systèmes quantiques en interaction, où il est à l'origine de transitions de phase et d'effets de localisation non-triviaux, représente aujourd'hui un défi majeur. En nous focalisant sur le cas d'un gaz de Bose dans le régime de faibles interactions, bien décrit par la théorie de Bogoliubov, nous étudions les transitions de localisation de ses excitations collectives dans différents contextes. Dans le cas d'un vrai désordre dans l'espace continu tout d'abord, nous développons un formalisme de désordre fort allant au-delà des études antérieures, aboutissant à une description complète des propriétés de localisation des excitations en dimension arbitraire. Nous présentons un diagramme de localisation générique, et une interprétation microscopique de la propagation des excitations dans le désordre. Dans un second temps, nous considérons le cas d'un potentiel quasi-périodique unidimensionnel, aux propriétés intermédiaires entre un vrai désordre et un potentiel périodique. Notre traitement analytique et numérique du problème révèle une transition de localisation collective, que nous caractérisons et interprétons en termes de localisation dans un potentiel effectif multiharmonique. Pour finir, nous considérons le cas d'un gaz de Bose à deux composants. Nous développons le formalisme général pour étudier ces questions et décrivons la physique de base de ces systèmes qui présentent leurs propres spécificités.

Abstract

In this thesis, we theoretically investigate the collective localization properties of weakly-interacting Bose superfluids subjected to disordered or quasiperiodic potentials. While disorder has been recognized since Anderson to induce single-particle localization, the interplay between disorder and interactions in quantum systems is today among the most challenging questions in the field, and underlies fascinating phase transitions and non-trivial localization effetcs. Focusing on Bose gases in the weakly-interacting regime for which the Bogoliubov theory proves a successful tool, we study the localization transitions of collective excitations in several contexts. First, in the case of a continuous true disorder, we develop a strong-disorder formalism going beyond previous studies, providing us with a complete description of the localization behaviour of collective excitations in arbitrary dimension. A generic localization diagram is obtained and the transport of excitations in the disorder is microscopically interpreted. Secondly, we consider the case of one-dimensional quasiperiodic potentials, which are known to display intermediate properties between periodic and disordered ones. We perform a numerical and analytical treatment of the localization problem of collective excitations, allowing us to quantitatively characterize and interpret the localization transition in terms of an effective multiharmonic problem. Finally, we set up the general inhomogeneous formalism to address such issues in multicomponent Bose gases, and we enlighten the basic physics of such systems, which are known to exhibit their own specific features.